# Bivalent cations conductive solid ionogel electrolytes for metal-ion applications

Nicolas Demarthe

COLLEGE DOCTORAL PAYS DE LA LOIRE
ED MATIERE,MOLECULES MATERIAUX ET GEOSCIENCES

Nantes Université

University of South Australia

# THESE DE DOCTORAT

NANTES UNIVERSITE & UNIVERSITY OF SOUTH AUSTRALIA

ECOLE DOCTORALE N° 596
*Matière, Molécules, Matériaux et Géosciences*
Spécialité : Sciences des Matériaux

Par

**Nicolas DEMARTHE**

## Bivalent cations conductive solid ionogel electrolytes for metal-ion applications

**Électrolytes ionogels solides conducteurs d'ions divalents pour application métal-ion**

**Thèse présentée et soutenue à Nantes, le 21 décembre 2023**

**Unité de recherche : Institut des Matériaux de Nantes Jean Rouxel / Future Industries Institute**

**Rapporteurs avant soutenance** :

| | |
|---|---|
| Mérièm ANOUTI | Professeure, PCM2E, Université de Tours |
| Michael DESCHAMPS | Professeur, CEMHTI, Université d'Orléans |

**Composition du Jury :**

| | | |
|---|---|---|
| Président : | Cristina IOJOIU | |
| Examinateurs : | Cristina IOJOIU | Directrice de Recherche, LEPMI, Grenoble INP UGA |
| | Monika SCHÖNHÖFF | Professeure, Institute of Physical Chemistry, Univesität Münster |
| Dir. de thèse : | Jean LE BIDEAU | Professeur, IMN, Nantes Université |
| Co-dir. de thèse : | Thierry BROUSSE | Professeur, IMN, Nantes Université |
| | Dario ARRUA | Professeur, FII, University of South Australia |
| | Drew EVANS | Professeur, FII, University of South Australia |
| **Invité(s)** | | |
| | Luke O'DELL | Professeur, IFM, Deakin University, Geelong |

*Aux cinq doigts de la main,*

# Table of content

# Acknowledgements

Three years ago in 2020, I had just completed my end-of-study internship in the dark covid-19 period, and even before graduating as an engineer from ENSMAC (formerly ENSCBP), I had the brightening opportunity to apply for a thesis at the Institut des Matériaux de Nantes (IMN). I would like to mention my dear, sweet friend **Etienne Le Calvez,** who, saddened to be separated from me on leaving school, suggested I come to Nantes to share the adventure of the doctorate - a suggestion that I finally acted on.

I would like to acknowledge **Nantes Université** and the **University of South Australia** for the financing of this project and both of their respective administrative teams who undeniably put a lot of energy into making this international thesis possible. I hope that my first experience of studying abroad under this co-tutelle agreement will make the formalities even easier for future Franco-Australian generations. A quick note to thank **Florent Boucher**, Director of the IMN (my home institution), for allowing me to flourish within the Institute, with its many shared facilities and resources.

I personally thank again all the jury members who took the time to evaluate my work in an exhaustive and interested manner in order to conclude the scientific discussion and bring the three-year study program to a close. A special thank for whom came to Nantes on the day of my thesis defence. Thanks also to all the online members, some of whom had to stay up late on the other side of the world! **Pr Mérièm Anouti**, **Pr Michael Deschamps**, **Dr Cristina Iojoiu, Pr Monika Schönhöff** and **Pr Luke O'Dell**.

First, I would like to thank my thesis supervisors, without whom all this work would not have been possible. **Jean le Bideau** for his formative presence and sharing of scientific knowledge, experience on the professional environment and the overall operation of an academic research laboratory, even beyond the thesis. **Thierry Brousse** for his incredible scientific culture and his many ingenious ideas on electrochemical devices, which really trained me to imagine applications for a rather fundamental subject. **Dario Arrua** for his kindness and availability to make my stay in Adelaide and Australia perfectly enjoyable both inside and outside the laboratory. He was essential in teaching me how to adapt to an international environment where operations were different from what I known and he was able to reassure me about the quality of the work generated by this type of co-tutelle. **Drew Evans** for his for its enriching discussions and its positivism towards any result, his daily support as well as for his pertinent questions, which always inspire us to strive for excellence in scientific

reasoning. Finally, I would like to emphasize that this complementary management team has enabled me to express myself and develop my research in a respectful and efficient manner. They were all good listeners and very encouraging when it came to discussing the interpretation of results, and all four helped forge my ethics and my future research career. I am very grateful for this excellent training journey.

I would like to make a special mention of the members of my "Commité de suivi individuel" (CSI) comprising **Mireille Richard** and **Pierre-Louis Taberna.** Thank you for guiding me through the organizational side of the PhD project.

Secondly, I would like to thank specifically **Luke O'Dell**, **Bernard Humbert**, **Maxime Bayle**, **Patrick Gerlach**, **Charlotte Bodin, Elodie Grange**, **Camille Douard**, **Françoise Lari**, **Bob Chivell**, **Fanch Guillou**, **John Denman, Patrick Sherman, Susie Ritch, Yann Claveau, Chris Ewels, Philippe Poizot, Patrick Soudan** and of course my colleague and friend **Thibaud Guillemin** for their help during the PhD. Thanks to them for helping me set up my experiments and interpreting some of the results with me.

Then, I want to thank **Carlos Ogouché** and **Tojo Rasoanarivo** the two interns who worked alongside me. **Youssef El Moussaoui** and **Samanvitha Kunigal Vijaya Shankar** who have put up with me in the office all this time.

**Théo Cavignac** and **Sandro Stal,** all three doctors now, who became very close friends after testing all the wackiest but always excellent recipes imaginable, the long hours spent playing role-playing games, and our great trip to Italy (bons baisers de Florence !).

More generally, I would like to thank all the PhD students and post-docs who have made my working environment so pleasant, with a lightness that the constraints of thesis work tend to make us forget. Thanks again for having been by my side during my cruciate ligament operation in the first year, my driving test in the second year, and the long administrative procedures involved in my move to Australia in the final year! **Etienne Le Calvez, Julio Espinosa, Thibaud Guillemin, Mathieu, Louise Burot, Juliette Théodore, Hugues Macé, Nicolas Goubard, Patrick Gerlach, Charlotte Bodin, Mohamad Haydoura, Cédric Mannequin, Florian Chabanais, Florent Pawula, Théo Cavignac, Sandro Stal, Justine Cordiez, Lucas Huet, Joëlle Zgheib, Hélène Roberge, Lou Bernard, Angelica Laurita, Thibault Amiaud, Aurely Bagghi, Pablo Castellani, Thomas le Néel, Youssef El moussaoui, Arthur Chadaigne, Clément Meyssonier, Eva Ros, Eugène Bertin, Allan Lebreton, Côme Archinard, Alexandre Merieau, Alberto Urutchu, Simon Guillonneau, Valentin Brard, Tojo Rasoanarivo, Eva Maria, Samanvitha Kunigal Vijaya Shankar, Boluwatife Igbaroola (Matt), Julien Chevet, Aline Kneubl, Marcelo Andrade, Pierre-Louis Martin, Nouridine Zemal, Bastien Anézo, Nathanaël Blond**, and all the others…

Of course, I will never forget the wonderful encounters I made in Australia thanks to my exchange at the University of South Australia, to all our hikes and long DnD evenings, to barbies: **Ravi Raj, Nam Mai, Max, Bodie Fuller, Jake Atkinson, Jacob Dalgleish, Minh Le Nguyen, Bianca Jong, Ting Chong Chen, André Hatem**… Thank you mates!

I am also grateful to my childhood friends for coming to my thesis defense; even if they did not understand everything, they had the strength to stay until the questions. **Lucas Bonnet-Gammard**, **Arthur Granger** and **Nicolas Seinturier**. Thanks to **Jean Castillon** for coming too and to **Luana Cuvillier** who has always been a great source of motivation.

Finally, I would like to end by thanking my family, who have been very much there for me, and whose presence counts a great deal in my professional success. As a sign of my gratitude, I dedicate this manuscript to **Hervé**, **Patricia**, **Marie** and **Lucie**.

# French summary

Le développement de dispositifs de stockage d'énergie tout solide implique l'utilisation de nouveaux matériaux innovants dont les électrolytes. Ceux-ci doivent être compétitifs vis-à-vis des électrolytes liquides organiques commerciaux en termes de conductivité ionique et de stabilité électrochimique et apporter plus de sécurité.

Les liquides ioniques (LIs) sont déjà utilisés pour leurs propriétés intéressantes telles que leur pression de vapeur très faible, leur point de fusion bas, leur non-flammabilité et leur large fenêtre électrochimique. Néanmoins, cette famille d'électrolytes reste liquide et peut présenter des problèmes de fuite et donc de packaging (électrolytes encerclés en rouge sur la Figure 1).

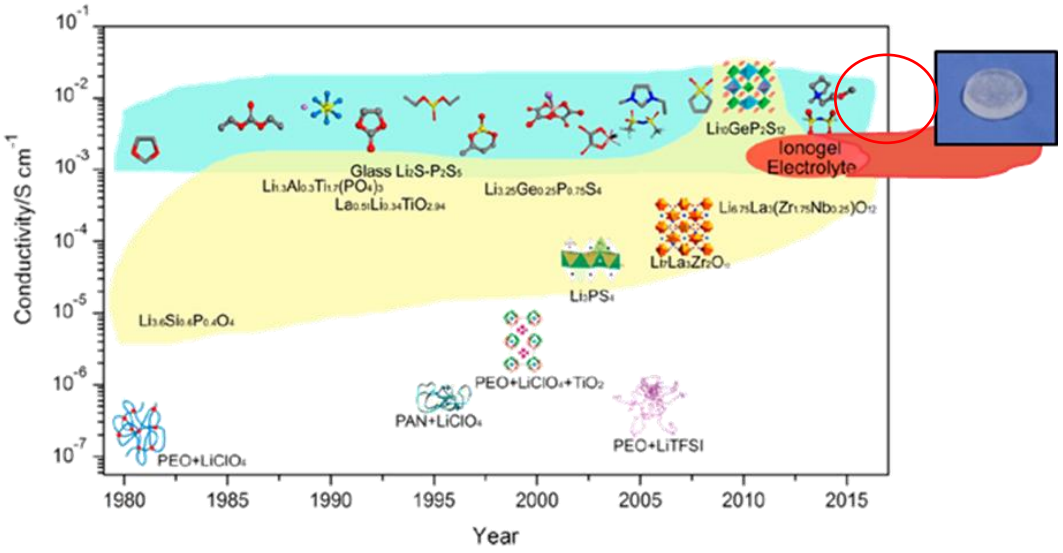


(Wu, F.; Chen, N.; Chen, R.; Zhu, Q.; Qian, J.; Li, L. *Chem. Mater.* **2016**, *28* (3), 848–856)

**Figure 1 : Etat de l'art des électrolytes liquides organiques, solides inorganiques, LIs et ionogels en fonctions de leur conductivité ionique**

L'usage de LIs confinés (ionogels), dans le polymère polyfluorure de vinylidène (PVDF) par exemple, évite tout risque de fuite, simplifie le packaging et permet de limiter le risque d'emballement thermique dans les dispositifs électrochimiques contrairement aux électrolytes liquides organiques classiques. Les ionogels sont des matériaux biphasiques à interface continue entre un liquide ionique et la matrice solide qui le confine, cette dernière pouvant être faite d'oxydes ou de polymères (électrolytes surlignés en rouge sur la Figure 1). Ils présentent une conductivité ionique très élevée comparée à celle des autres électrolytes solides inorganiques car les propriétés du liquide confiné sont préservées. L'ajout de sels de Li, Mg ou Zn dans le LI permet d'adapter les ionogels à des applications

spécifiques telles que les supercondensateurs et les batteries métal-ion. Le passage des cations monovalents ($Li^+$, $Na^+$ ou $K^+$) aux ions divalents ($Mg^{2+}$, $Ca^{2+}$ ou $Zn^{2+}$) garantit une densité d'énergie théorique plus élevée dans le dispositif. De plus, l'élaboration de dispositifs ne reposant pas sur la surexploitation des ressources en lithium, permet de s'affranchir de problématiques géographique et géopolitique.

Les systèmes étudiés dans ce manuscrit sont les mélanges ternaires composés du liquide ionique 1-ethyl-3-methylimidazolium bis(trifluoromethanesulfonyl)imide (EMImTFSI) avec des sels de LiTFSI, $Mg(TFSI)_2$ et $Zn(TFSI)_2$. Ces mêmes LIs sont ensuite confinés dans une matrice polymère pour former des gels physiques. La synthèse de ionogels à base de PVDF est présentée en Figure 2.

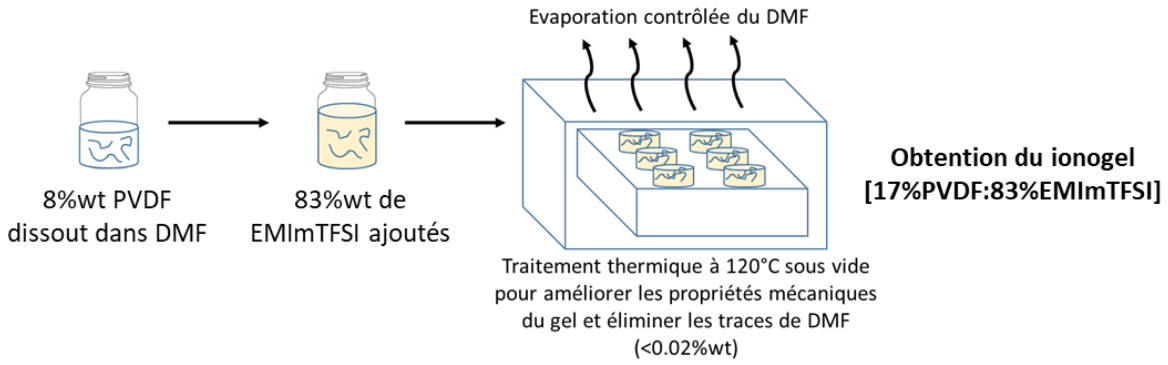


**Figure 2 : Illustration de la synthèse de ionogels physique par évaporation de solvant**

La stratégie de l'étude est de comparer le comportement des LIs non confinés et celui des ionogels afin de comprendre la différence de dynamique dans ces électrolytes avec une interface solide-liquide. S'il est contrintuitif d'ajouter un polymère qui ne participe pas à la conductivité ionique macroscopique des ions du liquide ionique, il est de prime abord surprenant de constater que ce confinement ne modifie pas les valeurs de conductivité mesurées (Figure 3).

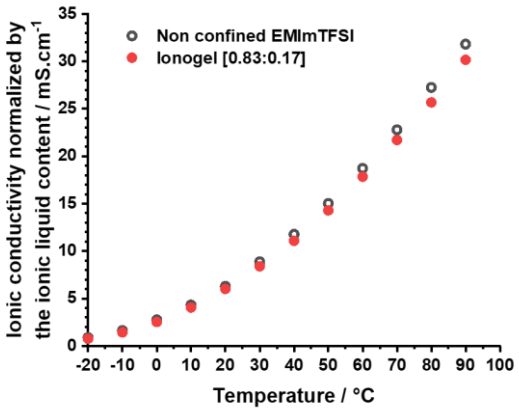


**Figure 3 : Conductivité ionique de EMImTFSI comparée à celle d'un ionogel PVDF 83%wt EMImTFSI**

Il semble que l'on passe d'un électrolyte liquide à un électrolyte solide (gel) sans perte de propriétés de transport. *Quelles sont les explications fondamentales de cette très haute conductivité ionique du ionogel riche en liquide ionique ?*

Ces travaux de recherche se focalisent sur les interactions et la mobilité des ions dans les LIs ternaires et les ionogels. Nous étudions les interactions coulombiennes en compétitions entre le cation d'intérêt ($Li^+/Mg^{2+}/Zn^{2+}$) et, soit avec l'anion de l'IL ($TFSI^-$), soit avec la matrice de confinement (Figure 4). Ces études apportent des connaissances sur la haute diffusivité de ces cations dans les ionogels.

La démonstration établie dans ce manuscrit tend à prouver que le confinement du LI incluant l'interface solide-liquide et les propriétés chimiques et physiques du polymère, joue un rôle essentiel dans les mécanismes de diffusion qui ont lieu à cette même interface solide-liquide. Le confinement permet de sélectionner une interaction privilégiée avec le réseau hôte pour les cations d'intérêt, avec un mécanisme de diffusion par saut possible à l'interface continue, ce qui est à l'origine des meilleures propriétés de transport observées dans les ionogels à fortes concentration en sel de cation métallique.

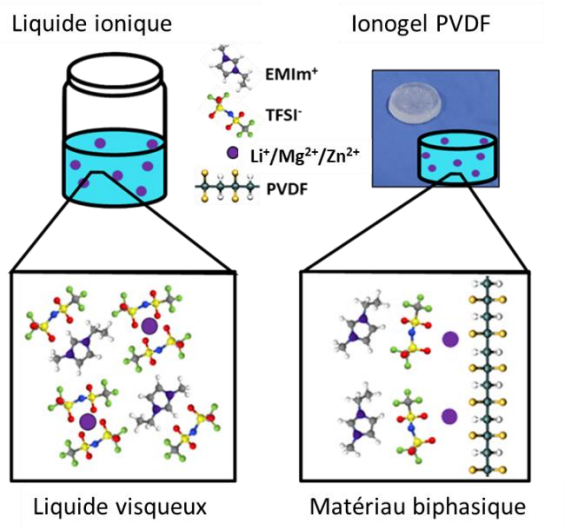


**Figure 4 : Présentation des systèmes étudiées et représentation schématique des interactions ioniques**

## 1. Analyse thermique

La Calorimétrie différentielle à balayage permet de mesurer les températures de transition vitreuse ($T_g$) dans les liquides et les matériaux solides. Cette transition de phase se produit à basse température en phase solide désordonnée. Les échantillons sont refroidis par une trempe de +150°C à -100°C avec une vitesse de refroidissement de -58°C/min. Les variations de températures de transitions vitreuse donnent des informations sur la force des interactions ioniques et la facilité des molécules à se mouvoir à basse températures (Figure 5).

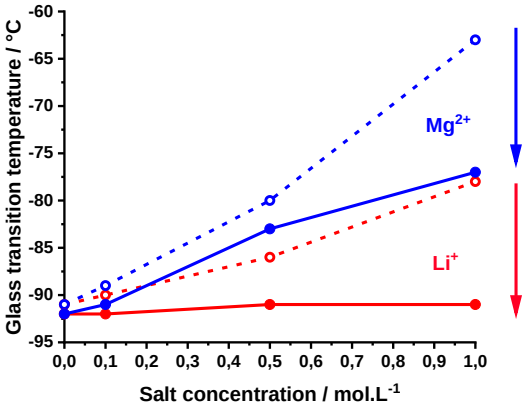


**Figure 5 : Comparaison des températures de transition vitreuse entre les LIs (cerlces ouverts) et les ionogels (cercles pleins) contenant du lithium (rouge) ou du magnésium (bleu)**

Les températures de transitions vitreuses des LIs confinés sont plus basses que celles des LIs non confinés. Ceci montre qu'à l'interface solide-liquide dans les ionogels l'énergie moyenne nécessaire à la réorganisation des ions est minimisée. La viscosité moyenne attendue est donc plus faible dans les ionogels que dans les LIs non confinés. Cette diminution moyenne de Tg et de viscosité pourrait être due à l'immédiate proximité de l'interface liquide ionique-polymère. Cet effet augmente avec la concentration en sel montrant l'effet important de l'interface sur la viscosité.

## 2. Conductivité ionique macroscopique

La spectroscopie d'impédance complexe a été utilisée pour mesurer les valeurs de conductivité ionique des échantillons liquides et solides. Ces mesures permettent d'évaluer la mobilité des espèces chargées qui sont en capacité de voyager d'une électrode à une autre à travers l'électrolyte sous l'application d'un champ électrique. Plusieurs conclusions peuvent être dégagées des mesures de conductivité ionique pour les systèmes présentés ci-dessus.

- La conductivité ionique de tous les échantillons augmente avec la température car la mobilité des molécules est liée par une loi d'Arrhenius ou dérivée (VTF) à la température.
- Le nombre d'ions libres et leur mobilité est liée aux interactions entre les ions du liquide ionique. La présence de cations polarisant lors d'ajout de sel métallique est à l'origine de l'augmentation de la viscosité et donc de la baisse de conductivité ionique (flèches rouges sur la Figure 6).

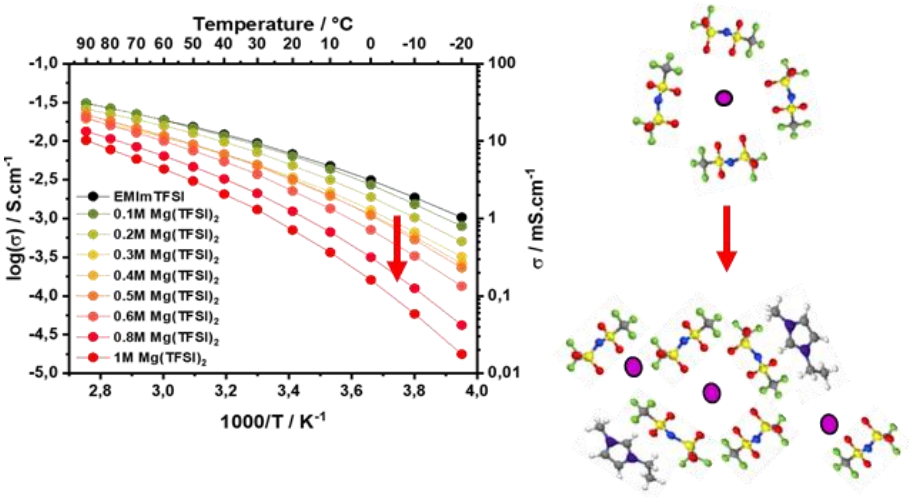


**Figure 6 : Conductivité ionique des LIs avec $Mg(TFSI)_2$ et formation d'agrégats en fonction de la concentration en sel**

- Dans le cas des LIs contenant du magnésium, la baisse de conductivité ionique due à l'ajout de sel est plus marquée que pour les LIs contenant des sels de lithium ou de zinc. La configuration électronique et la taille du cation métallique a une influence sur la force des interactions coulombiennes et donc sur la formation d'agrégats. En particulier, le magnésium possède un pouvoir polarisant (déformation du nuage électronique des autres molécules) plus élevé que celui de $Li^+$ ou $Zn^{2+}$.
- Le confinement maintient la conductivité ionique des LIs dans les ionogels PVDF contenant 83%wt de liquide ionique. A forte concentration en sel, la conductivité ionique macroscopique est égale voire supérieure dans les ionogels comparée à celle des LIs (Figure 7). On retrouve ici les conclusions de l'analyse thermique précédente, à savoir que la viscosité moyenne dans les ionogels est plus faible que celle des LIs non confinés.

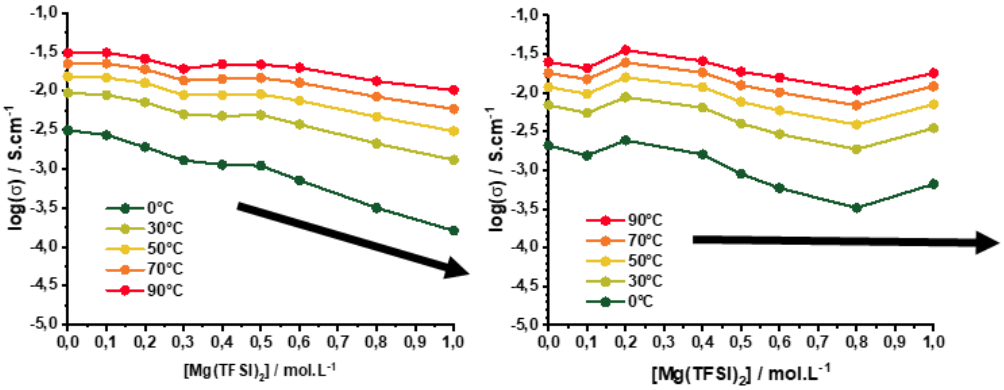


**Figure 7 : Conductivité ionique des LIs (gauche) et ionogels (gauche) avec $Mg(TFSI)_2$ en fonction de la concentration**

Les tendances sont présentées pour la mobilité à échelle macroscopique d'espèces chargées sous potentiel électrique. Plus d'informations seront apportées sur la diffusion individuelle des ions à une échelle moléculaire. Il s'agira de suivre la diffusion de toutes les espèces indépendamment de leur charge. C'est l'objet de la prochaine partie.

## 3. Coefficients de diffusion

La Résonance Magnétique Nucléaire à gradient de champ permet de sonder spécifiquement certains noyaux présents uniquement sur chaque type d'ion, et donc de mesurer les coefficients de diffusion propres à chaque ion du liquide ionique ternaire. Ces mesures en températures permettent aussi d'obtenir l'énergie d'activation nécessaire pour la diffusion de $EMIm^+$, $TFSI^-$ et $Li^+$. Le couplage de la spectroscopie d'impédance complexe et de la mesure des coefficients de diffusion permettent d'obtenir des informations sur la quantité d'ions libres (non associés à d'autres ions sous forme d'agrégats) disponibles pour la conductivité ionique macroscopique sous potentiel électrique dans l'électrolyte.

- Les coefficients de diffusion de $EMIm^+$, $TFSI^-$ et $Li^+$ diminuent avec l'ajout de sel de lithium dans les LIs non confinés, alors que les coefficients de diffusion de tous les ions sont presque constants dans les ionogels, indépendamment de la concentration en sel.
- A partir d'une certaine concentration qui varie d'un système à l'autre, la diffusion ionique dans les ionogels est meilleure que dans les LIs (cercles pleins sur la Figure 8). Le confinement améliore donc la diffusion dans les LIs concentrés en sel.

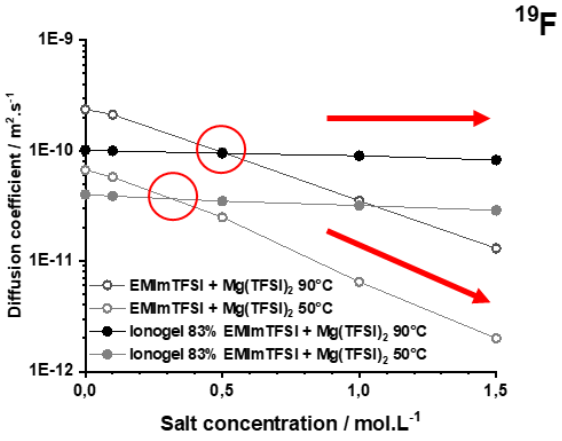


**Figure 8 : Coefficients de diffusion de $TFSI^-$ dans les LIs (cercles ouverts) et ionogels (cerlces pleins) avec $Mg(TFSI)_2$ à 50°C (gris) et 90°C (noir) en fonction de la concentration**

- Les énergies d'activation de diffusion sont plus faibles dans les ionogels que dans les LIs, comme montré sur la Figure 9. Les énergies d'activation de diffusion du lithium sont divisées

par deux, suggérant un mécanisme de diffusion différents dans les deux systèmes. Une hypothèse serait la transition d'un mécanisme de diffusion véhiculaire du lithium dans les LIs non confinés à un mécanisme de diffusion par saut à l'interface solide-liquide lors du confinement avec le polymère.

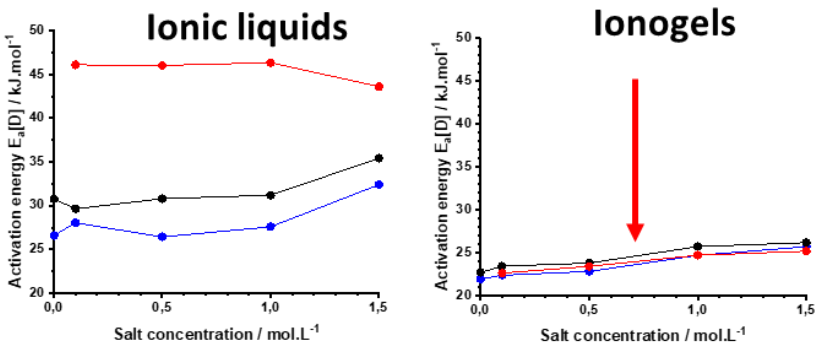


**Figure 9 : Energies d'activation pour la diffusion de $EMIm^+$ (bleu), $TFSI^-$ (noir) et $Li^+$ (rouge) dans les LIs (gauche) et ionogels (droite) avec LiTFSI en fonction de la concentration**

Ces conclusions sont également valables pour les échantillons au magnésium et au zinc. Même si les coefficients de diffusion des noyaux de Mg et Zn ne sont pas mesurables en RMN à gradient de champ, on observe une chute d'énergie d'activation de diffusion pour $EMIm^+$ et $TFSI^-$.

A ce stade, il semble que les propriétés de transport soient améliorées dans les ionogels lorsque le liquide ionique confiné est concentré en sel en comparaison du même liquide ionique non confiné (Figure 10). Lors de l'ajout de sel, la décroissance de la conductivité ionique dans les LIs non confinés est plus abrupte que la décroissance de conductivité ionique dans les ionogels, ce qui est confirmé par les études de diffusion en RMN à gradient de champ.

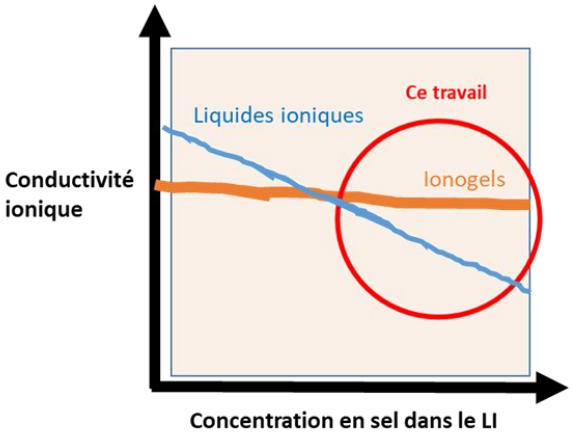


**Figure 10 : Illustrations des meilleures propriétés de transport dans les ionogels à LIs concentrés par rapport à leurs équivalents non confinés**

## 4. Interactions et coordination dans les LIs et ionogels

La spectroscopie Raman permet ici d'évaluer la grandeur des interactions coulombiennes principales entre les cations et l'anion TFSI. Le mode de vibration attribué à l'expansion et la contraction symétrique de l'anion $TFSI^-$ est très intense sur le spectre Raman de EMImTFSI obtenu avec une longueur d'onde d'excitation laser de 1064 nm (Fig. 11, trait plein vert foncé pour le LI sans sel ajouté). En suivant l'évolution de ce mode de vibration de $TFSI^-$ on en déduit son environnement proche.

- L'interaction entre $TFSI^-$ et le cation métallique augmente avec l'ajout de sel comme le montre la Figure 11 (le trait pointillé noir correspond au sel seul, *i.e.* en l'absence de LI). Cela confirme la formation d'agrégats de $TFSI^-$ autour de $Li^+$, $Mg^{2+}$ et $Zn^{2+}$. Dans le liquide ionique ternaire, il y a une compétition d'interaction entre $TFSI^-$ et soit $EMIm^+$ ou $Li^+/Mg^{2+}/Zn^{2+}$.

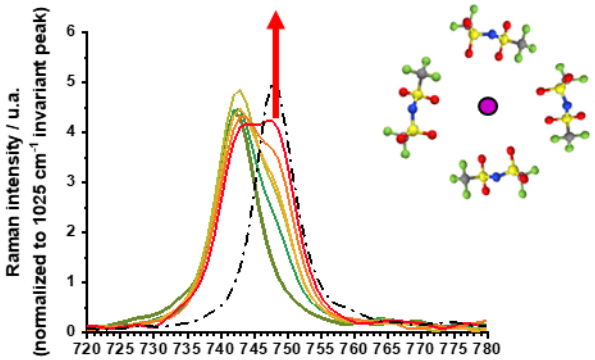


**Figure 11 : Apparition d'une nouvelle bande de vibration de $TFSI^-$ due à la présence de $Li^+$ dans le liquide ionique dont l'intensité dépend de la concentration en sel**

- Il y a une diminution drastique de l'interaction entre $TFSI^-$ et le cation métallique, lors du confinement des Lis avec sel, dans les ionogels (Figure 12).

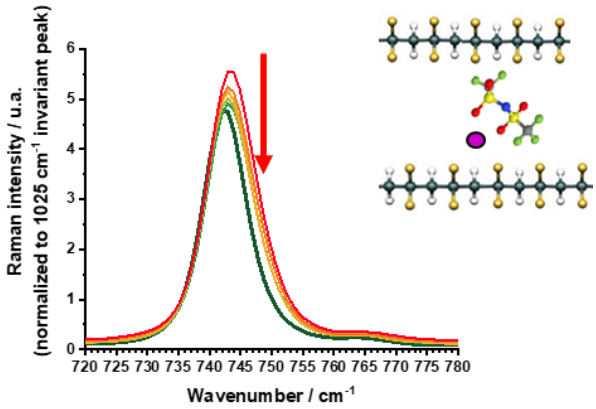


**Figure 12 : Disparition de la seconde bande de vibration de $TFSI^-$ due au confinement du liquide ionique contenant $Li^+$**

- Les nombres de coordination obtenus par des décompositions des spectres Raman laissent suggérer une diminution moyenne de l'interaction cation métallique - TFSI, induite par le confinement, ce qui est cohérent avec les meilleures propriétés de transport observées dans les ionogels à base de PVDF, et ce sans grande influence de la concentration en sel.

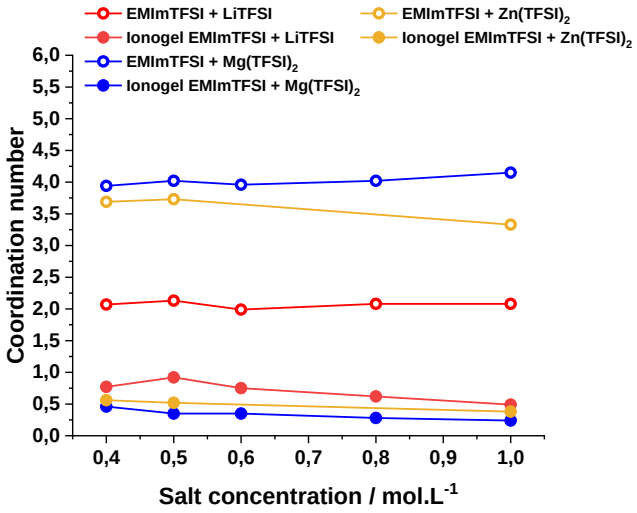


**Figure 13 Nombre de coordination de TFSI- autour du cation métallique dans les LIs (cercles ouverts) et dans les ionogels (cercles pleins) pour les échantillons contenant du lithium (rouge), du magnésium (bleu) ou du zinc (orange)**

- Dans une autre gamme spectrale, de nouvelles bandes de vibration, attribuées uniquement au PVDF, sont observées autour de 867 et 868 $cm^{-1}$, uniquement dans les ionogels avec sels de cation métallique. Elles sont attribuées à une interaction cation-polymère dont l'énergie dépend de la valence du cation.

Pour conclure, les propriétés de transport dans les LIs sont réduites par l'ajout du sel de cation métallique. Toutefois, la présence du cation d'intérêt est nécessaire dans la composition de l'électrolyte car il joue le rôle de réservoir pour les réactions d'oxydoréduction aux électrodes. Néanmoins, le confinement de ces LIs offre une interface solide-liquide qui favorise la diminution des interactions dans des paires d'ions, induisant un plus grand nombre d'ions libres et donc de meilleures propriétés de conductivité et de diffusion. La présence de doublets non liants sur les atomes de fluor du polymère provoque une compétition d'interactions du cation métallique avec soit l'anion du liquide ionique soit la surface du polymère. L'apparition d'une nouvelle bande de vibration dans la zone spectrale caractéristique du PVDF confirme l'interaction entre le cation métallique et l'environnement proche des motifs F-C-F de la chaîne polymère. D'autre part, la mobilité de $Li^+$ est facilitée par cette interaction dans les ionogels car l'énergie d'activation de diffusion du cation est divisée par deux par rapport à l'énergie d'activation de diffusion dans les LIs non confinés. Cette baisse significative permet

d'émettre l'hypothèse d'un changement de mécanisme de diffusion de $Li^+$ dans les ionogels. Ces résultats sont extrapolables pour les cations divalents qui présentent les mêmes baisses d'énergie d'activation pour $EMIm^+$ et $TFSI^-$.

En perspective, les ionogels conçus pour les prototypes de supercondensateurs hybrides métal-ion pourront être étudiés dans les cellules symétriques entre deux électrodes métalliques afin de confirmer que les propriétés de transport sont meilleures dans les ionogels fortement concentrés en sel que dans les LIs eux-mêmes.

# General introduction

Modern society, and more specifically the design of habitats for human beings on Earth, is governed by energy. The development of megacities comprising millions of people as well as the global supply chain for food, water and electricity to densely populated and rural areas would not have been possible without machines. These machines, including trucks, cement industries, and oil extraction plants, do consume energies such as coal, oil and gas to provide power.

However, the dependency on fossil fuels has raised two major questions for humankind. The first question is about the self-dependency on energy resources of most nations. The vulnerability of many countries to fuel imports establishes economical inequalities and peace instabilities. The second issue is about the greenhouse gases emissions ($CO_2$, methane etc…) due to human activities. This overproduction of gas is accelerating global warming, strengthening the inequalities mentioned above because we are not all equal when it comes to natural resources availabilities to thrive or natural disasters to survive.

Nevertheless, beyond this bleak picture of the Anthropocene era, there are a few strategies to start changing the way we consume energy resources. Hopefully, politicians, economists and scientists will agree on getting rid of fossil fuel and carbon-emissive energies dependency. Numerous efforts are being made to limit the consumption of coal, oil and gas in favour of more sustainable and responsible alternatives such as nuclear energy, renewables or even energy sobriety to guarantee an equal distribution of resources.

Secondary batteries and supercapacitors can substitute the internal combustion engine by powering electric vehicles. Stationary rechargeable batteries plants can store efficiently electrical energy generated by nuclear, solar and wind power, and provide a flexibility in the geographical distribution of electrical energy. The resources needed to redesign this electrical landscape is colossal but progress on energy storage devices development allow being more flexible in the electricity production and consumption at small and large scales. The scientific community agree on increasing the range of choices in the energy density and power levels of our portable electrical appliances so that the consumer can intelligently choose according to what is strictly necessary. This transition must be accompanied by the development of new performant devices based on natural resources that are abundant and if possible with an equitable geographical distribution to avoid geopolitical tensions. The emergence of Na-ion batteries as an alternative to the historical Li-ion batteries raises many hopes in

this area of research. As the earth is a closed planet with limited resources, this is very interesting to study electrolytes and electrode materials containing less critical elements than cobalt or lithium.

The work presented in this thesis is one point of view on how the study of bivalent metal cations electrolytes can be a good approach to develop new energy storage systems. The goal here is to synthetize magnesium and zinc conductive ionogels electrolytes for hybrid supercapacitors devices. This project is funded by *Nantes Université*, the *Institut des Matériaux de Nantes Jean Rouxel* (IMN) and the *University of South Austrlia* (UniSA). A co-tutelle agreement was settled and I was personally the first student taking part in this fresh new collaboration with Australia.

The first chapter of the manuscript is a state of the art on the study of non-confined and confined ionic liquids-based electrolytes for batteries and supercapacitors applications.

The second chapter first describes the series of ionic liquids doped with lithium, magnesium and zinc salts used in this research project. In a second part, the synthesis of biphasic solid electrolytes containing ionic liquids (ionogels) will be detailed with a strategy to unravel the dynamics in both liquid and solid state electrolytes.

The third chapter is a systematic methodology to produce an exhaustive study of physical and chemical properties of ionic-liquid based electrolytes. First, the structural organization and thermal stability are assessed by Differential Scanning Calorimetry (DSC) measurements. Then, Electrochemical Impedance Spectroscopy (EIS) and Pulsed-Field Gradient Nuclear Magnetic Resonance (PFG NMR) are coupled to understand the diffusion on a molecular scale. Finally, Raman Spectroscopy (RS) enables to obtain the nature of the coordination sphere around metal cations in the electrolyte.

The fourth chapter includes the direct application of the previous methodology on ternary ionic liquids as a reference to compare the properties of liquid state electrolytes to the one of ionogels.

The fifth and final chapter is a complete study of the dynamics in ionogels electrolytes. Some consideration about the effect on the salt concentration and the valence of the metal cation is offered with hypothesis on the diffusion mechanisms at the solid-to-liquid interface

# Chapter 1 - State of the art: Diffusion and electrochemistry in ionic liquids-based electrolytes

# Introduction

This chapter aims of presenting a brief introduction to the context of the research project lead in the present thesis. First, some generalities about electrolytes for energy storage applications will be presented. Secondly, the ionic liquids electrolytes family will be described more specifically. Finally, the ionogels electrolytes, which combine ionic liquids and solid electrolytes properties, as well as their integration in all-solid electrochemical devices will be discussed.

# 1.1 Liquid electrolytes for hybrid supercapacitors

Electrolytes are responsible for the mass transport between two electrodes in batteries and supercapacitors devices. The motivation for understanding and improving the mobility of charged species in electrolyte is to optimize wisely the rates of ions adsorption and chemical reactions at the electrolyte-to-electrode interface. The rate at which electrons are reversibly stored at the electrodes, and eventually transferred between an electrode and the species in solution, affects the properties of the resulting device in term of power and energy, cyclability and safety.[1]

## 1.1.1 Energy storage systems

There is a trade-off between increasing the energy density in energy storage systems and safety. Operating principles of these devices will be described here.

### a) Hybrid capacitors: a combination of a battery and a supercapacitor

Batteries and supercapacitors are energy storage systems[2] composed of an electrolyte between two electrodes. However, besides their structural similarities, the processes that occur at the electrodes control their charge-storage properties.

#### Batteries

Batteries are energy devices that deliver relatively low currents for very long time. The insertion of the metal cation in the electrode material is necessary to allow redox reactions (Figure 1B and 1D). The change of oxidation state of both electrode material and metal cation from the electrolyte is at the origin of the current delivered by the device.[3] This process is called faradaic, is diffusion-controlled and the kinetic is slow. The cyclic voltammogram signature of batteries is a characterized by redox peaks (Figure 1F).The applications for batteries are high energy density systems such as

wireless devices (computers, satellites…), battery-powered energy storage plants or transportation (cars, trains…).

Supercapacitors

Electrochemical capacitors or supercapacitors are power devices; they deliver high energy in very short times of the order of magnitude of the second. The charged species in the electrolytes are adsorbed on the polarized electrodes by fast surface processes under an applied voltage (Figure 1A and 1C).[4] This capacitive process is generally very fast. Two phenomenon can occur at the electrode:

- The double layer in Electrical Double Layer Capacitors (EDLCs)[5]
- Redox reactions in the superficial layers of pseudo-capacitive electrode materials.[6]

Globally, the cyclic voltammogram signature of supercapacitors is a rectangular shape (Figure 1E). The applications for these systems are high power delivery systems such as transportation (cars, buses, tramways, cranes …), or aeronautics.[7]

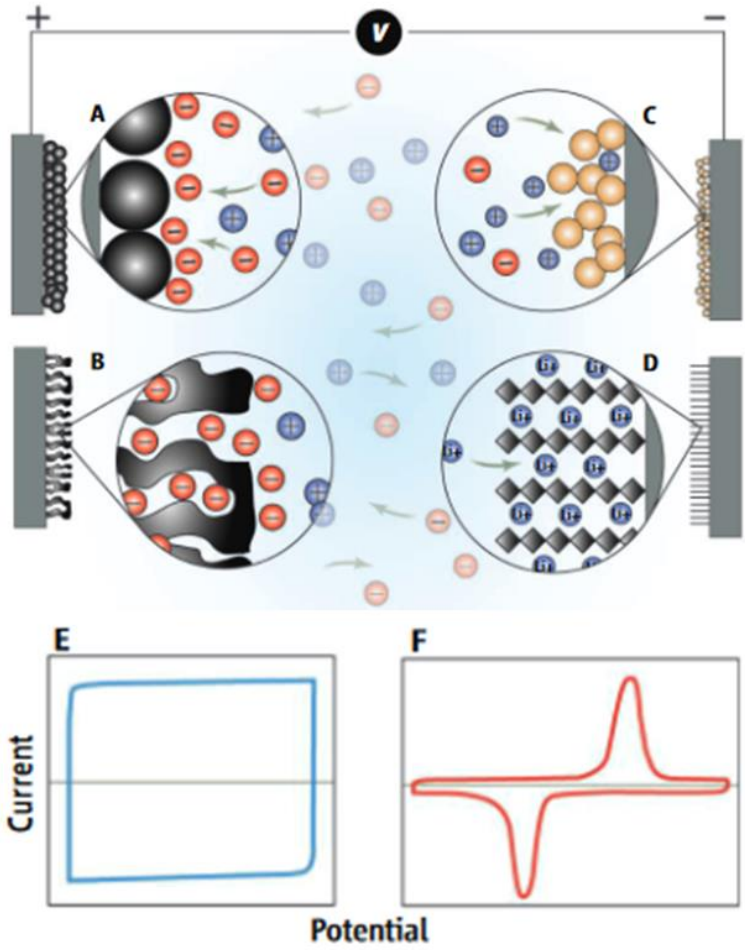


**Figure 1.1: Comparison between batteries and supercapacitors (adapted from [8])**

Hybrid devices

Hybrid devices, sometimes called supercapatteries, are assembled with a battery type negative electrode that could be made of graphite[9] or $Li_4Ti_5O_{12}$,[10] and a positive activated carbon electrode or a positive electrode made of $PbO_2$[11] or $Ni(OH)_2$[12] for example, with the corresponding complementary negative carbon electrode.

Recently, new studies show that is possible to use metal anode and find an appropriate electrolytes with promising results.[13] For instance, Han et al. developed a Zn-ion supercapacitor with an aqueous acetate-based electrolyte with a specific capacity of 60 $mAh.g^{-1}$ at 5 $A.g^{-1}$ over 10,000 cycles.[14]

The present thesis is part of a context where improving the specific power density of metal-ion batteries (see Figure 2) is a priority. The goal is to develop an ionogel electrolyte for bivalent metal hybrid capacitors with metal negative electrode and a positive carbon electrode.

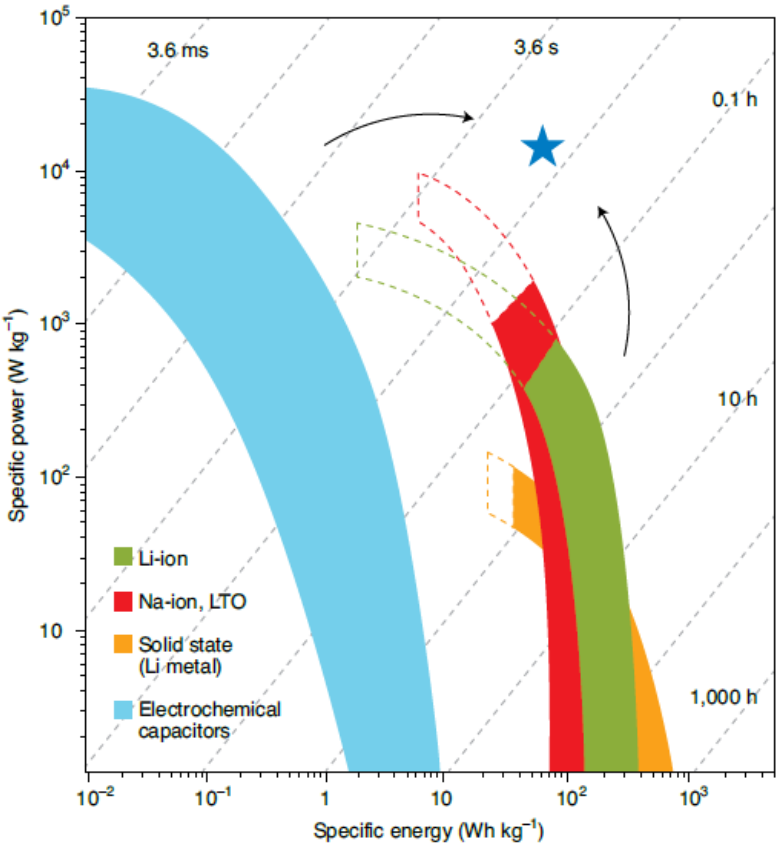


**Figure 1.2: Ragone plot of batteries and supercapacitors families showing the consensus regarding the targeted power and energy performance for energy storage systems in the next future**[15]

### b) Bivalent metal cations

Bivalent-ion batteries and supercapacitors attract a great deal of attention thanks to their low cost, attractive specific volumetric capacity and potential application in stationary storage systems (see Figure 1.3).[16] In particular, Mg and Zn anodes do have low mass specific capacities but interesting redox potentials and are cheaper than lithium anodes because more abundant in nature.[17]

Magnesium

Magnesium metal is considered as a possible alternative to lithium for energy storage applications.[18] Its specific volumetric capacity, charge to volume ratio and its low reduction potential (-2.37V vs. Standard Hydrogen Electrode), make this metal promising for batteries and supercapacitors.[19] Moreover, the absence of dendrites formation on magnesium could insure safety in the Mg batteries.[20] One of the main issue encountered with magnesium-based devices is the passivation layer on the magnesium metal electrode in most common electrolytes.[21] There is a need in finding safe and chemically compatible electrolytes that allow electrochemical reactions at the electrode/electrolyte interface.[22] Many studies focus on ionic liquids composites by adding some additives or nanoparticles in the liquid phase.[23,24]

Zinc

Zinc is also seriously considered as an alternative to lithium for energy storage devices. Its potential is much higher than for $Li^+/Li$ or $Mg^{2+}/Mg$ redox couples but is negative enough to make Zn metal a negative electrode material, particularly in various aqueous batteries. Zn is more abundant in the earth's crust, and has a higher theoretical volumetric charge capacity (5851 $mAh.cm^{-3}$ vs. 2062 $mAh.cm^{-3}$). However, dendrites formation and the increased irreversibility of the $Zn/Zn^{2+}$ redox couple during the charging and discharging processes affect the cycling life of the devices. Here again, a lot of studies focus on ionic liquids based electrolytes to tackle this issues.[25]

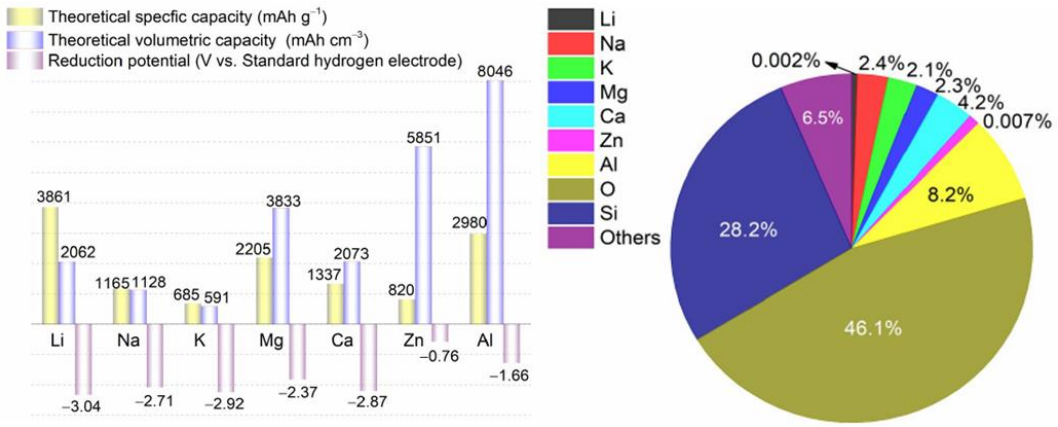


**Figure 1.3: Theoretical specific capacity, volumetric capacity and reduction potential of different metal anodes and their corresponding abundance in the earth's crust**[26]

## 1.1.2 Role of electrolytes in energy storage applications

### a) Generalities on mass transport

The transport properties include the ability to transfer matter, energy, or some other specified property from one place to another. Diffusion is the migration of matter down a concentration gradient, thermal conduction is the migration of energy down a temperature gradient, electrical conduction is the migration of electric charge down a potential gradient and viscosity is the migration of linear momentum down a velocity gradient.[27] More specifically, the transport properties for ions in electrolytes is known to follow a Brownian motion in solutions up to 2 mol.$L^{-1}$. The particles moves randomly in the liquid medium.[28] For highly concentrated electrolyte solutions, the validity of the Brownian motion theories for ions is no more applicable.[29]

The transport mechanisms in solutions are divided in two types illustrated in Figure 4: Brownian translational random motion mentioned for diluted electrolytes (vehicular mechanism) and the hopping mechanism for highly concentrated electrolytes (hopping-type mechanism).

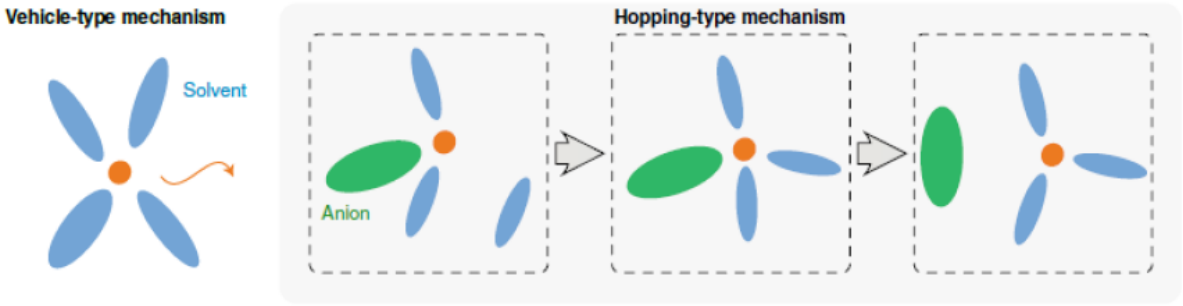


**Figure 1.4: Schematic representation of transport mechanism in electrolyte solutions**[30]

In liquid solutions, molecule mobility depends on the energy provided to the systems. The probability for this molecule to obtain this energy is mostly proportional to $e^{-Ea/RT}$: The mobility of species in liquids should mostly follow an Arrhenius-like temperature dependency: viscosity decreases exponentially with increasing temperature and so the ionic conductivity increases.

However, it is not easy to measure the viscosity and the intermolecular forces between the molecules govern the magnitude of Ea.

Another method to analyse motions in liquids is through the motion of ions in solution by potential difference applied between two electrodes. Transport of charges through electrolyte

solutions is a classical efficient way to quantify these intermolecular forces because ions drift steadily through the solution towards one electrode or the other. This is particularly interesting in electrochemistry because this model to study molecular motion is the closest one to the reality in electrochemical devices.

b) Common electrolytes and performance

Electrolyte is too often neglected at the expense electrode materials in full cell prototypes of energy storage devices. Nevertheless, electrolytes are essential in the energy storage as they are both ionic conductive (adsorptions/reactions kinetics) and electrons insulators (preventing short-circuits). They can be liquids, solids or composites and must meet the following requirements[31,32] according to the targeted applications: a wide electrochemical stability window , a high ionic conductivity (see Figure 5), good thermal and chemical stabilities and be safe, non-toxic and economically interesting.

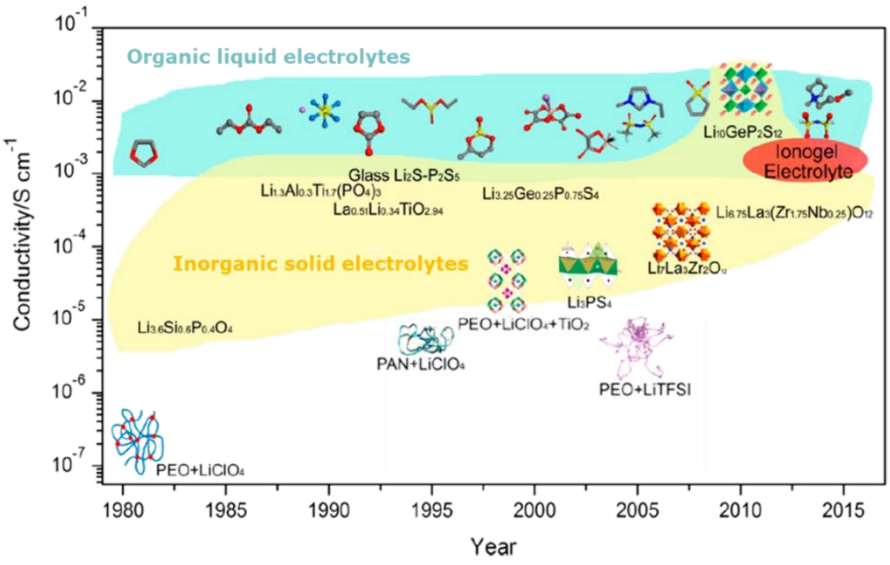


**Figure 1.5: Ionic conductivity order of magnitude for common liquid and solid electrolytes (adapted from [33])**

Liquid electrolytes can be divided into several categories depending on the nature of the solvent and the number or complexity of their constituents.

Aqueous electrolytes

Historically, the first batteries were composed of aqueous electrolytes. The voltaic primary battery by Alessandro Volta used brine as electrolyte.

They do present very good ionic conductivities and they are non-flammable[34]. The commonly lithium nitrates and sulphates salts used in aqueous electrolytes reduce considerably the price of these electrolytes.[35] Finally, they are good candidates for high power delivery devices because of the unsurpassed ionic conductivity (around 15 $mS.cm^{-1}$ for 0.1M KCL in water at room temperature). However, the main drawback of this family is the very low operating window limited by $H_2O$ reduction (ESW of 1.23V). Therefore, most of the research is about extending this narrow ESW.

Organic electrolytes

Organic electrolytes are composed of salt and organic solvents, they do present a wider ESW than that of aqueous electrolytes (>2.8V).[36] Generally composed of alkyl carbonates with dissolved lithium salt, they do present acceptable electrochemical stability, high ionic conductivity and low toxicity. They can be tuned with additives to reach very high operating potential (up to 4.5V)[37]. Moreover, the use of alkali and alkali earth metals is possible with organic solvents and the electrolyte-to-metal interface could be easily studied. Nevertheless, this family of electrolytes faces the safety issue because of the high flammability of the organic solvents and cannot be used for high temperatures applications as shown in Figure 1.6.[38]

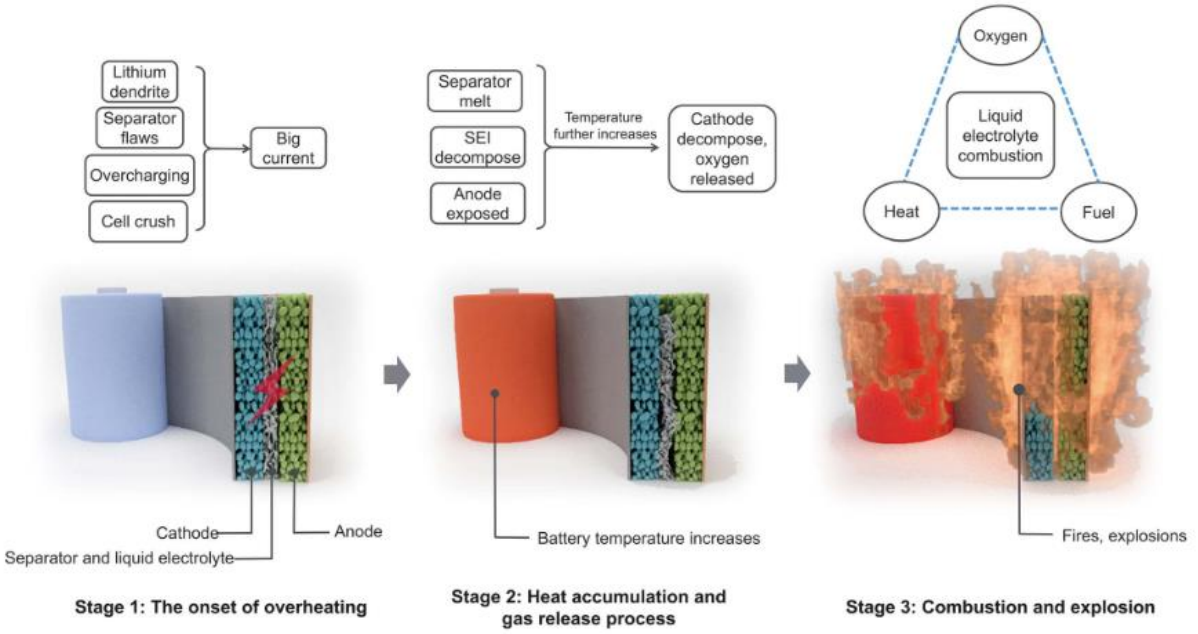


**Figure 1.6: The steps for thermal runaways in batteries**[39]

# 1.2. Ionic liquids: a trade-off between safety and viscosity

The increase in energy density implies the development of non-flammable liquid electrolytes.[40] On one hand, some strategies consist of adding non-flammable co-solvent or flame retardant additives into the electrolytes.[41,42] On the other hand, ionic liquids (ILs), which are part of the molten salt's family, are composed of large asymmetric cations and anions.[43] A common definition for ILS is a molten salt with a melting point below 100°C.[44] Some of them do have melting point below room temperature.[45] ILs are known to be good candidates as electrolytes for energy storage devices.[15,46] Due to specific association of ion pairs, they present interesting physico-chemical properties such as low vapour pressure, non-flammability, and relatively good ionic conductivity.[47] Thermal stability of ILs is one of the main motivation to use them as electrolytes in electrochemical devices. They avoid thermal runaways that can occurs in battery at high temperatures.[48] Nevertheless, they are expansive for now and present high viscosity. In consequence, some strategies are studied to improve their transport properties.

## 1.2.1 Properties of ionic liquids

The variation of ions structure in ILs allow to design a mixture according to the targeted application: ion conductive materials for electrochemical devices, solvents for chemical reaction, or bioscience.[49] The anion and cation are chosen to decrease the cohesive energy between them. Cations in ILs are often imidazoliums, ammoniums, phosphoniums, pyrrolidiums or piperidiniums while there is an almost infinite variety of anions among acetates, fluoroborates, triflates, phosphates, nitrates…

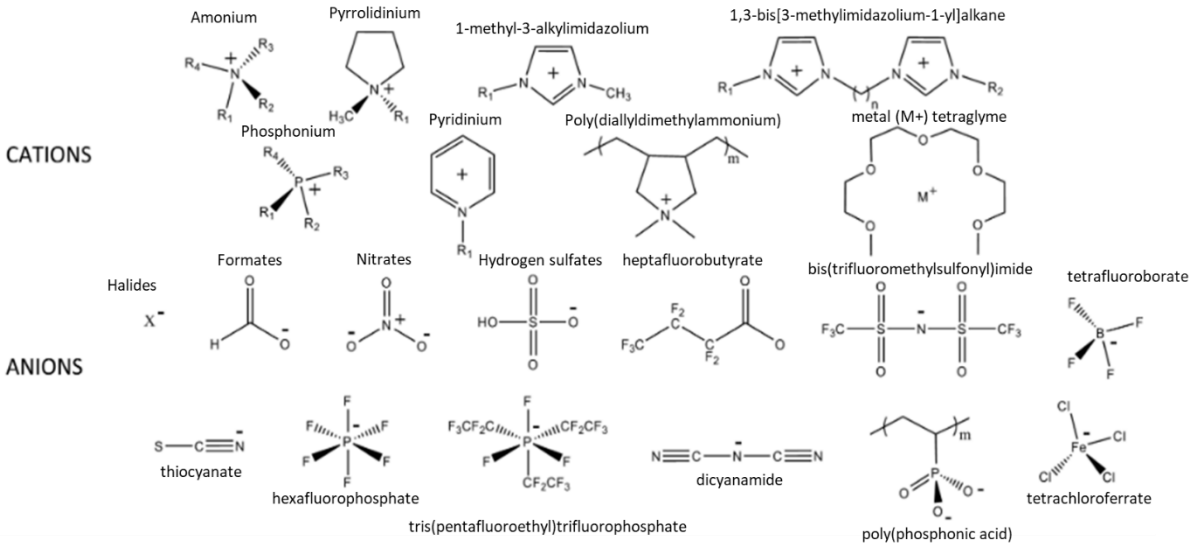


**Figure 1.7: Overview of ionic liquids cations and anions**[50]

### Thermal properties

The thermal stability of ILs is defined by their (very low) melting point and degradation temperatures, last of which is usually comprised between 200°C and 400°C.[51,52] The details of the Differential Scanning Calorimetry (DSC) technique to characterize the thermal stability and phase transitions in ILs will be decribed in Chapter 3.

### Electrochemical stability window (ESW)

The ESW for ionic liquids varies from 2V to 6V and can be measure either by linear sweep voltammetry (LSV) of cyclic voltammetry (CV).[53] This voltage goes from the cation reduction at low potential (between –3V and -0.5V vs. Li) to the anion oxidation at high potential (above 1.5V).[54,55] This ESW is strongly reduced by the water content in the electrolyte.[56]

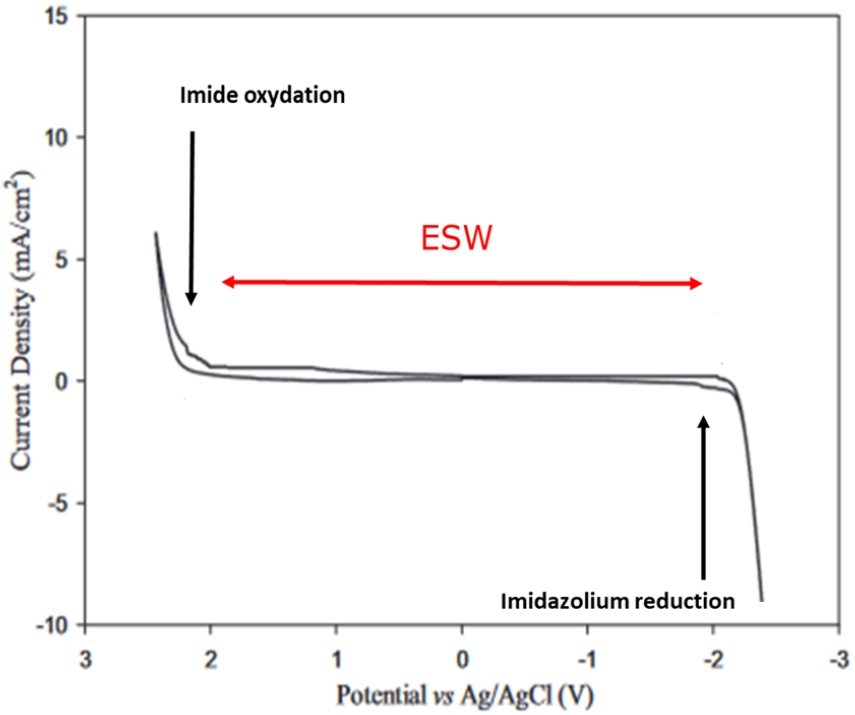


**Figure 1.7: Cyclic voltammetry of 1-ethyl-3-methylimidazolium bis(trifluoromethansulfonyl)imide (EMImTFSI) using glassy carbon macro-electrode at 100 mV.s$^{-1}$ at 25°C (adapted from [57])**

Sustainability

ILs are often known as green solvents and environmentally sustainable.[58] This is not the case for all ILs, some are even toxic and they are expensive to synthetise.[59] In every industrial process, the cycle life analysis need to be perform to accurately assess the ”greenness” of using ILs instead of traditional solvents (Figure 1.8).

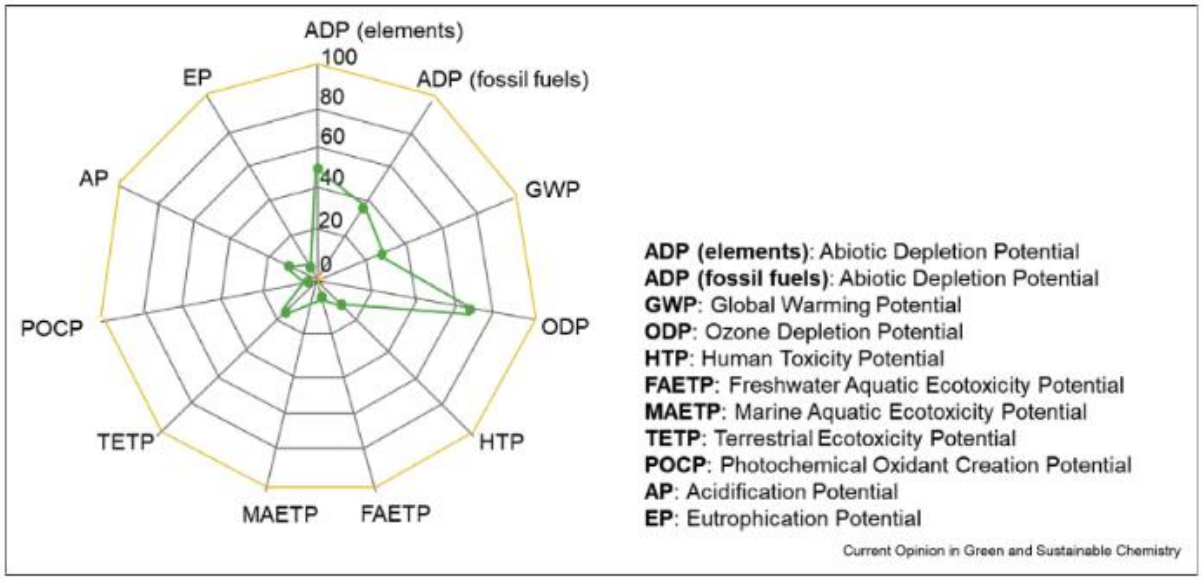


**Figure 1.8: Questioning the sustainability of EMImTFSI (green line) compared to triethylene glycol (orange line) by cycle life analysis for natural gas dehydration process**[60]

Nevertheless, ILs are still promising in numerous fields and present opportunities to reduce costs thanks to their easy and high recyclability.[61]

## 1.2.2 Dynamics in ionic liquids

### a) Theory on the mobility in ionic liquids

The performance of ILs are often assessed on their viscosity and according to their interaction forces between cation and anion.[43] These interactions depend on the size of ions and their chemical functions. They are coulomb interactions[62], Van der Walls[63] and hydrogen bonding[64] and their forces control the mobility of ions in a very polarizable medium.

The Walden product is given by the following equation:

$$\Lambda * \eta = \frac{1}{r} * cste$$

Where $\Lambda$ is the molar conductivity (S.m$^2$.mol$^{-1}$), $\eta$ the apparent viscosity (Po), and $r$ the ion radius (m).

The reference for this relation is a 1M solution of KCl diluted in water. From this "ideal" conductive solution with an entire proportion of free ions, all electrolyte solutions can be sorted in function of their ability to create free ions instead of ions pairs and aggregates (Figure 1.9). Angell et al. theorised the ions structure and thermodynamics behaviour of liquids and glassy phases by studying the relaxation times and the Arrhenius dependency of dynamics in such complex systems.[65]

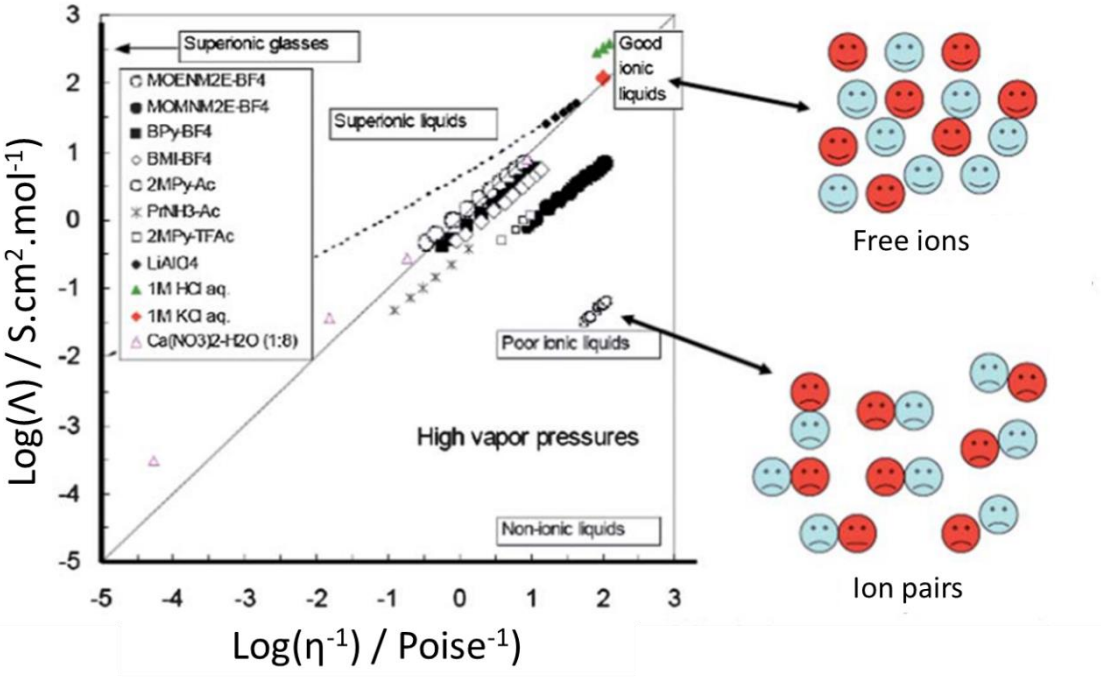


**Figure 1.9 : Walden plot to classify ILs according to their related equivalent ionic conductivity and apparent viscosity (adapted from[43])**

The presence of aggregates and ion pairing is the main factor for the viscosity increase in ILs. Therefore, their ionic conductivity is favoured in the case of low viscosity, which is a parameter to take into account when choosing IL for electrochemical applications.

Watanabe et al. have undertaken a comprehensive study of transport properties in ILs in order to derive general rules for optimizing the geometry of cations and anions. In particular, they conclude on the non-Arrhenius behaviour of the macroscopic ionic conductivity and ions diffusion measured respectively by Electrochemical Impedance Spectroscopy (EIS) and by Pulsed-Field Gradient Nuclear Magnetic Resonance (PFG NMR).[66]

Thus they confirm the Vogel-Fulcher-Tamman model that should be used instead to describe transport properties P in ILs, mentioned by Angell:

$$P = P_0 * \exp(\frac{D.T_0}{T - T_0})$$

Where $P_0$ is a constant representing the value of the variable at infinite temperature, $D$ is a constant proportional to the classical activation energy: D was presented as the fragility index by A. Angell, and the lower D is, the more fragile the medium is, the more it shows a low viscosity and a high ionic conductivity. ·$T_0$ is a finite divergence temperature (corrected from the absolute zero in Arrhenius law) often called ideal glass transition temperature.

Finally, the quantification of the fraction of ions available to take part in conduction (not paired nor aggregated ions), called ionicity, is possible by coupling the two techniques mentioned above and remain the main challenge while developing new ionic-liquid based- system.[67]

### b) Ionic liquids in electrochemical applications

As mentioned above, the wide ESW, the relatively high ionic conductivities (0.01 S.cm$^{-1}$ at room temperature), and the thermal stability of ILs are all favourable properties for the use of ionic liquids as electrolytes.[44] For example, 1-ethyl-3-methylimidazolium bis(trifluoromethansulfonyl)imide (EMImTFSI) shows high conductivity and self-diffusivity,[63,68] rather wide electrochemical window,[55] and temperature stability window.[69]

However, dynamics in ILs is known to be strongly dependent on metal salt addition due to pairs and aggregates formation.[43,70–72] For lithium transport, negative transference number were reported for the lithium motion in ILs-based electrolytes due to the strong interactions between metal cations and IL anions.[130] Besides the resulting viscosity, aggregates would reduce ions diffusion and thus the ionic conductivity performance (Figure 1.10).[67,73] A comment on the aqueous $LiNO_3$-based electrolyte can be made at higher temperatures. The water evaporation led to a decrease in and failure of the conductivity measurements above 30°C, which does not occur for IL-based electrolytes.

Some strategies are developed in order to reduce these aggregates, thus enhance the amount of ions available for charge transport (free ions); the ratio between free ions and total number of ions is quantified by the ionicity. These approaches include the use of very high concentrated electrolytes,[74–76] the use of anions mixtures[77], hybrid composite, or confined ionic liquid based electrolytes to improve the mobility of targeted metal cations.[78–81] Furthermore, these strategies

sometimes lead to new diffusion mechanisms for ion in the electrolyte, bringing about favoured hopping mechanism that improves drastically the conduction properties of the ILs.[82,83]

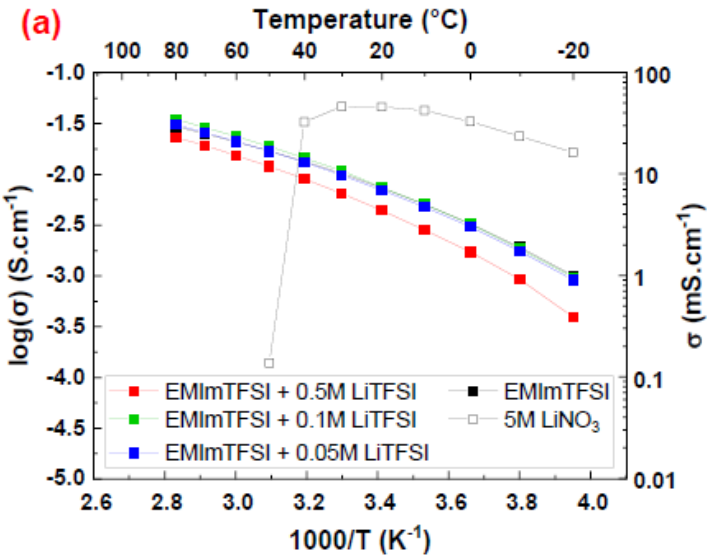


**Figure 1.10: Li salt concentration dependency of ionic conductivity in Li-doped ILs compared with aqueous electrolyte**[84]

Many studies focuses on the affinity of ILs and performance with electrodes materials in every kind of energy storage applications.[85] These studies will not be detailed in this summary of transport properties in ILs-based electrolytes because many recent reviews exist on the topic, that the reader is invited to read.[86,87] Nevertheless, particular attention is being paid to the development of electrolytes compatible with the use of magnesium metal as electrode because of the passivating surface layer generated from the reduction of Mg salt, polar aprotic solvents, and contaminations or impurities.[26,88] For instance, this study includes the use of $Mg(TFSI)_2/MgCl_2$ in dimethoxyethane (DME),[89]

In parallel, the development of theoretical dynamics models in ILs is expending.[90,91] Especially, complex ionic liquids mixtures can be now modelled thanks to Molecular Dynamics (MD) at metal interfaces.[92] And new polarizable force fields are specifically designed for complex ILs with very polarizing cations.[93]

# 1.3. Ionogels: solid-state performant electrolytes

## 1.3.1 Tunable properties for a solid that behaves like a liquid

### a) Generalities

Ionogels are biphasic liquid-solid materials with a high amount of IL (above 50 %wt) confined within a host network. This porous matrix can be made of organic materials such as polymer,[94,95] inorganic materials such as carbon nanotubes or silica,[96,97] or hybrid materials.[98] The motivation to use ionogels is to confine ionic liquids and preserving the physics of the liquid while shaping the ionogel as a solid, resistant, and leakage-free electrolyte.[99,100] The solid phase generally interacts with the IL, which changes slightly the properties depending on the chemical nature of this host matrix.[101–103] These variations can be exploited to improve locally these properties.

Synthesis of ionogels are generally divided in three different routes.

- Sol gel route for silica-based ionogels (chemical gels) using silica precursors dissolved in ILs and pH-controlled solution in order to control the morphology of the future solid phase.[97,104]
- In situ polymerization (chemical gels) using monomers dissolved in ILs by photo-polymerization[105,106], free-radical polymerization[107] or even in-situ phase separation[108]
- Physical gels obtained from the percolation of polymer chains dissolved in a solvent under controlled evaporation.[109]

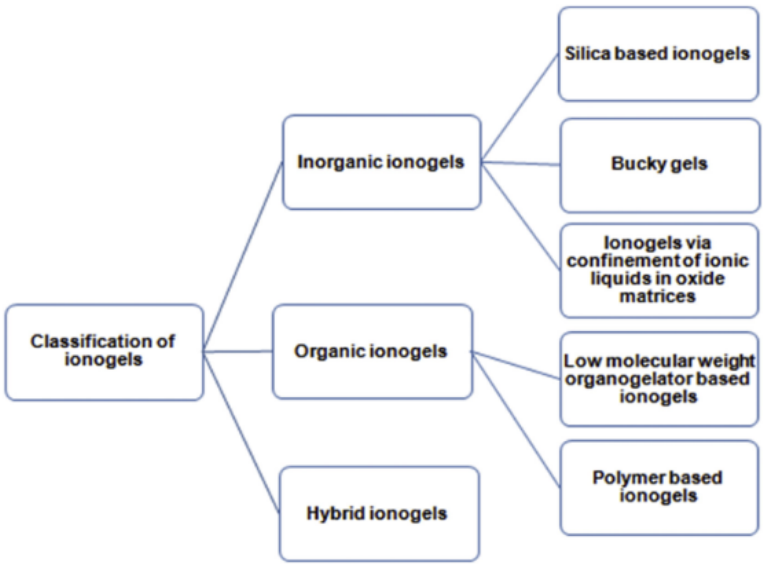


**Figure 1.10: Classification of ionogels regarding the nature of the host matrix**[110]

b) The targeted properties of the confined ionic liquid

Both the IL and the host network can be customized to fulfil requirements for an infinite versatility of applications. Ionogels are attractive for their mechanical properties, they can be flexible,[111] very though,[107] stretchable[112] or even self-healing.[106,113]

They can be biologically compatible and used as wearable sensors for biomedical applications.[113] They are also used as electrolytes in solar cells[114,115] and fuel cells.[116,117]

In Figure 1.11 is presented an ionogel based on co-polymers matrix that can be tuned for electrical, mechanical or even optical properties depending on the liquid-to-solid ratio and the co-polymer composition.

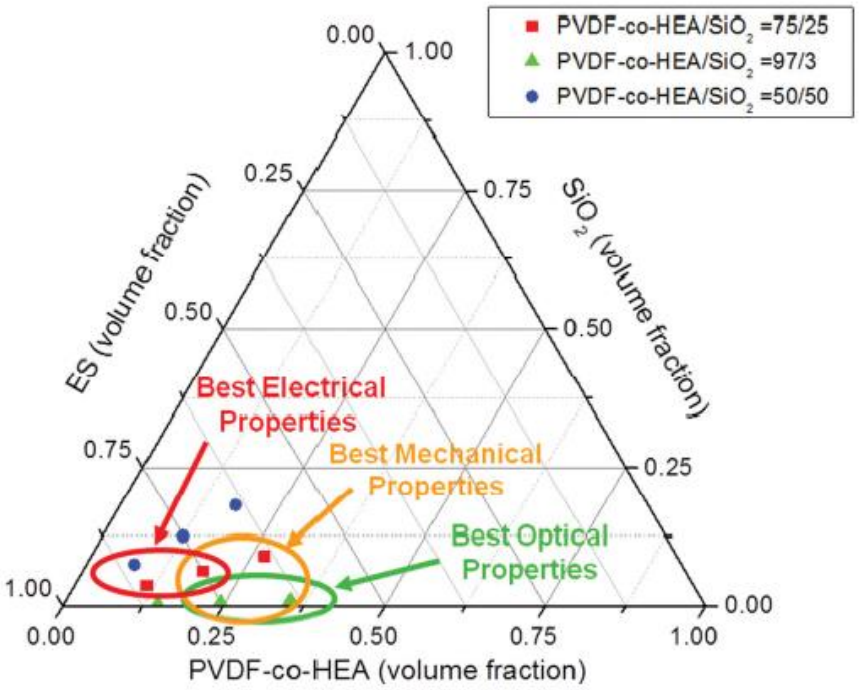


**Figure 1.11: Ternary diagram of the composition of a polymer-based hybrid ionogel designed according to the intended application[98]**

## 1.3.2 Ionogels in energy storage applictions

Confining ionic liquids is another interesting approach to tackle viscosity in ILs, with the advantage of dealing with solid-state electrolytes.

a) Ionogels electrolytes

Few studies have proven that such solid electrolytes could be integrated in electrochemical devices.[111,118,119] Consequently, in the last few years, many energy storage devices prototypes emerged such as Li-ion batteries,[120] and high voltage supercapacitors.[121]They showed promising results regarding bivalent metal cations conduction by increasing the number of free ions in such viscous electrolytes.[122]

b) Dynamics within the ionogel and solid-to-liquid interface characterization

Ion mobility in ionogels is very similar to the dynamics of ILs themselves.[101] Therefore, the macroscopic ionic conductivity is expected to be very close to the one of the corresponding IL (Figure 1.11).

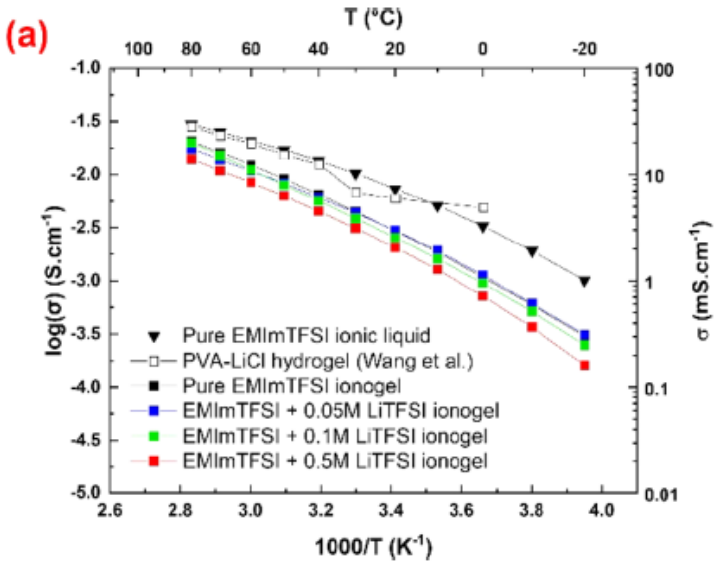


**Figure 1.12: Li salt concentration dependency of ionic conductivity in Li-doped ionogel compared to hydrogel electrolyte**[119]

The self-diffusion coefficients strongly depend on the liquid-to-solid ratio[123] and the morphology of the confining matrix[101,104] and the chemistry at the solid-liquid interface (Figure 1.14).[124]

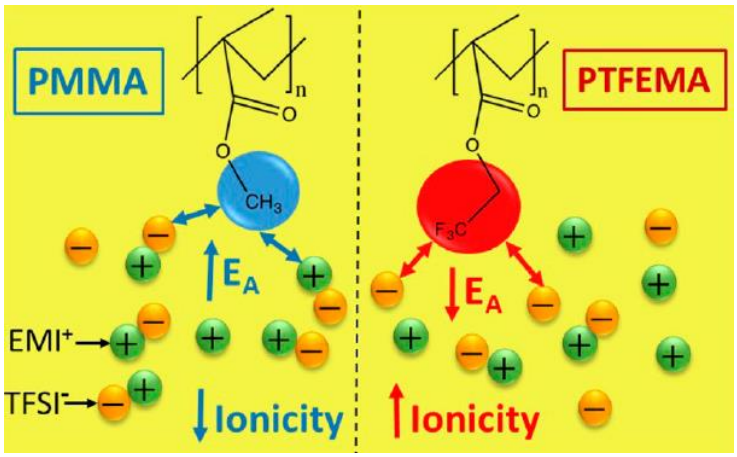


**Figure 1.14: The role of the interface chemistry in ionicity enhancement within hybrid polymer-based ionogels**[124]

In ionogels, the ionic liquid is divided in two regions: the bulk region where the IL does not interact with the matrix, and the region nearby the interface.[125] These two regions show different transport properties because of the adsorption and re-organization of ions in the liquid phase nearby the solid interface.[126] Indeed, in silica based-ionogels containing tri(fluoromethylsulfonyl)imide (TFSI), the formation of hydrogen bonds between the silanols functions of the matrix and the fluorine atoms of the anion has been proven.[127,128]

Confining ternary ionic liquids with an added metal cation is strongly affecting the interactions forces within the ionogel. The main variation is about the coordination number (i.e. the number of anions around this metal cation) measured by Raman spectroscopy, which decrease upon confinement.[104] This result is due to a competitive interaction and better affinity of $Li^+$ with the silica matrix than with the $TFSI^-$ anion.All these observations bring insights on the organisation of ions interactions within the ionogel and need to be strengthen by more studies that are fundamental and theoretical (Figure 1.13) in order to optimize this liquid-to solid interface for a better metal cation diffusion (Figure 1.14). In particular, the specific selective diffusion of the metal cation is an essential parameter to take into account when designing an ionogel for electrochemical applications.

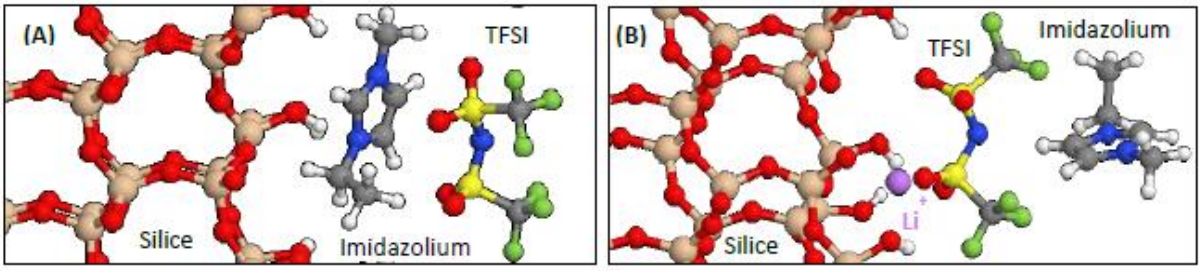


**Figure 1.14: DFT calculations on the adsorption of ions within a silica-based ionogel A) without lithium and B) with lithium**

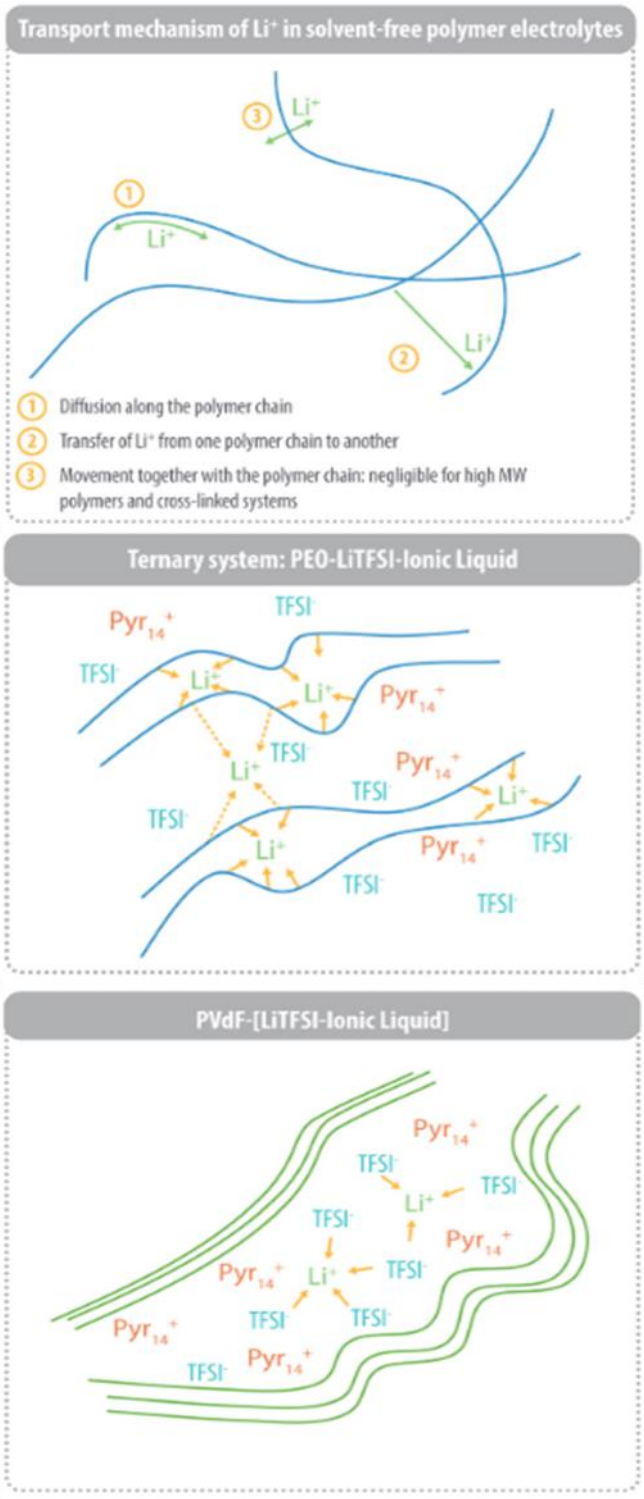


**Figure 1.14: a) Transport mechanism of $Li^+$ in polymer-based electrolytes, b) Structural organisation of ions in PEO-based ionogel and c) in PVDF-based ionogels (adapated from[129])**

# Conclusion

An overview of the challenges in studying dynamics in ILs-based electrolytes and ionogels was presented. The aim of this thesis is to present a robust, step-by-step methodology for demonstrating the improved transport properties of ionogels compared with conventional metal cations doped-ionic liquids. The second chapter presents the systems chosen to synthetize bivalent cations-conductive ionogels. The third chapter will give the systematic methodology used herein to compare the dynamics in non-confined and confined ionic liquids electrolytes. The fourth chapter summarizes the results obtained for several series of non confined ternary ionic liquids doped with lithium, magnesium and zinc salts. Finally, the fifth chapter brings conclusions and insights on the benefits using confined ILs instead of non-confined ILs with some fundamental considerations about the transport of monovalent and bivalent metal cations in PVDF-based ionogels. A *Conclusion and Perspectives* will point out the ways for possible future advances.

# References


(1) Xia, L.; Yu, L.; Hu, D.; Chen, G. Z. Electrolytes for Electrochemical Energy Storage. *Mater. Chem. Front.* **2017**, *1* (4), 584–618. https://doi.org/10.1039/C6QM00169F.

(2) Chen, G. Z. Supercapacitor and Supercapattery as Emerging Electrochemical Energy Stores. *International Materials Reviews* **2017**, *62* (4), 173–202. https://doi.org/10.1080/09506608.2016.1240914.

(3) Goodenough, J. B.; Park, K.-S. The Li-Ion Rechargeable Battery: A Perspective. *J. Am. Chem. Soc.* **2013**, *135* (4), 1167–1176. https://doi.org/10.1021/ja3091438.

(4) MacFarlane, D. R.; Tachikawa, N.; Forsyth, M.; Pringle, J. M.; Howlett, P. C.; Elliott, G. D.; Davis, J. H.; Watanabe, M.; Simon, P.; Angell, C. A. Energy Applications of Ionic Liquids. *Energy Environ. Sci.* **2014**, *7* (1), 232–250. https://doi.org/10.1039/C3EE42099J.

(5) Pandolfo, A. G.; Hollenkamp, A. F. Carbon Properties and Their Role in Supercapacitors. *Journal of Power Sources* **2006**, *157* (1), 11–27. https://doi.org/10.1016/j.jpowsour.2006.02.065.

(6) Brousse, T.; Bélanger, D.; Long, J. W. To Be or Not To Be Pseudocapacitive? *J. Electrochem. Soc.* **2015**, *162* (5), A5185–A5189. https://doi.org/10.1149/2.0201505jes.

(7) Simon, P.; Gogotsi, Y. Materials for Electrochemical Capacitors. *Nature Mater* **2008**, *7* (11), 845–854. https://doi.org/10.1038/nmat2297.

(8) Simon, P.; Gogotsi, Y.; Dunn, B. Where Do Batteries End and Supercapacitors Begin? *Science* **2014**, *343* (6176), 1210–1211. https://doi.org/10.1126/science.1249625.

(9) Aida, T.; Yamada, K.; Morita, M. An Advanced Hybrid Electrochemical Capacitor That Uses a Wide Potential Range at the Positive Electrode. *Electrochem. Solid-State Lett.* **2006**, *9* (12), A534. https://doi.org/10.1149/1.2349495.

(10) Amatucci, G. G.; Badway, F.; Du Pasquier, A.; Zheng, T. An Asymmetric Hybrid Nonaqueous Energy Storage Cell. *J. Electrochem. Soc.* **2001**, *148* (8), A930. https://doi.org/10.1149/1.1383553.

(11) Pell, W. G.; Conway, B. E. Peculiarities and Requirements of Asymmetric Capacitor Devices Based on Combination of Capacitor and Battery-Type Electrodes. *Journal of Power Sources* **2004**, *136* (2), 334–345. https://doi.org/10.1016/j.jpowsour.2004.03.021.

(12) Zheng, J. P. The Limitations of Energy Density of Battery/Double-Layer Capacitor Asymmetric Cells. *J. Electrochem. Soc.* **2003**, *150* (4), A484. https://doi.org/10.1149/1.1559067.

(13) Zuo, W.; Li, R.; Zhou, C.; Li, Y.; Xia, J.; Liu, J. Battery-Supercapacitor Hybrid Devices: Recent Progress and Future Prospects. *Advanced Science* **2017**, *4* (7), 1600539. https://doi.org/10.1002/advs.201600539.

(14) Han, J.; Mariani, A.; Zarrabeitia, M.; Jusys, Z.; Behm, R. J.; Varzi, A.; Passerini, S. Zinc-Ion Hybrid Supercapacitors Employing Acetate-Based Water-in-Salt Electrolytes. *Small* **2022**, *18* (31), 2201563. https://doi.org/10.1002/smll.202201563.

(15) Simon, P.; Gogotsi, Y. Perspectives for Electrochemical Capacitors and Related Devices. *Nat. Mater.* **2020**, *19* (11), 1151–1163. https://doi.org/10.1038/s41563-020-0747-z.

(16) Xu, C.; Chen, Y.; Shi, S.; Li, J.; Kang, F.; Su, D. Secondary Batteries with Multivalent Ions for Energy Storage. *Sci Rep* **2015**, *5* (1), 14120. https://doi.org/10.1038/srep14120.

(17) Chamoun, M.; Hertzberg, B. J.; Gupta, T.; Davies, D.; Bhadra, S.; Van Tassell, B.; Erdonmez, C.; Steingart, D. A. Hyper-Dendritic Nanoporous Zinc Foam Anodes. *NPG Asia Mater* **2015**, *7* (4), e178–e178. https://doi.org/10.1038/am.2015.32.

(18) Yoo, H. D.; Shterenberg, I.; Gofer, Y.; Gershinsky, G.; Pour, N.; Aurbach, D. Mg Rechargeable Batteries: An on-Going Challenge. *Energy Environ. Sci.* **2013**, *6* (8), 2265–2279. https://doi.org/10.1039/C3EE40871J.

(19) Bucur, C. B.; Gregory, T.; Oliver, A. G.; Muldoon, J. Confession of a Magnesium Battery. *J. Phys. Chem. Lett.* **2015**, *6* (18), 3578–3591. https://doi.org/10.1021/acs.jpclett.5b01219.

(20) Matsui, M. Study on Electrochemically Deposited Mg Metal. *Journal of Power Sources* **2011**, *196* (16), 7048–7055. https://doi.org/10.1016/j.jpowsour.2010.11.141.
(21) Aurbach, D.; Lu, Z.; Schechter, A.; Gofer, Y.; Gizbar, H.; Turgeman, R.; Cohen, Y.; Moshkovich, M.; Levi, E. Prototype Systems for Rechargeable Magnesium Batteries. *Nature* **2000**, *407* (6805), 724–727. https://doi.org/10.1038/35037553.
(22) Muldoon, J.; Bucur, C. B.; Gregory, T. Quest for Nonaqueous Multivalent Secondary Batteries: Magnesium and Beyond. *Chem. Rev.* **2014**, *114* (23), 11683–11720. https://doi.org/10.1021/cr500049y.
(23) Kar, M.; Ma, Z.; Azofra, L. M.; Chen, K.; Forsyth, M.; MacFarlane, D. R. Ionic Liquid Electrolytes for Reversible Magnesium Electrochemistry. *Chem. Commun.* **2016**, *52* (21), 4033–4036. https://doi.org/10.1039/C5CC09324D.
(24) Ma, Z.; Kar, M.; Xiao, C.; Forsyth, M.; MacFarlane, D. R. Electrochemical Cycling of Mg in Mg[TFSI]2/Tetraglyme Electrolytes. *Electrochemistry Communications* **2017**, *78*, 29–32. https://doi.org/10.1016/j.elecom.2017.03.018.
(25) Zhao, Z.; Lai, J.; Ho, D. T.; Lei, Y.; Yin, J.; Chen, L.; Schwingenschlögl, U.; Alshareef, H. N. A Novel "Water-in-Ionic Liquid" Electrolyte for Zn Metal Batteries. *ACS Energy Lett.* **2023**, *8* (1), 608–618. https://doi.org/10.1021/acsenergylett.2c02520.
(26) Zhang, H.; Qiao, L.; Armand, M. Organic Electrolyte Design for Rechargeable Batteries: From Lithium to Magnesium. *Angewandte Chemie International Edition* **2022**, *61* (52), e202214054. https://doi.org/10.1002/anie.202214054.
(27) Atkins, P. W. *Physical Chemistry*, Oxford.; 1994.
(28) *The Feynman Lectures on Physics Vol. I Ch. 41: The Brownian Movement*. https://www.feynmanlectures.caltech.edu/I_41.html (accessed 2023-11-08).
(29) Dufrêche, J.-F.; Bernard, O.; Turq, P. Transport in Electrolyte Solutions: Are Ions Brownian Particles? *Journal of Molecular Liquids* **2005**, *118* (1–3), 189–194. https://doi.org/10.1016/j.molliq.2004.07.036.
(30) Yamada, Y.; Wang, J.; Ko, S.; Watanabe, E.; Yamada, A. Advances and Issues in Developing Salt-Concentrated Battery Electrolytes. *Nat Energy* **2019**, *4* (4), 269–280. https://doi.org/10.1038/s41560-019-0336-z.
(31) Aurbach, D.; Talyosef, Y.; Markovsky, B.; Markevich, E.; Zinigrad, E.; Asraf, L.; Gnanaraj, J. S.; Kim, H.-J. Design of Electrolyte Solutions for Li and Li-Ion Batteries: A Review. *Electrochimica Acta* **2004**, *50* (2–3), 247–254. https://doi.org/10.1016/j.electacta.2004.01.090.
(32) Palomares, V.; Serras, P.; Villaluenga, I.; Hueso, K. B.; Carretero-González, J.; Rojo, T. Na-Ion Batteries, Recent Advances and Present Challenges to Become Low Cost Energy Storage Systems. *Energy Environ. Sci.* **2012**, *5* (3), 5884. https://doi.org/10.1039/c2ee02781j.
(33) Wu, F.; Chen, N.; Chen, R.; Zhu, Q.; Qian, J.; Li, L. "Liquid-in-Solid" and "Solid-in-Liquid" Electrolytes with High Rate Capacity and Long Cycling Life for Lithium-Ion Batteries. *Chem. Mater.* **2016**, *28* (3), 848–856. https://doi.org/10.1021/acs.chemmater.5b04278.
(34) Posada, J. O. G.; Rennie, A. J. R.; Villar, S. P.; Martins, V. L.; Marinaccio, J.; Barnes, A.; Glover, C. F.; Worsley, D. A.; Hall, P. J. Aqueous Batteries as Grid Scale Energy Storage Solutions. *Renewable and Sustainable Energy Reviews* **2017**, *68* (2), 1174–1182.
(35) Kim, H.; Hong, J.; Park, K.-Y.; Kim, H.; Kim, S.-W.; Kang, K. Aqueous Rechargeable Li and Na Ion Batteries. *Chem. Rev.* **2014**, *114* (23), 11788–11827. https://doi.org/10.1021/cr500232y.
(36) Zhong, C.; Deng, Y.; Hu, W.; Qiao, J.; Zhang, L.; Zhang, J. A Review of Electrolyte Materials and Compositions for Electrochemical Supercapacitors. *Chem. Soc. Rev.* **2015**, *44* (21), 7484–7539. https://doi.org/10.1039/C5CS00303B.
(37) Xu, M.; Dalavi, S.; Lucht, B. L. Electrolytes for Lithium-Ion Batteries with High-Voltage Cathodes. In *Lithium Batteries*; John Wiley & Sons, Ltd, 2013; pp 71–87. https://doi.org/10.1002/9781118615515.ch4.
(38) Hess, S.; Wohlfahrt-Mehrens, M.; Wachtler, M. Flammability of Li-Ion Battery Electrolytes: Flash Point and Self-Extinguishing Time Measurements. *J. Electrochem. Soc.* **2015**, *162* (2), A3084. https://doi.org/10.1149/2.0121502jes.

(39) Liu, K.; Liu, Y.; Lin, D.; Pei, A.; Cui, Y. Materials for Lithium-Ion Battery Safety. *Sci Adv* **2018**, *4* (6), eaas9820. https://doi.org/10.1126/sciadv.aas9820.
(40) Gond, R.; Van Ekeren, W.; Mogensen, R.; Naylor, A. J.; Younesi, R. Non-Flammable Liquid Electrolytes for Safe Batteries. *Mater. Horiz.* **2021**, *8* (11), 2913–2928. https://doi.org/10.1039/D1MH00748C.
(41) Chawla, N.; Bharti, N.; Singh, S. Recent Advances in Non-Flammable Electrolytes for Safer Lithium-Ion Batteries. *Batteries* **2019**, *5* (1), 19. https://doi.org/10.3390/batteries5010019.
(42) Wang, Q.; Jiang, L.; Yu, Y.; Sun, J. Progress of Enhancing the Safety of Lithium Ion Battery from the Electrolyte Aspect. *Nano Energy* **2019**, *55*, 93–114. https://doi.org/10.1016/j.nanoen.2018.10.035.
(43) Austen Angell, C.; Ansari, Y.; Zhao, Z. Ionic Liquids: Past, Present and Future. *Faraday Discuss.* **2012**, *154*, 9–27. https://doi.org/10.1039/C1FD00112D.
(44) Watanabe, M.; Thomas, M. L.; Zhang, S.; Ueno, K.; Yasuda, T.; Dokko, K. Application of Ionic Liquids to Energy Storage and Conversion Materials and Devices. *Chem. Rev.* **2017**, *117* (10), 7190–7239. https://doi.org/10.1021/acs.chemrev.6b00504.
(45) Reichardt, C. Solvents and Solvent Effects: An Introduction. *Org. Process Res. Dev.* **2007**, *11* (1), 105–113. https://doi.org/10.1021/op0680082.
(46) Galiński, M.; Lewandowski, A.; Stępniak, I. Ionic Liquids as Electrolytes. *Electrochimica Acta* **2006**, *51* (26), 5567–5580. https://doi.org/10.1016/j.electacta.2006.03.016.
(47) Endres, F.; Abedin, S. Z. E. Air and Water Stable Ionic Liquids in Physical Chemistry. *Phys. Chem. Chem. Phys.* **2006**, *8* (18), 2101–2116. https://doi.org/10.1039/B600519P.
(48) Tian, X.; Yi, Y.; Fang, B.; Yang, P.; Wang, T.; Liu, P.; Qu, L.; Li, M.; Zhang, S. Design Strategies of Safe Electrolytes for Preventing Thermal Runaway in Lithium Ion Batteries. *Chem. Mater.* **2020**, *32* (23), 9821–9848. https://doi.org/10.1021/acs.chemmater.0c02428.
(49) Armand, M.; Endres, F.; MacFarlane, D. R.; Ohno, H.; Scrosati, B. Ionic-Liquid Materials for the Electrochemical Challenges of the Future. *Nature Mater* **2009**, *8* (8), 621–629. https://doi.org/10.1038/nmat2448.
(50) Hayes, R.; Warr, G. G.; Atkin, R. Structure and Nanostructure in Ionic Liquids. *Chem. Rev.* **2015**, *115* (13), 6357–6426. https://doi.org/10.1021/cr500411q.
(51) Maton, C.; Vos, N. D.; Stevens, C. V. Ionic Liquid Thermal Stabilities: Decomposition Mechanisms and Analysis Tools. *Chem. Soc. Rev.* **2013**, *42* (13), 5963–5977. https://doi.org/10.1039/C3CS60071H.
(52) Baranyai, K. J.; Deacon, G. B.; MacFarlane, D. R.; Pringle, J. M.; Scott, J. L. Thermal Degradation of Ionic Liquids at Elevated Temperatures. *Aust. J. Chem.* **2004**, *57* (2), 145–147. https://doi.org/10.1071/ch03221.
(53) Fedorov, M. V.; Kornyshev, A. A. Ionic Liquids at Electrified Interfaces. *Chem. Rev.* **2014**, *114* (5), 2978–3036. https://doi.org/10.1021/cr400374x.
(54) Ohno, H. Electrochemical Aspects of Ionic Liquids; 2011.
(55) Kazemiabnavi, S.; Zhang, Z.; Thornton, K.; Banerjee, S. Electrochemical Stability Window of Imidazolium-Based Ionic Liquids as Electrolytes for Lithium Batteries. *J. Phys. Chem. B* **2016**, *120* (25), 5691–5702. https://doi.org/10.1021/acs.jpcb.6b03433.
(56) O'Mahony, A. M.; Silvester, D. S.; Aldous, L.; Hardacre, C.; Compton, R. G. Effect of Water on the Electrochemical Window and Potential Limits of Room-Temperature Ionic Liquids. *J. Chem. Eng. Data* **2008**, *53* (12), 2884–2891. https://doi.org/10.1021/je800678e.
(57) Hayyan, M.; Mjalli, F. S.; Hashim, M. A.; AlNashef, I. M.; Mei, T. X. Investigating the Electrochemical Windows of Ionic Liquids. *Journal of Industrial and Engineering Chemistry* **2013**, *19* (1), 106–112. https://doi.org/10.1016/j.jiec.2012.07.011.
(58) Choudhary, G.; Dhariwal, J.; Saha, M.; Trivedi, S.; Banjare, M. K.; Kanaoujiya, R.; Behera, K. Ionic Liquids: Environmentally Sustainable Materials for Energy Conversion and Storage Applications. *Environ Sci Pollut Res* **2023**. https://doi.org/10.1007/s11356-023-25468-w.
(59) Kuroda, K. A Simple Overview of Toxicity of Ionic Liquids and Designs of Biocompatible Ionic Liquids. *New J. Chem.* **2022**, *46* (42), 20047–20052. https://doi.org/10.1039/D2NJ02634A.

(60) Wu, B.; Dai, C.; Chen, B.; Yu, G.; Liu, N.; Xu, R. Ionic Liquid versus Traditional Volatile Organic Solvent in the Natural Gas Dehydration Process: A Comparison from a Life Cycle Perspective. *ACS Sustainable Chem. Eng.* **2019**, *7* (23), 19194–19201. https://doi.org/10.1021/acssuschemeng.9b05194.
(61) Mai, N. L.; Ahn, K.; Koo, Y.-M. Methods for Recovery of Ionic Liquids—A Review. *Process Biochemistry* **2014**, *49* (5), 872–881. https://doi.org/10.1016/j.procbio.2014.01.016.
(62) Tokuda, H.; Hayamizu, K.; Ishii, K.; Susan, Md. A. B. H.; Watanabe, M. Physicochemical Properties and Structures of Room Temperature Ionic Liquids. 2. Variation of Alkyl Chain Length in Imidazolium Cation. *J. Phys. Chem. B* **2005**, *109* (13), 6103–6110. https://doi.org/10.1021/jp044626d.
(63) Martinelli, A.; Maréchal, M.; Östlund, Å.; Cambedouzou, J. Insights into the Interplay between Molecular Structure and Diffusional Motion in 1-Alkyl-3-Methylimidazolium Ionic Liquids: A Combined PFG NMR and X-Ray Scattering Study. *Phys. Chem. Chem. Phys.* **2013**, *15* (15), 5510–5517. https://doi.org/10.1039/C3CP00097D.
(64) Dong, K.; Zhang, S.; Wang, J. Understanding the Hydrogen Bonds in Ionic Liquids and Their Roles in Properties and Reactions. *Chem. Commun.* **2016**, *52* (41), 6744–6764. https://doi.org/10.1039/C5CC10120D.
(65) Angell, C. A. Structural Instability and Relaxation in Liquid and Glassy Phases near the Fragile Liquid Limit. *Journal of Non-Crystalline Solids* **1988**, *102* (1–3), 205–221. https://doi.org/10.1016/0022-3093(88)90133-0.
(66) Noda, A.; Hayamizu, K.; Watanabe, M. Pulsed-Gradient Spin−Echo $^{1}$H and $^{19}$F NMR Ionic Diffusion Coefficient, Viscosity, and Ionic Conductivity of Non-Chloroaluminate Room-Temperature Ionic Liquids. *J. Phys. Chem. B* **2001**, *105* (20), 4603–4610. https://doi.org/10.1021/jp004132q.
(67) MacFarlane, D. R.; Forsyth, M.; Izgorodina, E. I.; Abbott, A. P.; Annat, G.; Fraser, K. On the Concept of Ionicity in Ionic Liquids. *Phys. Chem. Chem. Phys.* **2009**, *11* (25), 4962–4967. https://doi.org/10.1039/B900201D.
(68) Liu, S.-H.; Chen, C.-C.; Zhang, B.; Wu, J.-H. Fire and Explosion Hazards of 1-Ethyl-3-Methylimidazolium Bis(Trifluoromethylsulfonyl)Imide. *RSC Adv.* **2020**, *10* (38), 22468–22479. https://doi.org/10.1039/D0RA01821J.
(69) Rotnicki, K.; Sterczyńska, A.; Fojud, Z.; Jażdżewska, M.; Beskrovnyi, A.; Waliszewski, J.; Śliwińska-Bartkowiak, M. Phase Transitions, Molecular Dynamics and Structural Properties of 1-Ethyl-3-Methylimidazolium Bis(Trifluoromethylsulfonyl)Imide Ionic Liquid. *Journal of Molecular Liquids* **2020**, *313*, 113535. https://doi.org/10.1016/j.molliq.2020.113535.
(70) Lassègues, J.-C.; Grondin, J.; Aupetit, C.; Johansson, P. Spectroscopic Identification of the Lithium Ion Transporting Species in LiTFSI-Doped Ionic Liquids. *J. Phys. Chem. A* **2009**, *113* (1), 305–314. https://doi.org/10.1021/jp806124w.
(71) Zhou, Q.; Boyle, P. D.; Malpezzi, L.; Mele, A.; Shin, J.-H.; Passerini, S.; Henderson, W. A. Phase Behavior of Ionic Liquid–LiX Mixtures: Pyrrolidinium Cations and $TFSI^-$ Anions – Linking Structure to Transport Properties. *Chem. Mater.* **2011**, *23* (19), 4331–4337. https://doi.org/10.1021/cm201427k.
(72) Giffin, G. A.; Moretti, A.; Jeong, S.; Passerini, S. Complex Nature of Ionic Coordination in Magnesium Ionic Liquid-Based Electrolytes: Solvates with Mobile $Mg^{2+}$ Cations. *J. Phys. Chem. C* **2014**, *118* (19), 9966–9973. https://doi.org/10.1021/jp502354h.
(73) Ueno, K.; Tokuda, H.; Watanabe, M. Ionicity in Ionic Liquids: Correlation with Ionic Structure and Physicochemical Properties. *Phys. Chem. Chem. Phys.* **2010**, *12* (8), 1649–1658. https://doi.org/10.1039/B921462N.
(74) Girard, G. M. A.; Hilder, M.; Zhu, H.; Nucciarone, D.; Whitbread, K.; Zavorine, S.; Moser, M.; Forsyth, M.; MacFarlane, D. R.; Howlett, P. C. Electrochemical and Physicochemical Properties of Small Phosphonium Cation Ionic Liquid Electrolytes with High Lithium Salt Content. *Phys. Chem. Chem. Phys.* **2015**, *17* (14), 8706–8713. https://doi.org/10.1039/C5CP00205B.

(75) Rakov, D. A.; Sun, J.; Ferdousi, S. A.; Howlett, P. C.; Simonov, A. N.; Chen, F.; Forsyth, M. Polar Organic Cations at Electrified Metal with Superconcentrated Ionic Liquid Electrolyte and Implications for Sodium Metal Batteries. *ACS Materials Lett.* **2022**, *4* (10), 1984–1990. https://doi.org/10.1021/acsmaterialslett.2c00496.

(76) Arano, K.; Begic, S.; Chen, F.; Rakov, D.; Mazouzi, D.; Gautier, N.; Kerr, R.; Lestriez, B.; Le Bideau, J.; Howlett, P. C.; Guyomard, D.; Forsyth, M.; Dupre, N. Tuning the Formation and Structure of the Silicon Electrode/Ionic Liquid Electrolyte Interphase in Superconcentrated Ionic Liquids. *ACS Appl. Mater. Interfaces* **2021**, *13* (24), 28281–28294. https://doi.org/10.1021/acsami.1c06465.

(77) Kerner, M.; Plylahan, N.; Scheers, J.; Johansson, P. Ionic Liquid Based Lithium Battery Electrolytes: Fundamental Benefits of Utilising Both TFSI and FSI Anions? *Phys. Chem. Chem. Phys.* **2015**, *17* (29), 19569–19581. https://doi.org/10.1039/C5CP01891A.

(78) Delacroix, S.; Sauvage, F.; Reynaud, M.; Deschamps, M.; Bruyère, S.; Becuwe, M.; Postel, D.; Tarascon, J.-M.; Van Nhien, A. N. SiO2/Ionic Liquid Hybrid Nanoparticles for Solid-State Lithium Ion Conduction. *Chem. Mater.* **2015**, *27* (23), 7926–7933. https://doi.org/10.1021/acs.chemmater.5b02944.

(79) Garaga, M. N.; Aguilera, L.; Yaghini, N.; Matic, A.; Persson, M.; Martinelli, A. Achieving Enhanced Ionic Mobility in Nanoporous Silica by Controlled Surface Interactions. *Phys. Chem. Chem. Phys.* **2017**, *19* (8), 5727–5736. https://doi.org/10.1039/C6CP07351D.

(80) Yu, J.; Wang, C.; Li, S.; Liu, N.; Zhu, J.; Lu, Z. Li+-Containing, Continuous Silica Nanofibers for High Li+ Conductivity in Composite Polymer Electrolyte. *Small* **2019**, *15* (44), 1902729. https://doi.org/10.1002/smll.201902729.

(81) Lu, C.; Chen, X. In Situ Synthesized PEO/NBR Composite Ionogels for High-Performance All-Solid-State Supercapacitors. *Chem. Commun.* **2019**, *55* (58), 8470–8473. https://doi.org/10.1039/C9CC03401C.

(82) Dokko, K.; Watanabe, D.; Ugata, Y.; Thomas, M. L.; Tsuzuki, S.; Shinoda, W.; Hashimoto, K.; Ueno, K.; Umebayashi, Y.; Watanabe, M. Direct Evidence for Li Ion Hopping Conduction in Highly Concentrated Sulfolane-Based Liquid Electrolytes. *J. Phys. Chem. B* **2018**, *122* (47), 10736–10745. https://doi.org/10.1021/acs.jpcb.8b09439.

(83) Harte, T.; Dharmasiri, B.; Dobhal, G. S.; Walsh, T. R.; Henderson, L. C. Accelerated Lithium-Ion Diffusion via a Ligand 'Hopping' Mechanism in Lithium Enriched Solvate Ionic Liquids. *Phys. Chem. Chem. Phys.* **2023**, *25* (43), 29614–29623. https://doi.org/10.1039/D3CP04666D.

(84) Guillemin, T. Micro-Supercondensateurs 3D Tout-Solide à Base de Dioxyde de Manganèse et d'électrolyte Ionogel. These de doctorat, Nantes Université, 2022. https://www.theses.fr/2022NANU4013 (accessed 2023-11-10).

(85) R. MacFarlane, D.; Tachikawa, N.; Forsyth, M.; M. Pringle, J.; C. Howlett, P.; D. Elliott, G.; H. Davis, J.; Watanabe, M.; Simon, P.; Austen Angell, C. Energy Applications of Ionic Liquids. *Energy & Environmental Science* **2014**, *7* (1), 232–250. https://doi.org/10.1039/C3EE42099J.

(86) Liu, H.; Yu, H. Ionic Liquids for Electrochemical Energy Storage Devices Applications. *Journal of Materials Science & Technology* **2019**, *35* (4), 674–686. https://doi.org/10.1016/j.jmst.2018.10.007.

(87) Zhou, T.; Gui, C.; Sun, L.; Hu, Y.; Lyu, H.; Wang, Z.; Song, Z.; Yu, G. Energy Applications of Ionic Liquids: Recent Developments and Future Prospects. *Chem. Rev.* **2023**, *123* (21), 12170–12253. https://doi.org/10.1021/acs.chemrev.3c00391.

(88) Muldoon, J.; Bucur, C. B.; Oliver, A. G.; Sugimoto, T.; Matsui, M.; Kim, H. S.; Allred, G. D.; Zajicek, J.; Kotani, Y. Electrolyte Roadblocks to a Magnesium Rechargeable Battery. *Energy Environ. Sci.* **2012**, *5* (3), 5941–5950. https://doi.org/10.1039/C2EE03029B.

(89) Shterenberg, I.; Salama, M.; Yoo, H. D.; Gofer, Y.; Park, J.-B.; Sun, Y.-K.; Aurbach, D. Evaluation of $(CF_3SO_2)_2N^-$ (TFSI) Based Electrolyte Solutions for Mg Batteries. *J. Electrochem. Soc.* **2015**, *162* (13), A7118–A7128. https://doi.org/10.1149/2.0161513jes.

(90) Jónsson, E. Ionic Liquids as Electrolytes for Energy Storage Applications – A Modelling Perspective. *Energy Storage Materials* **2020**, *25*, 827–835. https://doi.org/10.1016/j.ensm.2019.08.030.

(91) Canongia Lopes, J. N. A.; Pádua, A. A. H. Nanostructural Organization in Ionic Liquids. *J. Phys. Chem. B* **2006**, *110* (7), 3330–3335. https://doi.org/10.1021/jp056006y.
(92) Docampo-Álvarez, B.; Gómez-González, V.; Cabeza, O.; Ivaništšev, V. B.; Gallego, L. J.; Varela, L. M. Molecular Dynamics Simulations of Novel Electrolytes Based on Mixtures of Protic and Aprotic Ionic Liquids at the Electrochemical Interface: Structure and Capacitance of the Electric Double Layer. *Electrochimica Acta* **2019**, *305*, 223–231. https://doi.org/10.1016/j.electacta.2019.03.010.
(93) Goloviznina, K.; Gong, Z.; Padua, A. A. H. The CL&Pol Polarizable Force Field for the Simulation of Ionic Liquids and Eutectic Solvents. *WIREs Computational Molecular Science* **2022**, *12* (3), e1572. https://doi.org/10.1002/wcms.1572.
(94) Bara, J. E.; Lessmann, S.; Gabriel, C. J.; Hatakeyama, E. S.; Noble, R. D.; Gin, D. L. Synthesis and Performance of Polymerizable Room-Temperature Ionic Liquids as Gas Separation Membranes. *Ind. Eng. Chem. Res.* **2007**, *46* (16), 5397–5404. https://doi.org/10.1021/ie0704492.
(95) Ye, Y.-S.; Rick, J.; Hwang, B.-J. Ionic Liquid Polymer Electrolytes. *J. Mater. Chem. A* **2013**, *1* (8), 2719–2743. https://doi.org/10.1039/C2TA00126H.
(96) Katakabe, T.; Kaneko, T.; Watanabe, M.; Fukushima, T.; Aida, T. Electric Double-Layer Capacitors Using "Bucky Gels" Consisting of an Ionic Liquid and Carbon Nanotubes. *J. Electrochem. Soc.* **2005**, *152* (10), A1913. https://doi.org/10.1149/1.2001187.
(97) Bideau, J. L.; Viau, L.; Vioux, A. Ionogels, Ionic Liquid Based Hybrid Materials. *Chem. Soc. Rev.* **2011**, *40* (2), 907–925. https://doi.org/10.1039/C0CS00059K.
(98) Guyomard-Lack, A.; Abusleme, J.; Soudan, P.; Lestriez, B.; Guyomard, D.; Bideau, J. L. Hybrid Silica-Polymer Ionogel Solid Electrolyte with Tunable Properties. *Adv. Energy Mater.* **2014**, *4* (8), 1301570. https://doi.org/10.1002/aenm.201301570.
(99) Néouze, M.-A.; Bideau, J. L.; Leroux, F.; Vioux, A. A Route to Heat Resistant Solid Membranes with Performances of Liquid Electrolytes. *Chem. Commun.* **2005**, No. 8, 1082–1084. https://doi.org/10.1039/B416267F.
(100) Néouze, M.-A.; Le Bideau, J.; Vioux, A. Versatile Heat Resistant Solid Electrolytes with Performances of Liquid Electrolytes. *Progress in Solid State Chemistry* **2005**, *33* (2–4), 217–222. https://doi.org/10.1016/j.progsolidstchem.2005.11.049.
(101) Le Bideau, J.; Gaveau, P.; Bellayer, S.; Néouze, M.-A.; Vioux, A. Effect of Confinement on Ionic Liquids Dynamics in Monolithic Silica Ionogels: 1H NMR Study. *Phys. Chem. Chem. Phys.* **2007**, *9* (40), 5419. https://doi.org/10.1039/b711539c.
(102) Ueno, K.; Kasuya, M.; Watanabe, M.; Mizukami, M.; Kurihara, K. Resonance Shear Measurement of Nanoconfined Ionic Liquids. *Phys. Chem. Chem. Phys.* **2010**, *12* (16), 4066. https://doi.org/10.1039/b923571j.
(103) Wang, T.-H.; Wu, M.-S.; Chang, H.-Chou. Characterization of Local Structures of Confined Imidazolium Ionic Liquids in PVdF-Co-HFP Matrices by High Pressure Infrared Spectroscopy. *Nanomaterials* **2020**, *10* (Copyright (C) 2021 American Chemical Society (ACS). All Rights Reserved.), 1973. https://doi.org/10.3390/nano10101973.
(104) Marie, A.; Said, B.; Galarneau, A.; Stettner, T.; Balducci, A.; Bayle, M.; Humbert, B.; Le Bideau, J. Silica Based Ionogels: Interface Effects with Aprotic and Protic Ionic Liquids with Lithium. *Phys. Chem. Chem. Phys.* **2020**, *22* (41), 24051–24058. https://doi.org/10.1039/D0CP03599H.
(105) Aidoud, D.; Guy-Bouyssou, D.; Guyomard, D.; Bideau, J. L.; Lestriez, B. Photo-Polymerized Organic Host Network of Ionogels for Lithium Batteries: Effects of Mesh Size and of Ethylene Oxide Content. *Journal of The Electrochemical Society* **2018**.
(106) Tie, J.; Mao, Z.; Zhang, L.; Zhong, Y.; Xu, H. Stretchable, Self-Healing, and Remodelable Ionogel via In Situ Phase Separation as a Highly Sensitive Multimode Sensor. *ACS Appl. Polym. Mater.* **2023**, *5* (11), 9092–9102. https://doi.org/10.1021/acsapm.3c01611.
(107) Wang, M.; Hu, J.; Dickey, M. D. Tough Ionogels: Synthesis, Toughening Mechanisms, and Mechanical Properties–A Perspective. *JACS Au* **2022**, *2* (12), 2645–2657. https://doi.org/10.1021/jacsau.2c00489.

(108) Zhou, R.; Jin, Y.; Li, Y.; Jin, H.; Zeng, W.; Mei, J.; Liu, Y. In-Situ Phase Separation Constructing Robust Hydrophobic Ionogels with Multifunction. *Chemical Engineering Journal* **2023**, *476*, 146840. https://doi.org/10.1016/j.cej.2023.146840.
(109) Shi, Y.; Wang, Y.; Gu, Y.; Zheng, L.; Ma, S.; Xu, X. Self-Healable and Stretchable Ionogels Serve as Electrolytes and Substrates for Integrated All-in-One Micro-Supercapacitors. *Chemical Engineering Journal* **2020**, *392*, 123645. https://doi.org/10.1016/j.cej.2019.123645.
(110) Sahrash, R.; Siddiqa, A.; Razzaq, H.; Iqbal, T.; Qaisar, S. PVDF Based Ionogels: Applications towards Electrochemical Devices and Membrane Separation Processes. *Heliyon* **2018**, *4* (11), e00847. https://doi.org/10.1016/j.heliyon.2018.e00847.
(111) Balo, L.; Shalu; Gupta, H.; Kumar Singh, V.; Kumar Singh, R. Flexible Gel Polymer Electrolyte Based on Ionic Liquid EMIMTFSI for Rechargeable Battery Application. *Electrochimica Acta* **2017**, *230*, 123–131. https://doi.org/10.1016/j.electacta.2017.01.177.
(112) Wang, M.; Zhang, P.; Shamsi, M.; Thelen, J. L.; Qian, W.; Truong, V. K.; Ma, J.; Hu, J.; Dickey, M. D. Tough and Stretchable Ionogels by in Situ Phase Separation. *Nat. Mater.* **2022**, *21* (3), 359–365. https://doi.org/10.1038/s41563-022-01195-4.
(113) Xu, L.; Huang, Z.; Deng, Z.; Du, Z.; Sun, T. L.; Guo, Z.-H.; Yue, K. A Transparent, Highly Stretchable, Solvent-Resistant, Recyclable Multifunctional Ionogel with Underwater Self-Healing and Adhesion for Reliable Strain Sensors. *Advanced Materials* **2021**, *33* (51), 2105306. https://doi.org/10.1002/adma.202105306.
(114) Wang, P.; Zakeeruddin, S. M.; Exnar, I.; Grätzel, M. High Efficiency Dye-Sensitized Nanocrystalline Solar Cells Based on Ionic Liquid Polymer Gel Electrolyte. *Chem. Commun.* **2002**, No. 24, 2972–2973. https://doi.org/10.1039/B209322G.
(115) Kang, Y.; Li, R.; Wang, A.; Kang, J.; Wang, Z.; Bi, W.; Yang, Y.; Song, Y.; Dong, Q. Ionogel-Perovskite Matrix Enabling Highly Efficient and Stable Flexible Solar Cells towards Fully-R2R Fabrication. *Energy Environ. Sci.* **2022**, *15* (8), 3439–3448. https://doi.org/10.1039/D2EE01326F.
(116) Zhang, X.; Fu, X.; Yang, S.; Zhang, Y.; Zhang, R.; Hu, S.; Bao, X.; Zhao, F.; Li, X.; Liu, Q. Design of Sepiolite-Supported Ionogel-Embedded Composite Membranes without Proton Carrier Wastage for Wide-Temperature-Range Operation of Proton Exchange Membrane Fuel Cells. *J. Mater. Chem. A* **2019**, *7* (25), 15288–15301. https://doi.org/10.1039/C9TA03666K.
(117) Zou, M.; Luo, J.; Wang, X.; Tan, S.; Wang, C.; Wu, Y. In Situ Polymerized Protic Ionogels for Fuel Cells at Elevated Temperatures. *Ind. Eng. Chem. Res.* **2021**, *60* (9), 3589–3596. https://doi.org/10.1021/acs.iecr.0c04882.
(118) Marr, P. C.; Marr, A. C. Ionic Liquid Gel Materials: Applications in Green and Sustainable Chemistry. *Green Chem.* **2016**, *18* (1), 105–128. https://doi.org/10.1039/C5GC02277K.
(119) Guillemin, T.; Douard, C.; Robert, K.; Asbani, B.; Lethien, C.; Brousse, T.; Le Bideau, J. Solid-State 3D Micro-Supercapacitors Based on Ionogel Electrolyte: Influence of Adding Lithium and Sodium Salts to the Ionic Liquid. *Energy Storage Materials* **2022**, *50*, 606–617. https://doi.org/10.1016/j.ensm.2022.05.041.
(120) Chen, N.; Zhang, H.; Li, L.; Chen, R.; Guo, S. Ionogel Electrolytes for High-Performance Lithium Batteries: A Review. *Advanced Energy Materials* **2018**, *8* (12), 1702675. https://doi.org/10.1002/aenm.201702675.
(121) Pan, S.; Yao, M.; Zhang, J.; Li, B.; Xing, C.; Song, X.; Su, P.; Zhang, H. Recognition of Ionic Liquids as High-Voltage Electrolytes for Supercapacitors. *Frontiers in Chemistry* **2020**, *8*.
(122) Asmara, S. N.; Kufian, M. Z.; Majid, S. R.; Arof, A. K. Preparation and Characterization of Magnesium Ion Gel Polymer Electrolytes for Application in Electrical Double Layer Capacitors. *Electrochimica Acta* **2011**, *57*, 91–97. https://doi.org/10.1016/j.electacta.2011.06.045.
(123) Abdou, N.; Alonso, B.; Brun, N.; Devautour-Vinot, S.; Paillet, M.; Landois, P.; Mehdi, A.; Hesemann, P. Confinement Effects on the Ionic Liquid Dynamics in Ionosilica Ionogels: Impact of the Ionosilica Nature and the Host/Guest Ratio. *J. Phys. Chem. C* **2022**, acs.jpcc.2c06565. https://doi.org/10.1021/acs.jpcc.2c06565.

(124) D'Angelo, A. J.; Grimes, J. J.; Panzer, M. J. Deciphering Physical versus Chemical Contributions to the Ionic Conductivity of Functionalized Poly(Methacrylate)-Based Ionogel Electrolytes. *J. Phys. Chem. B* **2015**, *119* (47), 14959–14969. https://doi.org/10.1021/acs.jpcb.5b08250.
(125) Wang, Y.-L.; Li, B.; Sarman, S.; Mocci, F.; Lu, Z.-Y.; Yuan, J.; Laaksonen, A.; Fayer, M. D. Microstructural and Dynamical Heterogeneities in Ionic Liquids. *Chem. Rev.* **2020**, *120* (13), 5798–5877. https://doi.org/10.1021/acs.chemrev.9b00693.
(126) Zhang, S.; Zhang, J.; Zhang, Y.; Deng, Y. Nanoconfined Ionic Liquids. *Chem. Rev.* **2017**, *117* (10), 6755–6833. https://doi.org/10.1021/acs.chemrev.6b00509.
(127) Liu, Y.; Wu, G.; Fu, H.; Jiang, Z.; Chen, S.; Sha, M. Immobilization and Melting Point Depression of Imidazolium Ionic Liquids on the Surface of Nano-SiOx Particles. *Dalton Trans.* **2010**, *39* (13), 3190. https://doi.org/10.1039/b924042j.
(128) Néouze, M.-A.; Le Bideau, J.; Gaveau, P.; Bellayer, S.; Vioux, A. Ionogels, New Materials Arising from the Confinement of Ionic Liquids within Silica-Derived Networks. *Chem. Mater.* **2006**, *18* (17), 3931–3936. https://doi.org/10.1021/cm060656c.
(129) Osada, I.; de Vries, H.; Scrosati, B.; Passerini, S. Ionic-Liquid-Based Polymer Electrolytes for Battery Applications. *Angewandte Chemie International Edition* **2016**, *55* (2), 500–513. https://doi.org/10.1002/anie.201504971.
(130) Gouverneur, M.; Schmidt F.; Schönhoff M. Negative effective Li transference numbers in Li salt/ionic liquid mixtures: does Li drift in the "Wrong" direction? *Phys. Chem. Chem. Phys.* **2018,** *20,* (11), 7470-7478.

# Chapter 2 - Ionic liquids and confined ionic liquids (ionogels) synthesis

# Introduction

The development of all-solid-state energy storage devices implies the use of new solid materials as electrolytes. They must be competitive to current liquid electrolytes in terms of ionic conductivity, thermal and electrochemical stabilities.[1,2] The challenge of my research project is to design and understand a new family of solid-state electrolytes: polymer-based ionogels. This work mainly focuses on fundamental understanding on ions dynamics in ionic liquid-based electrolytes. However, it is essential to keep in mind the targeted application, which is integrating ionogels in high energy and power densities hybrid supercapacitors. The choices made are with respect for these specifications i.e., very high ionic conductivity (above 1 $mS.cm^{-1}$), wide temperature stability window (from - 20°C to + 90°C), wide electrochemical window (around 4 V) and satisfying mechanical properties (self-standing gels).

Ionics liquids (ILs) are well known for their interesting properties such as very low vapour pressure, low melting point, non-flammability, and wide electrochemical window.[3] As ILs are stable in temperature, they are good candidates to tackle the thermal runaways that could occur in batteries and supercapacitors at high temperatures.[4,5] They could even become the main alternative to classical organic electrolytes for extreme conditions application such as space satellites or oil drilling. Nevertheless, they present relatively high viscosity. It has been reported that the viscosity is increasing with alkali and alkaline earth salts addition.[6,7] This is a major drawback in energy storage devices where the electrolyte is considered as a reservoir for the cation of interest ($Li^+$, $Na^+$, $Zn^{2+}$…). Moreover, they remain liquids and could bring about leakage and packaging issues.

Finally, ionogels are biphasic materials with a bicontinuous interface between the solid matrix and the ionic liquid phase.[8] They are composed of an IL confined in a solid electron doublet-rich matrix such as silica or certain polymers. These solid electrolytes have attracted attention in the last decades for their high ionic conductivities, the safety regarding thermal runaways and their tuneable mechanical, optical and electrochemical properties.[9–11]

This chapter describes how the liquid and solid electrolytes will be synthetized and their study will be the topics of the following chapters. First, in the current chapter, the preparation and synthesis of ternary/salt doped ionic liquids and ionogels is presented with a few discussions on the major key parameters. Then in the following chapter, the methodology used to measure the physicochemical properties and fundamental interactions in these electrolytes will be presented through an example: EMImTFSI + 0.5M LiTFSI (Chapter 3).

The research focuses on understanding the diffusion mechanisms and limitations that occurs in ionic liquid-based electrolytes to optimize electrochemical devices performance. Having access to such information implies probing the matter at an atomic or electronic scale during very short times to capture sensitive and fast phenomenon like ions aggregation. Therefore, spectroscopies are very interesting to compare some fundamental concepts such as ionicity or coordination sphere of metal cations. Some techniques including Differential Scanning Calorimetry (DSC), Electrochemical Impedance Spectroscopy (EIS), Raman Spectroscopy (RS) and Pulsed Field Gradient Nuclear Magnetic Resonance (PFG NMR) will be described in the next chapter.

# 2.1 Ionic liquid preparation

Ionic liquids (ILs) are molten salt that are liquid on a wide range of temperature. They all have specific phase transitions and thermodynamics is essential to study them. Coulombic interactions, Van der Walls, and hydrogen bonding controls ions mobility in ILs [10].

As soon as an IL is doped with a salt, we will name it ternary or quaternary IL with cations or anions of different nature which imply a more complex phase diagram. The interactions between cations and anions change and become competitive depending on the geometry, polarizability, and polarization power.

## 2.1.1 Choice of the ionic liquid

To develop an electrolyte for energy storage applications, the main properties to consider, with priorities based on each specific device, are the temperature and electrochemical stability windows, the ionic conductivity, and diffusion of the cation of interest. Here, the ionic liquids considered for this study and their main properties is reported. They are widely used and studied for electrochemical devices.[7,12,13]

Finally, regarding the properties summarized in Table 2.1., 1-ethyl-3-methylimidazolium bis(trifluoromethanesulfonyl)imide (EMImTFSI) was chosen based on its very good ionic conductivity and electrochemical window sufficient for supercapacitors devices. On the other hand, the pyrrolidinium cations present better electrochemical stability windows but lower ionic conductivity and thus they are better candidates for batteries applications. Even if EMIMFSI seems to be an excellent candidate too, this ionic liquid could present some chemical instability issues because of the FSI anion or remaining impurities from its synthesis. Indeed, LiFSI is very hygroscopic and could degrades with water in an exothermic reaction at relatively high temperatures.[14]

**Table 2.1: Physico-chemical properties of the main ILs used in electrochemistry**

| Ionic liquid | $\sigma_{RT}$ (mS.cm$^{-1}$) | Melting point (°C) | Decomposition temperature (°C) | Electrochemical window (V) | References |
|---|---|---|---|---|---|
| **EMImTFSI** | 8 - 8.4 | -18 | 439 | 4.6 | 15–19 |
| **EMImFSI** | 15.4 -16.5 | -13 | 225 | 4.5 | 19,20 |
| **Pyr$_{13}$TFSI** | 3.9 | 12 | 417 | 5.3 | 16,21 |
| **Pyr$_{13}$FSI** | 8.3 | -17.5 | 217 | 5.3 | 19,20 |

Power density in supercapacitors is not only brought by the electrode material loading, topology and design. It comes also from the ion's concentration and conductivity of the electrolyte.[22] In that sense, metal salts could be added in the ionic liquid to provide the electrochemical active cation in the electrolyte reacting with pseudocapacitive material. In the following sections the term ternary ionic liquid is used to describe EMImTFSI mixtures by adding lithium, magnesium or zinc bis(trifluoromethanesulfonyl)imide salts (Figure 2.1). In all cases, the corresponding salt with the same anion than the IL's one was chosen in order to avoid adding complexity to the mixture. Even if some studies have shown that it could be interesting to mix anions together to improve the transport properties by changing the solvation sphere of metal cations.[23]

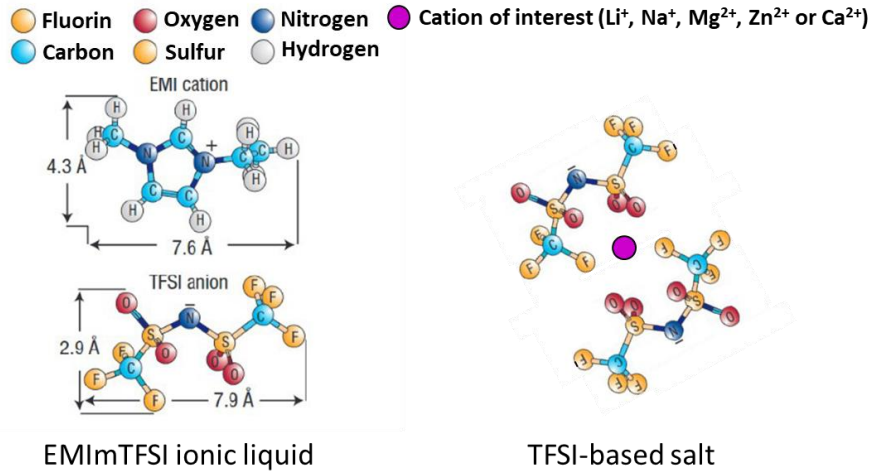


**Figure 2.1: Schematical representation of ionic liquid and salt used in following studies[24]**

## 2.1.2 Water management

To prepare ionic liquids as electrolytes for electrochemical applications, the priority is to avoid moisture. Notably, the following undesirable reactions can occur between water and alkali and alkaline earth metals and metal oxides:

$$2Li_{(s)} + 2H_2O_{(aq)} \rightarrow 2Li(OH)_{(aq)} + H_{2(g)} \uparrow$$

$$Li_2O_{(s)} + 2H_2O_{(aq)} \rightarrow 2Li(OH)_{(aq)}$$

$$Mg_{(s)} + 2H_2O_{(aq)} \xrightarrow{\Delta} Mg(OH)_{2(aq)} + H_{2(g)} \uparrow$$

$$MgO_{(s)} + H_2O_{(aq)} \rightarrow Mg(OH)_{2(aq)}$$

**Equations 2.1**

As these metals are used to characterize electrodes materials, the electrolytes should not bring water that may precipitate metal electrodes and disrupt the operation of energy storage systems. Moreover, it has been reported that the presence of water strongly shortens the electrochemical stability window of such electrolytes.[3,25]

Neat ionic liquid and salts have been purchased from Solvionic with a purity of 99.5%. Metal cation salts were added in a glovebox after drying the ionic liquid and salts at 50°C under $3.10^{-2}$ mbar vacuum for 24 hours. Karl Fischer water titration is performed on the neat ionic liquid: the water amount measured after the drying process is below 20 ppm (a more precise value would not be reliable). Most of the salts are hygroscopic hence the ternary ionic liquids may have higher water amount, especially at high concentrations. However, it has not been measured on every sample of the numerous series of the studies A water amount below 50 ppm was considered as negligible to change the physicochemical properties of ionic liquids without or with salt. To check this, we have measured conductivities of two samples, one spontaneously saturated with water from ambient atmosphere, the other dried following the conditions presented above. The results are presented on Figure 2.2. EMImTFSI ionic conductivity measured by Electrochemical Impedance Spectroscopy for two different water content in the ionic liquid.

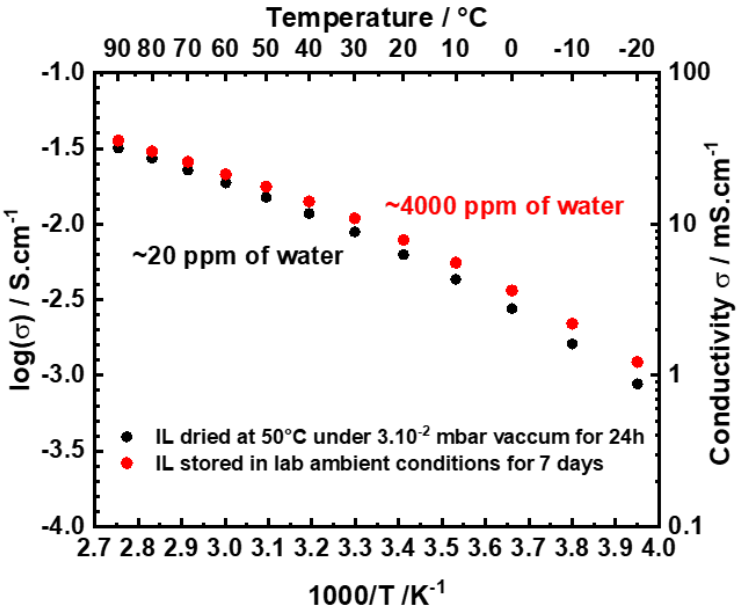


**Figure 2.2: EMImTFSI ionic conductivity for dried and undried samples**

The undried sample shows better ionic conductivity because of water molecules, especially at low temperatures. This result clearly shows the importance of adequate storage and drying process for ionic liquids and salts in order to communicate accurate conductivities.

## 2.1.3 Molecular volume and concentration calculations

Density of salts are generally not reported in the Safety Data Sheet of the chemicals neither provided by the producer. All densities for the purchased solid salts are measured with a pycnometer and tabulated with the corresponding molecular mass in Table 2.1.

**Table 2.2: Molar volume calculations for ionic liquid and salts**

| Chemical name | Formula | Molar mass ($g.mol^{-1}$) | Density ($g.cm^{-3}$) | Molar volume ($cm^3.mol^{-1}$) |
|---|---|---|---|---|
| **1-ethyl-3-methylimidazolium bis(trifluoromethanesulfonyl)imide** | EMImTFSI | 391.3 | 1.52 | 257.4 |
| **Lithium bis(trifluoromethanesulfonyl)imide** | LiTFSI | 287.1 | 1.33 | 215.9 |
| **Sodium bis(trifluoromethanesulfonyl)imide** | NaTFSI | 303.1 | 2.28* | 132.9 |
| **Magnesium(II) Di[bis(trifluoromethanesulfonyl)imide]** | $Mg(TFSI)_2$ | 584.6 | 2.25* | 259.8 |
| **Zinc(II) Di[bis(trifluoromethanesulfonyl)imide]** | $Zn(TFSI)_2$ | 625.7 | 2.42* | 258.6 |
| **Calcium(II) Di[bis(trifluoromethanesulfonyl)imide]** | $Ca(TFSI)_2$ | 600.4 | 2.12* | 283.2 |

*Measured by pycnometry

The mixture has been prepared considering that the molar volume of all constituents may not change. This is an approximation because of the interactions between ions in the ionic liquids that may bring small changes in density for the mixture. Moreover, the density of the ionic liquid itself varies with temperature.[26] The following calculations have been made considering the density at room temperature.

However, neglecting these changes was an easier way to calculate concentrations. This study, aims to discuss some trends between series of samples rather than precisely measuring the exact concentration of the samples accurately. The molar fraction of monovalent salt in the mixture is given by the following equation:

$$x_{salt} = \frac{\frac{m_{salt}}{M_{salt}}}{2\frac{m_{salt}}{M_{salt}} + 2\frac{m_{I.L}}{M_{I.L}}}$$

The molar fraction of bivalent salt in the mixture is given by the following equation:

$$x_{salt} = \frac{\frac{m_{salt}}{M_{salt}}}{3\frac{m_{salt}}{M_{salt}} + 2\frac{m_{I.L}}{M_{I.L}}}$$

**Equations 2.2**

Where $m_{I.L}$ is the mass of ionic liquid; $m_{salt}$ the mass of the salt; $M_{I.L}$ and $M_{salt}$ their molar masses respectively.

Similarly, the salt molar concentration is given by the following equation if we hypothesise that the total volume of the mixture is equal to the sum of the ionic liquid and salt volumes:

$$[salt] = 1000 * \frac{\frac{m_{salt}}{M_{salt}}}{\frac{m_{salt}}{M_{salt}} * V_{salt} + \frac{m_{I.L}}{M_{I.L}} * V_{I.L.}}$$

**Equation 2.3**

Where $V_{salt}$ is the salt's molar volume in $cm^3.mol^{-1}$; $V_{I.L.}$ is the IL's molar volume in $cm^3.mol^{-1}$.

Finally, the salt molar fraction as a function of its concentration is calculated using the following equation:

$$x_{salt} = [salt] * \frac{\frac{m_{salt}}{M_{salt}} * V_{salt} + \frac{m_{I.L}}{M_{I.L}} * V_{I.L.}}{1000 * [2\frac{m_{salt}}{M_{salt}} + 2\frac{m_{I.L}}{M_{I.L}}]} \text{ (monovalent)}$$

$$x_{salt} = [salt] * \frac{\frac{m_{salt}}{M_{salt}} * V_{salt} + \frac{m_{I.L}}{M_{I.L}} * V_{I.L.}}{1000 * [3\frac{m_{salt}}{M_{salt}} + 2\frac{m_{I.L}}{M_{I.L}}]} \text{ (bivalent)}$$

**Equations 2.4**

It is essential to mention the main difference between monovalent and bivalent cations: for each mole of $Li^+$ added, one mole of TFSI is added to the neat ionic liquid whereas two moles of TFSI are added for $Mg(TFSI)_2$ (Figure 2.3).

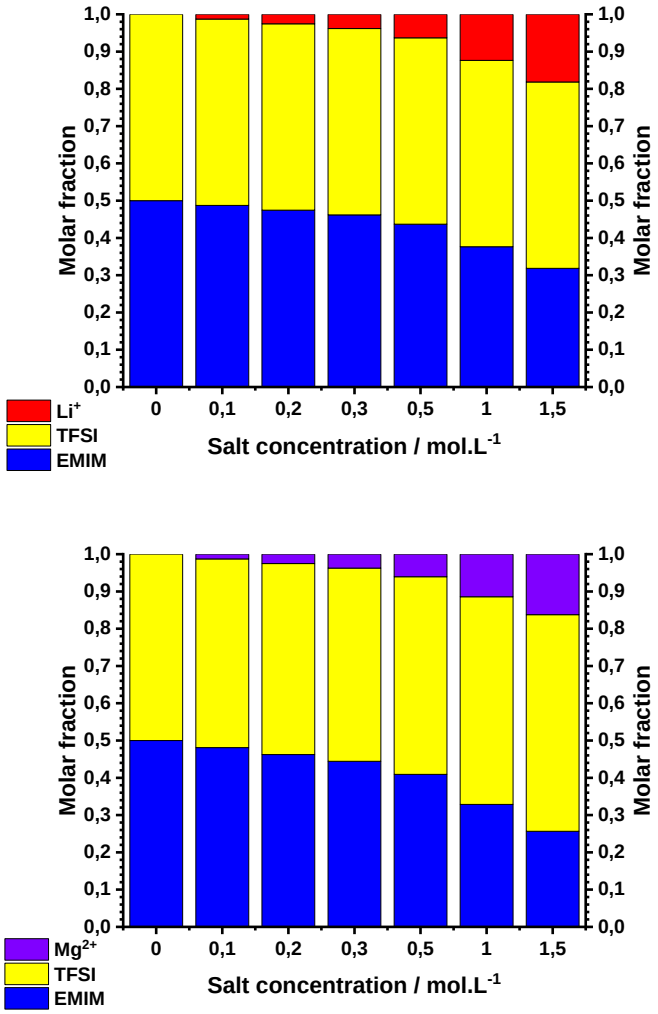


**Figure 2.3: Molar fractions in [EMImTFSI + LiTFSI] and [EMImTFSI + $Mg(TFSI)_2$] in function of salt concentration**

## 2.1.4 Dissolving salts in ionic liquids

Ionic liquids can be doped with metal cation salt of interest for the targeted device. In Figure 2.4 is shown two ternary ILs series for $Li^+$ (yellow) and $Ca^{2+}$ (blue) doped ILs.

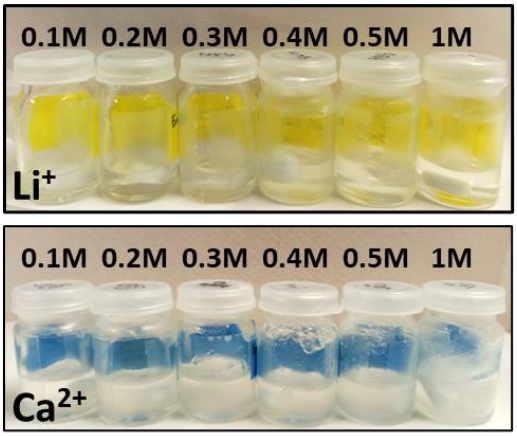


**Figure 2.4: Ternary ILs with different molar concentration of LiTFSI (yellow) and $Ca(TFSI)_2$ (blue)**

The first comment should be about the qualitative difference of dissolution between both salts. For instance, 1 moles of LiTFSI are easily dissolved in EMImTFSI before the mixture becomes very viscous, whereas no more than 0.3 moles of $Ca(TFSI)_2$ could dissolve in EMImTFSI at room temperature. This difference is mainly due to the volume difference between these two cations. Charge to volume ratios for the different cations are represented below in Table 2.2 according to Agmon work on cationic radii,[27] which will be helpful for future discussion.

**Table 2.3: Charge to volume ratio for cations**

| Cation | Formula | Electrons configuration | Theoretical charge | Calculated ionic radius (Å) [27] | Polarization power factor ($Å^{-1}$) | Charge to volume ratio ($Å^{-3}$) |
|---|---|---|---|---|---|---|
| **Lithium** | $Li^+$ | $1s^2 2s^0$ | +1 | 0.75 | 1.33 | 0.57 |
| **Sodium** | $Na^+$ | $[Ne]^{10} 3s^0$ | +1 | 0.99 | 1.01 | 0.25 |
| **Magnesium** | $Mg^{2+}$ | $[Ne]^{10} 3s^0$ | +2 | 0.69 | 2.90 | 1.45 |
| **Zinc** | $Zn^{2+}$ | $[Ar]^{18} 4s^0 3d^{10}$ | +2 | 0.74 | 2.70 | 1.18 |
| **Calcium** | $Ca^{2+}$ | $[Ar]^{18} 4s^0$ | +2 | 0.96 | 2.08 | 0.54 |

The higher the charge to volume is, the more concentrated the cation charge is and so are the attractive properties of polarizable ions.

# 2.2 PVDF-based ionogels preparation

## 2.2.1 Physical gels synthesis – Polymer in salt approach

Ionogels are solid gels made of a confined ionic liquid in a solid matrix. In the present work, a polyvinylidene fluoride (PVDF) was used as a polymer host network. There is no chemical reaction at stake in the synthesis. The gelation process occured by percolation of the already polymerized polymer chains. This process is known as a physical gel synthesis, as opposed to chemical gel synthesis involving chemical/polymerization reactions for the gel formation.

Ionogels were prepared from the ILs and a polyvinylidene fluoride (PVDF Solef 6008, Solvay) confining matrix. Firstly, the PVDF was solubilized in dimethylformamide solvent (DMF, Acros Organics) at 8 wt% at room temperature and let to homogenize in a sealed vial under stirring. Then, dried IL was added to the latter mixture up to 83 wt% and stirred for a few minutes. The ionogel precursor (~ 3 $cm^3$) obtained was casted in Teflon molds and let to age under ambient conditions, following two steps. First, the molds are placed for two days in a closed box (~ 100 $cm^3$) to slow down the evaporation of the DMF, to allow the PVDF chains unfolding and to prevent any cracks. Secondly, the molds are kept without cover for two more days to allow the final evaporation of DMF. Finally, a heat treatment is performed on ionogels at 120°C under $3.10^{-2}$ mbar during 40 min to improve their mechanical strength and get rid of the last DMF traces.

The end-up gel is a solid than can be easily handled with no leakage (Figure 2.5). It can be shaped according to the characterization technique needs or for the targeted application (thin membrane).

a)

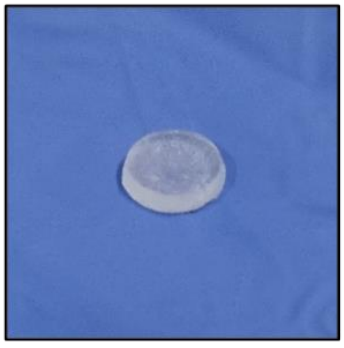

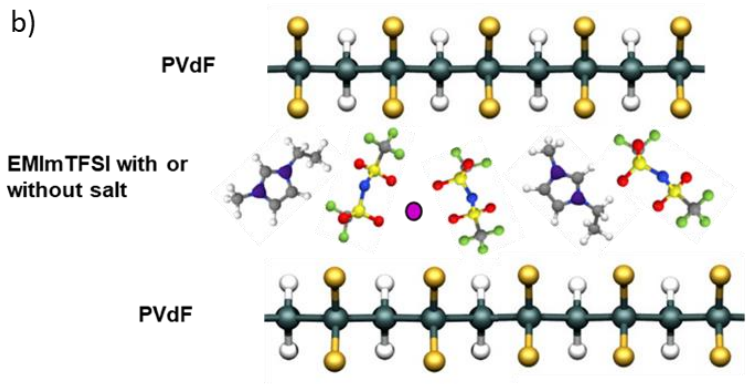


**Figure 2.5: Picture (a) and schematical representation (b) of PVDF-based ionogels**

## 2.2.2 Solid-to-liquid ratio

To be called ionogels, the gels should have a minimum of 50 % wt. of ionic liquid. Otherwise, the physicochemical properties are too different from the neat ionic liquid. The liquid-to-solid ratio, more precisely the liquid-to-interface ratio, in an essential parameter in ionogel science .[28] It should be chosen in function of the targeted properties. Figure 2.6 shows the ionic conductivity for two different confinement proportions.

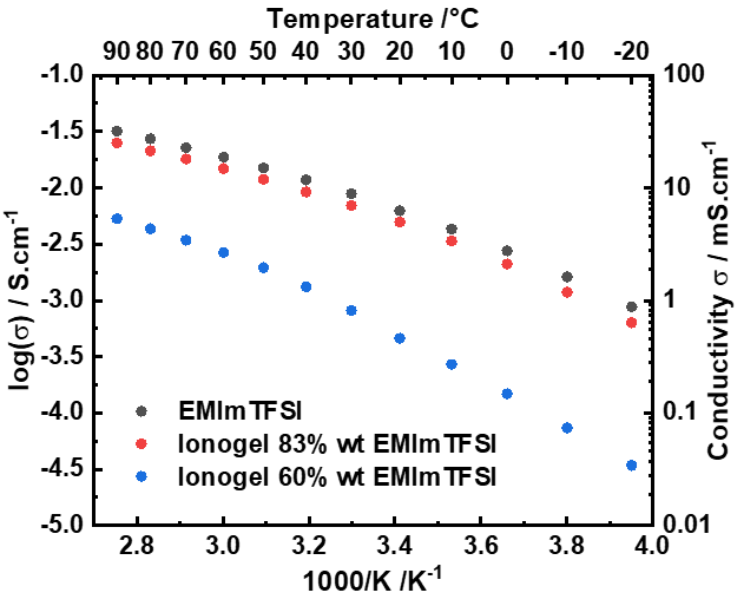


**Figure 2.6: Ionic conductivity for EMImTFSI (black dots), Ionogel [0.83:0.17] wt. (red dots) and ionogel [0.6:0.4] wt. (blue dots)**

Overall, the ionic conductivity increases with temperature for all the samples. However, the mobility of charged species decreases drastically with polymer addition (less wt% of IL). This could be understood since the polymer is not participating in the macroscopic ionic conductivity of the IL ions. It could even be a physical barrier for diffusion, and this aspect will be discussed later in the manuscript. Nevertheless, this decrease is not directly proportional to the liquid content, which assumes that a specific optimised solid to liquid ratio does exist to maximise the ionic conductivity property. Figure 2.7 shows the ionic conductivity percentage relative to the IL's conductivity alone confined within the two previous ionogels.

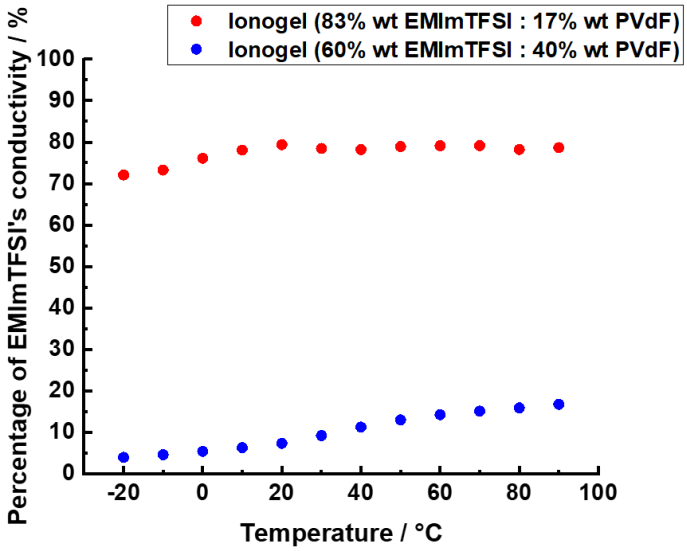


**Figure 2.7: Ionic conductivity conservation for two confinement degrees in an ionogel [0.83:0.17] wt. (red dots) and ionogel [0.6:0.4] wt. (blue dots)**

In the case of the IL rich ionogel (red dots), the macroscopic ionic conductivity is proportional to the liquid content, around 80% of the neat ionic liquid conductivity. That means all the confined ionic liquid is taking part in the macroscopic conductivity of the ionogel. Whereas for the 60%wt ionic liquid ionogel the ionic conductivity drastically decreased (blue dots). The confinement is changing the dynamics in the liquid phase and these changes depend on the mesh size of the polymer matrix, as well as presumably to the surface of interface.

There is a trade-off between the solid mechanical properties and the ionic conductivity. The minimum amount of PVDF used in the synthesis to obtain a solid gel is around [EMImTFSI 89%wt : PVDF 11%wt] and in the following studies, all the ionogels do have these proportions: [EMImTFSI 83%wt : PVDF 17%wt], because of the very good mechanical properties and very high conductivity for these solid electrolytes.

## 2.3 Problematic and strategy

At this stage, a solid electrolyte which present very promising properties for macroscopic ionic conductivity was obtained. The benefit of dealing with a solid electrolyte that presents no gas release, which is leakage-free and can be shaped as needed, is of great interest for several device families.

These useful properties will be the starting point for the following studies in Chapter 4 and 5. *What are the fundamental explanations for the very high ionic conductivity of IL-rich PVDF-based ionogels?*

The motivation of this research project is to bring understandings about the small loss in ionic conductivity compared to the ionic liquid itself. Some studies formulate the hypothesis that the liquid to solid interface brings new dynamics in the ionic liquid that could be favourable for ions mobility.[29] Nevertheless, there is a research gap for the unequivocal and quantitative study of this previous hypothesis especially about bivalent cations conductive ionogels.

Ionic liquids doped with salts will be studied to understand the changes in dynamics brought by the salts' addition in Chapter 4. Then the effect of confinement and salts' addition in ionogels will be discussed in Chapter 5. As ionogels are compliant to specific systems thanks to the versatility of salts that can be dissolved in the IL, the primary study will focus on lithium-based ionogels with the aim of understanding the challenges of moving from a monovalent cation system to a bivalent cation system ($Mg^{2+}$ and $Zn^{2+}$). Finally, the first electrochemical tests performed in symmetric cells with metal electrodes will be presented in a final conclusive chapter in order to validate the fundamental study hypothesis and conclusions.

## Conclusion

This chapter aim to present the context of the research project and the strategy put to work in the next chapters.

Obtaining solid biphasic electrolytes is an easy task, especially physical gels made of PVDF polymer chains. Nevertheless, the study of the dynamics in these complex electrolytes and understanding the diffusion mechanism is not trivial and is the objective of this thesis.

# References


(1) Zhang, M.; Zuo, Q.; Wang, L.; Yu, S.; Mai, Y.; Zhou, Yongfeng. Poly(Ionic Liquid)-Based Polymer Composites as High-Performance Solid-State Electrolytes: Benefiting from Nanophase Separation and Alternating Polymer Architecture. *Chem. Commun. (Cambridge, U. K.)* **2020**, *56* (Copyright (C) 2021 American Chemical Society (ACS). All Rights Reserved.), 7929–7932. https://doi.org/10.1039/d0cc03281f.

(2) Balo, L.; Shalu; Gupta, H.; Kumar Singh, V.; Kumar Singh, R. Flexible Gel Polymer Electrolyte Based on Ionic Liquid EMIMTFSI for Rechargeable Battery Application. *Electrochimica Acta* **2017**, *230*, 123–131. https://doi.org/10.1016/j.electacta.2017.01.177.

(3) Ohno, H. Electrochemical Aspects of Ionic Liquids; 2011.

(4) Tian, X.; Yi, Y.; Fang, B.; Yang, P.; Wang, T.; Liu, P.; Qu, L.; Li, M.; Zhang, S. Design Strategies of Safe Electrolytes for Preventing Thermal Runaway in Lithium Ion Batteries. *Chem. Mater.* **2020**, *32* (23), 9821–9848. https://doi.org/10.1021/acs.chemmater.0c02428.

(5) Sun, H.; Zhu, G.; Zhu, Y.; Lin, M.-C.; Chen, H.; Li, Y.-Y.; Hung, W. H.; Zhou, B.; Wang, X.; Bai, Y.; Gu, M.; Huang, C.-L.; Tai, H.-C.; Xu, X.; Angell, M.; Shyue, J.-J.; Dai, Hongjie. High-Safety and High-Energy-Density Lithium Metal Batteries in a Novel Ionic-Liquid Electrolyte. *Adv. Mater. (Weinheim, Ger.)* **2020**, *32* (Copyright (C) 2021 American Chemical Society (ACS). All Rights Reserved.), 2001741. https://doi.org/10.1002/adma.202001741.

(6) Borodin, O.; Giffin, G. A.; Moretti, A.; Haskins, J. B.; Lawson, J. W.; Henderson, W. A.; Passerini, S. Insights into the Structure and Transport of the Lithium, Sodium, Magnesium, and Zinc Bis(Trifluoromethansulfonyl)Imide Salts in Ionic Liquids. *J. Phys. Chem. C* **2018**, 14.

(7) Guillemin, T.; Douard, C.; Robert, K.; Asbani, B.; Lethien, C.; Brousse, T.; Le Bideau, J. Solid-State 3D Micro-Supercapacitors Based on Ionogel Electrolyte: Influence of Adding Lithium and Sodium Salts to the Ionic Liquid. *Energy Storage Materials* **2022**, *50*, 606–617. https://doi.org/10.1016/j.ensm.2022.05.041.

(8) Néouze, M.-A.; Bideau, J. L.; Leroux, F.; Vioux, A. A Route to Heat Resistant Solid Membranes with Performances of Liquid Electrolytes. *Chem. Commun.* **2005**, No. 8, 1082–1084. https://doi.org/10.1039/B416267F.

(9) Marr, P. C.; Marr, A. C. Ionic Liquid Gel Materials: Applications in Green and Sustainable Chemistry. *Green Chem.* **2016**, *18* (1), 105–128. https://doi.org/10.1039/C5GC02277K.

(10) Guyomard-Lack, A.; Abusleme, J.; Soudan, P.; Lestriez, B.; Guyomard, D.; Bideau, J. L. Hybrid Silica-Polymer Ionogel Solid Electrolyte with Tunable Properties. *Adv. Energy Mater.* **2014**, *4* (8), 1301570. https://doi.org/10.1002/aenm.201301570.

(11) Le Bideau, J.; Ducros, J.-B.; Soudan, P.; Guyomard, D. Solid-State Electrode Materials with Ionic-Liquid Properties for Energy Storage: The Lithium Solid-State Ionic-Liquid Concept. *Adv. Funct. Mater.* **2011**, *21* (21), 4073–4078. https://doi.org/10.1002/adfm.201100774.

(12) Brachet, M.; Gaboriau, D.; Gentile, P.; Fantini, S.; Bidan, G.; Sadki, S.; Brousse, T.; Le Bideau, J. Solder-Reflow Resistant Solid-State Micro-Supercapacitors Based on Ionogels. *J. Mater. Chem. A* **2016**, *4* (30), 11835–11843. https://doi.org/10.1039/C6TA03142K.

(13) Zheng, S.; Huang, H.; Dong, Y.; Wang, S.; Zhou, F.; Qin, J.; Sun, C.; Yu, Y.; Wu, Z.-S.; Bao, X. Ionogel-Based Sodium Ion Micro-Batteries with a 3D Na-Ion Diffusion Mechanism Enable Ultrahigh Rate Capability. *Energy Environ. Sci.* **2020**, *13* (3), 821–829. https://doi.org/10.1039/C9EE03219C.
(14) Huang, J.; Hollenkamp, A. F. Thermal Behavior of Ionic Liquids Containing the FSI Anion and the Li+ Cation. *J. Phys. Chem. C* **2010**, *114* (49), 21840–21847. https://doi.org/10.1021/jp107740p.
(15) Fujii, K.; Soejima, Y.; Kyoshoin, Y.; Fukuda, S.; Kanzaki, R.; Umebayashi, Y.; Yamaguchi, T.; Ishiguro, S.; Takamuku, T. Liquid Structure of Room-Temperature Ionic Liquid, 1-Ethyl-3-Methylimidazolium Bis-(Trifluoromethanesulfonyl) Imide. *J. Phys. Chem. B* **2008**, *112* (14), 4329–4336. https://doi.org/10.1021/jp7105499.
(16) MacFarlane, D. R.; Meakin, P.; Sun, J.; Amini, N.; Forsyth, M. Pyrrolidinium Imides: A New Family of Molten Salts and Conductive Plastic Crystal Phases. *J. Phys. Chem. B* **1999**, *103* (20), 4164–4170. https://doi.org/10.1021/jp984145s.
(17) Tokuda, H.; Tsuzuki, S.; Susan, Md. A. B. H.; Hayamizu, K.; Watanabe, M. How Ionic Are Room-Temperature Ionic Liquids? An Indicator of the Physicochemical Properties. *J. Phys. Chem. B* **2006**, *110* (39), 19593–19600. https://doi.org/10.1021/jp064159v.
(18) Tokuda, H.; Hayamizu, K.; Ishii, K.; Susan, Md. A. B. H.; Watanabe, M. Physicochemical Properties and Structures of Room Temperature Ionic Liquids. 2. Variation of Alkyl Chain Length in Imidazolium Cation. *J. Phys. Chem. B* **2005**, *109* (13), 6103–6110. https://doi.org/10.1021/jp044626d.
(19) Matsumoto, H.; Sakaebe, H.; Tatsumi, K.; Kikuta, M.; Ishiko, E.; Kono, M. Fast Cycling of Li/LiCoO2 Cell with Low-Viscosity Ionic Liquids Based on Bis(Fluorosulfonyl)Imide [FSI]−. *Journal of Power Sources* **2006**, *160* (2), 1308–1313. https://doi.org/10.1016/j.jpowsour.2006.02.018.
(20) Ishikawa, M.; Sugimoto, T.; Kikuta, M.; Ishiko, E.; Kono, M. Pure Ionic Liquid Electrolytes Compatible with a Graphitized Carbon Negative Electrode in Rechargeable Lithium-Ion Batteries. *Journal of Power Sources* **2006**, *162* (1), 658–662. https://doi.org/10.1016/j.jpowsour.2006.02.077.
(21) Brandt, A.; Pohlmann, S.; Varzi, A.; Balducci, A.; Passerini, S. Ionic Liquids in Supercapacitors. *MRS Bulletin* **2013**, *38* (7), 554–559. https://doi.org/10.1557/mrs.2013.151.
(22) Brandt, A.; Balducci, A. Theoretical and Practical Energy Limitations of Organic and Ionic Liquid-Based Electrolytes for High Voltage Electrochemical Double Layer Capacitors. *Journal of Power Sources* **2014**, *250*, 343–351. https://doi.org/10.1016/j.jpowsour.2013.10.147.
(23) Kerner, M.; Plylahan, N.; Scheers, J.; Johansson, P. Ionic Liquid Based Lithium Battery Electrolytes: Fundamental Benefits of Utilising Both TFSI and FSI Anions? *Phys. Chem. Chem. Phys.* **2015**, *17* (29), 19569–19581. https://doi.org/10.1039/C5CP01891A.
(24) Simon, P.; Gogotsi, Y. Materials for Electrochemical Capacitors. *Nature Mater* **2008**, *7* (11), 845–854. https://doi.org/10.1038/nmat2297.
(25) O'Mahony, A. M.; Silvester, D. S.; Aldous, L.; Hardacre, C.; Compton, R. G. Effect of Water on the Electrochemical Window and Potential Limits of Room-Temperature Ionic Liquids. *J. Chem. Eng. Data* **2008**, *53* (12), 2884–2891. https://doi.org/10.1021/je800678e.

(26) Seki, S.; Tsuzuki, S.; Hayamizu, K.; Umebayashi, Y.; Serizawa, N.; Takei, K.; Miyashiro, H. Comprehensive Refractive Index Property for Room-Temperature Ionic Liquids. *J. Chem. Eng. Data* **2012**, *57* (8), 2211–2216. https://doi.org/10.1021/je201289w.
(27) Agmon, N. Isoelectronic Theory for Cationic Radii. *J. Am. Chem. Soc.* **2017**, *139* (42), 15068–15073. https://doi.org/10.1021/jacs.7b07882.
(28) Abdou, N.; Alonso, B.; Brun, N.; Devautour-Vinot, S.; Paillet, M.; Landois, P.; Mehdi, A.; Hesemann, P. Confinement Effects on the Ionic Liquid Dynamics in Ionosilica Ionogels: Impact of the Ionosilica Nature and the Host/Guest Ratio. *J. Phys. Chem. C* **2022**, acs.jpcc.2c06565. https://doi.org/10.1021/acs.jpcc.2c06565.
(29) Marie, A.; Said, B.; Galarneau, A.; Stettner, T.; Balducci, A.; Bayle, M.; Humbert, B.; Le Bideau, J. Silica Based Ionogels: Interface Effects with Aprotic and Protic Ionic Liquids with Lithium. *Phys. Chem. Chem. Phys.* **2020**, *22* (41), 24051–24058. https://doi.org/10.1039/D0CP03599H.

# Chapter 3 – Methodology: [EMImTFSI + 0.5M LiTFSI] physico-chemical properties

# Introduction

In this chapter, the techniques and the methodology used to characterize all the liquid and solid electrolyte samples are described. The aim of this methodology is to offer here a systematic method to compare ionic liquids and ionogels with exactly the same experimental conditions. The strategy is to measure the effect of salt addition in ILs and the effect of confinement on structural and transport properties.

## 3.1 Assessing the electrolyte thermal stability

In part 2.1.1, the necessity to study the thermodynamics of ILs was discussed. We are interested in the stable temperatures range in which the IL will not change phase and stay in a liquid state. DSC is a common technique to assess the phase transitions of mixtures and sometimes obtain the phase diagram. Figure 3.1 shows the thermal stability diagram for the mixture EMImTFSI + 0.5M LiTFSI from -100°C to +150°C measured by Differential Scanning Calorimetry (DSC). The following thermograms were recorded after heating the sample up to +150°C to erase the thermal history. Then the samples are cooled down to -100°C with a cooling rate of 58°C/min which was the fastest rate possible on the machine and considered as a rapid cooling.

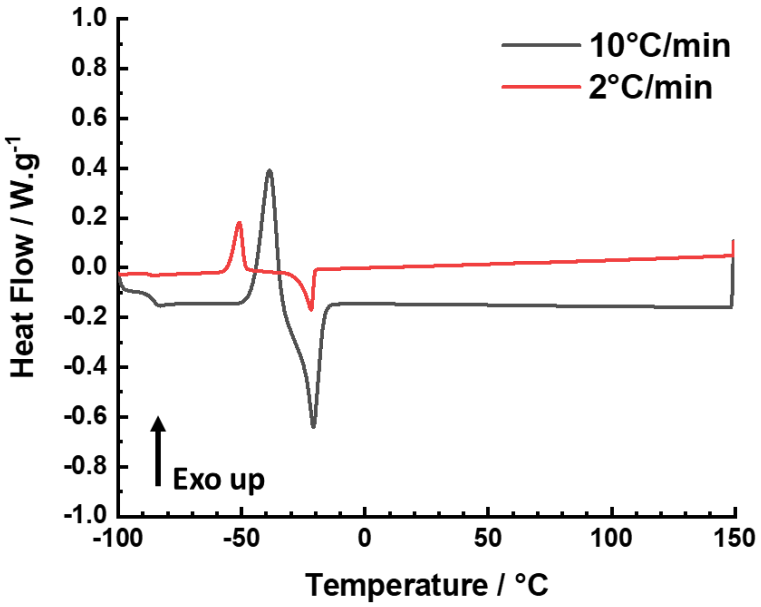


**Figure 3.1: Thermogram for the mixture EMImTFSI + 0.5M LiTFSI**

On EMImTFSI+0.5M LiTFSI thermal stability plot we can note that from -10°C up to 150°C the ternary ionic liquid does not present any phase change. In this range of temperatures, it remains in a liquid state with supposedly all lithium salt crystals dissolved. Nevertheless, it has been reported that the melting of EMImTFSI is inhomogeneous and ionic liquid crystals traces could be found under -6°C.[1] DSC needs to be coupled with other techniques such as Neutrons Diffraction (ND) and X-rays Diffraction (WAXS) if the exact transition temperature and structure of residual crystals need to be studied especially in the case of mixtures. This work focused on the change of phase transitions temperatures between samples. The priority here is to identify the main transitions and their variations.

Three main transitions can be identified below -10°C on Figure 3.2. Two kind of phase transitions exist: first order phase transitions which are the non-reversing part of the heat flow and second order which are the reversing part of the heat flow. For example, in this case study, the glass transition is a first order transition whereas the cold crystallization or solid-to-solid phase transition, and melting are second order phase transitions. This detail is important to justify the study of the thermal stability window through two different heat scan rates. The 10°C/min scan rate is fast and then is more appropriate to visualize first order phase transitions (insert in Figure 3.2). On the other hand, the 2°C/min scan rate is slower and brings more accuracy on second-order phase transition temperatures due to a smoother thermodynamic equilibrium. Main phase transitions of this specific mixture is reported in Table 3.1.

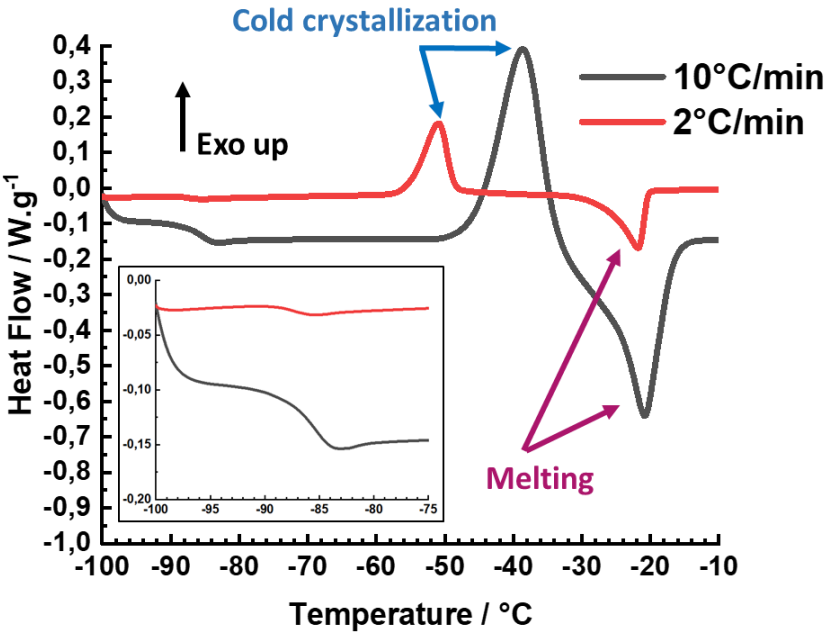


**Figure 3.2: Phase transitions in EMImTFSI + 0.5M LiTFSI electrolyte**

**Table 3.1: Phase transitions for EMImTFSI + 0.5M LiTFSI**

| | Glass transition temperature | Cold crystallization temperature | Melting point |
|---|---|---|---|
| **EMImTFSI+0.5M LiTFSI (10°C.min$^{-1}$)** | -86°C | -46°C (offset)<br>-38°C (maximum) | -29°C (offset)<br>-21°C (minimum) |
| **EMImTFSI+0.5M LiTFSI (2°C.min$^{-1}$)** | -86°C | - 56°C (offset)<br>-51°C (maximum) | -28°C (offset)<br>-22°C (minimum) |

## 3.2 Measuring the macroscopic ionic conductivity

The mobility of ions in ILs is controlled by different interactions between those ions. Macroscopic ionic conductivity of electrolytes can be measured by Electrochemical Impedance Spectroscopy (EIS). The value of the ion's conductivity measured by EIS is based on the migration of charged species under an electric field.[2] Ions pairs or aggregates that are uncharged will not participate in the macroscopic ionic conductivity. These aggregates take part in the global viscosity of the mixture, lowering down the ionic conductivity (Figure 3.3).

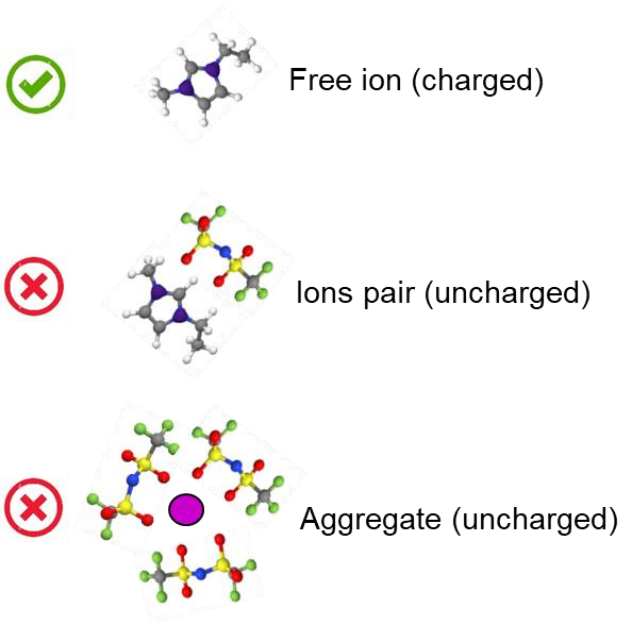


**Figure 3.3: Ionic species considered in the macroscopic ionic conductivity**

The macroscopic ionic conductivity is a concept which describes the internal impedance of an electrolyte between two conductive electrodes (Figure 3.4). This simple cell can be described as an

electric circuit with $R_b$ the bulk resistance, which is essential in the electrolyte conductivity study, $C_g$ the geometrical capacitance and $C_{dl}$ the double layer capacitance.

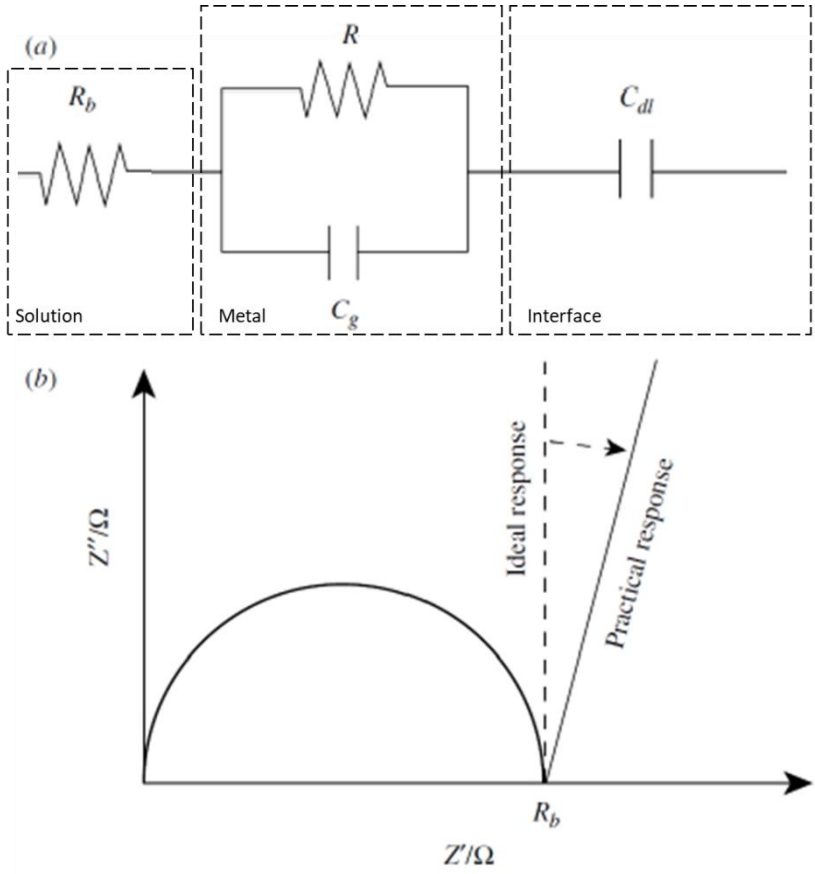


**Figure 3.4: Equivalent circuit for internal impedance of an electrolyte between two conductive electrodes (a) and the corresponding Nyquist plot (b) (adapted from [3])**

EIS principle is based on the Ohm law:

$$U = R.I$$

**Equation 3.1**

Where $U$ is potential difference applied between the two electrodes (V); $R$ the internal resistance of the electrolyte (Ω); and $I$ the resulting current (A).

For a given sinusoidal tension applied the resultant sinusoidal current is measured and then the electrolyte complex impedance. By extracting the real and imaginary part of this complex impedance the corresponding Nyquist plot for [EMImTFSI + 0.5M LiTFSI] at different temperatures was obtained (see Figure 3.6.).

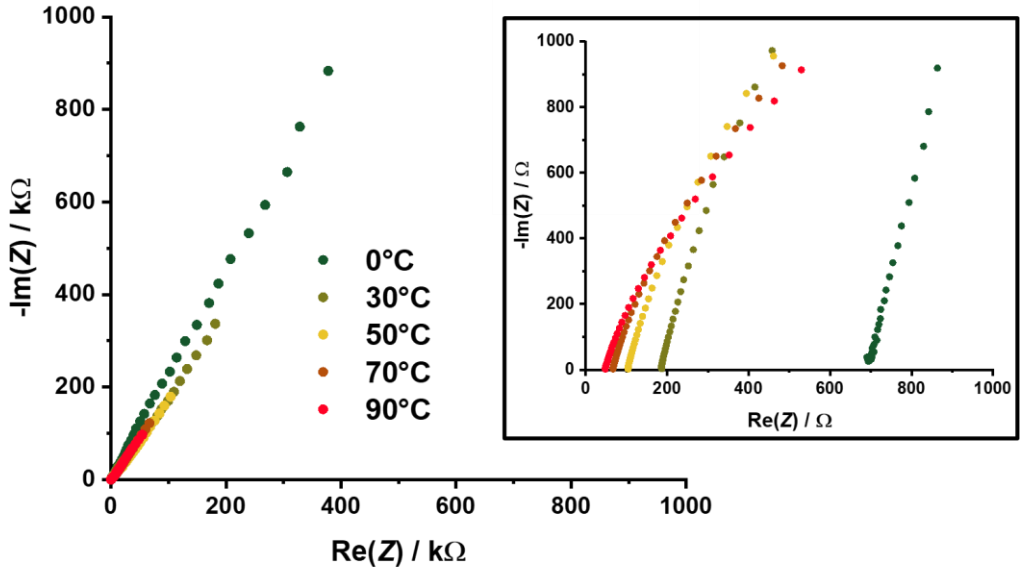


**Figure 3.5: Nyquist plots of EMImTFSI + 0.5M LiTFSI at different temperatures**

The ionic conductivity of the electrolyte is given by the following equation:

$$\sigma = \frac{e}{R.S}$$

**Equation 3.2**

Where $\sigma$ is the ionic conductivity in S.cm$^{-1}$; $e$ the thickness of the sample in cm; $S$ the surface area of the sample in contact with the stainless steel electrodes in cm$^2$ and $R$ the real part of the complex Impedance in Ω. In other words, the ionic conductivity is normalized by the sample's shape factor. The molar conductivity $\Lambda_m$ [4] is also defined as:

$$\Lambda_m = \sigma.V_m$$

**Equation 3.3**

In the case of mixture, as mentioned in part 2.1.1.c, we will consider that the entire molar volume of the electrolyte solution is proportional to the molar ratio of each species. For example, 1 mole of EMIMTFSI + 0.5M LiTFSI, contains:

- 0.874 mole of EMImTFSI with a molar volume of 257.4 cm$^3$.mol$^{-1}$;
- 0.126 mole of LiTFSI with a molar volume of 215.9 cm$^3$.mol$^{-1}$.

In the end, the approximative molar volume for EMIMTFSI + 0.5M LiTFSI is equal to 252.1 cm$^3$.mol$^{-1}$ and the measured ionic conductivity for this sample at 50°C is 10 mS.cm$^{-1}$.

The calculated molar conductivity for this electrolyte at 50°C is **2.52 S.cm$^2$.mol$^{-1}$**. This value is crucial and will be discussed later to define an essential concept in ionic liquid-based electrolyte: the ionicity.

By convention, a plot of the decimal logarithm of the ionic conductivity in function of 1000/T is used in this work (Figure 3.7).

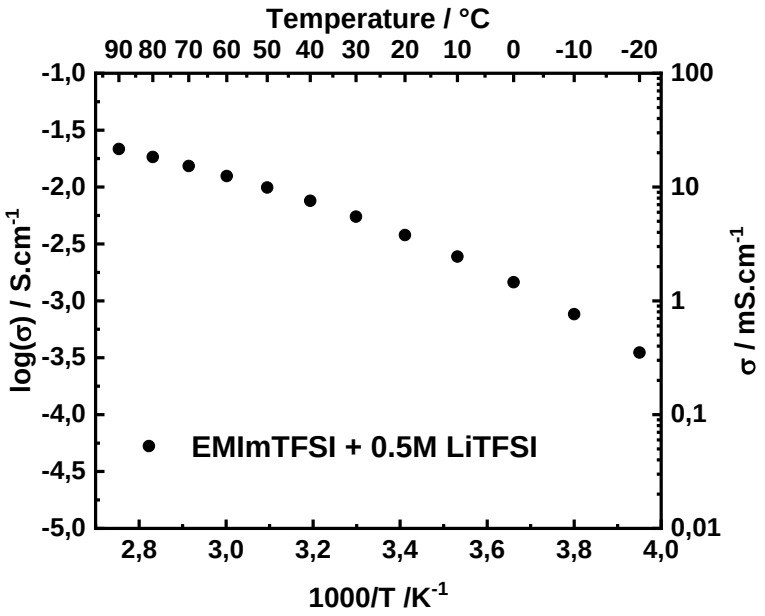


**Figure 3.6: Ionic conductivity at different temperatures of [EMImTFSI + 0.5M LiTFSI] electrolyte**

These measurements are cycled twice on each cell on two identical samples to obtain a approximate standard deviation showed in Annex 1.

Here again the ionic conductivity increases with temperature for this ternary ionic liquid. The nonlinear profile at low temperatures is mainly due to the melting phase transition mentioned in the previous subpart. However, it is interesting to describe the evolution of ionic conductivity in function of 1/T as an Arrhenius function only for data points at high temperatures:

$$\sigma = \sigma_0 . exp(\frac{-E_a}{k_B . T})$$

$$\ln(\sigma) = \ln(\sigma_0) - \frac{E_a}{k_B . T}$$

**Equations 3.4**

Where $\sigma$ is the ionic conductivity in S.cm$^{-1}$; $\sigma_0$ is the theoretical ionic conductivity at infinite temperature in S.cm$^{-1}$; $E_a$ is the activation energy for charged species' mobility in an electric field in J; and $k_B$ is the Boltzmann's constant.

The slope of the previous function shown on Figure 3.7 gives the activation energy for charged species mobility in the electrolyte. The infinite temperature conductivity is given by the interception with Y axis and the values are reported in Table 3.2.

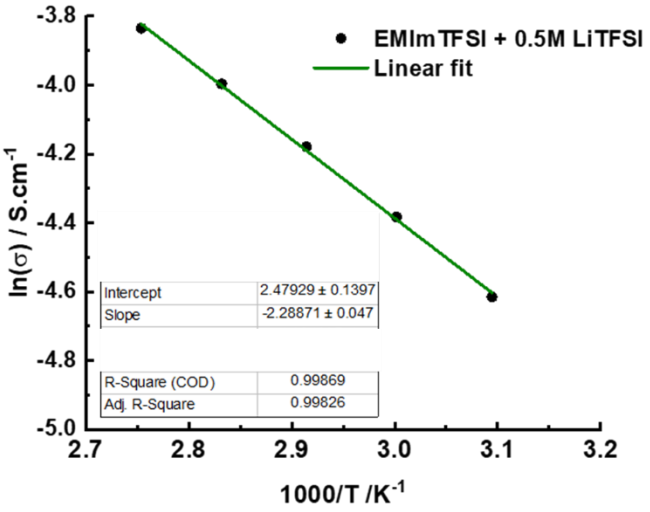


**Figure 3.7: Arrhenius fit for ionic conductivity of EMImTFSI + 0.5M LiTFSI electrolyte**

**Table 3.2: Key parameters for [EMIMTFSI + 0.5M LiTFSI] Arrhenius fit**

| | $\sigma_0$ (S.cm$^{-1}$) | $E_A$ (kJ.mol$^{-1}$) |
|---|---|---|
| **EMImTFSI+0.5M LiTFSI** | 11.93 | 19.03 |

Even at high temperature, the ionic conductivity dependency with temperature is not linear and so the Arrhenius fit quality is not optimal. One better model to describe evolutionof ionic conductivity in function of 1/T is the Vogel-Fulcher-Tammann (VFT) equation:

$$\sigma = \sigma_0 . exp(\frac{-B}{T - T_0})$$

$$\ln(\sigma) = \ln(\sigma_0) - \frac{B}{T - T_0}$$

**Equation 3.5**

Where $\sigma$ is the ionic conductivity in S.cm$^{-1}$; $\sigma_0$ is the theoretical ionic conductivity at infinite temperature in S.cm$^{-1}$; $B$ is pseudo-activation barrier dependant on the free volume in the ionic solution; and $T_0$ is the ideal glass transition temperature at which the molecular motion stops (Vogel's temperature).

Another important parameter is the fragility index D, which was proposed by Angell [5,6] and it can be defined as a quantification of the thermal sensitivity of the liquid structure:

$$\mathrm{D} = \frac{B}{T_0}$$

**Equation 3.6**

If the ionic conductivity of an ionic liquid solution diverges from Arrhenius behaviour that means the solution is fragile. Its fragility index D is low, and the mobility of ions is facilitated. In other words, a fragile liquid can re-arrange easily under weak constraints. This dynamic is characterized by short relaxation times and a non-Fick diffusion. VTF-fitting is shown on Figure 3.8. with the main parameters tabulated in Table 3.3.

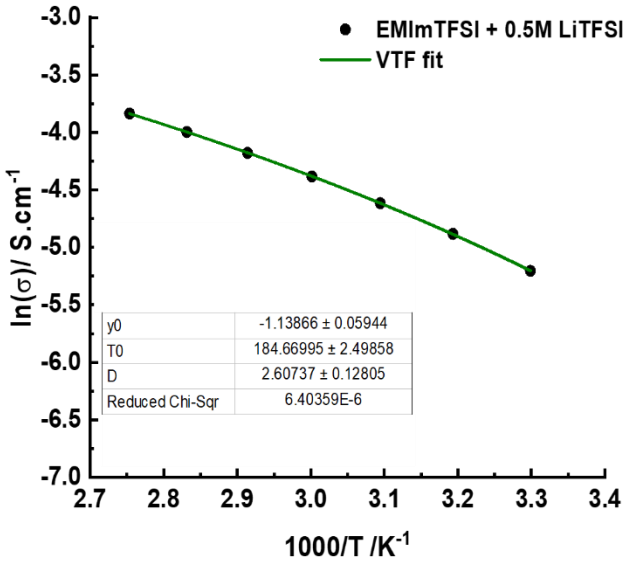


**Figure 3.8: VTF fit for ionic conductivity of EMImTFSI + 0.5M LiTFSI electrolyte**

**Table 3.3: Key parameters for EMIMTFSI + 0.5M LiTFSI VFT fit**

| | $\sigma_0$ (S.cm$^{-1}$) | To (K$^{-1}$) | $T_0/T_g$ * | D index (S.cm$^{-1}$) |
|---|---|---|---|---|
| **EMImTFSI+0.5M LiTFSI** | 390.6 | 184.7 | 0.99 | 2.6 |

*The ratio between the fitted value of $T_0$ and the measured glass transition temperature $T_g$ is another way to assess the fragility of a mixture.[7]

# 3.3 Self-Diffusion coefficients for every ion in the mixture

Once the macroscopic ionic conductivity was obtained by EIS, it is interesting to look at the specific diffusion for every species in the IL. Indeed, the measure of self-diffusion coefficients (D) is the best option to understand the ions dynamics at a molecular scale. Pulsed-Field Gradient Nuclear Magnetic Resonance (PFG NMR) experiment is a direct technique to obtained diffusion coefficient values for all the IL-based electrolyte molecules. The only limitation for this technique is the targeted nuclei isotope abundance. All nuclei involved in the IL-based electrolyte systems are summarized on figure 3.9 and their NMR isotopes characteristics are reported in Table 3.4.

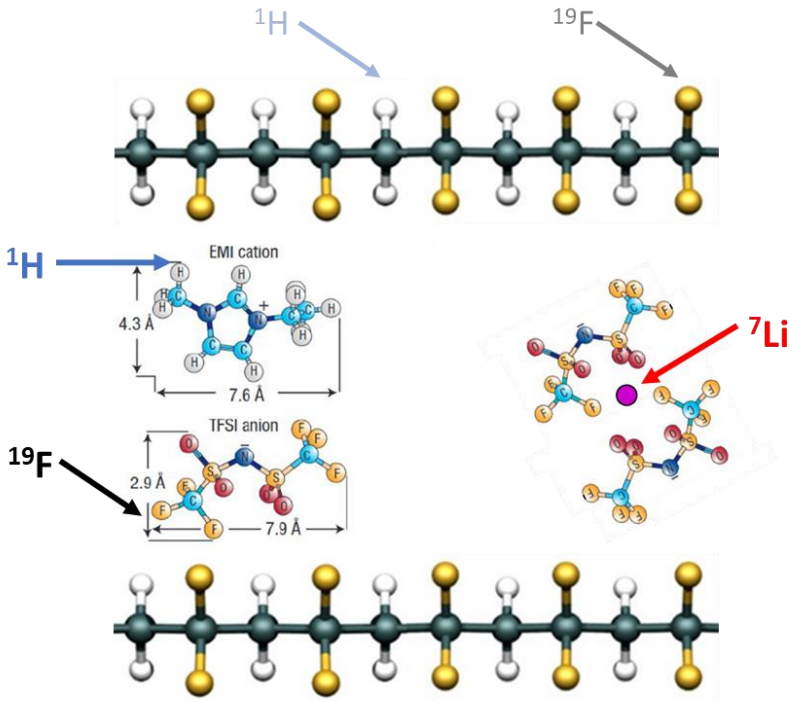


**Figure 3.9: Active nuclei for PFG NMR measurements in our systems**

**Table 3.4: Active nuclei for PFG NMR measurements and properties**

| Ion | Active nuclei | Abundance of the isotope (%)* | Frequency (MHz)* | Spin* |
|---|---|---|---|---|
| **EMIM** | $^{1}H$ | 99.9 | 750 | 1/2 |
| **TFSI** | $^{19}F$ | 100 | 706 | 1/2 |
| **$Li^{+}$** | $^{7}Li$ | 92.6 | 291.5 | 3/2 |
| **$Na^{+}$** | $^{23}Na$ | 100 | 198.5 | 3/2 |
| **$Mg^{2+}$** | $^{25}Mg$ | 10.1 | 46 | 5/2 |
| **$Zn^{2+}$** | $^{67}Zn$ | 4.11 | 47 | 7/2 |
| **$Ca^{2+}$** | $^{43}Ca$ | 0.15 | 50.5 | 5/2 |

*https://nmr.cemhti.cnrs-orleans.fr/dmfit/tables/tableisotopes.aspx

This PFG NMR measurements do not distinguish ionic pairs or aggregates from free ions during the NMR time scale. This is a major distinction compared to the dynamics measured by EIS (Figure 3.10). In the case of EIS, the macroscopic ionic conductivity is an average of the mobility of charged species whereas for PFG NMR the self-diffusion coefficient is an average of the diffusion of each nucleus. [8]

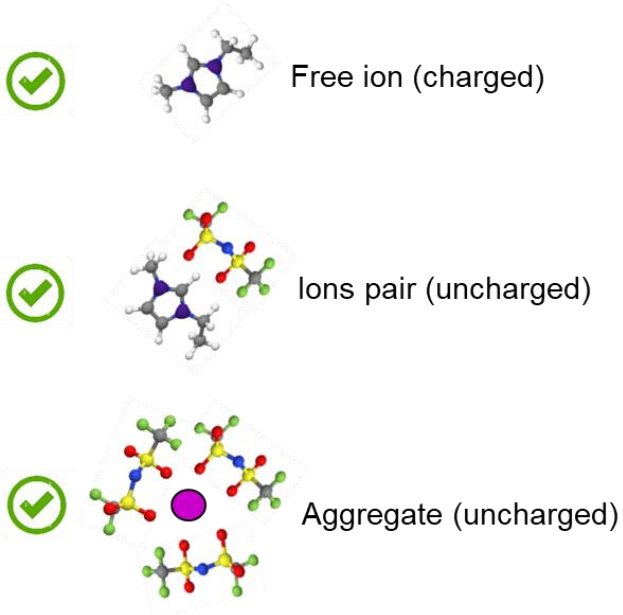


**Figure 3.10: Ionic species considered in PFG NMR**

Although for usual NMR measurements the magnetic field needs to be perfectly constant, in PFG NMR a magnetic field gradient is applied (Figure 3.11).

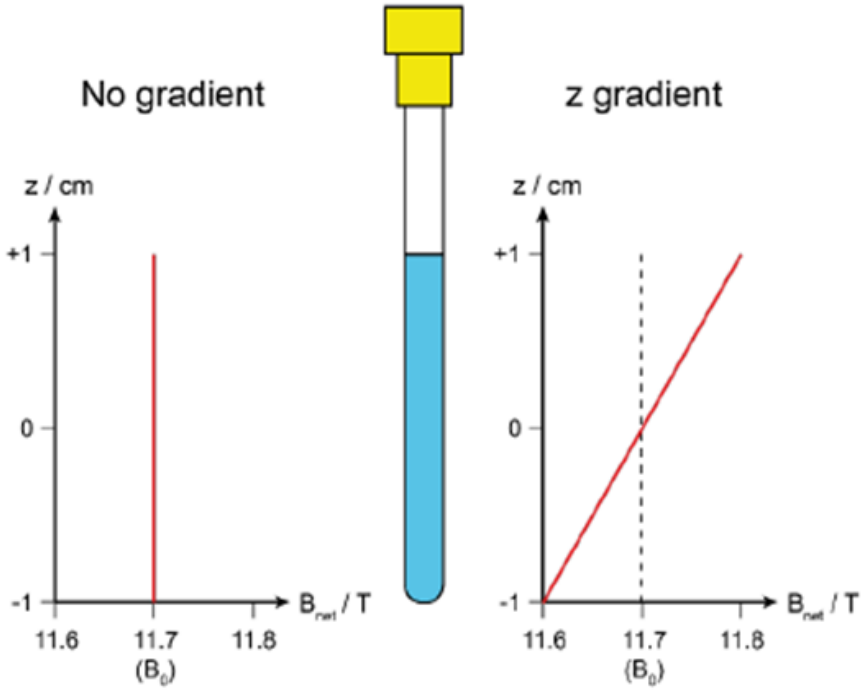


**Figure 3.11: Field gradient through the sample in PFG NMR (credit to Pr. Luke O'Dell)**

Both liquid and solid samples were placed in small rotors (around 1 cm high, and Ø1mm) in a classical NMR tube with controlled height of the rotor in order to insure its position in the field gradient. The whole sequence including the strength of the gradient, the pulses and their duration is controlled. Self-diffusion (D) measurements for $^{1}H$, $^{19}F$, and $^{7}Li$ were performed at 50°C, 70°C, and 90°C using a pulsed field gradient stimulated echo NMR pulse sequence with a Bruker Advance III 7.05 T spectrometer equipped with a 5mm Bruker Diff50 probe with a maximum strength of 3,000 $G.cm^{-1}$. The gradient pulse length was 2 ms and the diffusion time was 20 ms. To extract the diffusion coefficients, the data were fitted in the Brucker Topspin software using the Stejskal-Tanner equation:

$$I = I_0 . \exp(-D\gamma^2 g^2 \delta^2 \left(\Delta - \frac{\delta}{3}\right))$$

**Equation 3.7**

Where $I$ is the observed signal intensity; $I_0$ is the maximum signal intensity; $\gamma$ is the the gyromagnetic ratio of the nucleus being observed; $g$ is the gradient strength; $\delta$ is the gradient pulse duration and $\Delta$ is diffusion time.

The corresponding coefficients are shown in Figure 3.12 for the mixture [EMIMTFSI + 0.5M LiTFSI]. The water content could affect the self-diffusion coefficients measurements by increasing slightly the D value. Precautions has been taken to dry the samples before each measurements. In any case, the signal for $EMIm^{+}$ is stronger than $H_2O$ signal because of the proportions in the ternary IL.

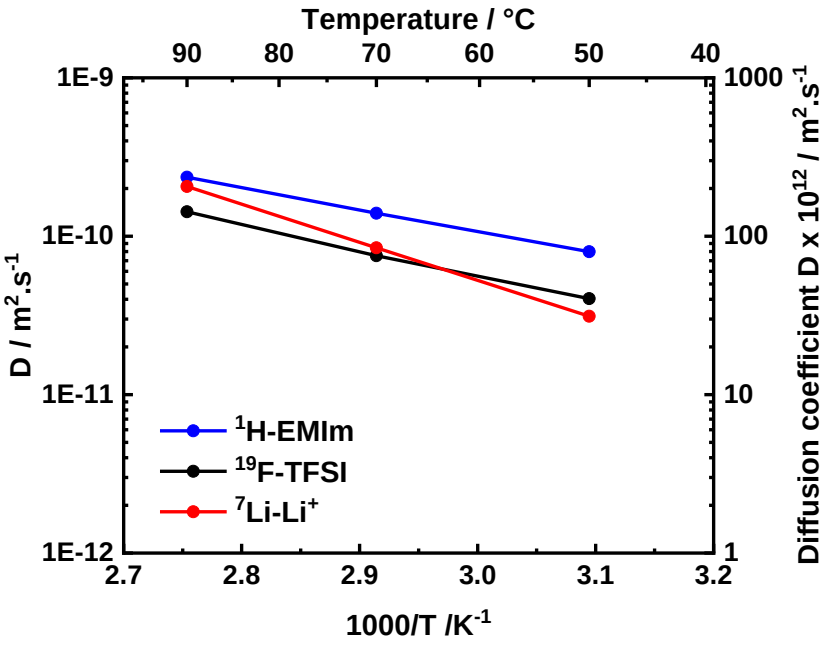


**Figure 3.12: Self-diffusion coefficients in [EMIMTFSI + 0.5M LiTFSI]**

Self-diffusion coefficients for every species decrease with temperature. This is coherent with the thermal energy brought in the system that enable better mobility at high temperatures. The profile is linear here and again it is interesting to describe the dependency on temperatures with an Arrhenius function:

$$D = D_0 . exp(\frac{-E_a}{k_B . T})$$

$$\ln(D) = \ln(D_0) - \frac{E_a}{k_B . T}$$

**Equation 3.8**

Where $D$ is the self-diffusion coefficient in $m^2.s^{-1}$; $D_0$ is the theoretical diffusion coefficient at infinite temperature in $m^2.s^{-1}$; $E_a$ is the activation energy for the nucleus mobility in in J; and $k_B$ is the Boltzmann's constant.

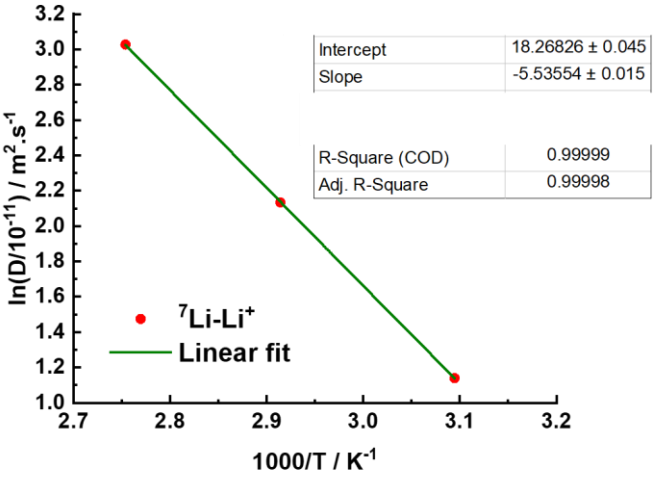


**Figure 3.13: Arrhenius fit for $D_{Li+}$ in EMImTFSI + 0.5M LiTFSI electrolyte**

The slope of the previous fit gives the activation energy for the molecule diffusion in the electrolyte and the infinite temperature self-diffusion coefficient is given by the interception with Y axis.

It is possible to use a VTF fit instead but more data points are needed.

**Table 3.5: Key parameters for diffusion coefficients of EMIMTFSI + 0.5M LiTFSI Arrhenius fit**

| | $D_{Li+}$ 50°C ($m^2.s^{-1}$) | $D_0$ ($m^2.s^{-1}$) | $E_A$ ($kJ.mol^{-1}$) |
|---|---|---|---|
| **EMImTFSI+0.5M LiTFSI** | $3.1.10^{-11}$ | $8.6.10^{-7}$ | 46.03 |

Last, the limiting molar conductivity from the measure of diffusion coefficients using the Nerst-Einstein equation for n ions in the mixture can be calculated [9]:

$$\Lambda_{NMR} = \frac{F^2}{R.T} \sum_{i=0}^{n} x_i {e_i}^2 D_i$$

**Equation 3.9**

Where $F$ is Faraday constant; $R$ is gas constant; $x$ is the molar ratio of the ion i; $e$ its theoretical charge D its self-diffusion coefficient.

For example, the limiting molar conductivity for EMIMTFSI + 0.5M LiTFSI at 50°C is equal to 3.952 $S.cm^2.mol^{-1}$.

Finally, it is possible to calculate the degree of ionicity (*I*) of the mixture using the following equation[10]:

$$I = \frac{\Lambda_m}{\Lambda_{NMR}}$$

**Equation 3.10**

Where $I$ is the ionicity degree; $\Lambda_m$ is the molar conductivity measured by EIS; $\Lambda_{NMR}$ is the calculated limiting molar conductivity from self-diffusion coefficients measurements.
For the mixture EMIMTFSI + 0.5M LiTFSI, the degree of ionicity is equal to 63.8%.
This result means that in this electrolyte, up to 63.8% of the ions are free on average, not taking part in pairs or aggregates.

## 3.4 Probing ionic interactions and coordination sphere

The last spectroscopy used to characterize the samples is the Raman vibrational spectroscopy. This technique is widely used in ILs science. Indeed, probing ionic interactions at a molecular scale is essential to assess and identify the formation of aggregates at the equilibrium in the electrolyte.

Raman spectroscopy was performed on dried ILs (in glass vials) and ionogels with a Fourier Transform Raman (Bruker). A Nd-YAG laser of wavelength and power of 1064 nm and 500 mW, respectively, was used with a spectral resolution of 2 and 3 $cm^{-1}$. The spectrums are measured between 200 and 3200 cm-1 with 400 scans repetition.

Figure 3.14. shows the signal for the vibration band attributed to the symmetrical elongation of the anion TFSI between 720 $cm^{-1}$ and 780 $cm^{-1}$ in the neat ionic liquid, in [EMImTFSI + 0.5M LiTFSI] mixture and in the LiTFSI salt. The spectra are normalized to the 1025 $cm^{-1}$ vibration band intensity which is attributed to the imidazolium ring in plane symmetric stretching (in plane), $CH_3$(N) and $CH_2$(N) stretching. [11] It is an invariant vibrational band specific for EMImTFSI, it is not disrupted by the salt addition or later the confinement. This vibration band is intense enough to be a reliable reference to normalize the intensity and more relevant that the more intense 741.4 $cm^{-1}$ vibration band that could be salt dependant.

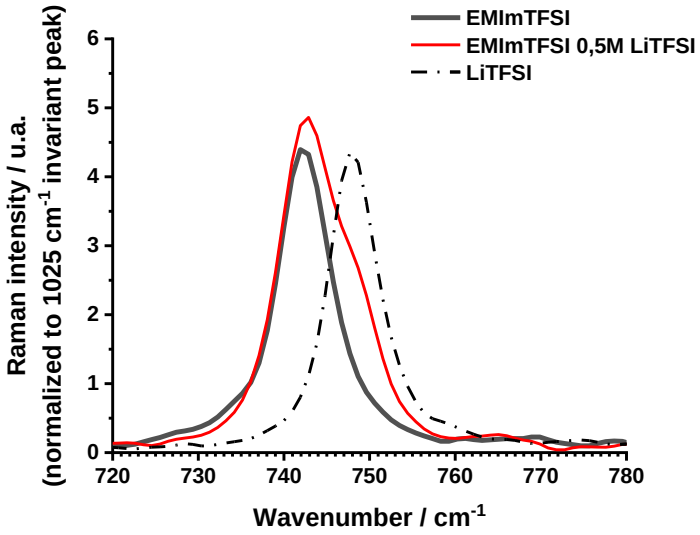


**Figure 3.14: Raman spectrum centred on the symmetrical expansion-contraction mode of TFSI for EMImTFSI, [EMImTFSI +0.5M LiTFSI] and LiTFSI**

In the pure EMImTFSI ionic liquid, the vibration band at 741.4 $cm^{-1}$ is the most intense signal. This band is attributed to the symmetrical expansion-contraction mode of TFSI. As the salt is added, a second population of vibrating TFSI appears. The shoulder or second band is related to the presence of metallic cations in TFSI environment (here $Li^+$). [12,13] Raman spectrum clearly show this second population of TFSI in the [EMImTFSI + 0.5M LiTFSI] mixture. This second band at 748.2 $cm^{-1}$ corresponds to the vibration band of TFSI in LiTFSI (Table 3.6). The energy at stake depends on the strength of the TFSI to cation interaction. The more attractive the cation is, the more energy is needed for TFSI to vibrate compared to the EMIm-TFSI interaction.

**Table 3.6: TFSI- expansion contraction bands in the neat ionic liquid, mixture and salt**

| | 1st vibration band position ($cm^{-1}$) | 2nd vibration band position ($cm^{-1}$) | Energy shift (eV) |
|---|---|---|---|
| **EMImTFSI** | 741.4 | - | - |
| **EMImTFSI + 0.5M LiTFSI** | 741.4 | 748.2 | 0.75 |
| **LiTFSI** | - | 748.2 | - |

The spectrum above can be decomposed to extract the different contributions of the different population of TFSI in the samples. In the literature, several methods are used to attribute all the contributions of TFSI populations with different physical justifications.[14,15] The following decomposition is made with 3 pseudo-Voigt functions in order to take into consideration the two

conformations of the "free" $TFSI^-$ in cis and trans conformations and one function attributed to the coordinated TFSI in interaction with metallic cation. The pseudo-Voigt functions are given with this equation:

$$y = y_0 + A[\mu \frac{2}{\pi} \frac{\omega}{4(x-x_c)^2+\omega^2} + (1-\mu) * \frac{\sqrt{4\ln(2)}}{\omega\sqrt{\pi}} * \exp(-\frac{4\ln(2)}{\omega^2} * (x-x_c)^2)]$$

**Equation 3.11**

Where $y_0$ is the offset, $x_c$ the band position, $A$ the integrated intensity, $\mu$ the shape factor due to Lorenzian function proportion compared to the Gaussian proportion et $\omega$ its width at mid-height.

Figure 3.15. shows the decomposition of the 741.4 $cm^{-1}$ the vibration band of EMImTFSI. Two populations coexist corresponding to the different states of TFSI in the IL. In the literature, this decomposition is justified by the conformation cis and trans of the TFSI anion in the neat IL.[16]

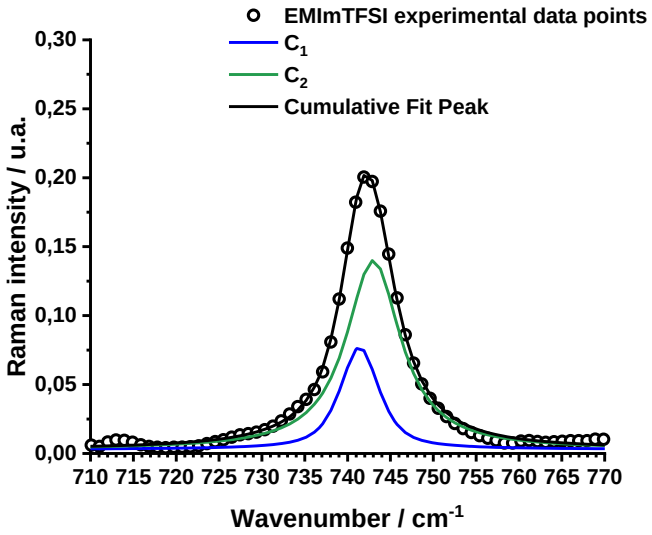


**Figure 3.15: Decomposition of Raman spectrum for EMImTFSI**

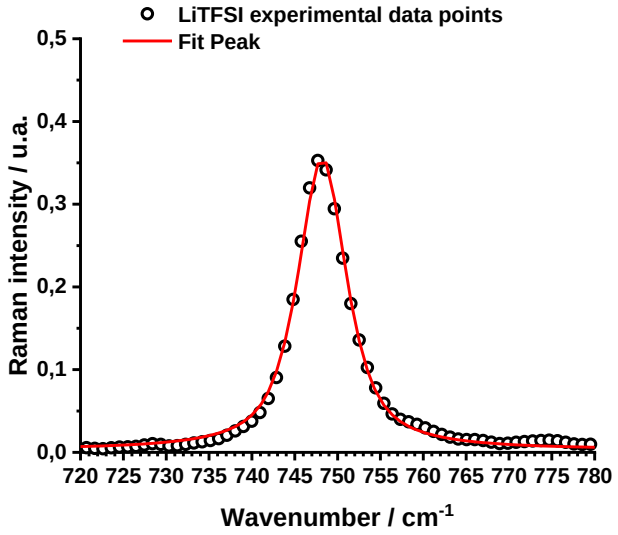


**Figure 3.16: Decomposition of Raman spectrum for LiTFSI**

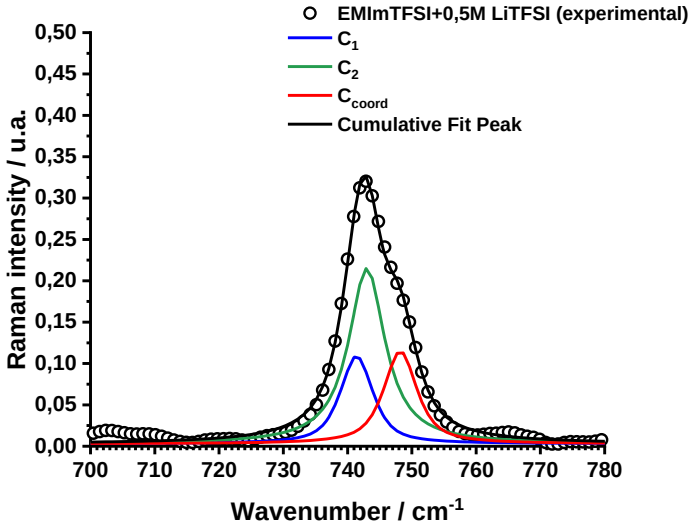


**Figure 3.17: Decomposition of Raman spectrum for [EMImTFSI +0.5M LiTFSI]**

**Table 3.6: Raman fit parameters to obtain the coordination number**

| | Pseudo-Voigt functions parameters | EMImTFSI | EMImTFSI + 0.5M LiTFSI | LiTFSI |
|---|---|---|---|---|
| | $y_0$ | **0.003** | **0.003** | **0.003** |
| $C_1$ | *A* | 0.659 | 0.963 | - |
| | *w* | **6** | **6** | - |
| | *μ* | **0.775** | **0.775** | - |
| | $x_c$ | **741.4** | **741.4** | - |
| **C2** | *A* | 1.458 | 2.114 | - |
| | *w* | **6.6** | **6.6** | - |
| | *μ* | **1** | **1** | - |
| | $x_c$ | **743** | **743** | - |
| $C_{ccord}$ | *A* | - | 1.099 | 3.456 |
| | *w* | - | **6.6** | **6.6** |
| | *μ* | - | **0.836** | **0.836** |
| | $x_c$ | - | **748.2** | **748.2** |

The coordination number is obtained from fitting the experimental Raman spectrum and the following equation:

$$n = \frac{A_{coord}}{A_{coord} + A_{non\ coord}} * \frac{1}{x}$$

**Equation 3.12**

Where $n$ is the coordination number, $A_{coord}$ the coordinated TFSI vibration band area, $A_{non\ coord}$ the sum of non-coordinated TFSI vibration band areas and $x$ the molar fraction of salt in the sample.

The calculated coordination number for the [EMImTFSI +0.5M LiTFSI] mixture is **2.01**. That means that on average, in this IL, 1.9 molecules of TFSI-surround the Li+ cations. This value is in accordance with the literature for similar pyrrolidinium-based ILs (2 $TFSI^-$ molecules).[16]

# Conclusion

For the last 20 years, research groups tried to bring a clear definition of ionic liquids properties and behaviour as a function of temperature or salt dopant. The conclusion on studying ternary ILs is that this family of molten salt is promising for energy storage electrolytes applications. More studies that are recent focused on the transport properties in these solutions. An overview of the different techniques used to characterize the series of samples is presented in this chapter. Especially the coupled EIS and PFG NMR, which is a power tool to understand the dynamics in such polarized environment. Furthermore, many specific physicochemical properties were given through a liquid sample electrolyte [EMIMTFSI + 0.5M LiTFSI], especially the glass transition temperature (-86°C), the ionicity (63.8%) and the coordination number (1.9) that help to understand how to optimize such electrolytes to tackle viscosity. The results showed that lowering the glass transition temperature, increasing the macroscopic ionic conductivity, increasing the self-diffusion coefficients, and reducing the coordination number around lithium are the main objectives to improve the electrolytes performance.

In the next two chapters, we will present and discuss the effect of adding metal salts to ionic liquids and the effect of confining them in the polymer matrix for monovalent and bivalent cations.

# References


(1) Rotnicki, K.; Sterczyńska, A.; Fojud, Z.; Jażdżewska, M.; Beskrovnyi, A.; Waliszewski, J.; Śliwińska-Bartkowiak, M. Phase Transitions, Molecular Dynamics and Structural Properties of 1-Ethyl-3-Methylimidazolium Bis(Trifluoromethylsulfonyl)Imide Ionic Liquid. *Journal of Molecular Liquids* **2020**, *313*, 113535. https://doi.org/10.1016/j.molliq.2020.113535.

(2) Tokuda, H.; Tsuzuki, S.; Susan, Md. A. B. H.; Hayamizu, K.; Watanabe, M. How Ionic Are Room-Temperature Ionic Liquids? An Indicator of the Physicochemical Properties. *J. Phys. Chem. B* **2006**, *110* (39), 19593–19600. https://doi.org/10.1021/jp064159v.

(3) Ohno, H. Electrochemical Aspects of Ionic Liquids; 2011.

(4) MacFarlane, D. R.; Meakin, P.; Sun, J.; Amini, N.; Forsyth, M. Pyrrolidinium Imides: A New Family of Molten Salts and Conductive Plastic Crystal Phases. *J. Phys. Chem. B* **1999**, *103* (20), 4164–4170. https://doi.org/10.1021/jp984145s.

(5) Angell, C. A. Structural Instability and Relaxation in Liquid and Glassy Phases near the Fragile Liquid Limit. *Journal of Non-Crystalline Solids* **1988**, *102* (1–3), 205–221. https://doi.org/10.1016/0022-3093(88)90133-0.

(6) Xu, W.; Cooper, E. I.; Angell, C. A. Ionic Liquids: Ion Mobilities, Glass Temperatures, and Fragilities. *J. Phys. Chem. B* **2003**, *107* (25), 6170–6178. https://doi.org/10.1021/jp0275894.

(7) Guyomard-Lack, A.; Delannoy, P.-E.; Dupré, N.; Cerclier, C. V.; Humbert, B.; Le Bideau, J. Destructuring Ionic Liquids in Ionogels: Enhanced Fragility for Solid Devices. *Phys. Chem. Chem. Phys.* **2014**, *16* (43), 23639–23645. https://doi.org/10.1039/C4CP03187C.

(8) Noda, A.; Hayamizu, K.; Watanabe, M. Pulsed-Gradient Spin−Echo $^{1}$H and $^{19}$F NMR Ionic Diffusion Coefficient, Viscosity, and Ionic Conductivity of Non-Chloroaluminate Room-Temperature Ionic Liquids. *J. Phys. Chem. B* **2001**, *105* (20), 4603–4610. https://doi.org/10.1021/jp004132q.

(9) Atkins, P. W. *Physical Chemistry*, Oxford.; 1994.

(10) MacFarlane, D. R.; Forsyth, M.; Izgorodina, E. I.; Abbott, A. P.; Annat, G.; Fraser, K. On the Concept of Ionicity in Ionic Liquids. *Phys. Chem. Chem. Phys.* **2009**, *11* (25), 4962. https://doi.org/10.1039/b900201d.

(11) Kiefer, J.; Fries, J.; Leipertz, A. Experimental Vibrational Study of Imidazolium-Based Ionic Liquids: Raman and Infrared Spectra of 1-Ethyl-3-Methylimidazolium Bis(Trifluoromethylsulfonyl)Imide and 1-Ethyl-3-Methylimidazolium Ethylsulfate. *Appl. Spectrosc., AS* **2007**, *61* (12), 1306–1311.

(12) Lassègues, J.-C.; Grondin, J.; Talaga, D. Lithium Solvation in Bis(Trifluoromethanesulfonyl)Imide-Based Ionic Liquids. *Phys. Chem. Chem. Phys.* **2006**, *8* (48), 5629–5632. https://doi.org/10.1039/B615127B.

(13) Guyomard-Lack, A.; Said, B.; Dupré, N.; Galarneau, A.; Le Bideau, J. Enhancement of Lithium Transport by Controlling the Mesoporosity of Silica Monoliths Filled by Ionic Liquids. *New J. Chem.* **2016**, *40* (5), 4269–4276. https://doi.org/10.1039/C5NJ03318G.

(14) Giffin, G. A.; Moretti, A.; Jeong, S.; Passerini, S. Complex Nature of Ionic Coordination in Magnesium Ionic Liquid-Based Electrolytes: Solvates with Mobile Mg $^{2+}$ Cations. *J. Phys. Chem. C* **2014**, *118* (19), 9966–9973. https://doi.org/10.1021/jp502354h.

(15) Borodin, O.; Giffin, G. A.; Moretti, A.; Haskins, J. B.; Lawson, J. W.; Henderson, W. A.; Passerini, S. Insights into the Structure and Transport of the Lithium, Sodium, Magnesium, and Zinc Bis(Trifluoromethansulfonyl)Imide Salts in Ionic Liquids. *J. Phys. Chem. C* **2018**, 14.

(16) Marie, A.; Said, B.; Galarneau, A.; Stettner, T.; Balducci, A.; Bayle, M.; Humbert, B.; Le Bideau, J. Silica Based Ionogels: Interface Effects with Aprotic and Protic Ionic Liquids with Lithium. *Phys. Chem. Chem. Phys.* **2020**, *22* (41), 24051–24058. https://doi.org/10.1039/D0CP03599H.

# Chapter 4 - Series of non-confined ionic liquids - effects of salt concentration and valence of the cation

# Introduction

It becomes essential to understand the thermodynamics and diffusion in these medium in order to optimise mass transport and insure safety in batteries and supercapacitors. As shown in Chapter 2, this molten salt family can be tailored to various applications because ILs can dissolve most of the salts used in electrolytes science.

To assess the effect of the confinement of ILs in polymer matrix in the next and last chapter, the evolution of physico-chemical properties induced by salt addition in ILs systems needs to be studied first. The goal here is to observe the influence of lithium, magnesium and zinc bis(trifluoromethansulfonyl)imide (respectively LiTFSI, $Mg(TFSI)_2$ and $Zn(TFSI)_2$) in 1-ethyl-3-methyimidazolium bis(trifluorosulfonyl)imide (EMImTFSI) IL. These systems are called ternary ionic liquids because of the second metal cation, which disrupts the EMIm-TFSI interactions in the neat IL, is fully part of the IL behaviour. Beforehand, a slowdown of dynamics is expected in doped ILs because of the strong attractive forces that these small and densely charged cations bring in this highly ionic environment.

To validate this hypothesis, the first step is to characterize the neat EMImTFSI following the methodology described in Chapter 3. Then, the influence of monovalent and bivalent metal cations in ILs will be discussed. Lithium is studied as a reference to compare the effect of the cation valence on the interactions and dynamics in the series of liquid samples. In a first part, the scientific argument and conclusions will be comprehensively presented. The second part focuses on the effect of metal cation valence. Finally, the comparison between series of samples will help to identify which mixtures are interesting for electrolytes applications. Especially, the following experiments aim to question the salt addition in ILs-based electrolyte as a charged species reservoir and the drawbacks that implies for transport properties.

# 4.1 Effect of salt concentration: lithium-based ternary ionic liquids

## 4.1.1 Thermal stability and phase transitions in Li-based ternary ionic liquids

First, the effect of salt addition on the phase transitions of the lithium-based ternary ILs is discussed. DSC experiments were performed at two different heating rate: 10°C/min and 2°C/min. On Figure 4.1.a. are represented the DSC plots for the neat IL and ternary ILs with increasing concentrations of lithium salt. The same phase transitions than in Chapter 3 are observed. The glass transitions occur at temperatures below - 70°C, the cold crystallizations between - 70°C and - 30°C and the melting transitions between - 30°C and + 10°C. Once again, there are no phase transitions between + 10°C and + 150°C. This is essential regarding the thermal stability of these electrolytes for ambient and high temperatures applications such as oil drilling or satellites power supply. Degradation temperature of the IL, measured by thermogravimetric analysis, need to be performed to conclude on the complete temperature range. Indeed, working at a temperature close to the melting point of an electrolyte will strongly affect equivalent series resistance (ESR) of the device because of the partial crystallization. The higher the ESR, the higher the amount of energy dissipated as heat and thus not stored in the device.

The thermograms are a fingerprint of the mixture. Indeed, each sample has specific phase transitions temperatures, which is a characteristics of the effect of salt addition on the thermodynamics properties of the ILs. However, up to a particular concentration, the thermogram flattens and the cold crystallization and melting are no longer visible with these experimental conditions. For example, the sample [EMImTFSI + 1M LiTFSI] do not present any phase transitions measurable but the glass transition: the glass transition is the only transition that enables a determination of the salt concentration, even at high concentration (Figure 4.1.b).

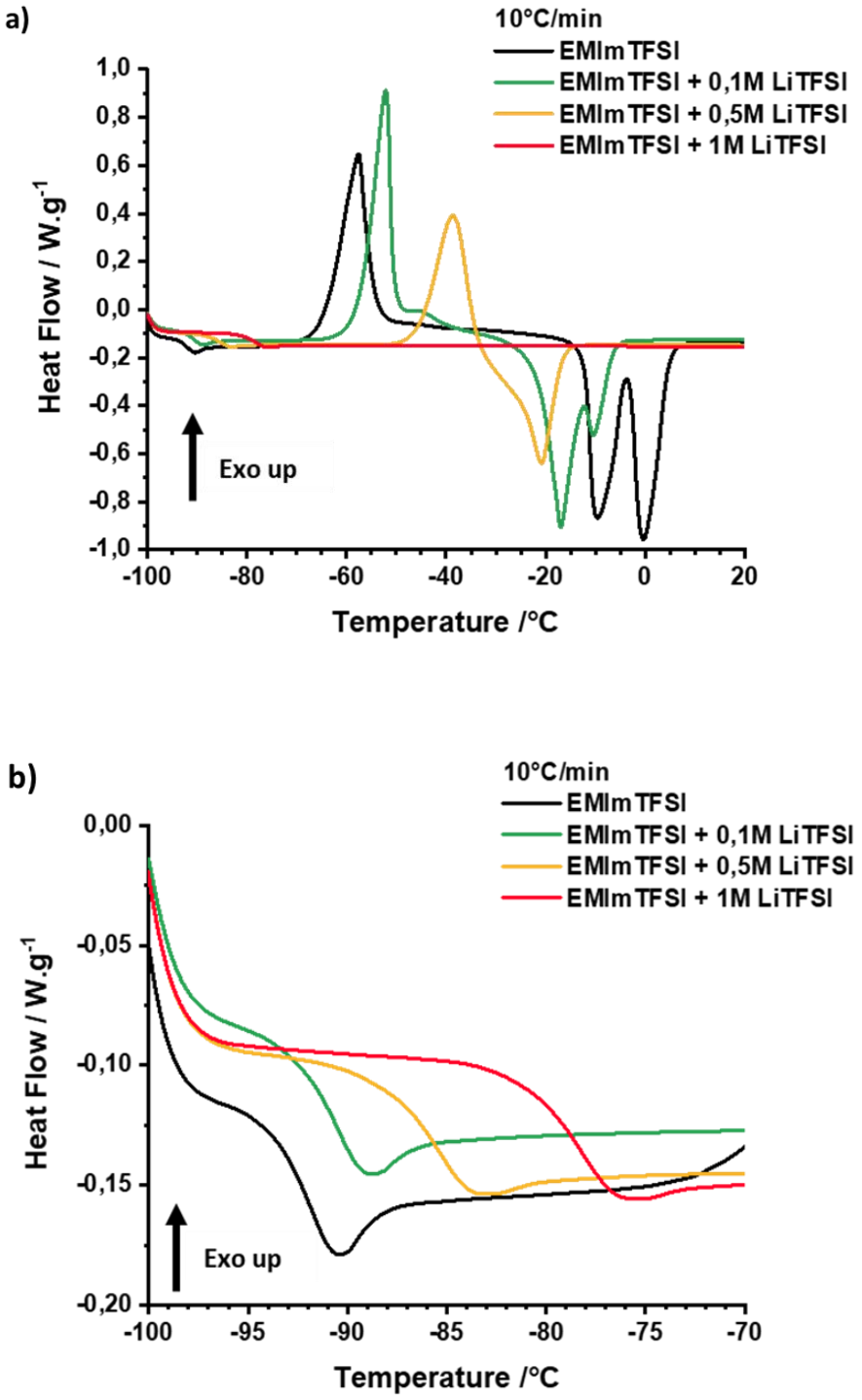


**Figure 4.1: a) Phase transitions for [EMImTFSI + LiTFSI] ternary ILs measured with a 10°C/min heating rate and b) a zoom on glass transitions**

Three observations can be made about the effect of lithium salts addition in EMImTFSI:

- The glass transition temperature increases with salt addition. More energy is needed to allow ions local dynamics in the solid amorphous phase when the concentration increases.

- The cold crystallization temperature increases with salt addition. More energy is needed to trigger the transition from amorphous phase to an crystalline solid phase when adding more LiTFSI
- The melting temperature decreases with salt addition. The liquid phase range starts at lower temperatures when adding lithium salt : although a crystalline phase was obtained for Li salt concentrations below 1M, some constraints lead to a decrease in reticular energy (unstability) of the solid phase. This is very interesting result because lowering the liquid to solid phase transition improves the thermal operating window of the electrolyte.

It is interesting to point out that similar conclusions were presented by others authors, e.g. by Zhou et al for the study of phase behaviour and crystalline structures for pyrrolidinium and imidazolium bis(trifluoromethanesulfonyl)imide.[1,2]

To conclude, more concentrated the mixture is, narrower the crystal phase temperature range and wider the amorphous and liquid phases temperature ranges are. To help understanding the firs orders phase transitions (crystallisation, melting), we plotted the same phase transitions but with a slower heating rate (Figure 4.2). As expected, on one hand the signal of the second order phase transition (glass transition) is much smaller. On the other hand, for first order phase transitions, we can more clearly observe the different phase's domains because the transitions temperatures are more accurate.

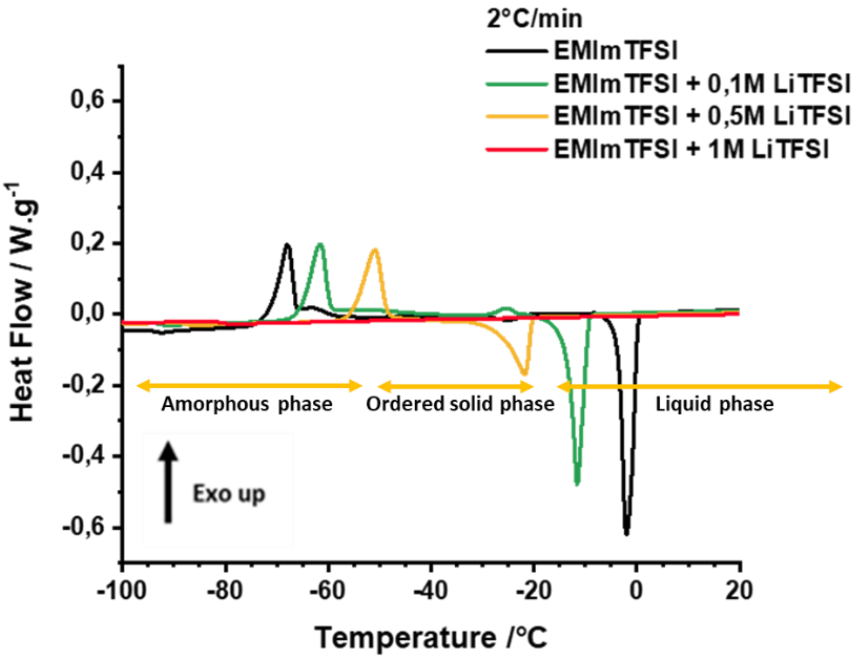


**Figure 4.2: Phase domains for [EMImTFSI + LiTFSI] ternary ILs measured with a 2°C/min heating rate**

A double peak for the melting is observed at 10°C/min, the first (upon heating) endothermic transition being related to solid α – solid β transition and the second to the melting of solid β, as expected for the fluorine based.[3] This is noticeable on Figure 4.1.a) for [EMImTFSI] and [EMImTFSI + 0.1M LiTFSI] samples. This is consistent with the dominance of the thermodynamics of EMImTFSI at very low concentrations of lithium salt. This double peak broadens and appears as one single signal at higher concentration. Such two endothermic signals were not observed at 2 °C.min$^{-1}$, thus showing that solid β is a metastable phase. These phase transitions temperatures are reported in Table 4.1.

**Table 4.1: Phase transitions temperatures for [EMImTFSI + LiTFSI] ternary ILs**

| | **Glass transition temperature** | **Cold crystallization temperature** | **Solid-to-solid and melting point** |
|---|---|---|---|
| **EMImTFSI (10°C.min$^{-1}$)** | -91°C [a] | -66°C [b]<br>-58°C [c] | $T_{s-s}$: -12°C [b]<br>-9°C [c]<br>$T_m$: -3°C [b]<br>-1°C [c] |
| **EMImTFSI (2°C.min$^{-1}$)** | -91°C [a] | -72°C [b]<br>-68°C [c] | -4°C b<br>-2°C c |
| **EMImTFSI + 0.1M LiTFSI (10°C.min$^{-1}$)** | -90°C [a] | -58°C [b]<br>-53°C [c] | $T_{s-s}$: -23°C [b]<br>-17°C [c]<br>$T_m$: -14°C [b]<br>-11°C [c] |
| **EMImTFSI + 0.1M LiTFSI (2°C.min$^{-1}$)** | -90°C [a] | -66°C [b]<br>-62°C [c] | -14°C [b]<br>-12°C [c] |
| **EMImTFSI + 0.5M LiTFSI (10°C.min$^{-1}$)** | -86°C [a] | -46°C [b]<br>-38°C [c] | -29°C [b]<br>-21°C [c] |
| **EMImTFSI + 0.5M LiTFSI (2°C.min$^{-1}$)** | -86°C [a] | -56°C [b]<br>-51°C [c] | -28°C [b]<br>-22°C [c] |
| **EMImTFSI + 1M LiTFSI (10°C.min$^{-1}$)** | -78°C [a] | / | / |
| **EMImTFSI + 1M LiTFSI (2°C.min$^{-1}$)** | -78°C [a] | / | / |

[a] measure at the inflexion point, [b] offset, [c] maximum in case of exothermic phase transition, minimum in case of endothermic phase transition

Finally, the phase transitions temperatures' shifts reflect the increasing viscosity of the ILs. The interaction forces between ions becomes stronger at higher lithium concentration. These interactions are responsible for the shift of the transitions i.e. the mixture needs more energy to initiate the molecule movement or reorganization. The cation of interest (here lithium) clearly disrupt the initial coulombic interactions between EMIm cation and TFSI anion.

### 4.1.2 Charged species motion in Li-based ternary ionic liquids

Dynamics in ILs is strongly dependent on salt addition due to pairs and aggregates formation.[4] This is directly in agreement with the previous results: stronger interactions leads to heightened viscosity. Besides the resulting viscosity, aggregates would reduce ions mobility and individual ions diffusion.

Instead of measuring viscosity, which is IL consuming and more difficult to set up for temperature studies, Electrochemical Impedance Spectroscopy was chosen to measure the ionic conductivity. These two physico-chemical variables are related through the Walden product, mentioned in Chapter 1. The Figure 4.3. shows the evolution of the ionic conductivities for Li-doped LIs in function of temperature. These measures are repeated at least twice for each sample to insure the veracity of the data sets. As expected, the ionic conductivity decreases when the temperature decreases. With an Arrhenius approach, the energy for the motion of molecules, and so for the motion of charged species in an electric field, is proportional to $e^{-Ea/RT}$. At high temperatures, the energy provided to the system enables the disaggregation of ions and thus enables a better mobility.

The ionic conductivity values are between 0.1 $mS.cm^{-1}$ and 8 $mS.cm^{-1}$ within the entire temperature range for all samples. That means the charged species mobility is good enough for the mass transport not to be a limitation during the device operation. It is interesting to note that the temperature dependency almost follows an Arrhenius model from + 20°C to + 90°C. However, below ~ +20°C the curves starts to drop. The VTF model is then more relevant than the Arrhenius one to describe the temperature dependency of ionic conductivity in ternary ILs.

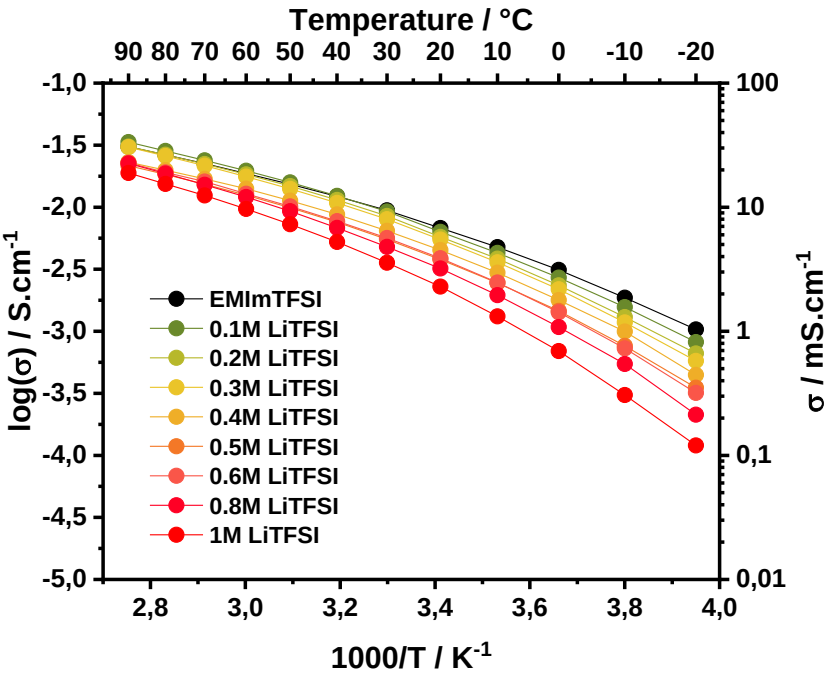


**Figure 4.3: Temperature dependency of ionic conductivity of [EMImTFSI + LiTFSI] ternary ILs**

Figure 4.4 shows the ionic conductivity as a function of LiTFSI concentration in EMImTFSI. Ionic conductivity decreases with the salt addition no matter the temperature. Nevertheless, the decrease is temperature dependant. The slopes are steeper for lower temperatures (here from 0°C to 90°C). For high temperatures applications, it is interesting to note that the salt addition does not impart significantly the ionic conductivities. At 90°C, the ionic conductivities of the Li-doped ILs are almost equal to that of the neat EMImTFSI one. This observation means that the drawbacks brought by the viscosity of highly concentrated ILs does not exist anymore at high temperatures. Hence, if a specific application is targeted for operation at temperatures higher than 70°C, there is no limitation to work at very high salt concentrations regarding the macroscopic ionic conductivity. This result is even more interesting knowing that most of commercial electrolytes are hard to use over 70°C because of the vapour pressure of the electrolyte and the fast decrease of lifetime for the battery. Ternary ILs could be the perfect fit for this range of temperatures.

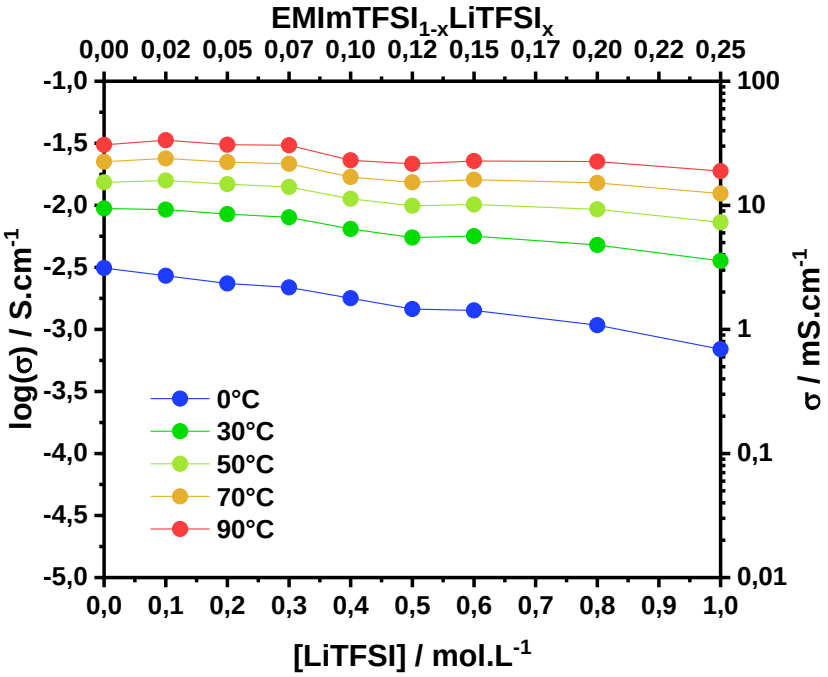


**Figure 4.4: Salt concentration dependency of ionic conductivity for [EMImTFSI + LiTFSI] ternary ILs**

In Table 4.2. are reported the ionic conductivity of several samples at 50°C and their VTF parameters. It is wiser to fit the data sets from Figure 4.3, deleting the points close to the melting temperature to avoid mistakes due to partial crystallization in the sample (from 0°C to + 90°C in the case of the neat IL and from - 10°C to + 90°C for all the other samples). All curves were fitted with a good match with the model with $R^2$ coefficients higher than 0.999.

**Table 4.2: Ionic conductivities and VTF parameters of [EMImTFSI + LiTFSI] ternary ILs**

| | $\sigma_{50°C}$ (mS.cm$^{-1}$) | Calculated Vm (cm$^3$.mol$^{-1}$)* | $\Lambda_m$ at 50°C (S.cm$^2$.mol$^{-1}$) | $\sigma_0$ (mS.cm$^{-1}$) | $T_0/T_g$ | D index (S.cm$^{-1}$) |
|---|---|---|---|---|---|---|
| **EMImTFSI** | 15.3 | 257.4 | 3.94 | 458.4 | 0.92 | 3.19 |
| **EMImTFSI + 0.1M LiTFSI** | 15.8 | 256.3 | 4.05 | 677.1 | 0.90 | 3.60 |
| **EMImTFSI + 0.5M LiTFSI** | 10 | 252.1 | 2.52 | 390.6 | 0.95 | 3.04 |
| **EMImTFSI + 1M LiTFSI** | 5.3 | 247.0 | 1.31 | 559.9 | 0.93 | 3.41 |

*As mentioned in Chapter 3, there is an approximation on the calculation of the mixture's molar volume

Molar conductivity $\Lambda_m$ decreases when the salt concentration increases. There is an exception with the [EMImTFSI + 0.1M LiTFSI] sample which present a slightly better absolute value of the macroscopic ionic conductivity and molar conductivity, but similar to the case without salt, given the uncertainty. The decrease of conductivity for higher concentration could be explained by the competition of interactions between $EMIm^+$ and $Li^+$ cations with the $TFSI^-$ anion. The lithium cation is more polarizing than the imidazolium, hence more TFSI- anions coordinate the lithium. At low lithium salt addition, the diffusion of $EMIm^+$ could thus slightly increase because less TFSI- are available for coordinating $EMIm^+$, and the amount is still .

The same trends are observed for the VTF parameters shown on Figure 4.5. The ideal conductivity at infinite temperature $\boldsymbol{\sigma_0}$ slightly is constant (from 500 to 600 mS.cm-1) with salt addition (Figure 4.5.a). That means that the growing number of charged species at higher concentration compensates the increased viscosity when temperature is not a limitation for the molecules motion.

The fragility of an IL (mentionned in Chapter 3) could be defined as its ability to dissociate the aggregates locally (i.e. increasing the ionicity with lower density and better ionic conductivity) under a constraint, and can be quantify thanks to the fragility index D represented in Figure 4.5.b).[5] Here again, this index is slightly increases (or within the uncertainties, from 3 to 3.5) which could confirm the decrease of mobility for charged species for the highest concentrations.

In summary, the viscosity increases with the salt addition and consequently the ionic conductivity decreases. However, based on the VTF study and on the calculation of molar conductivity, we observed that the series of [EMImTFSI + LiTFSI] samples are only slightly affected in terms of macroscopic transport properties. Indeed the molar conductivity between the neat IL and [EMImTFSI + 1M LiTFSI] sample belongs to same order of magnitude (# 1 $S.cm^2.s^{-1}$). A more precise study on each ion diffusion is needed to investigate on the aggregates formation and try to quantify it.

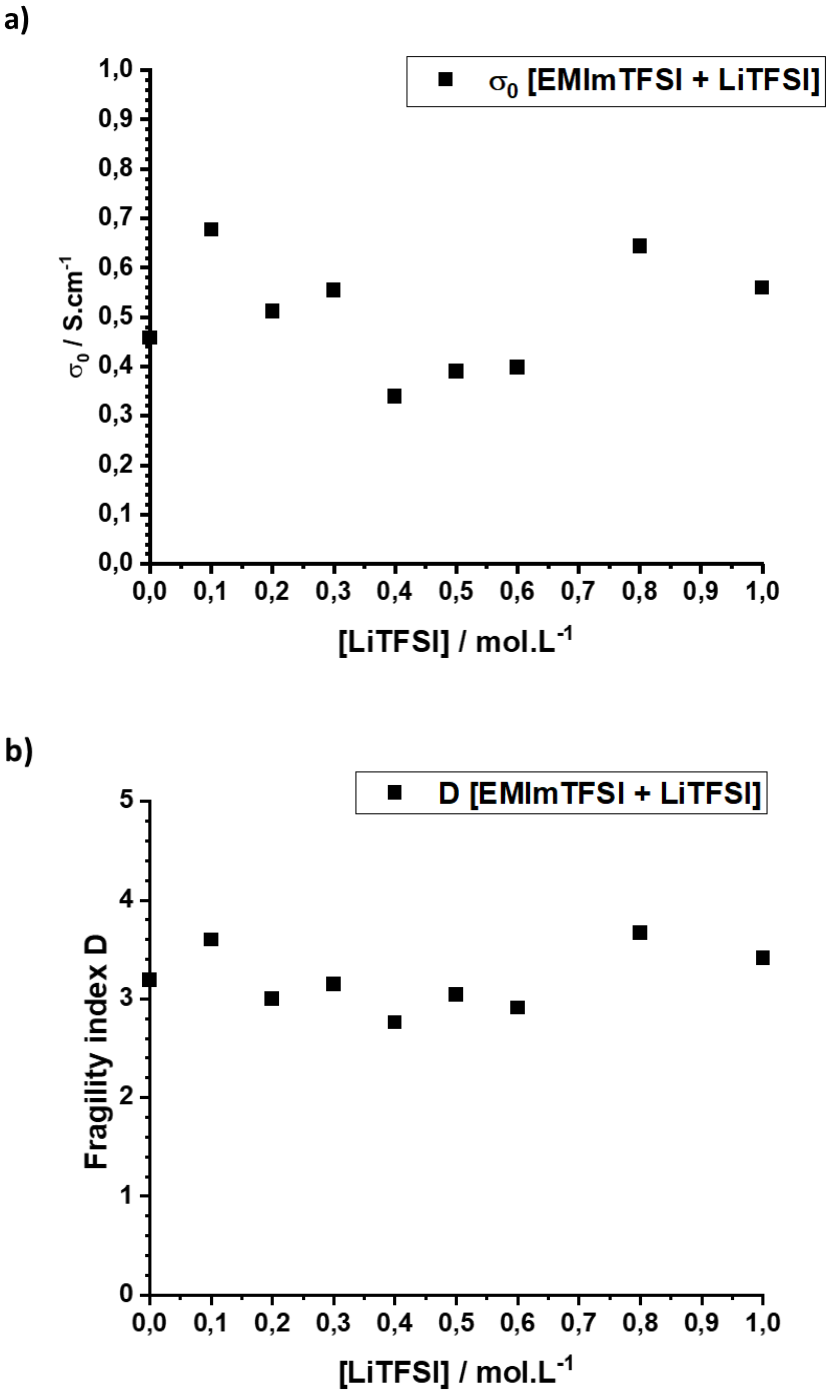


**Figure 4.5: a) Ideal ionic conductivity at infinite temperature and b) fragility index for [EMImTFSI + LiTFSI] ternary ILs**

## 4.1.3 Diffusion and free ions fraction in Li-based ternary ionic liquids

Ions mobility in ILs is controlled by Coulombic interactions, hydrogen bonding and Van der Walls interactions. Electrochemical impedance spectroscopy is advantageously coupled with Pulsed-Field Gradient Nuclear Magnetic Resonance to analyse ions self-diffusion coefficients in ILs based electrolytes. As mentioned in Chapter 3, these coupled techniques enables to quantify the proportions of free ions through the ionicity.

On Figure 4.6. are reported the self-diffusion coefficients measured at 50°C, 70°C and 90°C for ILs containing from 0 M to 1.5 M of Li salt. Self-diffusion coefficients decrease while cooling down the sample because motion of molecules is temperature-dependent. Here, the diffusion is not lead by any electric field. It is important to note than in an electrochemical device, the diffusion may change due to the energy brought by the potential difference between electrodes. Moreover, PFG NMR measurements allow measuring the average diffusion of nuclei mostly as free ions, but also as part of aggregates.

All the slopes of the temperature dependency for diffusion are similar for each ion showing that the diffusion is strongly correlated between ions with a unique 3D translation mechanism. This remark is even more relevant for $TFSI^-$ and $Li^+$ where the straight lines superimpose each other's. This is a first clue about the common dynamics of the $Li^+$-$TFSI^-$ pairs or aggregates, whereas the diffusion of $EMIm^+$ seems to be, on average, easier and more independent from other ions' mobility.

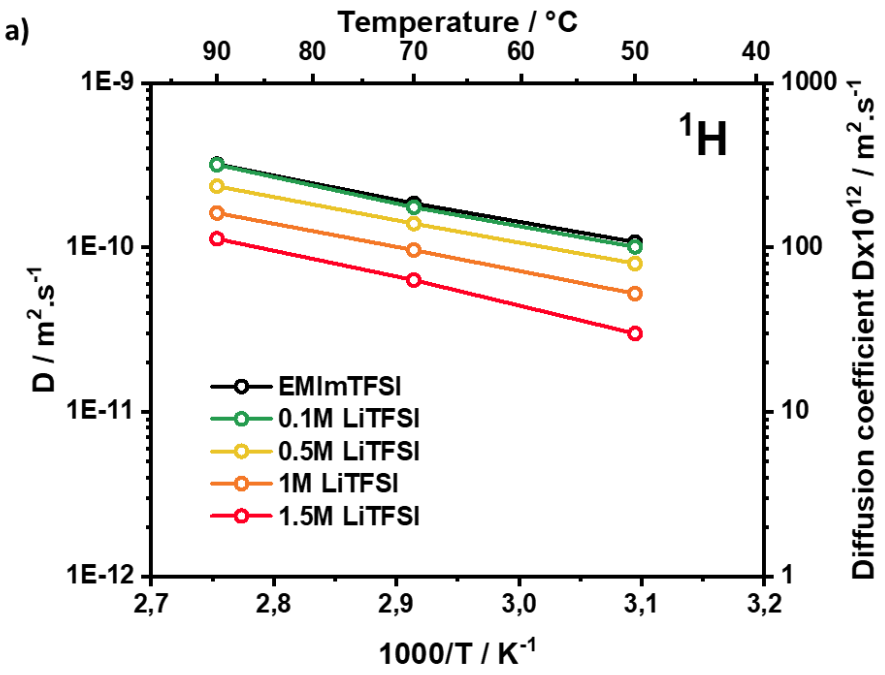

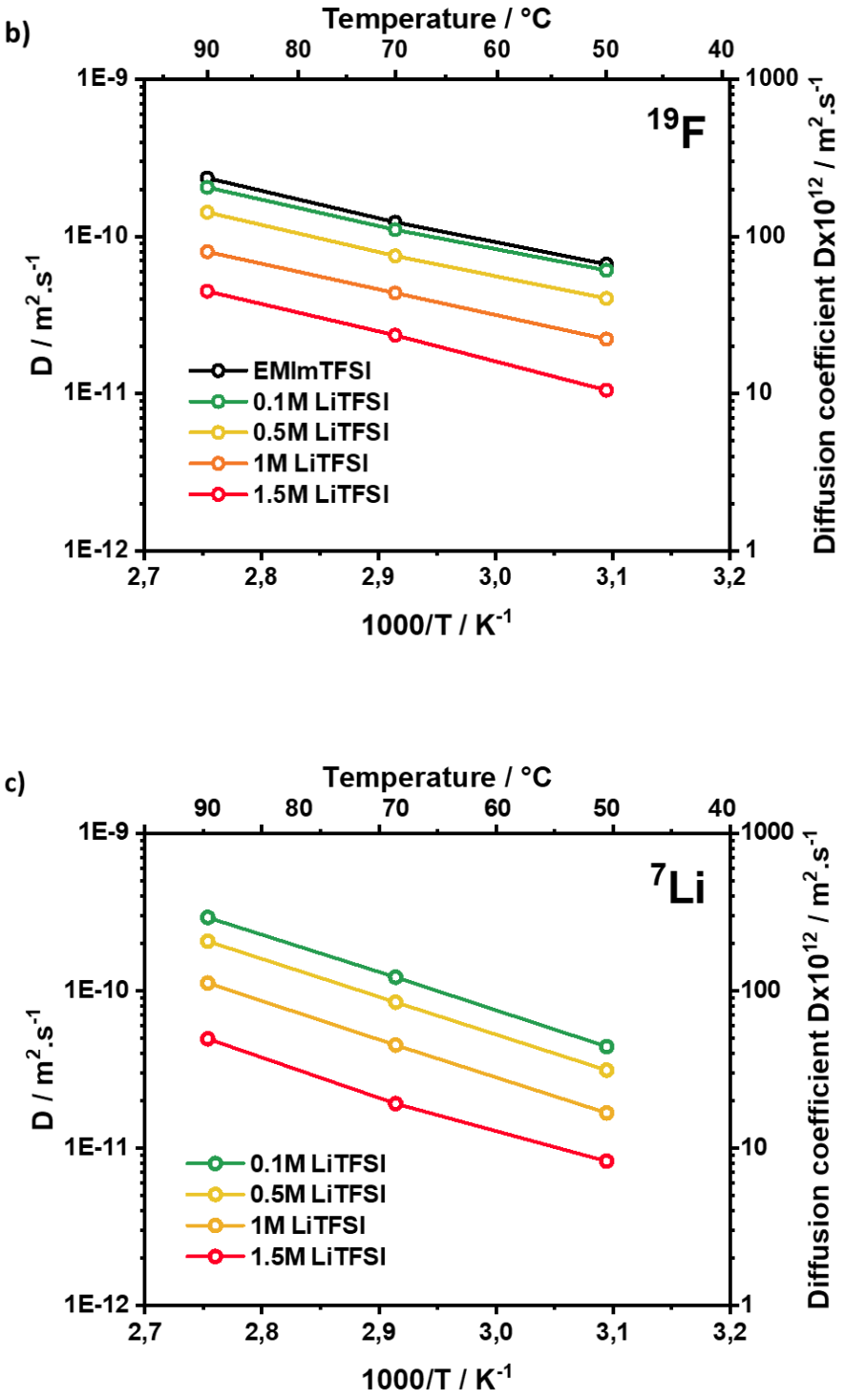


**Figure 4.6: Temperature dependency of self-diffusion coefficients of a) $EMIm^+$ b) $TFSI^-$ and c) $Li^+$ in [EMImTFSI + LiTFSI] ternary ILs**

To enlighten even more this phenomenon, self-diffusion coefficients in function of lithium salt concentration at 50°C and 90°C are shown in Figure 4.7. The first observation is that the salt addition lowers the diffusion of all ions in the electrolyte. In particular, TFSI- and metal cations mobility is reduced because of their mutual coordination. Indeed, all diffusion coefficients for $EMIm^+$, $TFSI^-$ and $Li^+$ decrease with salt addition. This mobility decrease is stronger for the fluorine and lithium nuclei: the slopes are steeper in the case of $Li^+$ and $TFSI^-$ confirming than their diffusion are correlated while $EMim^+$ is less affected by the presence of lithium.

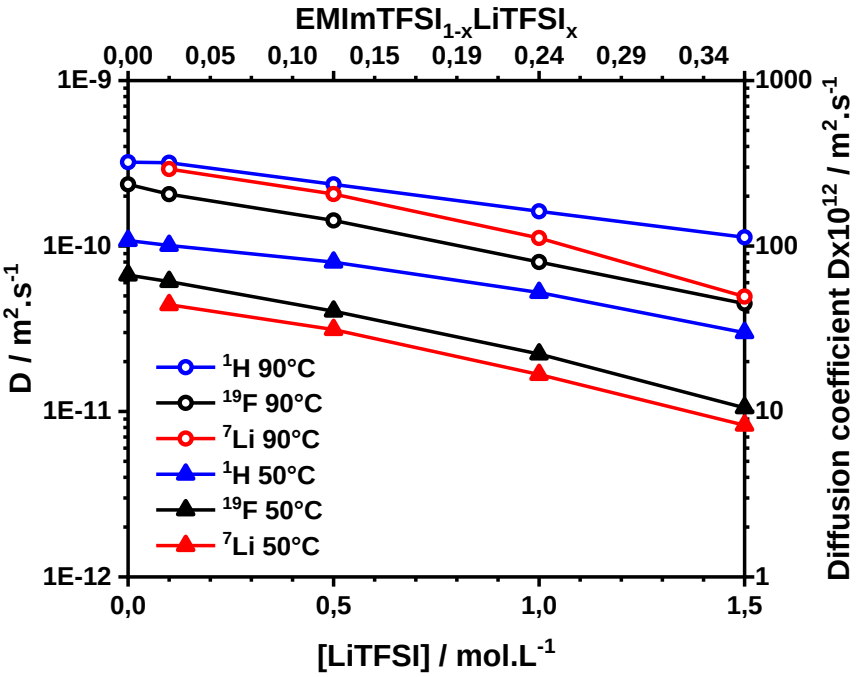


**Figure 4.7: Salt concentration dependency of self-diffusion coefficients of all ions in [EMImTFSI + LiTFSI] ternary ILs at 50°C and 90°C**

Secondly, the diffusion of $Li^+$ is better than that of $TFSI^-$ anion at 90°C but rather similar at 50°C. This is an interesting result showing that in these medium, there is a favoured selective cationic diffusion at high temperatures.

In Table 4.3 are reported the ions self-diffusion coefficients in [EMImTFSI + LiTFSI] ternary ILs, their calculated limiting molar conductivity, and their ionicty. The value for self-diffusion in EMImTFSI are consistent with the literature.[10]

Ionicity decreases clearly at 1M, but roughly stays constant below 0.5 M. This is not the case at very low concentrations where the presence of lithium is helping the motion of individual ions thanks to the competition of interactions, as presented in the ionic conductivity discussion.

**Table 4.3: Self-diffusion coefficients, limiting molar conductivity and ionicity of [EMImTFSI + LiTFSI] ternary ILs**

| | $D_{EMIm+}$ at 50°C x$10^{12}$ ($m^2.s^{-1}$) | $D_{TFSI-}$ at 50°C x$10^{12}$ ($m^2.s^{-1}$) | $D_{Li+}$ at 50°C x$10^{12}$ ($m^2.s^{-1}$) | $\Lambda_{NMR}$ at 50°C ($S.cm^2.mol^{-1}$) | $\Lambda_{EIS}$ at 50°C ($S.cm^2.mol^{-1}$) | Ionicity (%) |
|---|---|---|---|---|---|---|
| **EMImTFSI** | 107.9 | 66.7 | / | 6.05 | 3.94 | 65.1 |
| **EMImTFSI + 0.1M LiTFSI** | 100.7 | 61.0 | 44.2 | 5.553 | 4.05 | 72.9 |
| **EMImTFSI + 0.5M LiTFSI** | 79.8 | 40.4 | 31.3 | 3.953 | 2.52 | 63.7 |
| **EMImTFSI + 1M LiTFSI** | 52.4 | 22.3 | 16.7 | 2.283 | 1.31 | 57.4 |

Fitting the previous data sets with an Arrhenius function provide the activation energies related to the mobility of these ions in the ILs (Figure 4.8). $EMIm^+$ and $TFSI^-$ are constraint by the salt addition and more energy is needed for them to diffuse while increasing the amount of added LiTFSI, whereas for the lithium, this energy is almost constant, around 46 $kJ.mol^{-1}$, and much higher than the energies necessary for other ions to diffuse. Finally, the sum of all energies is increasing because diffusion is more difficult in concentrated ILs.

Moreover, the diffusion of $TFSI^-$ is slightly facilitated for the [EMImTFSI + 0.1M LiTFSI] mixture. This could be a clue of the better average transport properties observed previously for this sample, especially because $TFSI^-$ is the most abundance species in this mixture.

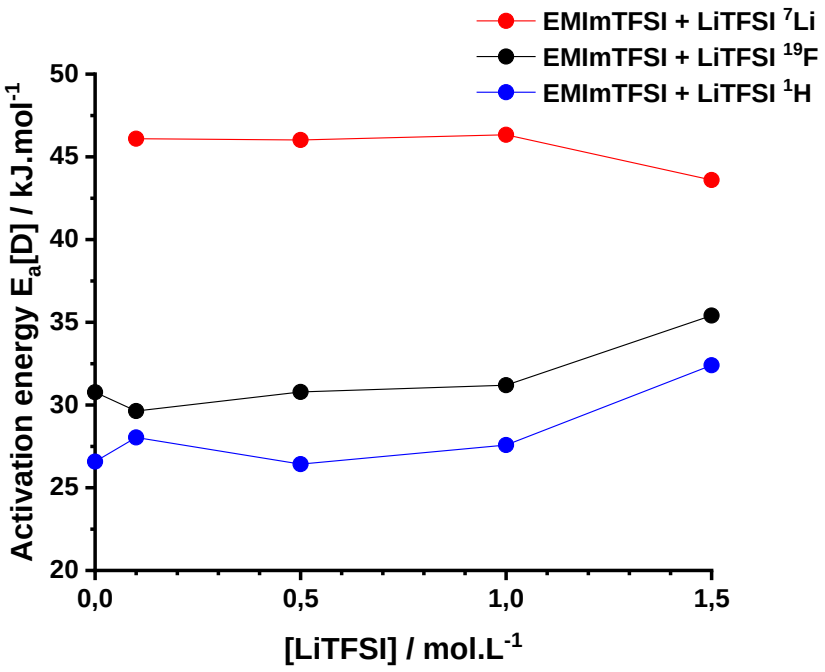


**Figure 4.8: Activation energies for the diffusion of all ions in [EMImTFSI + LiTFSI] ternary ILs**

To conclude on the diffusion of individual species, salt addition reduces their self-diffusion coefficients and as a result the macroscopic properties. The number of ions consumed in the aggregates formation increases with the concentration, which reduces the number of free charged species quantifiable with EIS measurement. In the next part, the structure of these aggregates will be studied by Raman spectroscopy.

## 4.1.4 Coordination sphere of lithium in EMImTFSI

The addition of LiTFSI in EMImTFSI brings a competition of interactions between $EMIm^+$ and $Li^+$. Coulombic interactions between anions ($TFSI^-$) and cations ($EMIm^+$, $Li^+$) decreases the ability for free ions to diffuse, which impact negatively the transport properties. Moreover, the small and locally charged cation is a more attractive center than imidazolium cation considering the geometry and charge to volume ratio. The interaction between $Li^+$ and $TFSI^-$ is to the detriment of the interaction between $EMIm^+$ and $TFSI^-$ since their polarizing powers are different. This polarizing effect of lithium is responsible for the viscosity increase when its concentration increase.

Selected spectral region of the Raman spectrum for [EMImTFSI + LiTFSI] ternary ILs are shown in Figure 4.9. In the pure EMImTFSI ionic liquid (dark green), the vibration band at 741.4 $cm^{-1}$ is the most intense signal. This band is attributed to the symmetrical expansion-contraction mode of $TFSI^-$ and can be decomposed in two distinct bands related to the conformation of the TFSI- anion (transoid at 741.4 $cm^{-1}$ and cisoid at 743 $cm^{-1}$).[6,7] As the salt is added, a second population of vibrating TFSI appears. The second band, slightly shifted toward higher energies at 748.2 $cm^{-1}$, is related to the presence of metal cations in $TFSI^-$ environment. Spectrum on Figure 4.9 clearly show this second population of TFSI in the ionic liquids with salt. Moreover, the intensity of this shoulder is directly proportional to the lithium concentration to a certain concentration where the $TFSI^-$ interact more with $Li^+$ than with $EMIm^+$ (above 1M).

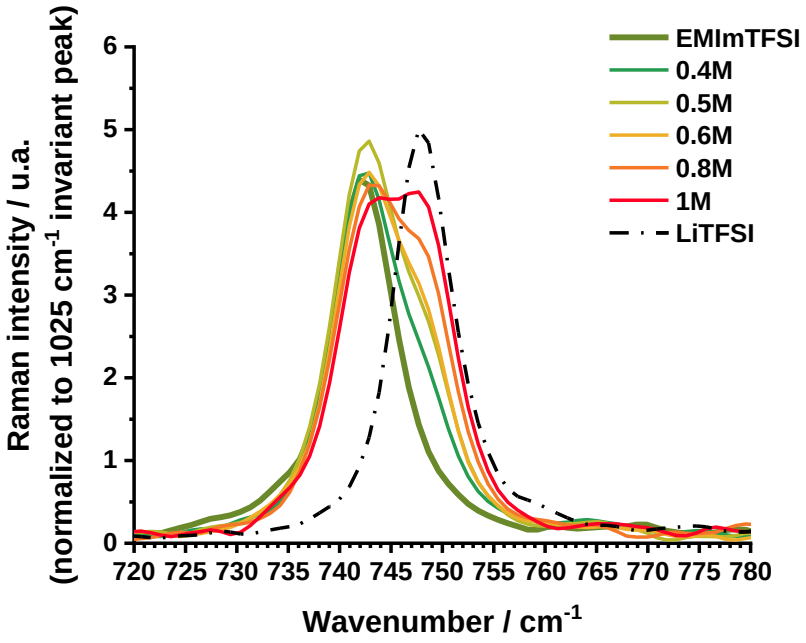


**Figure 4.9: Raman spectrum of [EMImTFSI + LiTFSI] ternary ILs at RT in the 720 to 780 $cm^{-1}$ region**

In the end, quantify the $TFSI^-$-$Li^+$ is another way to titrate the salt concentration in the electrolyte. The energy at stake depends on the strength of the TFSI-to-cation interaction (see table 4.4). The more attractive the cation is, the more energy is needed for TFSI to vibrate compared to its EMIm-TFSI interaction at the equilibrium in the neat IL.

**Table 4.4: Vibration mode wavenumber and its corresponding energy shift**

| | 1st vibration band energy ($cm^{-1}$) | 2nd vibration band energy ($cm^{-1}$) | 3rd vibration band energy ($cm^{-1}$) | Shift in energy (meV) |
|---|---|---|---|---|
| **EMImTFSI** | 741.4 | 743 | - | - |
| **LiTFSI** | - | - | 748 | - |
| **EMImTFSI + LiTFSI** | 741.4 | 743 | 748 | 0.75 |

All the samples are liquid at room temperature and there were no crystal in the solution. Indeed, by microscopic observation coupled with the previous DSC measurements no remaining solid salt crystal were observed.

That leads the discussion towards the coordination number of lithium in the IL, i.e. the number of $TFSI^-$ anions around the metal cation that can be quantify as described in Chapter 3. Figure 4.10 shows the evolution of the coordination number with lithium salt concentration.

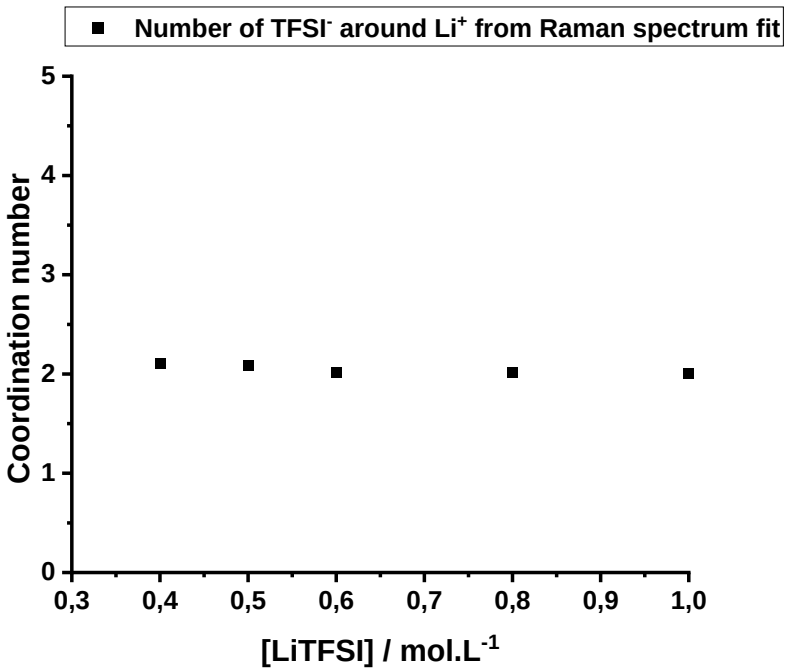


**Figure 4.10: TFSI molecules number in the $Li^+$ coordination sphere of [EMImTFSI + LiTFSI] ternary ILs from 0.4M to 1M**

On average, two molecules of $TFSI^-$ surround $Li^+$. This number only slightly decreases with concentration because the number of $TFSI^-$ per $Li^+$ decreases with salt addition. The origin of the disruption brought by the lithium in the IL is due to the fact that the lithium is more attractive than the imidazolium cation and attracts the $TFSI^-$ in its coordination sphere. At high concentration, the aggregates formation is the major phenomenon, bringing viscosity and a diffusion drop for each species on average. The energy needed for the diffusion of ions increases with the salt concentration and so the macroscopic ionic conductivity decreases. At high temperatures, this effect is lessened. These results are confirmed by the thermal behaviour of the ternary ILs, in particular because of the structuration of the ILs at high concentration.

In the next part, a similar study will be conducted on bivalent cations ILs, in order to validate these observations and be able to compare the behaviour of non confined ILs and ionogels in the next chapter.

# 4.2 Effect of salt concentration: bivalent cations in ternary ionic liquids

In this part, the same methodology will be applied to characterize $Mg^{2+}$ and $Zn^{2+}$-doped ILs. As the previous part offers a comprehensive description of series study, the figures and conclusion will be discussed directly in this second part. The comparison between monovalent and bivalent metal cations will validate our understanding of the dynamics in ternary ILs. Indeed, a stronger aggregation is expected due to the charge-to-volume of $Mg^{2+}$ and $Zn^{2+}$, which are much higher than for $Li^{+}$. Moreover, the electrons configuration between magnesium and zinc cations are different (respectively $[Ne]^{10}3s^{0}$ and $[Ar]^{18}4s^{0}3d^{10}$) but their sizes are similar [8]. Hence, this second comparison enables to understand to which extent the valence state of metal cations affects their diffusion in these electrolytes.

## 4.2.1 Thermal behaviour and phase transitions in bivalent metalcations ternary ionic liquids

Figures 4.11 and 4.12 show respectively the thermograms of [EMimTFSI + $Mg(TFSI)_2$] and [EMimTFSI + $Zn(TFSI)_2$] ternary ILs at 10°C/min and 2°C/min heating rate. The same conclusions than for lithium are observable. Glass transitions and cold crystallizations temperatures increase with salt addition whereas the melting temperatures decrease.

Once again, salt addition shifts the melting temperatures towards lower temperatures and this effect is stronger here at the same concentrations: for low concentrated ternary ILs with magnesium or zinc, the liquid range is extended to -15°C in the case of the [EMimTFSI + 0.1M $Mg(TFSI)_2$] and [EMimTFSI + 0.1M $Zn(TFSI)_2$]. It was not the case with lithium samples where the shift for [EMimTFSI + 0.1M LiTFSI] was around -10°C. Furthermore, the characteristic double peak attributed to the melting point of fluorine-based ILs for EMImTFSI is no longer visible for the mixtures mentioned above. This is an evidence that adding bivalent metal salt has a stronger impact on the thermal behaviour of the ILs than in the case of monovalent cation.

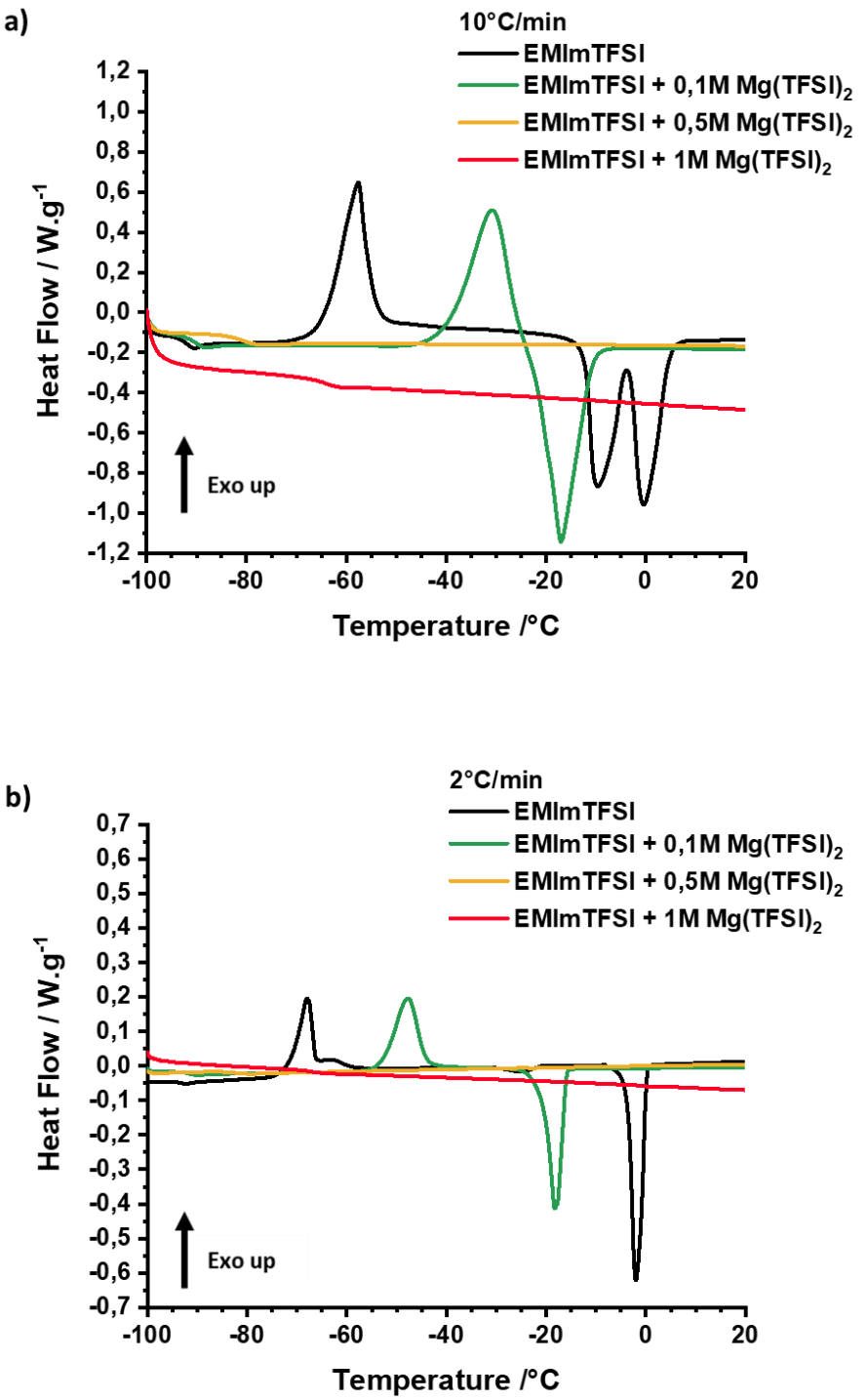


**Figure 4.11: Phase transitions for [EMImTFSI + $Mg(TFSI)_2$] ternary ILs at 10°C/min and 2°C/min**

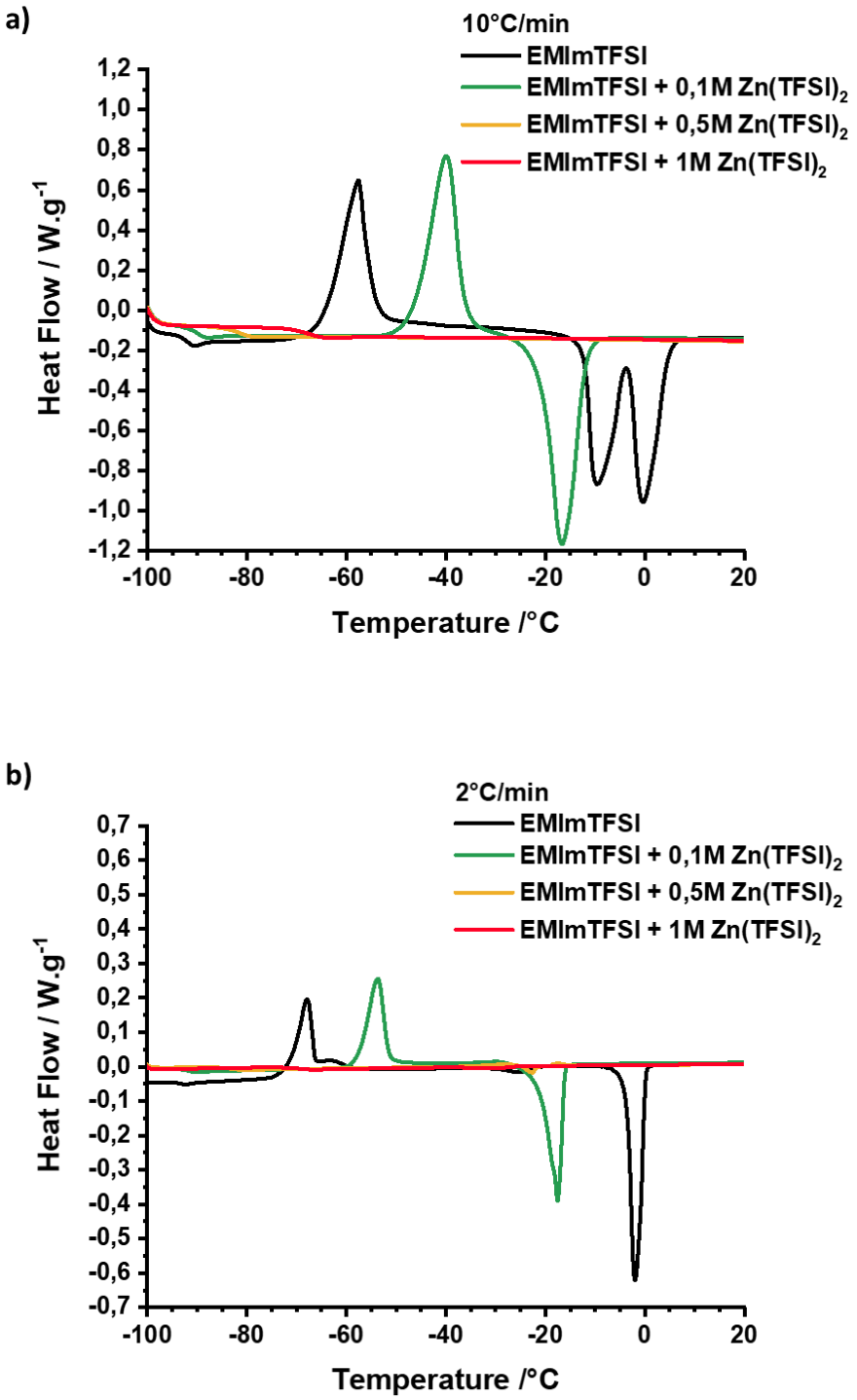


**Figure 4.12: Phase transitions for [EMImTFSI + $Zn(TFSI)_2$] ternary ILs at 10°C/min and 2°C/min**

. The evidence of this stronger effect on the shifts for bivalent cations is the flattening of reversible phase transitions in the 10°C/min experimental conditions from 0.5M (orange straight lines). For lithium samples, this flattening occurs for concentration only above 1M. The interaction forces are definitely stronger in ternary ILs doped with bivalent cations. The main phase transitions temperatures for these two series of samples are tabulated in Table 4.5.

**Table 4.5: Phase transitions temperatures for [EMImTFSI + $Mg(TFSI)_2$] and [EMImTFSI + $Zn(TFSI)_2$] ternary ILs**

| | Glass transition temperature | Cold crystallization | Melting point |
|---|---|---|---|
| **EMImTFSI (10°C.min$^{-1}$)** | -91°C [a] | -66°C [b]<br>-58°C [c] | $T_{s-s}$: -12°C [b]<br>-9°C [c]<br>$T_m$: -3°C [b]<br>-1°C [c] |
| **EMImTFSI (2°C.min$^{-1}$)** | -91°C [a] | -72°C [b]<br>-68°C [c] | -4°C b<br>-2°C c |
| **EMImTFSI + 0.1M $Mg(TFSI)_2$ (10°C.min$^{-1}$)** | -89°C [a] | -40°C [b]<br>-30°C [c] | -22°C [b]<br>-17°C [c] |
| **EMImTFSI + 0.1M $Mg(TFSI)_2$ (2°C.min$^{-1}$)** | -89°C [a] | -53°C [b]<br>-48°C [c] | -21°C [b]<br>-18°C [c] |
| **EMImTFSI + 0.5M $Mg(TFSI)_2$ (10°C.min$^{-1}$)** | -80°C [a] | / | / |
| **EMImTFSI + 0.5M $Mg(TFSI)_2$ (2°C.min$^{-1}$)** | -80°C [a] | / | / |
| **EMImTFSI + 1M $Mg(TFSI)_2$ (10°C.min$^{-1}$)** | -63°C [a] | / | / |
| **EMImTFSI + 1M $Mg(TFSI)_2$ (2°C.min$^{-1}$)** | -63°C [a] | / | / |
| **EMImTFSI + 0.1M $Zn(TFSI)_2$ (10°C.min$^{-1}$)** | -90°C [a] | -48°C [b]<br>-40°C [c] | -22°C [b]<br>-17°C [c] |
| **EMImTFSI + 0.1M Zn $(TFSI)_2$ (2°C.min$^{-1}$)** | -90°C [a] | -58°C [b]<br>-54°C [c] | -22°C [b]<br>-18°C [c] |
| **EMImTFSI + 0.5M Zn $(TFSI)_2$ (10°C.min$^{-1}$)** | -81°C [a] | / | / |
| **EMImTFSI + 0.5M Zn $(TFSI)_2$ (2°C.min$^{-1}$)** | -81°C [a] | / | -25°C [b]<br>-23°C [c] |
| **EMImTFSI + 1M Zn $(TFSI)_2$ (10°C.min$^{-1}$)** | -67°C [a] | / | / |
| **EMImTFSI + 1M Zn $(TFSI)_2$ (2°C.min$^{-1}$)** | -67°C [a] | / | / |

[a] measure at the inflexion point, [b] offset, [c] maximum in case of exothermic phase transition, minimum in case of endothermic phase transition

Here again, the melting point is shifted towards low temperatures, so the ternary ILs are still liquid at -17°C for all the bivalent cations doped-ILs.

Figure 4.12 shows the $T_g$ dependency on salt addition for each cation. First, this curve gives an easy way to determine precisely the salt concentration in EMImTFSI mixture. Secondly, this sorts the interactions energies at stake in the ternary ILs depending on the cation. Therefore, this thermodynamics consideration allows predicting the viscosity of the electrolytic solutions. A slower dynamics is expected in Mg-based ILs than in Zn-based ILs. In addition, both series should show slower dynamics than in the [EMImTFSI + LiTFSI] ternary ILs.

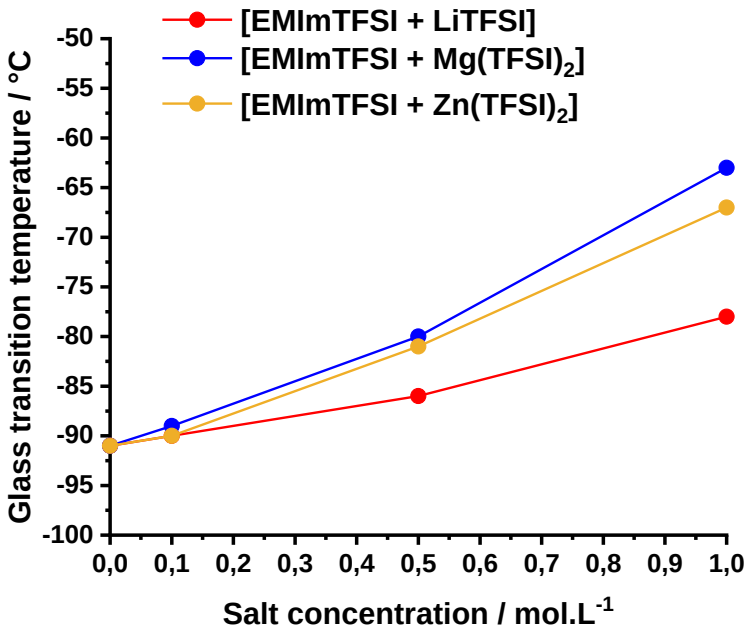


**Figure 4.13: Glass temperature dependency on salt concentration dissolved in EMImTFSI for Li+, $Mg^{2+}$ and $Zn^{2+}$**

## 4.2.2 Charged species motion in bivalent metal cations ternary ionic liquids

After the previous thermodynamics predictions, the transport properties need to be measured. Figure 4.14 shows the ionic conductivities for magnesium and zinc ILs series in the same temperatures and concentrations ranges than for the previous lithium samples.

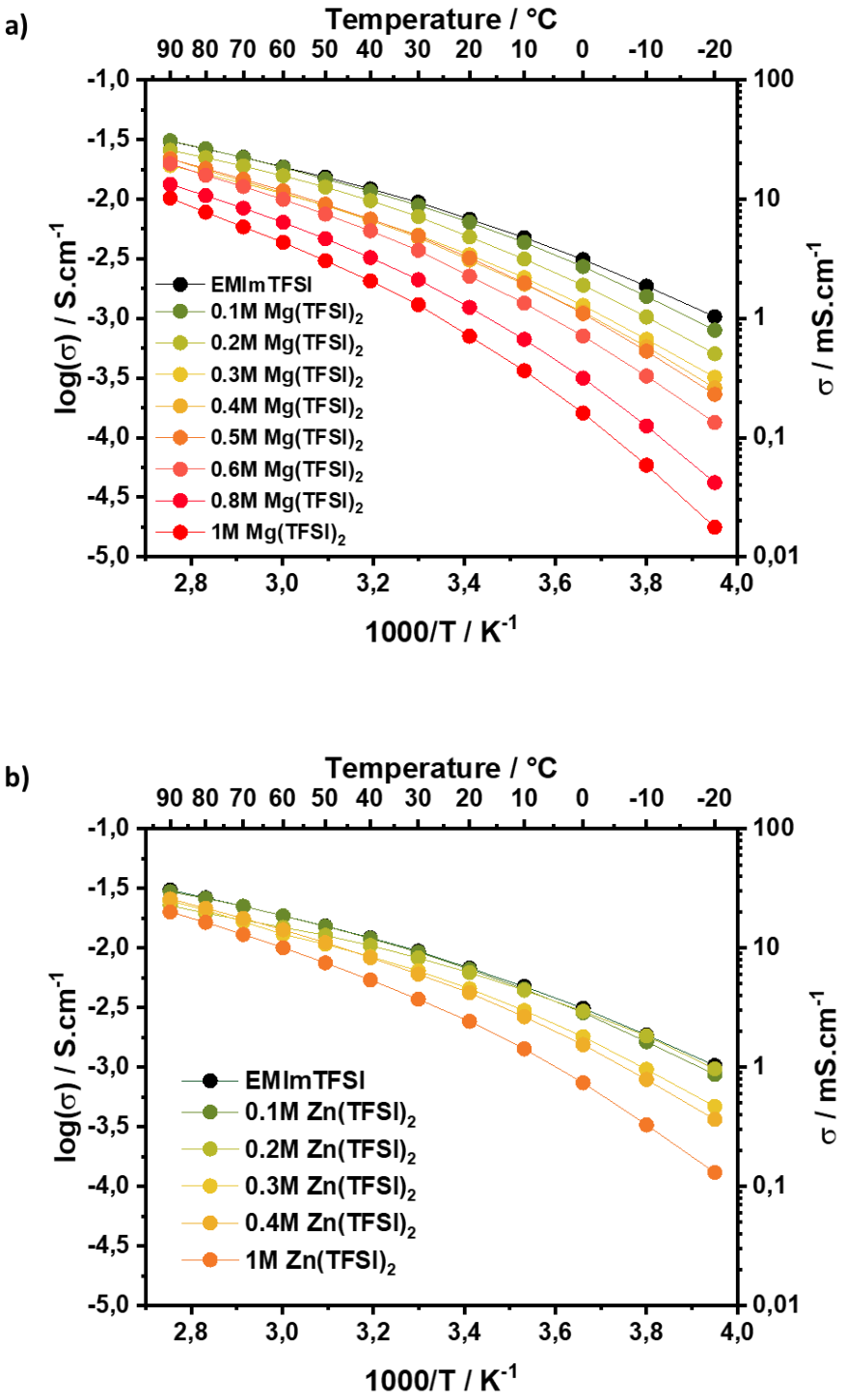


**Figure 4.14: Ionic conductivities for a) [EMImTFSI + $Mg(TFSI)_2$] and b)[EMImTFSI + $Zn(TFSI)_2$] ternary ILs**

As expected the ionic conductivity for [EMImTFSI + $Mg(TFSI)_2$] ternary ILs is much lower than with Li-based ILs. The ionic conductivities values go from 0.01 $mS.cm^{-1}$ to 8 $mS.cm^{-1}$ for all the temperature range. This result makes this series questionable for supercapacitors applications at room temperature, although the values at high temperatures are high enough to considered Mg-based ILs as electrolytes for high temperatures applications.

About the [EMImTFSI + $Zn(TFSI)_2$] series, the ionic conductivities are very similar to that of the lithium samples going from 0.1 $mS.cm^{-1}$ to 30 $mS.cm^{-1}$. Finally, the viscosity in Zn-based electrolytes is less important than expected and it is promising to develop zinc-ion devices because of the two charges of this cation.

Globally, the behaviour could be extrapolated from the VTF parameters:

- the ideal ionic conductivity at infinite temperature is increasing with the salt addition (higher values fort bivalent cations than for $Li^+$);

- the ratio between $T_0/T_g$ decreases and the fragility index D increases i.e. the liquid becomes more viscous and the local reorganization of interactions becomes more difficult.

Table 4.6 summarizes the macroscopic ionic conductivity parameters for these series of ternary ILs.

**Table 4.6: Ionic conductivities and VTF parameters of [EMImTFSI + $Mg(TFSI)_2$] and [EMImTFSI + $Zn(TFSI)_2$] ternary ILs**

| | $\sigma_{50°C}$ ($mS.cm^{-1}$) | Calculated Vm ($cm^3.mol^{-1}$)* | $\Lambda_m$ at 50°C ($S.cm^2.mol^{-1}$) | $\sigma_0$ ($mS.cm^{-1}$) | $T_0/T_g$ | D index ($S.cm^{-1}$) |
|---|---|---|---|---|---|---|
| **EMImTFSI** | 15.3 | 257.4 | 3.94 | 458.4 | 0.92 | 3.19 |
| **EMImTFSI + 0.1M $Mg(TFSI)_2$** | 14.8 | 257.5 | 3.81 | 458.4 | 0.94 | 2.97 |
| **EMImTFSI + 0.5M $Mg(TFSI)_2$** | 9.1 | 257.9 | 2.35 | 453.8 | 0.94 | 3.07 |
| **EMImTFSI + 1M $Mg(TFSI)_2$** | 3.1 | 258.4 | 0.80 | 670.3 | 0.86 | 4.21 |
| **EMImTFSI + 0.1M $Zn(TFSI)_2$** | 15.2 | 257.4 | 3.91 | 353.5 | 0.98 | 2.53 |
| **EMImTFSI + 0.5M $Zn(TFSI)_2$** | 11,1 | 257.6 | 2,86 | 571,2 | 0,91 | 3,37 |
| **EMImTFSI + 1M $Zn(TFSI)_2$** | 7.5 | 257.7 | 1.93 | 637.6 | 0.87 | 3.59 |

## 4.2.3 Diffusion and free ions fraction in bivalent metalcations ternary ionic liquids

A same evolution of the self-diffusion coefficient is observed for bivalent cations than for Li-based ternary ILs: diffusion is slowed down while cooling and with salt addition. Even if the coefficient measurement of $^{25}Mg$ and $^{67}Zn$ is not possible because of the low abundance of these two isotopes, a lot of information can be extracted from the $EMIm^+$ and $TFSI^-$ behaviour.

Figures 4.15. and 4.16 shows the temperature dependency, Arrhenius type, of self-diffusion coefficients for magnesium and zinc based electrolytes respectively. D values for $EMIm^+$ and $TFSI^-$ are lower in bivalent electrolytes. The same trend is noticeable about $EMIm^+$; its diffusion is less affected than the $TFSI^-$ diffusion with salt addition, which is expected because of the formation of metal cations –TFSI clusters. This result is enlighten in Figure 4.17 where the self-diffusion coefficients are presented in function of concentration at 50°C and 70°C.

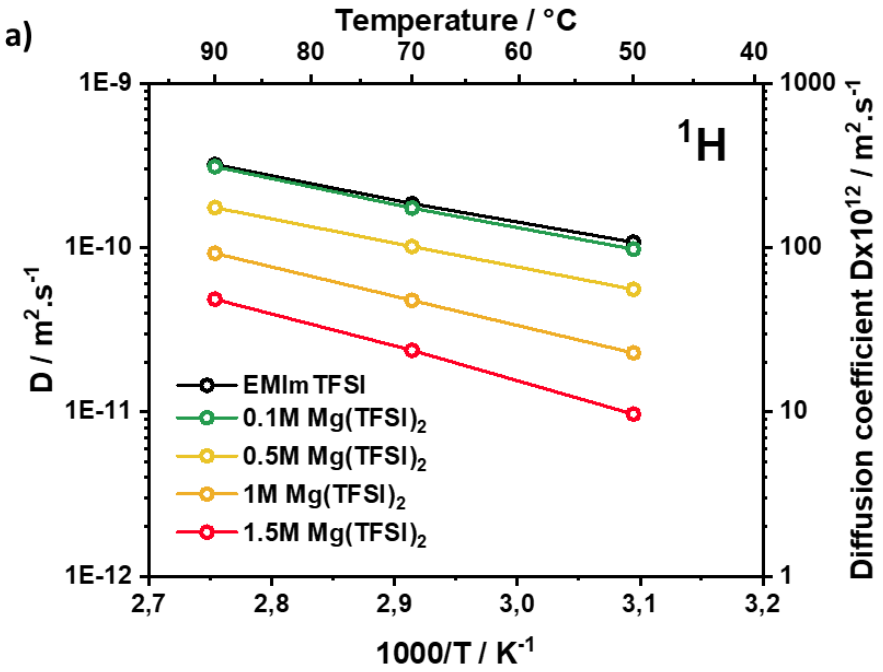

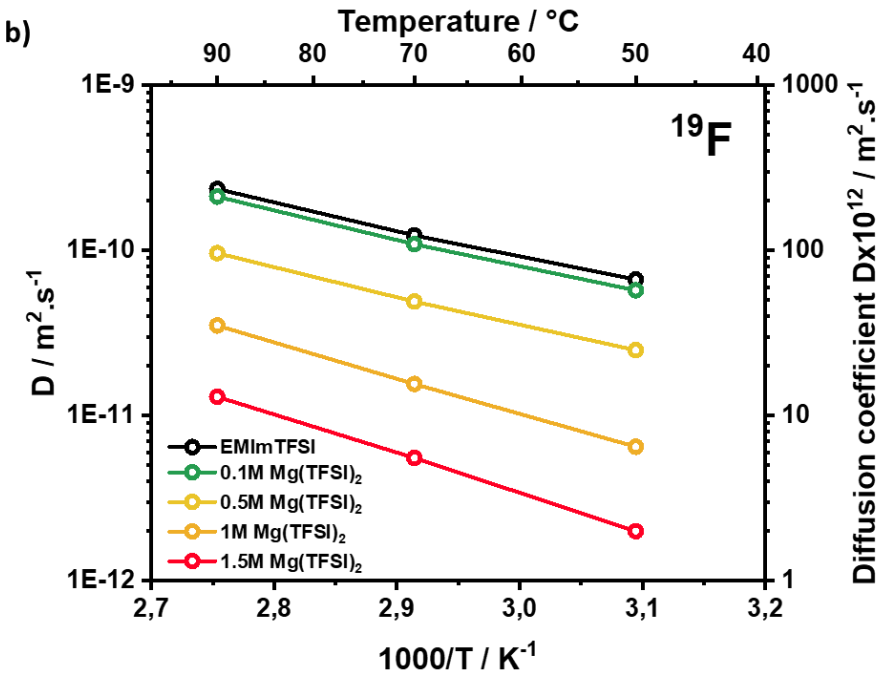


**Figure 4.15: Temperature dependency of self-diffusion coefficients of a) $EMIm^+$ and b) $TFSI^-$ in [EMImTFSI + Mg(TFSI)$_2$] ternary ILs**

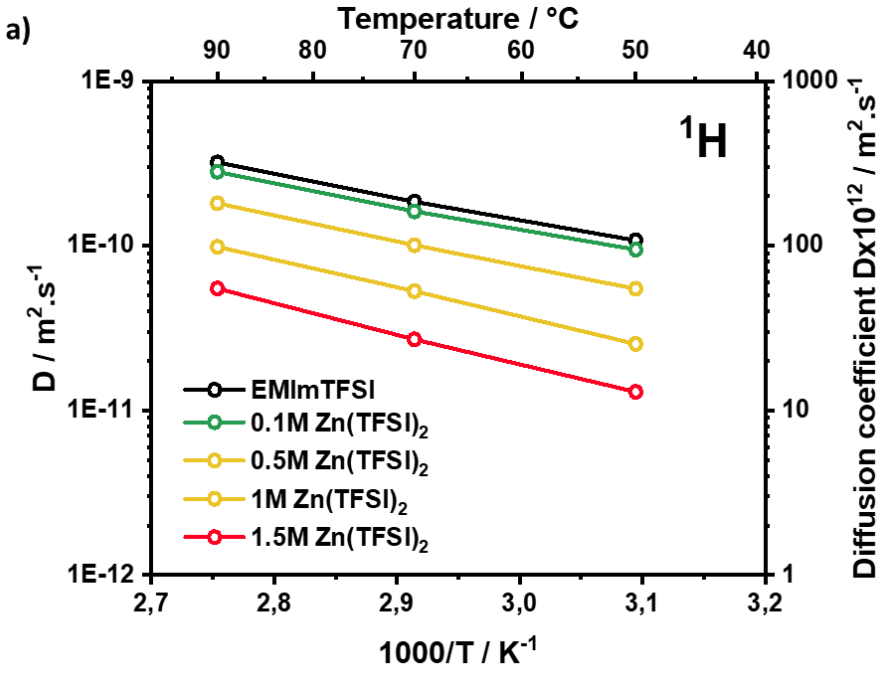

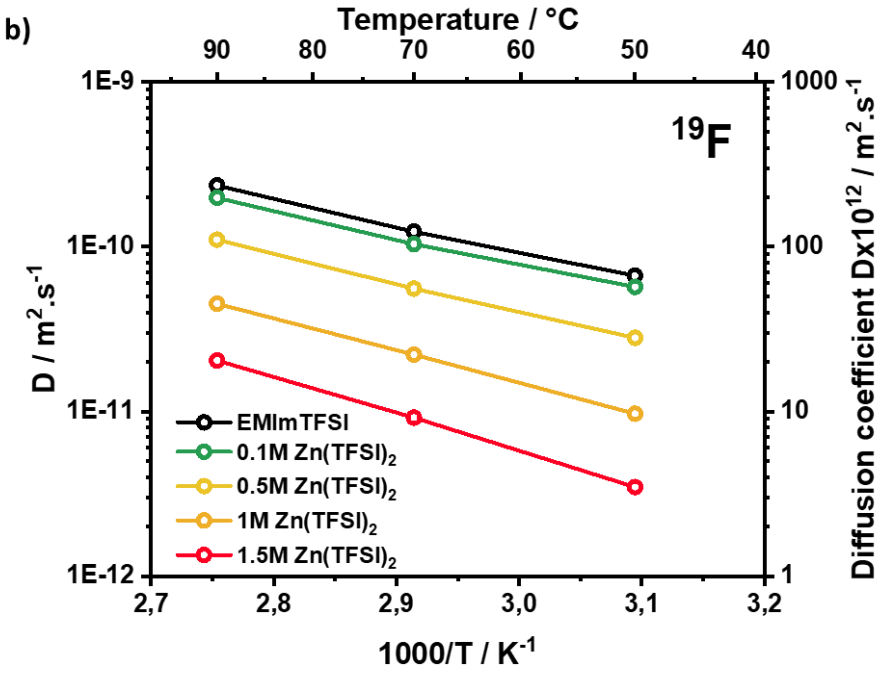


**Figure 4.16: Temperature dependency of self-diffusion coefficients of a) $EMIm^+$ and b) $TFSI^-$ in [EMImTFSI + $Zn(TFSI)_2$] ternary ILs**

The slopes for the diffusion of $EMIm^+$ cations are much less steep than the slopes for $TFSI^-$, showing that here again, the diffusion of $TFSI^-$ is strongly affected by the bivalent salt addition whereas $EMIm^+$ diffusion is less restraint. The drawback of salt addition on viscosity and aggregates formation is exacerbated with $Mg^{2+}$ and slightly higher$Zn^{2+}$ compared to Li-based ternary ILs.

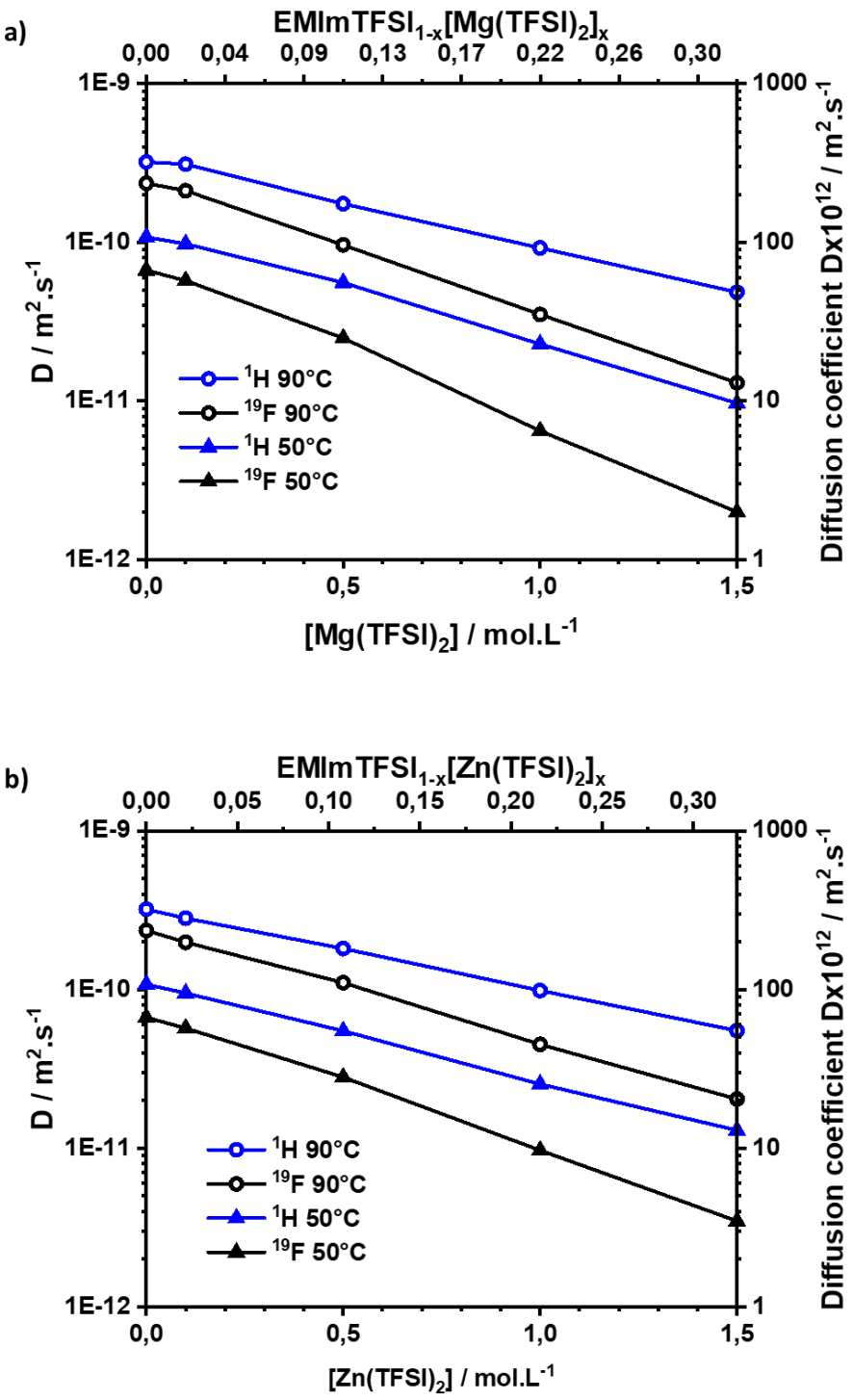


**Figure 4.17: Salt concentration dependency of $EMIm^+$ and $TFSI^-$ self-diffusion coefficients in a) [EMImTFSI + $Mg(TFSI)_2$] and b) [EMImTFSI + $Zn(TFSI)_2$] ternary ILs at 50°C and 90°C**

Finally, self-diffusion coefficients are tabulated in Table 4.7. In this case, the limiting ionic conductivities and ionicities can not be calculated because of the measurement of $Mg^{2+}$ and $Zn^{2+}$ self-diffusion coefficients which are not possible. Although the ionic conductivity values for [EMImTFSI + $Mg(TFSI)_2$] at their highest concentrations are much lower than for the [EMImTFSI + $Zn(TFSI)_2$] ternary

ILs, the self-diffusion coefficients are very close. This result means that the ionicity in [EMImTFSI + $Mg(TFSI)_2$] mixtures is expected to be much lower than in the zinc based ILs, which thus enlightens the great interest of [EMImTFSI + $Zn(TFSI)_2$] electrolytes.

**Table 4.7: Self-diffusion coefficients, limiting molar conductivity and ionicity of [EMImTFSI + $Mg(TFSI)_2$] and [EMImTFSI + $Zn(TFSI)_2$]**

| | $D_{EMIm+}$ at 50°C x$10^{12}$ ($m^2.s^{-1}$) | $D_{TFSI-}$ at 50°C x$10^{12}$ ($m^2.s^{-1}$) |
|---|---|---|
| **EMImTFSI** | 107.9 | 66.7 |
| **EMImTFSI + 0.1M $Mg(TFSI)_2$** | 97.9 | 57.4 |
| **EMImTFSI + 0.5M $Mg(TFSI)_2$** | 55.7 | 24.9 |
| **EMImTFSI + 1M $Mg(TFSI)_2$** | 22.8 | 6.5 |
| **EMImTFSI + 0.1M $Zn(TFSI)_2$** | 94.9 | 57.1 |
| **EMImTFSI + 0.5M $Zn(TFSI)_2$** | 54.9 | 28.0 |
| **EMImTFSI + 1M $Zn(TFSI)_2$** | 25.3 | 9.7 |

Finally, the same conclusion are made on the transport properties in monovalent cation or bivalent cation ternary ILs. The decrease in ionic conductivities and self-diffusion coefficient is clearly related to the interaction forces between the metal cation and TFSI anion. The aggregates formation seems to be enhanced in these two series of samples. Indeed, compared to the neat IL, $TFSI^-$ self-diffusion coefficient is 5-fold lower in [EMImTFSI + LiTFSI] ternary ILs, 15-fold in [EMImTFSI + $Zn(TFSI)_2$] ternary ILs and 25-fold in [EMImTFSI + $Mg(TFSI)_2$] ternary ILs.

In the next part, the relation between the transport properties and the structure of aggregates will be established.

## 4.2.4 Coordination sphere of magnesium and zinc in EMImTFSI

The coordination sphere around $Li^+$ has been presented above and is known to draw the viscosity increase and thus the negative consequences on transport properties. The correlation between the aggregates formation and the conductivity need to be deciphered for bivalent cations.

Raman spectrum for [EMImTFSI + $Mg(TFSI)_2$] and [EMImTFSI + $Zn(TFSI)_2$] ternary ILs are reported in Figure 4.18. The same two populations of $TFSI^-$ are observed at different wavenumbers: 752 $cm^{-1}$ for Mg-doped ILs and 750 $cm^{-1}$ for Zn-doped ILs. These energy shifts are tabulated in Table 4.6.

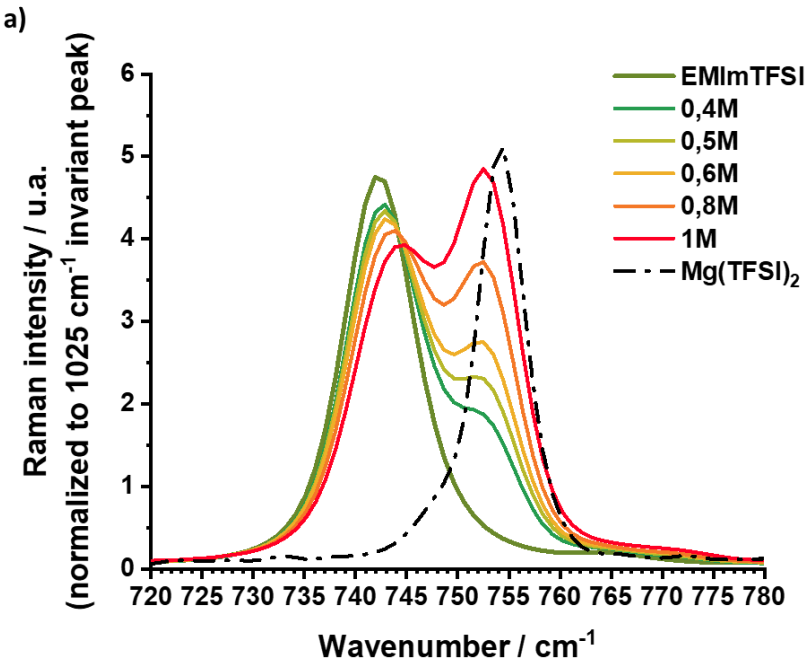

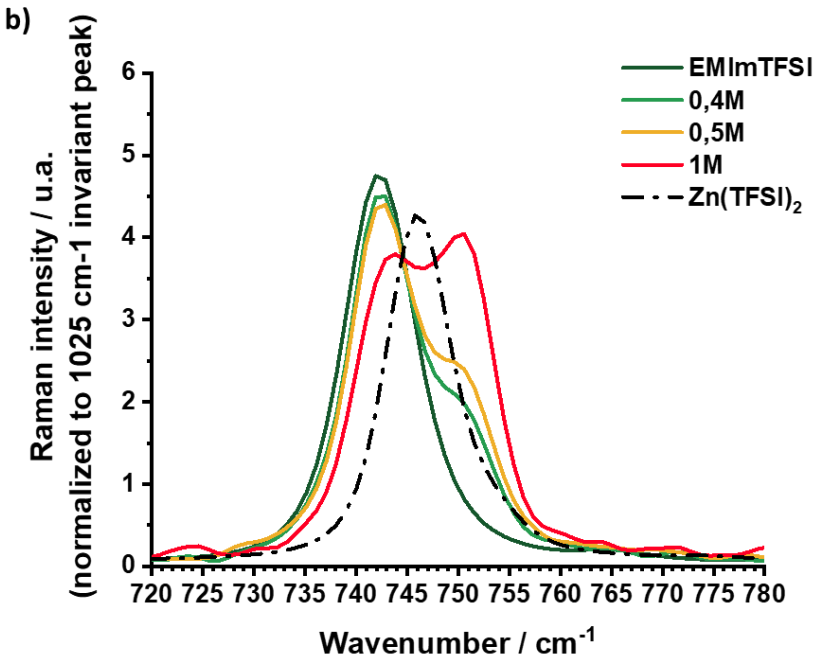


**Figure 4.18: Raman spectrum of a) [EMImTFSI + $Mg(TFSI)_2$] and b) [EMImTFSI + $Zn(TFSI)_2$] ternary ILs at RT in the 720 to 780 $cm^{-1}$ region**

This is interesting to note that the more intense peak in $Zn(TFSI)_2$ salt appears at 746 $cm^{-1}$ whereas the second population of TFSI- vibrations appear at higher energy (750 $cm^{-1}$). An hypothesis could be that the symmetric unit of $Zn(TFSI)_2$ does not allow to obtain an accurate energy for this vibration by Raman spectroscopy alone. This study needs to be coupled with IR spectroscopy to determine the correct average energy for this vibration mode. This value has not been reported in the literature.

**Table 4.8: Ionic conductivities and VTF parameters of [EMImTFSI + LiTFSI] ternary ILs**

| | 1st vibration band energy ($cm^{-1}$) | 2nd vibration band energy ($cm^{-1}$) | 3rd vibration band energy ($cm^{-1}$) | Shift in energy (meV) |
|---|---|---|---|---|
| **EMImTFSI** | 741.4 | 743 | - | - |
| **LiTFSI** | - | - | 748 | - |
| **$Mg(TFSI)_2$** | - | - | 754 | - |
| **$Zn(TFSI)_2$** | - | - | 746* | - |
| **EMImTFSI + LiTFSI** | 741.4 | 743 | 748 | 0.75 |
| **EMImTFSI + $Mg(TFSI)_2$** | 741.4 | 743.4 | 752 | 1.25 |
| **EMImTFSI + $Zn(TFSI)_2$** | 742 | 743 | 750 | 1 |

*Inaccurate because of the salt crystallography, needs to be coupled with an IR study of the TFSI expansion-contraction vibration mode.

Finally, Figure 4.19 shows the coordination number around $Mg^{2+}$ (blue dots) and $Zn^{2+}$ (orange dots). On average, $Mg^{2+}$ is surrounded by four $TFSI^-$ and $Zn^{2+}$ between three and four $TFSI^-$ molecules. The structuration of the IL around the metal cation is therefore correlated to its polarizing power and valence.

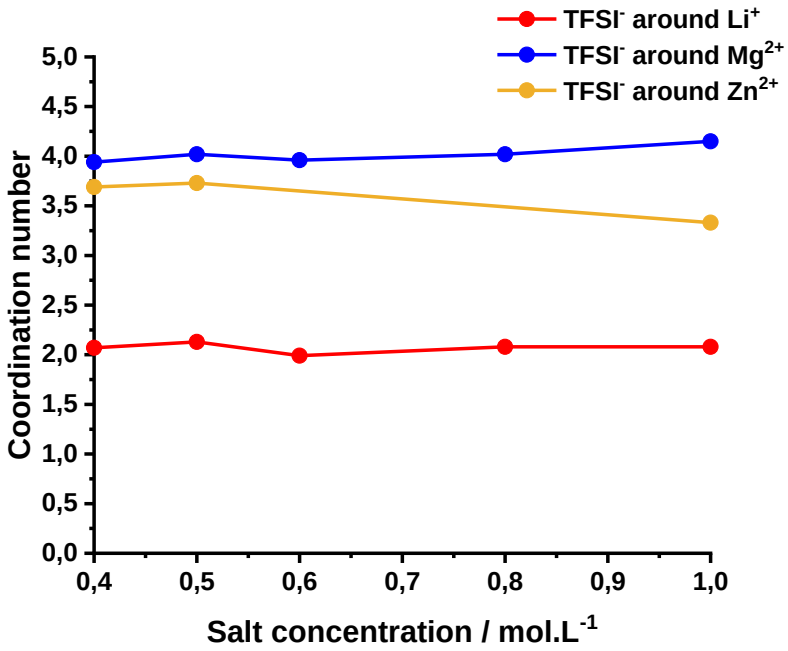


**Figure 4.19: Coordination number around the metalcation in ternary ILs from 0.4M to 1M**

This plot is to link with Figure 4.13. where the glass transition temperatures are sorted in function of the metal cation. Here, metal cations can be sorted in function of their energy shift on their Raman spectrum (Figure 4.18). Sodium and calcium cations were added on this figure because we recorded the Raman spectra, although not reported in this manuscript.

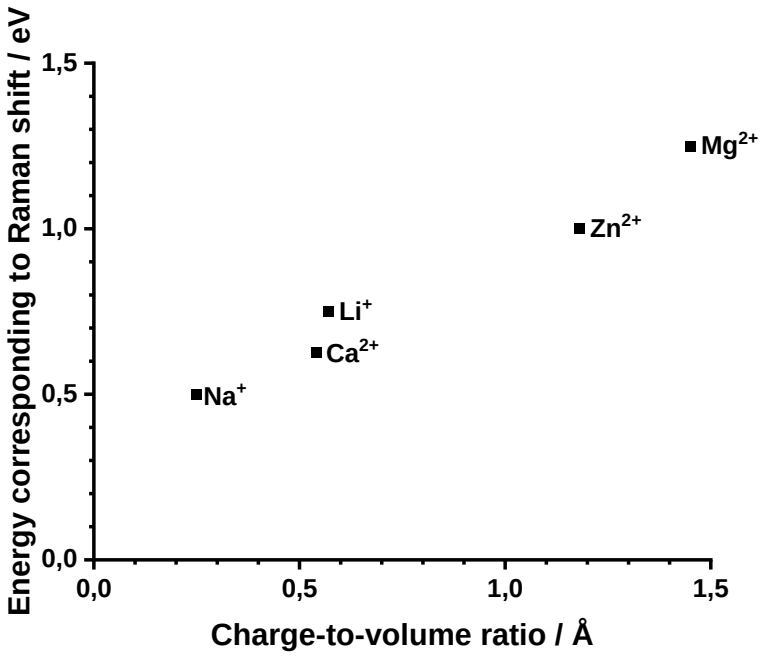


**Figure 4.20: Classification of the interaction strength of metal cations with $TFSI^-$ in EMImTFSI**

These experimental results are in agreement with the computational work on these ternary ILs from Borodin et al which also classify the cations regarding their viscosity, binding energies, size of coordination shell and speed of TFSI exchange rate around metalcations.[9] The possibility for $Na^+$, $Mg^{2+}$ and $Zn^{2+}$ coordination shell to be composed with fluorine atoms from $TFSI^-$ is mentioned.

The three spectroscopies studies allows to obtain structural and transport properties of the ternary ILs. Some fundamental aspects of the interactions at stake in these systems give insights on how bivalent cations behave in solutions compared to the traditional lithium cation.

# Conclusion

In this chapter, three series of ternary ILs ([EMImTFSI + LiTFSI], [EMImTFSI + Mg(TFSI)2] and [EMImTFSI + Zn(TFSI)2]) have been characterized in term of some thermodynamic point of view, transport properties and coordination sphere around the metal cation. The decrease in self-diffusion and thus in macroscopic ionic conductivity has been shown to be due to the increasing viscosity brought by the aggregates formation in these complex concentrated electrolytes.

First, this aggregation phenomenon is directly related to the polarizing power of the metal cation and its interaction ability toward $TFSI^-$ compared to the EMIm-TFSI interaction. The structure and proportion of these aggregates in the liquid phase are also depending on the nature of the cation and the salt concentration. In particular, the TFSI coordination number of around $Li^+$ is two, around $Mg^{2+}$ is five and around $Zn^{2+}$ is four. This structuration of the liquid is also at the origin of the phase transitions shifts observed in DSC. The liquid phase is cooled down very quickly, trapping the liquid phase arrangements for the ions and then heated up slowly.

Secondly, all these results together enable to predict the transport properties of the mixtures that are assessed in a second time thanks to the coupled EIS and PFG NMR. Even if the ionic conductivity and diffusion results are expected and predictable with basic models, analysing the dynamics in relatively complex systems such as ternary ILs, it is essential to understand how the aggregation occurs in these electrolytes. Numerous data were tabulated in this chapter, they will be the starting point to assess the effect of the confinement, within a PVDF polymer matrix, of this series of samples in the following chapter.

# References


(1) Zhou, Q.; Fitzgerald, K.; Boyle, P. D.; Henderson, W. A. Phase Behavior and Crystalline Phases of Ionic Liquid-Lithium Salt Mixtures with 1-Alkyl-3-Methylimidazolium Salts. *Chem. Mater.* **2010**, *22* (3), 1203–1208. https://doi.org/10.1021/cm902691v.

(2) Zhou, Q.; Boyle, P. D.; Malpezzi, L.; Mele, A.; Shin, J.-H.; Passerini, S.; Henderson, W. A. Phase Behavior of Ionic Liquid–LiX Mixtures: Pyrrolidinium Cations and TFSI– Anions – Linking Structure to Transport Properties. *Chem. Mater.* **2011**, *23* (19), 4331–4337. https://doi.org/10.1021/cm201427k.

(3) Pereiro, A. B.; Pastoriza-Gallego, M. J.; Shimizu, K.; Marrucho, I. M.; Lopes, J. N. C.; Piñeiro, M. M.; Rebelo, L. P. N. On the Formation of a Third, Nanostructured Domain in Ionic Liquids. *J. Phys. Chem. B* **2013**, *117* (37), 10826–10833. https://doi.org/10.1021/jp402300c.

(4) Lassègues, J.-C.; Grondin, J.; Aupetit, C.; Johansson, P. Spectroscopic Identification of the Lithium Ion Transporting Species in LiTFSI-Doped Ionic Liquids. *J. Phys. Chem. A* **2009**, *113* (1), 305–314. https://doi.org/10.1021/jp806124w.

(5) Guyomard-Lack, A.; Delannoy, P.-E.; Dupré, N.; Cerclier, C. V.; Humbert, B.; Le Bideau, J. Destructuring Ionic Liquids in Ionogels: Enhanced Fragility for Solid Devices. *Phys. Chem. Chem. Phys.* **2014**, *16* (43), 23639–23645. https://doi.org/10.1039/C4CP03187C.

(6) Giffin, G. A.; Moretti, A.; Jeong, S.; Passerini, S. Complex Nature of Ionic Coordination in Magnesium Ionic Liquid-Based Electrolytes: Solvates with Mobile $Mg^{2+}$ Cations. *J. Phys. Chem. C* **2014**, *118* (19), 9966–9973. https://doi.org/10.1021/jp502354h.

(7) Marie, A.; Said, B.; Galarneau, A.; Stettner, T.; Balducci, A.; Bayle, M.; Humbert, B.; Le Bideau, J. Silica Based Ionogels: Interface Effects with Aprotic and Protic Ionic Liquids with Lithium. *Phys. Chem. Chem. Phys.* **2020**, *22* (41), 24051–24058. https://doi.org/10.1039/D0CP03599H.

(8) Agmon, N. Isoelectronic Theory for Cationic Radii. *J. Am. Chem. Soc.* **2017**, *139* (42), 15068–15073. https://doi.org/10.1021/jacs.7b07882.

(9) Borodin, O.; Giffin, G. A.; Moretti, A.; Haskins, J. B.; Lawson, J. W.; Henderson, W. A.; Passerini, S. Insights into the Structure and Transport of the Lithium, Sodium, Magnesium, and Zinc Bis(Trifluoromethansulfonyl)Imide Salts in Ionic Liquids. *J. Phys. Chem. C* **2018**, 14.

(10) Stolwijk N.A.; Obeidi Sh. Combined analysis of self-diffusion, conductivity, and viscosity data on room temperature ionic liquids. *Electrochimica Acta* **2009**, 54, 1645-1653

# Chapter 5 - Series of confined ionic liquids (ionogels)

# Introduction

Dynamics in ternary ionic liquids (ILs) strongly depend on the viscosity. The salt addition increases the viscosity by the aggregates formation. As discussed in Chapter 4, this phenomenon affects negatively the cationic transport properties expected in an electrolyte.

Confining ILs is one of the strategy to control this phenomenon by bringing a solid-liquid interface, along with providing advantageously solid, shapable, leakage-free electrolyte. The physico-chemical properties of the polymer plays a key role on the impact of the interface. Poly(vinylidene) fluoride (PVDF) is a fluorine-rich polymer on a carbon backbone. The presence of fluorine atoms should have an effect on the hydrogen bonding and coulombic interactions observed in ternary ILs and thus on the inter-ions polarization near the interface. Hence, the behaviour of the ionic liquid at this interface is expected to be different.[1,2]

In this thesis, the parameters related to the polymer such as the chain length and the chemistry will be discussed in the *Perspectives*. Indeed, experimentally herein, PVDF was the only polymer used for the ionogels synthesis and its molar mass was not measured. However, the solid-to-liquid ratio could be controlled during the synthesis.

In this chapter, the methodology used previously for non confined electrolytes will be detailed for solid confined ternary ionic liquids (ILs). The comparison with the previous liquid samples will enable to assess the effect of the confinement on the intrinsic dynamics within the gel (Figure 1).

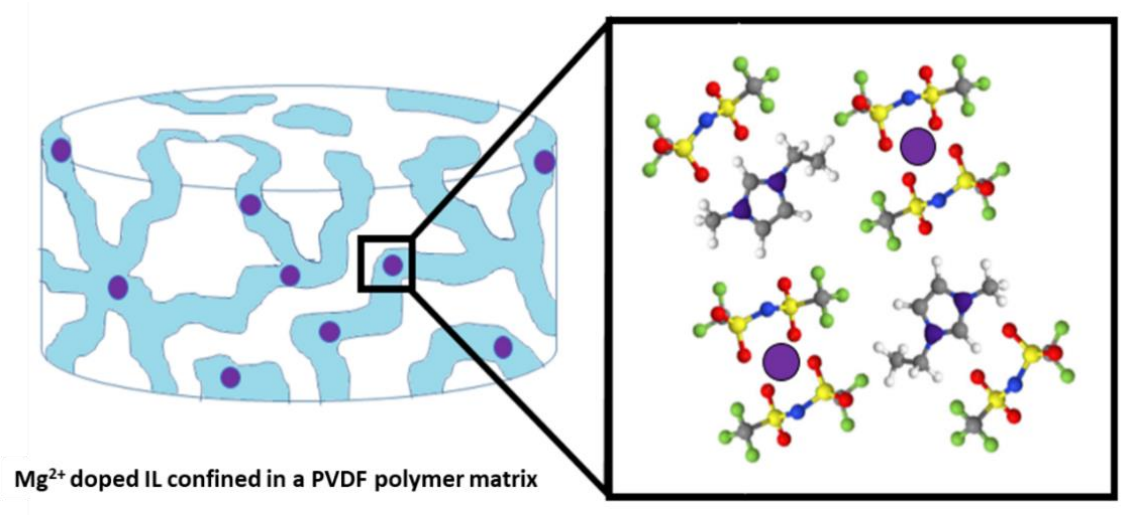


**Figure 5.1: Schematic representation of a solid bivalent-conductive ionogel electrolyte**

# 5.1 Nature of the confining host network: EMImTFSI in PVDF matrix

As mentioned briefly in Chapter 2 when presenting the ionogels synthesis, the following study is about solid-state electrolytes composed of an ionic liquid confined in a PVDF matrix. Figure 2 shows the ionic conductivities, for neat EMImTFSI and for ionogels with two different IL contents, as follow [EMImTFSI:PVDF]wt.: [0.60:0.40] and [0.83:0.17], i.e. 60 %wt and 83 %wt of IL respectively.

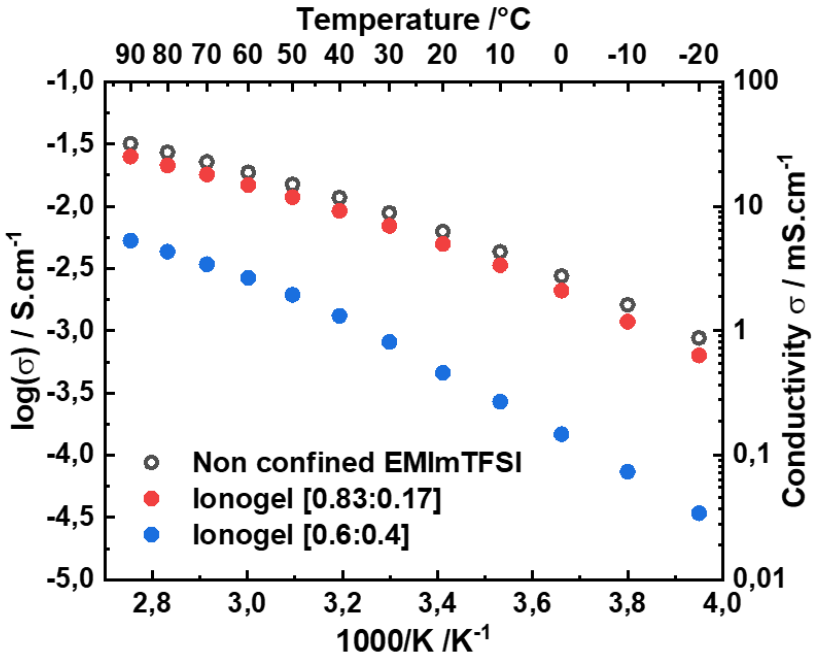


**Figure 5.2: Ionic conductivity for liquid and ionogels electrolytes**

Ionic conductivity increases with temperature for each sample. However, the mobility of charged species decreases with polymer addition. PVDF polymer is not taking part in the macroscopic ionic conductivity, although they are considered while taking into account the form factor of the entire ionogel for the overall ionic conductivity calculation. Nevertheless, the conductivity decrease is not directly proportional to the liquid content. The best solid-to-liquid ratio to maximise the ionic conductivity property is 83 %wt. of EMImTFSI in PVDF matrix. These proportions are close to the maximum content possibly confined in this polymer. The resulting ionogel presents satisfying mechanical properties in term of self-standing ability. On Figure 3 is reported the ionic conductivity normalized by the ionic liquid content in the ionogel for the previous samples.

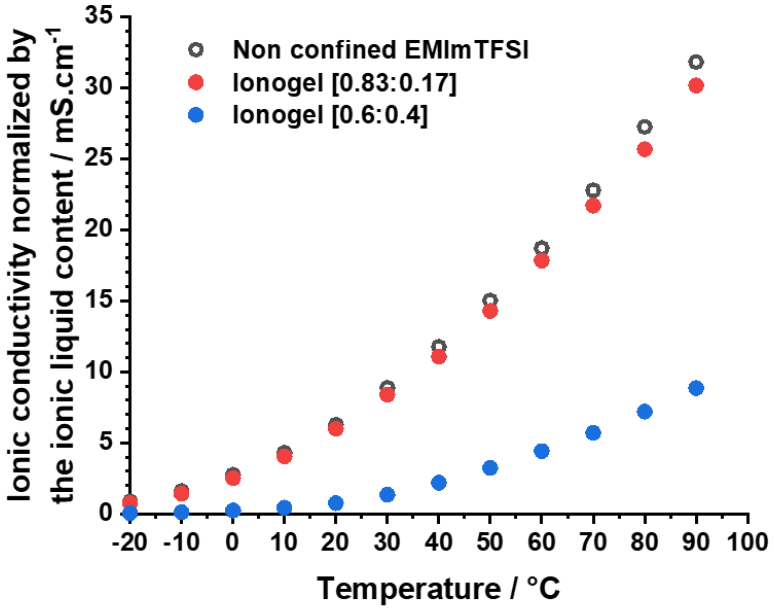


**Figure 5.3: Ionic conductivity of non-confined (open circles), and of confined IL within [0.83 IL : 0.17 PVDF] ionogel (red dots) and [0.60 IL : 0.40 PVDF] ionogel (blue dots).**

In the case of [0.83:0.17] ionogel (red dots), ionic conductivity for the confined ionic liquid is only slightly lower than the non-confined ionic liquid, whereas for the [0.6:0.4] ionogel the ionic conductivity of the confined ionic liquid drastically decreased (blue dots). The solid-liquid interface breaks down aggregates in the IL[3], and hence increases the ionic conductivity. This interface surface, which depends on the liquid-solid ratio, determines the overall dynamics and thus the ionic conductivity.

By means of NMR spectroscopy, restriction measurements were performed following the diffusion of fluorine nuclei ($TFSI^-$) in confined ionogels as a function of diffusion time (Figure 4). It appeared that confinement do not restrict the 3-D diffusion of the anion, which can move freely in the electrolyte up to at least 35 µm in both ionogels. The mean square distance $d_{RMS}$ for the 3D brownian random walk of the ions is given by:

$$d_{RMS} = \sqrt{6Dt}$$

Where $D$ is the diffusion coefficient in $m^2.s^{-1}$ and $t$ the diffusion time in s. This formula is valid for molecules in an isotropic liquid sample under Brownian motion. The direction of displacement is supposed to be random. In the case of ionogels, the polymer which represents a physical barrier for the molecules diffusion, may allow a favoured direction for the diffusion but the average in the sample

should be zero. This information needs to be checked by the following experiment, at least for the anion. It is noteworthy that the interface could be also seen as a 2D surface, thus leading to $\sqrt{4Dt}$, and also as a cylindrical pore to a 1D space restriction thus leading to $\sqrt{2Dt}$.

Here again, in the more confined IL ([0.60 IL : 0.40 PVDF] ionogel (blue dots), the less conducting, the slowing down of the TFSI diffusion is more important. In the less confined ionogel ([0.83 IL : 0.17 PVDF] ionogel (red dots), the most conductive, the slowing down is less important. Indeed the polymer matrix is more dense in the case of the ([0.60 IL : 0.40 PVDF] ionogel and the ions struggle to find a pathway without being slowed down. It is particularly interesting to note that the diffusion is very poorly restricted in the ionogel with 83 %wt of IL. The common conception of closed pores in the ionogel can not be applied with the polymer matrix. The polymer host network should be seen as a 3D net and self-diffusion coefficients are strongly dependant on the mesh size of this network.

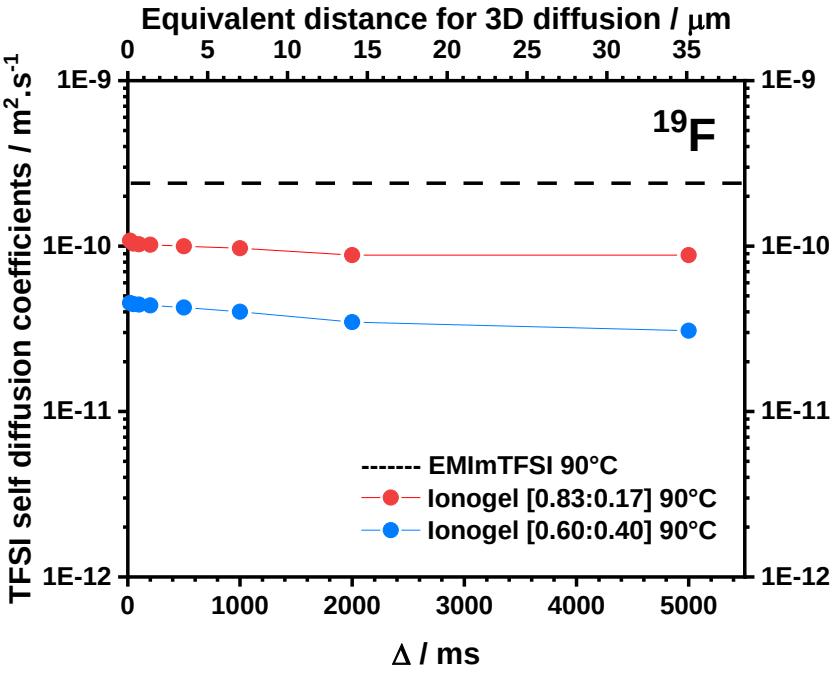


**Figure 5.4: TFSI diffusion dependency on diffusion time Δ for [0.83 IL : 0.17 PVDF] ionogel (red dots) and [0.60 IL : 0.40 PVDF] ionogel (blue dots) ; black dotted line shows the TFSI diffusion obtained with Δ= 20 ms.**

Therefore, the present study focuses on solid samples with a [0.83:0.17] proportions. This series of experiments aim to assess whether this positive effect of the confinement of binary ILs is also beneficial and to what extent in the case of ternary ILs. On one hand, the solid-liquid interface brings new pathways for the ions which will present a good dynamics in the ionogel. On the other hand, the electrons doublets rich matrix brings about new interactions for ions, breaking down aggregates, and leading to significant improvement in dynamics.

# 5.2 Effect of salt addition on the thermal stability and phase transitions of ionogels

## 5.2.1 Thermal stability of the poly(vinylidene) fluoride polymer

The first step is to characterize the polymer itself. Figure 5 shows the thermogram for the pristine powder of polymer chains. Only one phase transition is guessed: the melting point of the polymer occurs at temperature above 150°C. In the literature, the melting point of PVDF is known to be between 160°C and 190°C.[4] This is essential to note that the dissolution of the polymer in DMF and the contact with the IL once the ionogel is formed, changes the thermal properties of the polymer.[5] Zhou et. al reported that the melting of PVDF is facilitated in contact with an IL.[6] Therefore, a shift towards lower temperature is expected for this phase transition in ionogels. As shown Fig. 5, between -100 and +150°C no transition was observed for the PVDF alone.

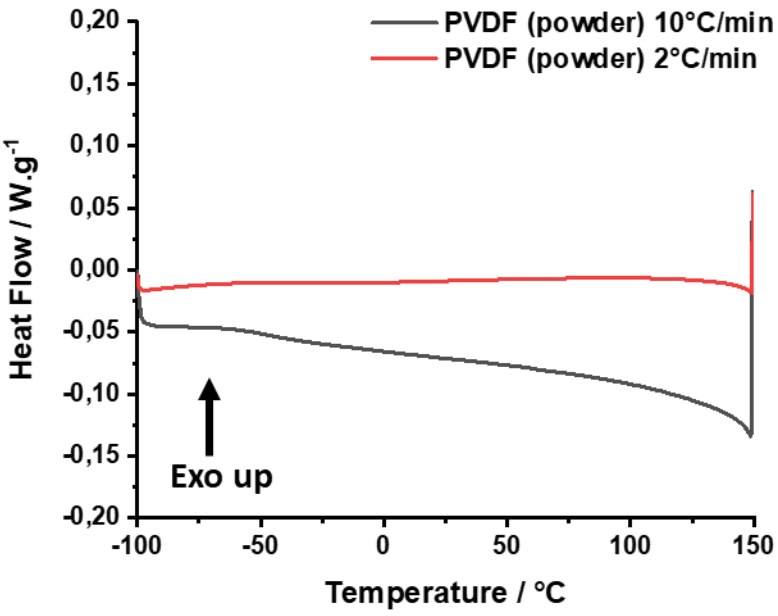


**Figure 5.5: PVDF thermal stability window from -100°C to 150°C**

## 5.2.2 Thermal stability and phase transitions in confined ternary ionic liquids

The phase transitions in ionogels containing Li, Mg and Zn-doped ILs are studied in this subpart. Thermograms are reported on Figure 6, 7 and 8 respectively. The experimental settings are 10°C/min

heating rate and the temperature range is -100 °C to +150 °C; a zoom on the glass transitions is shown. Here again, three main phase transitions are observed: the glass transitions temperatures between -100°C and -75°C, the cold crystallizations temperatures between -75°C and -40°C and the melting temperatures between -40°C and 10°C. A fourth transition is visible above 120°C which is the melting point of the polymer. As expected, this last transition is facilitated, i.e. requires less thermal energy compared to that of the neat PVDF powder since the melting occurs at lower temperatures.

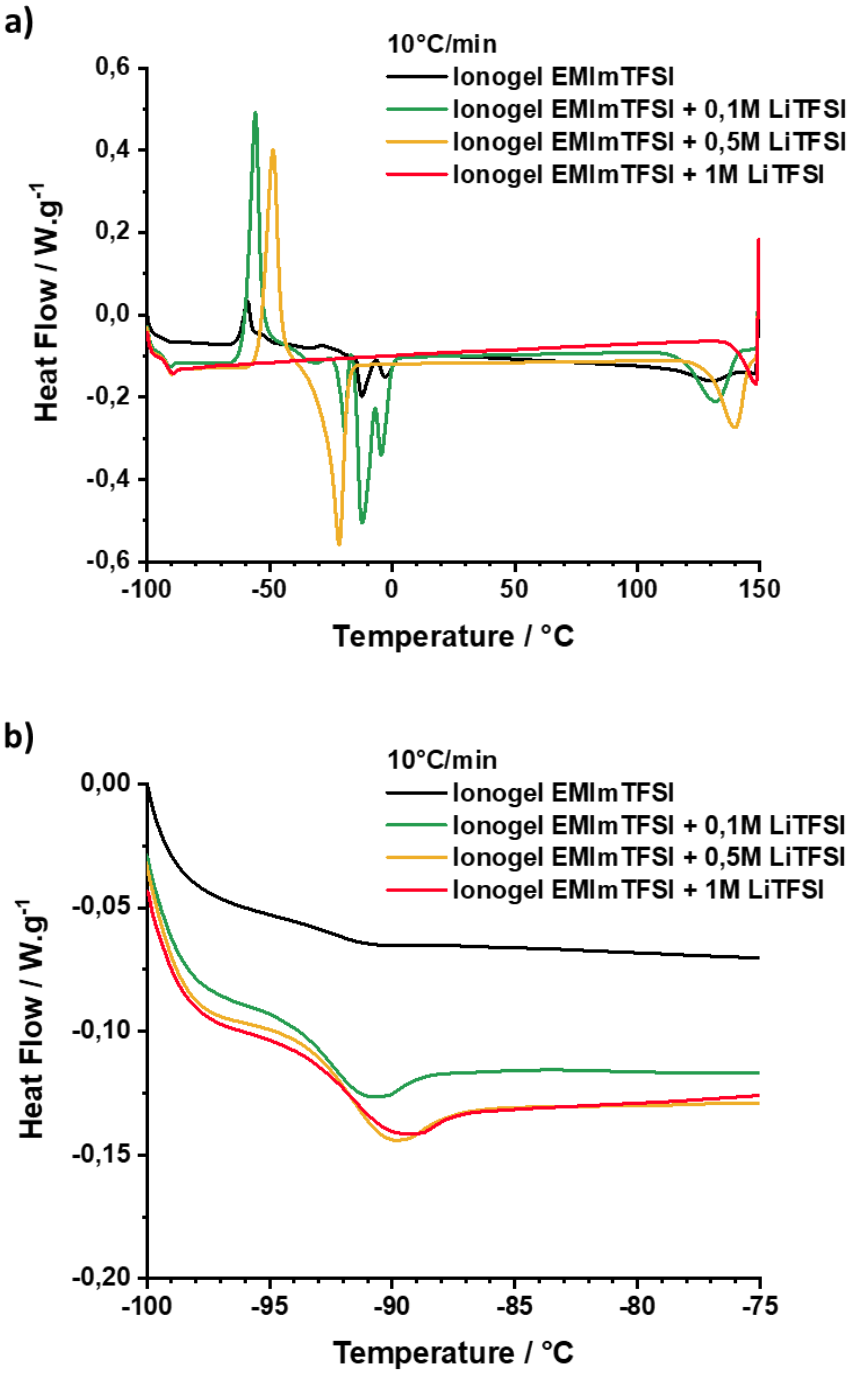


**Figure 5.6: a) Phase transitions for ionogel with [EMImTFSI + LiTFSI] ternary ILs measured with a 10°C/min heating from -100°C to 150°C rate and b) a zoom on glass transitions**

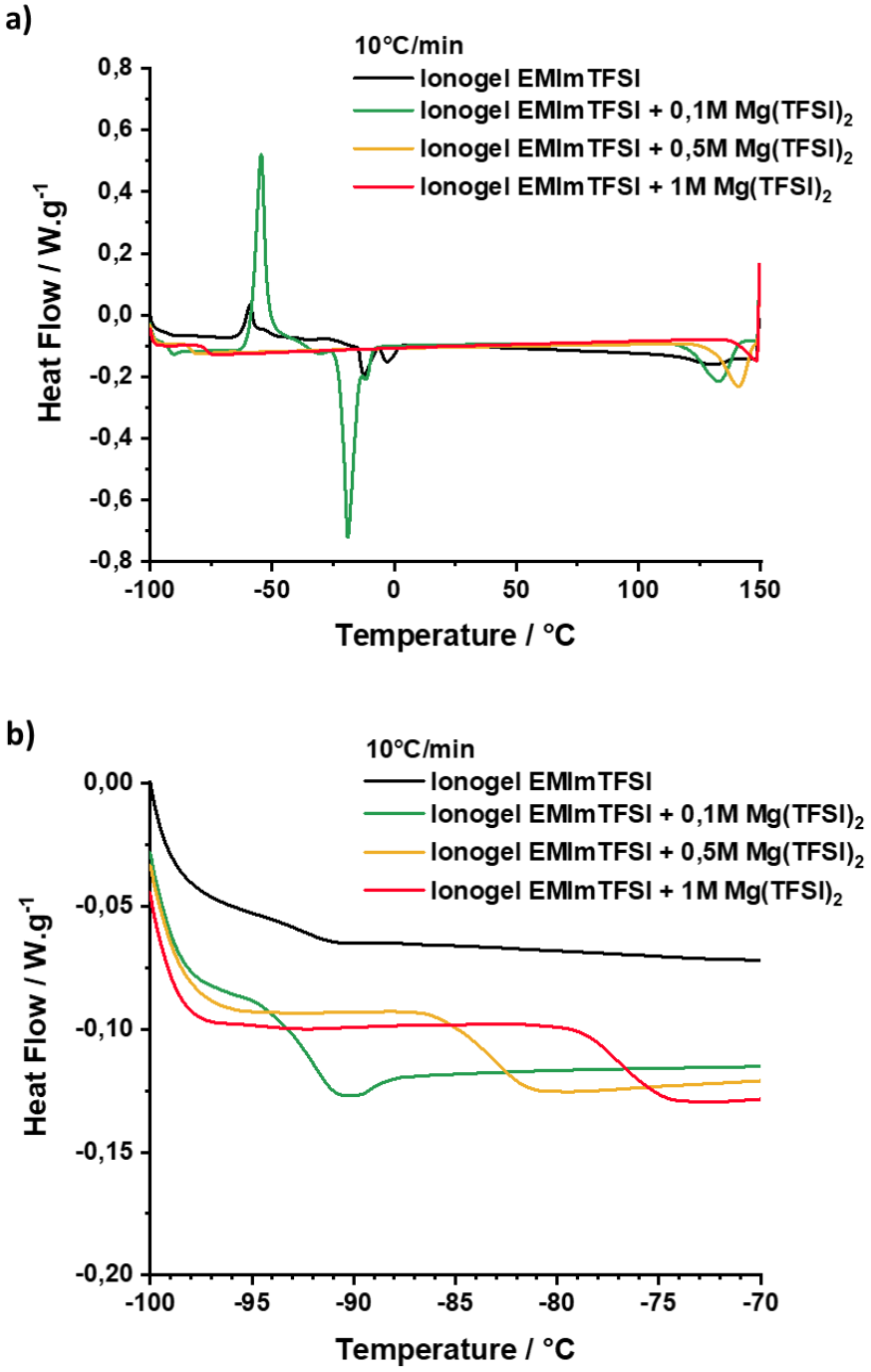


**Figure 5.7: a) Phase transitions for ionogel with [EMImTFSI + $Mg(TFSI)_2$] ternary ILs measured with a 10°C/min heating from -100°C to 150°C rate and b) a zoom on glass transitions**

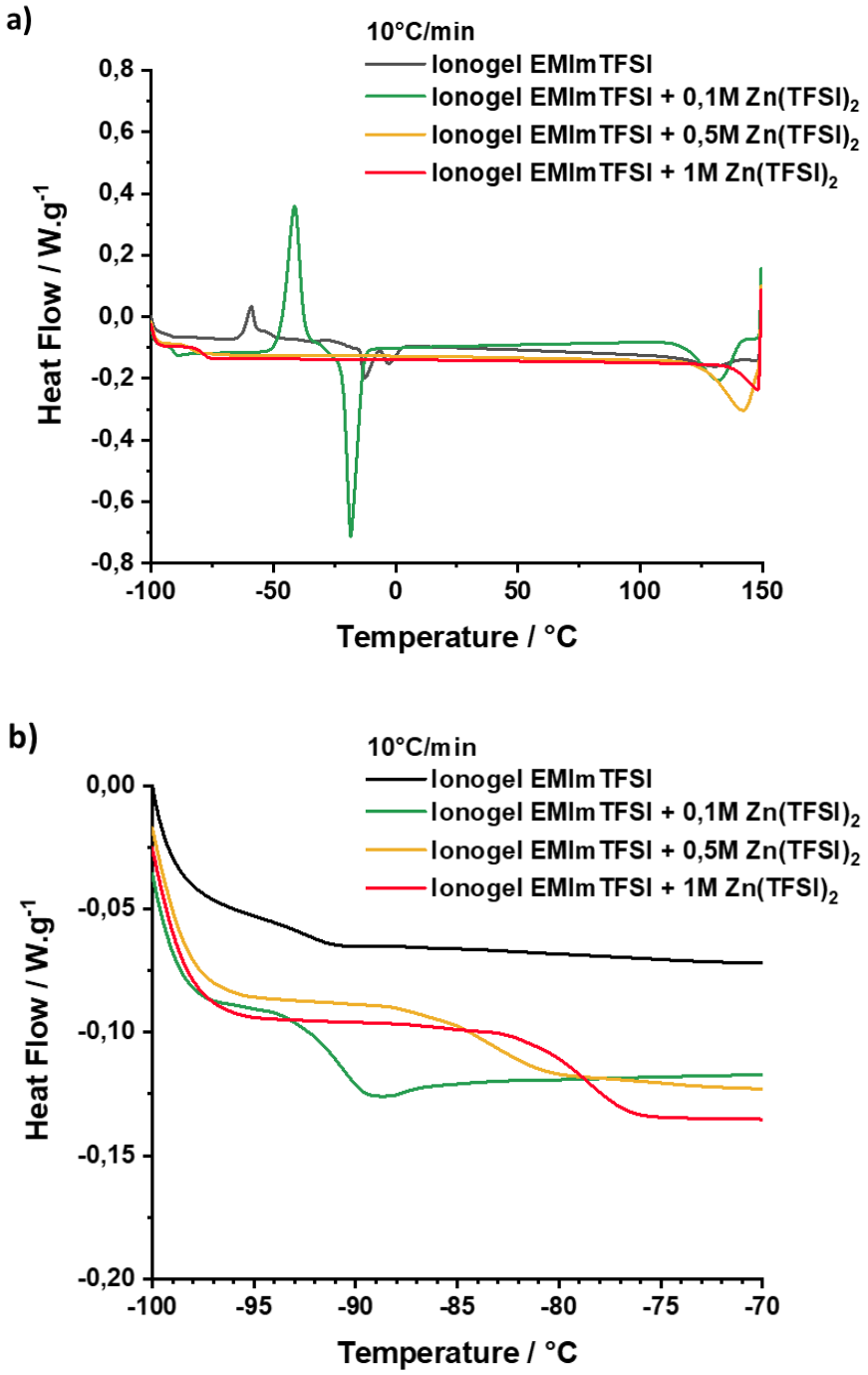


**Figure 5.8: a) Phase transitions for ionogel with [EMImTFSI + $Zn(TFSI)_2$] ternary ILs measured with a 10°C/min heating from -100°C to 150°C rate and b) a zoom on glass transitions**

For all the series, the same trends about the temperatures shifts of phase transitions are observed while adding salts. Salt addition increases the glass transition temperatures, increases the cold crystallization temperatures and decreases the melting temperatures. However, the phase transitions temperatures related to the IL are slightly less offset in the case of the ionogels than for the non-confined ternary ILs. These temperatures are tabulated in Table 5.1.

**Table 5.1: Phase transitions temperatures for ionogels series**

| Thermograms at 10°C/min | Glass transition temperature | Cold crystallization temperature | Solid-to-solid and melting point ionic liquid | Melting point polymer |
|---|---|---|---|---|
| **Ionogel EMImTFSI** | -92°C [a] | -63°C [b]<br>-59°C [c] | $T_{s-s}$: -15°C [b]<br>-12°C [c]<br>$T_m$: -7°C [b]<br>-4°C [c] | 130°C [c] |
| **Ionogel EMImTFSI + 0.1M LiTFSI** | -92°C [a] | -61°C°C [b]<br>-56°C [c] | $T_{s-s}$: -23°C [b]<br>-20°C [c]<br>$T_{s-s}$: -15°C [b]<br>-12°C [c]<br>$T_m$: -9°C [b]<br>-5°C [c] | 132°C [c] |
| **Ionogel EMImTFSI + 0.5M LiTFSI** | -91°C [a] | -54°C [b]<br>-49°C [c] | -29°C [b]<br>-21°C [c] | 140°C [c] |
| **Ionogel EMImTFSI + 1M LiTFSI** | -90°C [a] | / | / | ~150°C [c] |
| **Ionogel EMImTFSI + 0.1M $Mg(TFSI)_2$** | -91°C [a] | -58°C [b]<br>-55°C [c] | $T_{s-s}$: -23°C [b]<br>-19°C [c]<br>$T_m$: -15°C [b]<br>-11°C [c] | 133°C [c] |
| **Ionogel EMImTFSI + 0.5M $Mg(TFSI)_2$** | -83°C [a] | / | / | 141°C [c] |
| **Ionogel EMImTFSI + 1M $Mg(TFSI)_2$** | -77°C [a] | / | / | Above 150°C |
| **Ionogel EMImTFSI + 0.1M $Zn(TFSI)_2$** | -91°C [a] | -47°C [b]<br>-41°C [c] | -21°C [b]<br>-18°C [c] | 132°C [c] |
| **Ionogel EMImTFSI + 0.5M $Zn(TFSI)_2$** | -84°C [a] | / | / | 142°C [c] |
| **Ionogel EMImTFSI + 1M $Zn(TFSI)_2$** | -79°C [a] | / | / | Above 150°C |

[a] measure at the inflexion point, [b] offset, [c] maximum in case of exothermic phase transition, minimum in case of endothermic phase transition

About the polymer melting point, salt addition increases proportionally the transition phase temperature, and/or quenches this transition. This transition is related to the crystallized proportion of PVDF, which is a semi-crystalline polymer. The presence of Li, Mg and Zn salts makes more difficult the melting of this crystallized part, showing that the metal cation interacts with the polymer in its close environment.

The evolution of the glass transition temperatures in function of the salt concentration and the metal cation is shown in Figure 9. Indeed, the shift is less important in the case of ionogels than in the case of non confined ILs. In particular, there is almost no shift for lithium cation. That could be because most of the cations are located at the solid-liquid interface and do not disrupt the bulk IL the same way than in the non-confined IL. A thin layer of IL in contact with the polymer does not have the same thermal behaviour than the bulk IL.

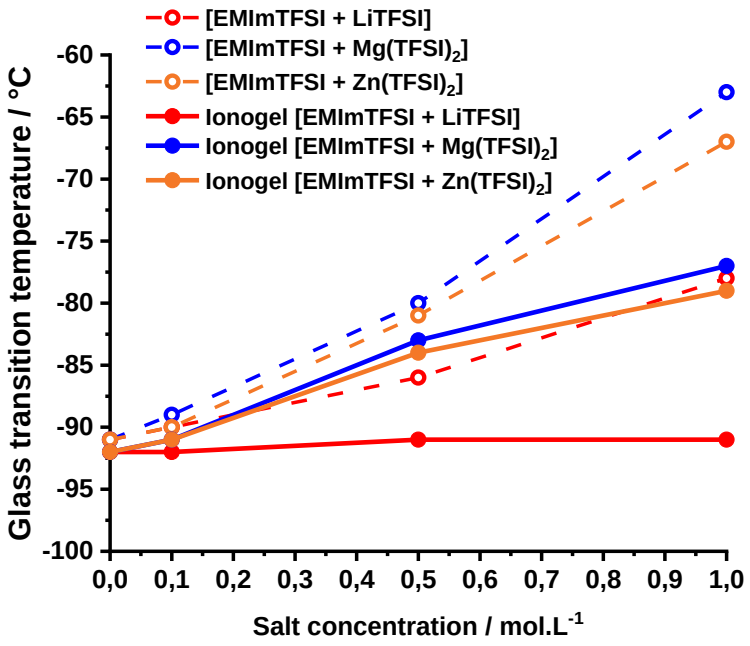


**Figure 5.9: Glass temperature dependency on salt concentration dissolved in non-confined and confined EMImTFSI with $Li^+$, $Mg^{2+}$ and $Zn^{2+}$**

Finally, the study of the thermograms showed that the salt addition has exactly the same effect on the phase transitions in the non-confined and confined ILs. However, the interface between the PVDF and the ionic liquid should bring a slight decrease in viscosity. Moreover, an interaction between the metal cation and the polymer is under consideration.

# 5.3 Macroscopic ionic conductivity evolution with salt addition in ionogels

Thermal analysis brought insights and prediction on the macroscopic viscosity of the IL confined in a polymer matrix. Confinement appears to have a positive effect on the average viscosity of the ILs compared to the non-confined ones. Transport properties are closely correlated to the viscosity through the Walden product. Macroscopic ionic conductivities of the solid electrolytes are shown on Figure 10.

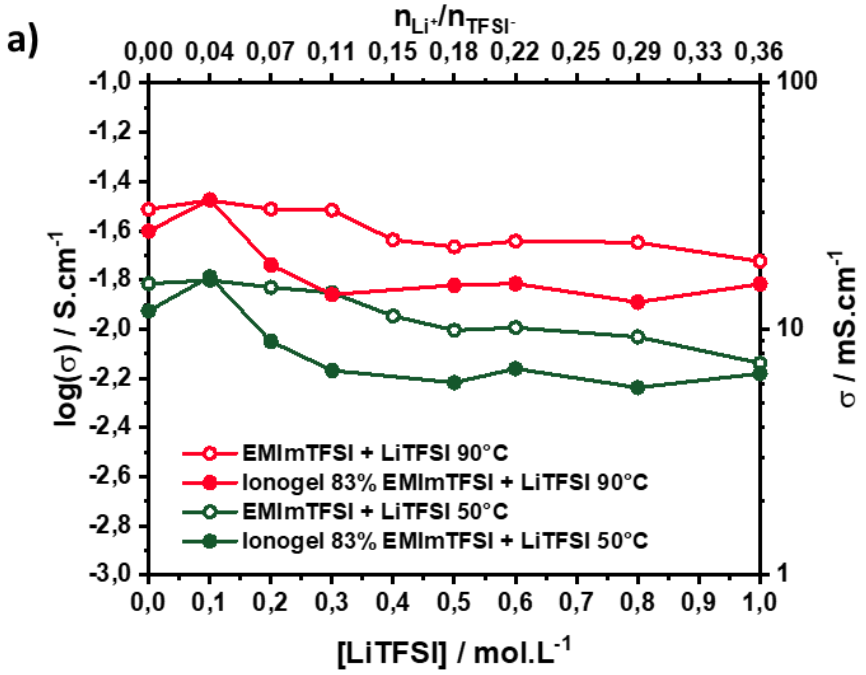

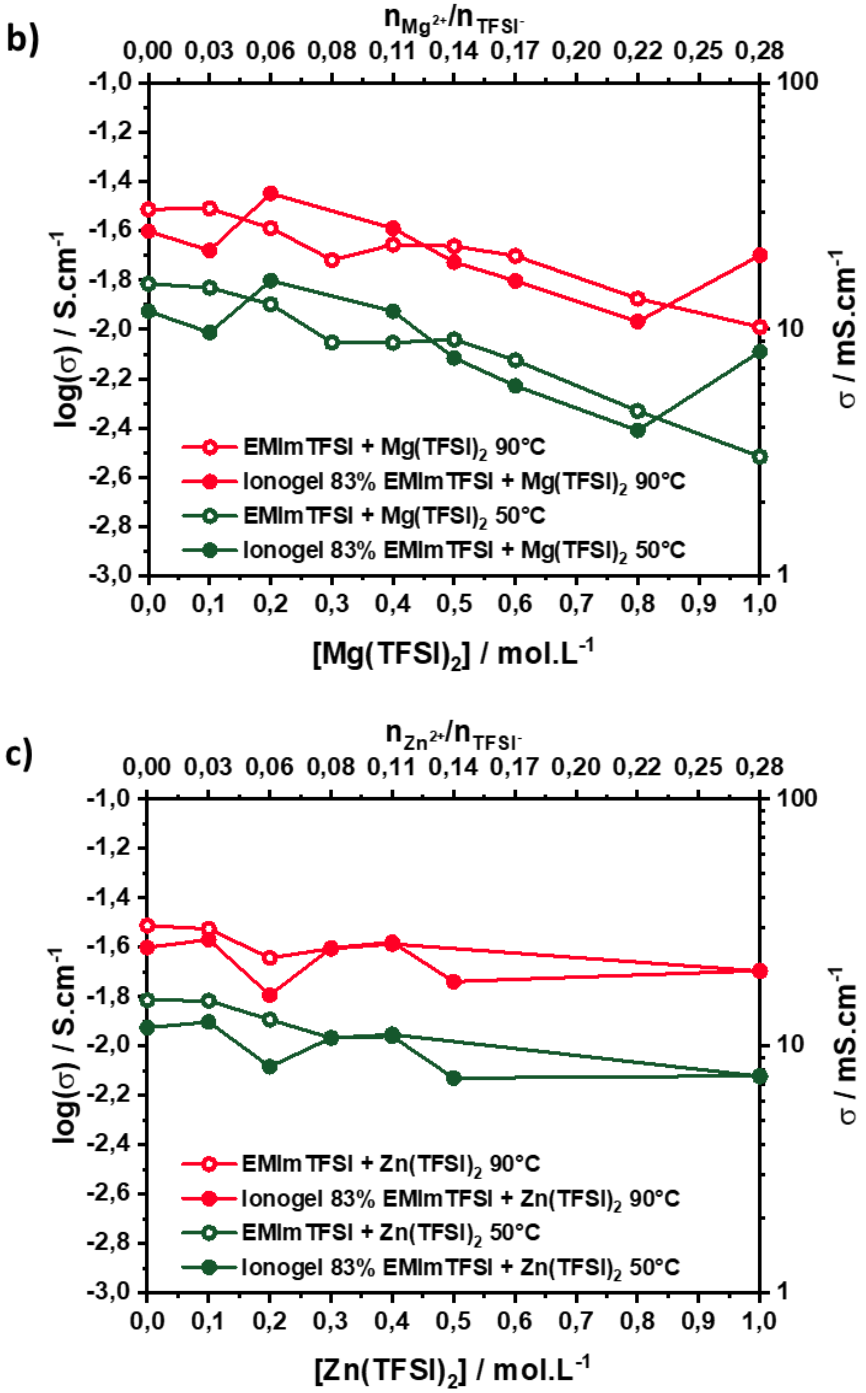


**Figure 5.10: Comparison of ionic conductivity between ionic liquids (open circles) and ionogels (full circles) containing a) lithium and b) magnesium and c) zinc salts.**

Ionic conductivity in ILs containing salts (Figure 5.10, open circles) decreases regularly with the salt addition up to 1 M for each salts (see Chapter 4). Salt addition brings about the formation of strongly coordinated TFSI- anions with metal cations, which enhances the viscosity.[3,7,8] This ionic conductivity decrease does not show the same slope in the case of ionogels, where surprisingly the ionic conductivity equalizes or even overcomes the IL one especially at high concentrations og Mg and

Zn. This is worth to be pointed out because of the current interest in highly concentrated electrolytes for energy storage applications.[9]

It appears that in the case of lithium and zinc the ionic conductivity at 50°C of ionogels at 1M is almost equal to that of the IL one. In the case of magnesium at 1M $Mg(TFSI)_2$, the ionogel conductivity and thus the calculated molar conductivity are even higher than for non confined ILs (Table 5.2 and Table 4.6).

**Table 5.2:** Conductivities neat and 1M Li and Mg concentrated ILs and ionogels

| | $\sigma_{50°C}$ (mS.cm$^{-1}$) | Calculated Vm (cm$^3$.mol$^{-1}$)* | $\Lambda_m$ (S.cm$^2$.mol$^{-1}$) | $\sigma_0$ (mS.cm$^{-1}$) | $T_0/T_g$ | D index |
|---|---|---|---|---|---|---|
| *Ionogel EMImTFSI* | 11.9 | 257.4 | 3.06 | 436.0 | 0.93 | 3.28 |
| *Ionogel EMImTFSI + 0.1M LiTFSI* | 12.3 | 258.6 | 3.15 | 453.8 | 0.96 | 2.84 |
| *Ionogel EMImTFSI + 0.5M LiTFSI* | 6.1 | 252.1 | 1.54 | 463.0 | 0.95 | 3.79 |
| *Ionogel EMImTFSI + 1M LiTFSI* | 6.6 | 247.0 | 1.63 | 319.8 | 1.00 | 2.94 |
| *Ionogel EMImTFSI + 0.1M $Mg(TFSI)_2$* | 9.7 | 257.5 | 2.50 | 423.2 | 0.93 | 3.41 |
| *Ionogel EMImTFSI + 0.5M $Mg(TFSI)_2$* | 7.7 | 257.9 | 1.99 | 612.6 | 0.89 | 3.95 |
| *Ionogel EMImTFSI + 1M $Mg(TFSI)_2$* | 7.1 | 258.4 | 1.83 | 436.0 | 0.95 | 3.03 |
| *Ionogel EMImTFSI + 0.1M $Zn(TFSI)_2$* | 12.5 | 257.4 | 3.22 | 463.0 | 0.94 | 3.19 |
| *Ionogel EMImTFSI + 0.5M $Zn(TFSI)_2$* | 7.4 | 257.6 | 1.91 | 559.9 | 0.90 | 3.92 |
| *Ionogel EMImTFSI + 1M $Zn(TFSI)_2$* | 7.6 | 257.7 | 1.96 | 650.6 | 0.92 | 3.60 |

*As mentioned in Chapter 3, there is an approximation on the calculation of the mixture's molar volume

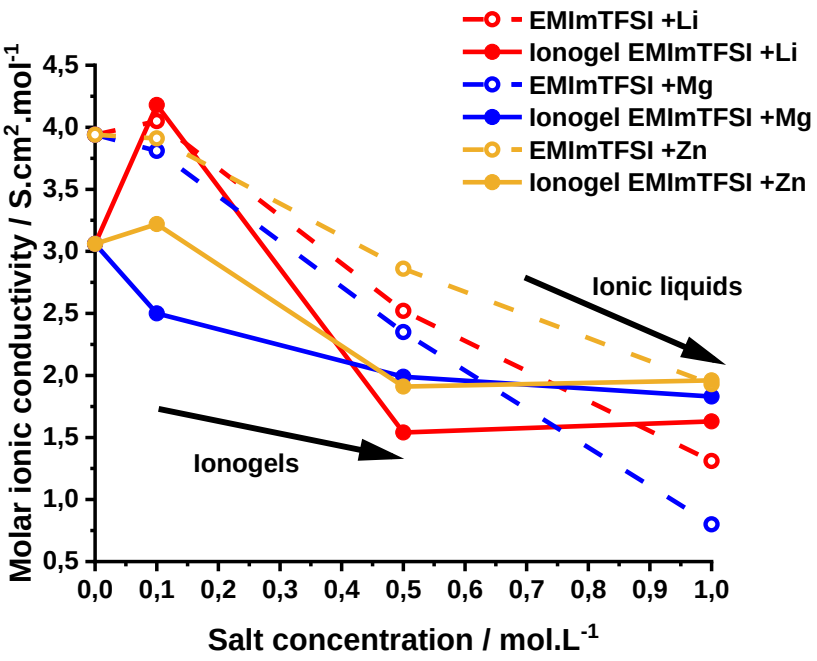


**Figure 5.11: Comparison of the molar ionic conductivity between ionic liquids (open circles) and ionogels (full circles) containing $Li^+$, $Mg^{2+}$ and $Zn^{2+}$**

Finally, the measurement of the macroscopic ionic conductivities showed that the concentration dependency in non-confined IL and ionogels are different (see Figure 5.11). The slopes are steeper for non-confined ternary IL than for ionogels. Dynamics in ionogels is more complex, the solid-to-liquid interface helping to break the aggregates and thus increasing the number of free charged species especially at high concentration.

# 5.4 Self-Diffusion and ionicity in ionogels

## 5.4.1 The better diffusion of $Li^+$ in PVDF ionogels

Here again, EIS is coupled with PFG NMR to analyse ions mobility in confined ILs. The study of individual self-diffusion coefficients helps to validate the hypothesis of disaggregation phenomenon brought by the PVDF matrix. In Figure 5.11, are reported the self-diffusion coefficients measured at 50°C and 90°C for ILs and ionogels containing from 0 M to 1.5 M of Li salt.

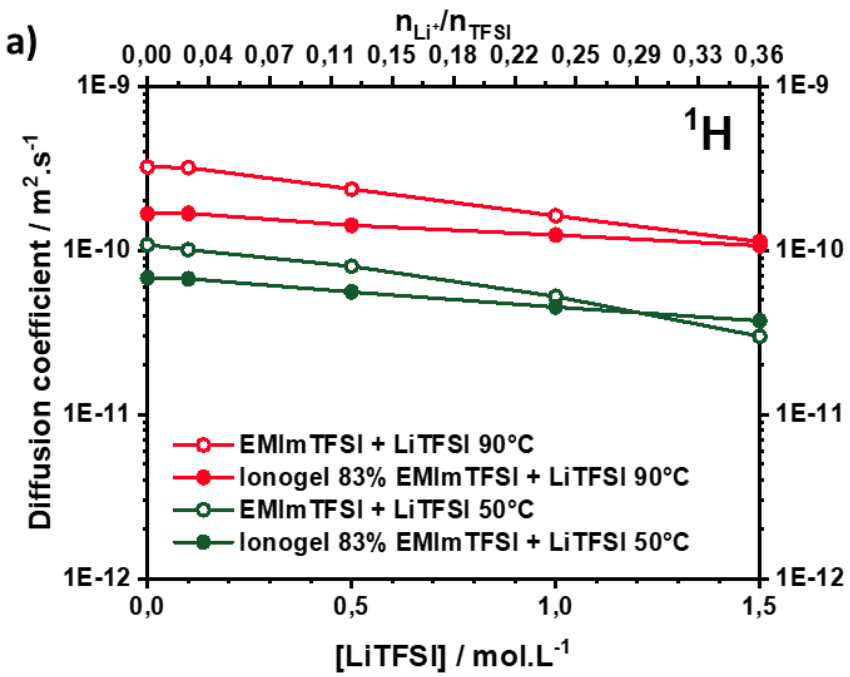
a)
$n_{Li^+}/n_{TFSI}$
0,00 0,04 0,07 0,11 0,15 0,18 0,22 0,25 0,29 0,33 0,36
$^1H$
Diffusion coefficient / $m^2.s^{-1}$
1E-9
1E-10
1E-11
1E-12
0,0
0,5
1,0
1,5
[LiTFSI] / $mol.L^{-1}$
EMImTFSI + LiTFSI 90°C
Ionogel 83% EMImTFSI + LiTFSI 90°C
EMImTFSI + LiTFSI 50°C
Ionogel 83% EMImTFSI + LiTFSI 50°C

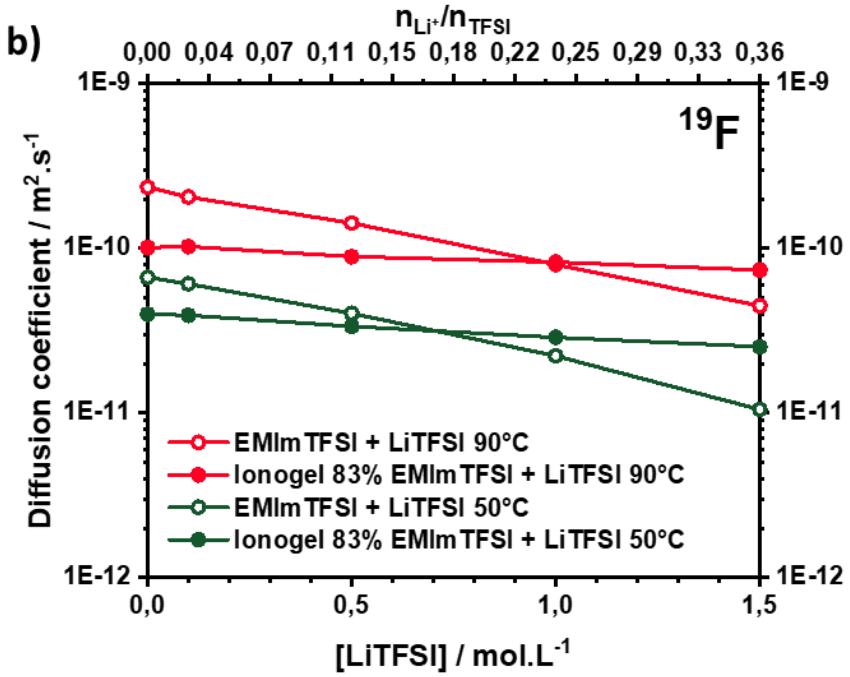
b)
$n_{Li^+}/n_{TFSI}$
0,00 0,04 0,07 0,11 0,15 0,18 0,22 0,25 0,29 0,33 0,36
$^{19}F$
Diffusion coefficient / $m^2.s^{-1}$
1E-9
1E-10
1E-11
1E-12
0,0
0,5
1,0
1,5
[LiTFSI] / $mol.L^{-1}$
EMImTFSI + LiTFSI 90°C
Ionogel 83% EMImTFSI + LiTFSI 90°C
EMImTFSI + LiTFSI 50°C
Ionogel 83% EMImTFSI + LiTFSI 50°C

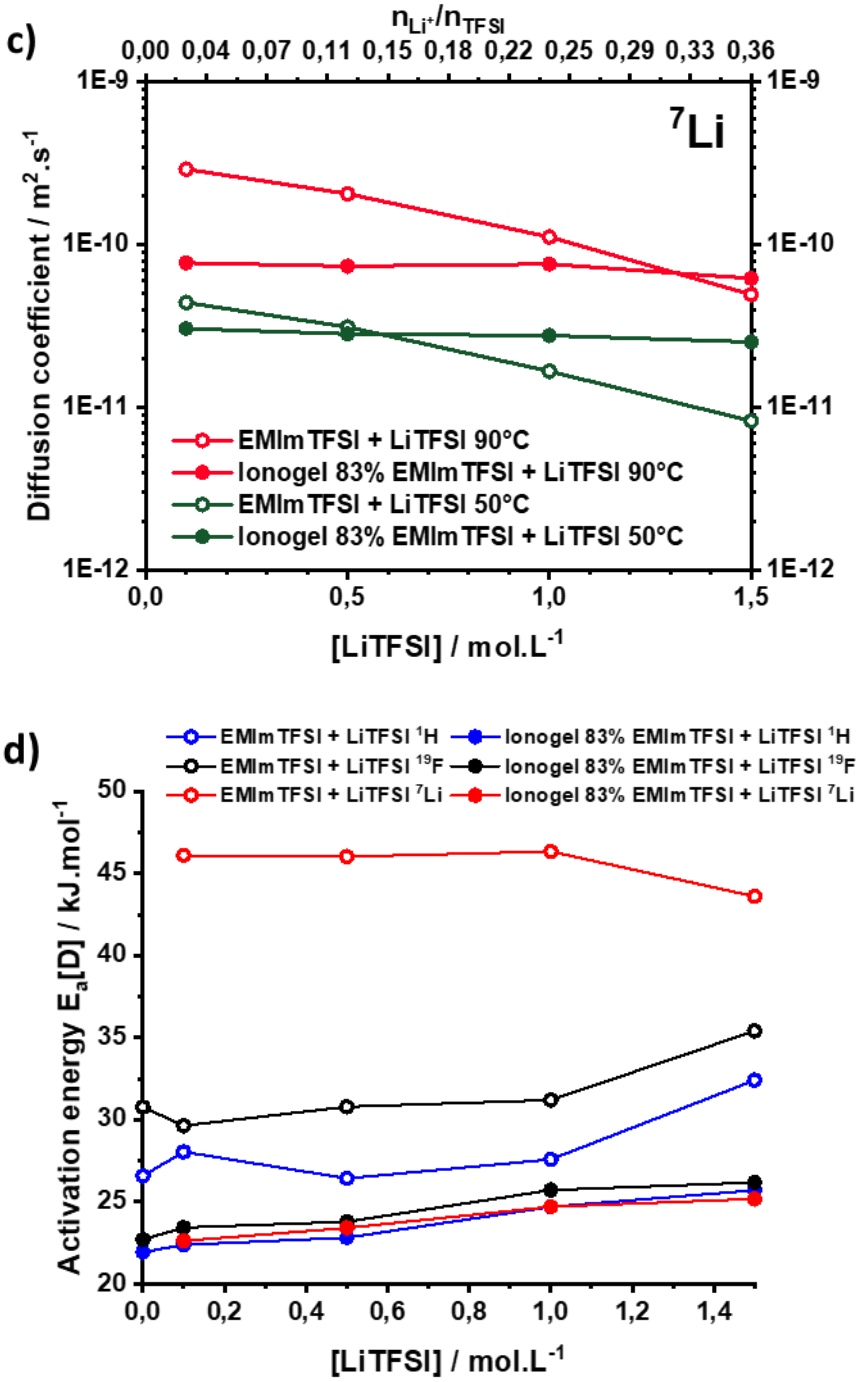


**Figure 5.11: Comparison of self-diffusion coefficients for a) $EMIm^+$, b) $TFSI^-$ and c) $Li^+$ between ILs (open circles) and ionogels (full circles) containing LiTFSI salt and d) their corresponding activation energies**

First, the self-diffusion coefficients are slightly lower at low salt concentrations for ionogels than for the ILs samples. According to the EIS results showing the decrease of macroscopic ionic conductivity, a decrease of self-diffusion coefficients for each species is expected. In particular, $TFSI^-$ and $Li^+$ cation mobility is reduced because of the Li-TFSI coordination. Indeed, all diffusion coefficients for $EMIm^+$, $TFSI^-$ and $Li^+$ decrease with salt addition, and this mobility decrease is stronger for the anions

and lithium ions. The slopes in the case of non-confined ILs are significantly steeper than the slopes for ionogels, showing the positive effect of the confinement.

It is striking that at high salt concentrations, a better diffusion was observed for all the ions in ionogels compared to those of ILs. It is another striking result that the activation energies necessary for the ions mobility are lower for each ion in ionogels (Figure 5.11.d). This confirms that the diffusion is facilitated in ionogels especially for lithium, at least in the range of added salt concentration investigated. Again, it appears that the confinement improves the diffusion, more specifically for highly concentrated ILs. For instance at 50°C, $Li^+$ diffusion in the ionogel is better than in the IL for above 0.6M of LiTFSI.

## 5.4.2 The case of bivalent cations

It is not possible to measure the diffusion of magnesium and zinc nuclei because of the low abundance of the $^{25}Mg$ and $^{67}Zn$ isotopes. Nevertheless, following $^{1}H$ and $^{19}F$ nuclei, the same behaviour for $EMIm^+$ and for $TFSI^-$ are observed in Figures 5.12 and 5.13. Here, as compared to Li-based samples, the steeper slopes show a more important slowdown of diffusion in non-confined ILs for $TFSI^-$ anion and $EMIM^+$ cation than in the corresponding ionogels were the slopes are almost zero. Here again, the diffusion is favoured in confined ILs for high concentrations. Moreover, it is worth noting that this positive effect appears to start at lower salt concentrations in the case of $Mg^{2+}$ and $Zn^{2+}$ than in the $Li^+$ case. The diffusion in ionogels is almost not affected by the salt addition. A hypothesis to explain this result is that the metal cations is adsorbed at the surface of the PVDF and does not participate as strongly in the aggregates formation as in the non-confined ternary ILs. The self-diffusion coefficients and calculated ionicity are tabulated in Table 5.3.

Of course, this raises the question of the strength of this adsorption and of the subsequent release for allowing metal ions diffusion. Nevertheless, since the diffusion of $TFSI^-$ is strongly correlated to the metal cation diffusion, an enhanced diffusion of $Mg^{2+}$ and $Zn^{2+}$ in ionogels compared to the corresponding non-confined ILs is expected. Activation energies for $EMIm^+$ and $TFSI^-$ are lower in the ionogels. Hence, the same behaviour is expected for the magnesium and zinc cations with a strong decrease of the energy needed to diffuse.

Another clue in favour of this advantageous phenomenon occuring in ionogels, is that the self-diffusion coefficients of $TFSI^-$ are higher in the case of bivalent cations than in the case of lithium especially at high concentrations. A competitive interaction of the metal cations with the polymer

implies the reduction of the cation-TFSI aggregates formation. Therefore, the mobility of the cation and $TFSI^-$ would be both enhanced. One the other hand, the diffusion of $EMIm^+$ is better in Li-based ionogels than in the bivalent cations ones, showing that probably, a proportion of $TFSI^-$ initially coordinated to the bivalent metal cations in the ternary ILs, is free again back in the bulk to form EMIm-TFSI pairs in the ionogel.

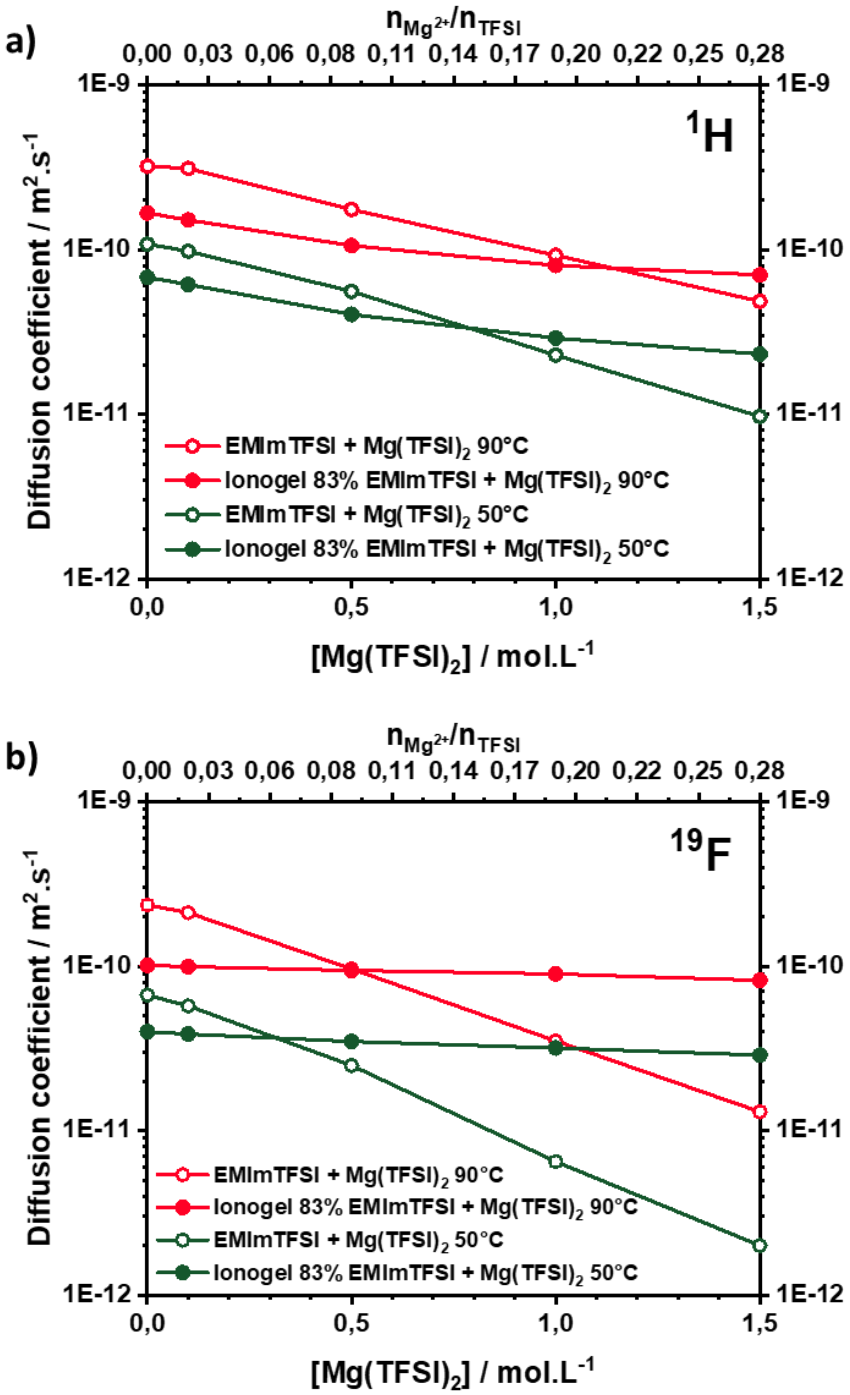

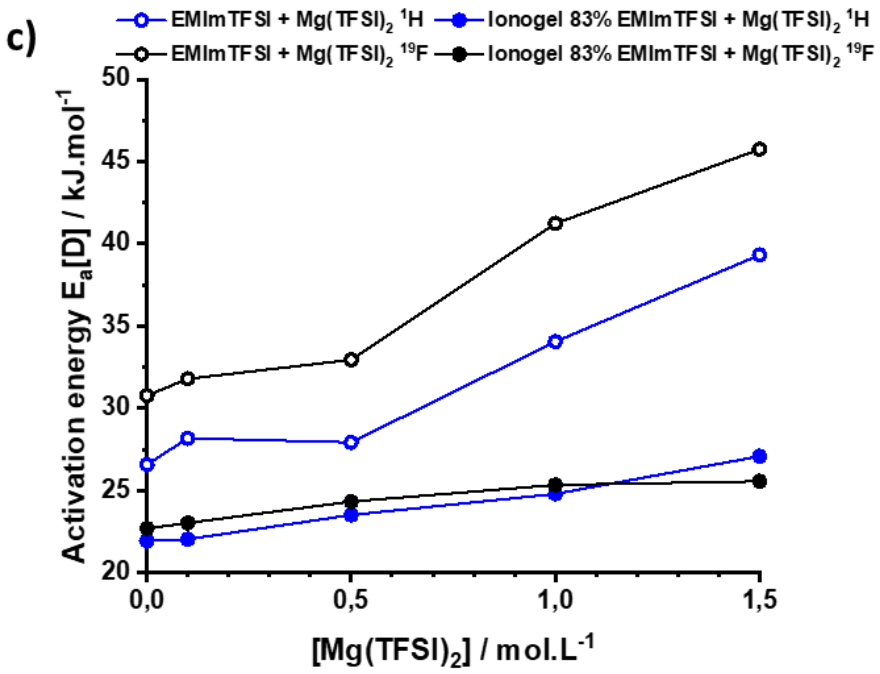


**Figure 5.12: Self-diffusion coefficients for a) $EMIm^+$ and b) $TFSI^-$ between ILs (open circles) and ionogels (full circles) containing $Mg(TFIS)_2$ salt and c) their corresponding activation energies**

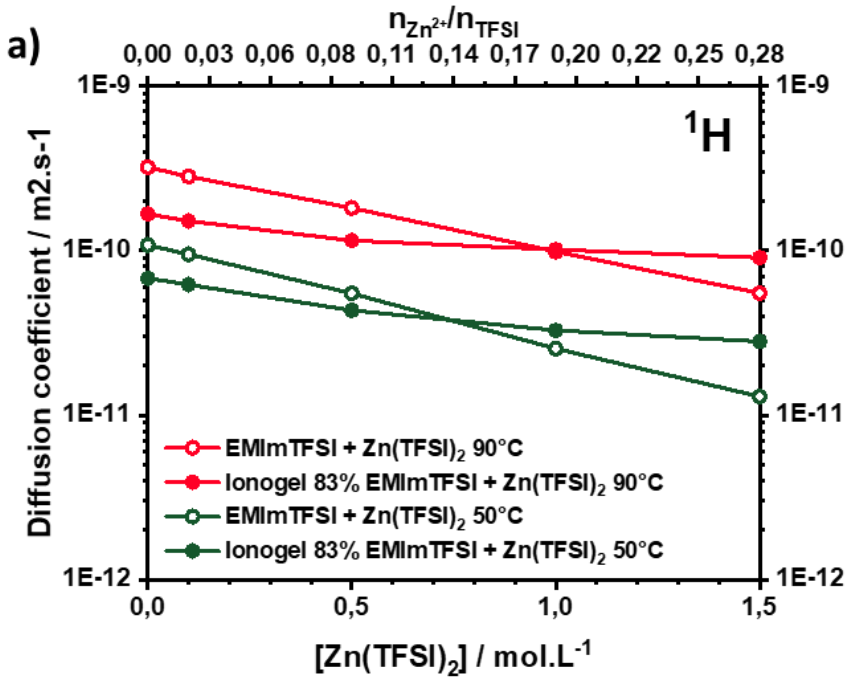

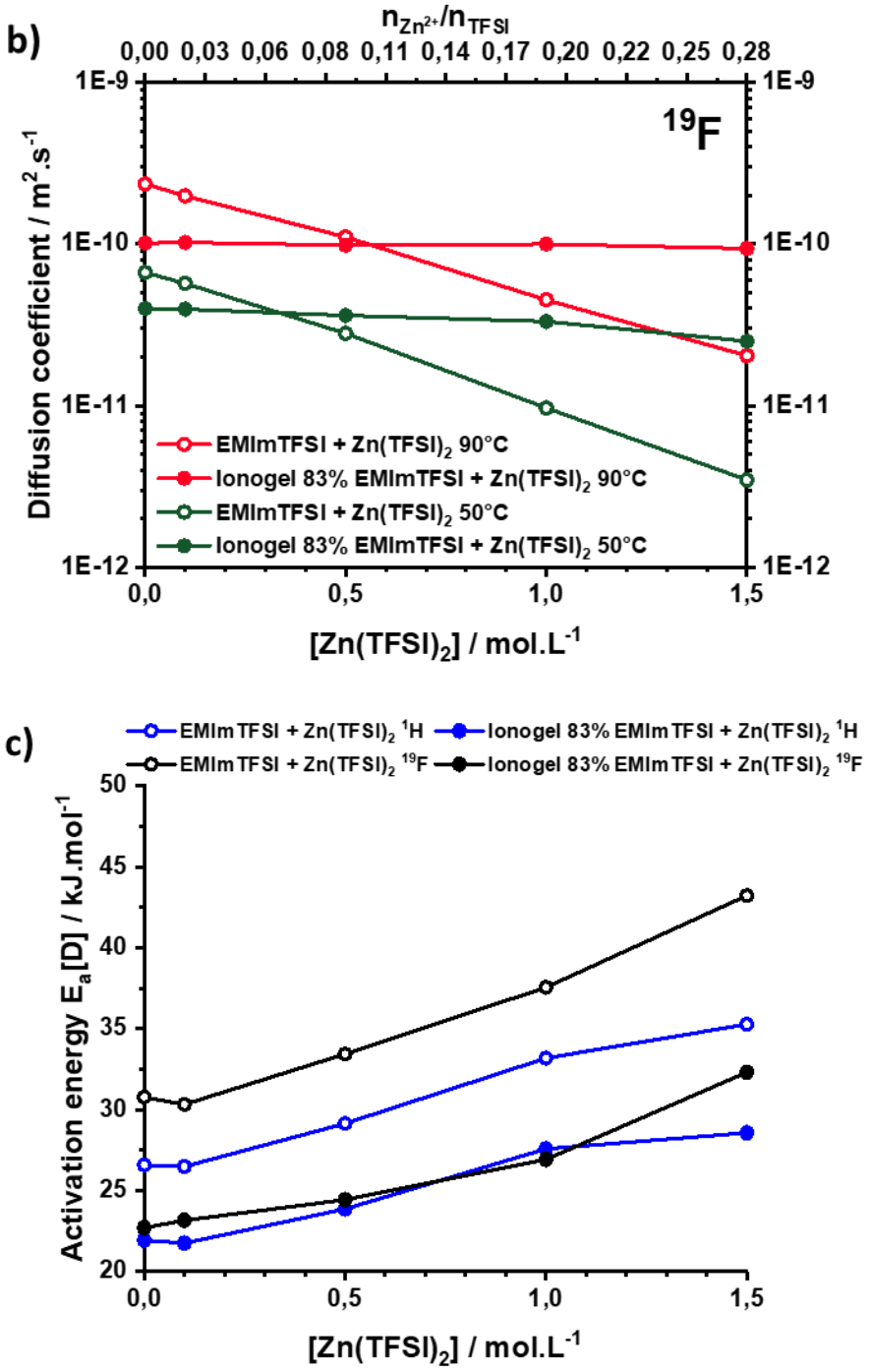


**Figure 5.13: Self-diffusion coefficients for a) $EMIm^+$ and b) $TFSI^-$ between ILs (open circles) and ionogels (full circles) containing $Zn(TFSI)_2$ salt and c) their corresponding activation energies**

**Table 5.3: Self-diffusion coefficients, limiting molar conductivity and ionicity of Li, Mg and Zn ionogels**

| | $D_{EMIm+}$ at 50°C x$10^{12}$ ($m^2.s^{-1}$) | $D_{TFSI-}$ at 50°C x$10^{12}$ ($m^2.s^{-1}$) | $D_{Li+}$ at 50°C x$10^{12}$ ($m^2.s^{-1}$) | $\Lambda_{NMR}$ at 50°C ($S.cm^2.mol^{-1}$) | $\Lambda_{EIS}$ at 50°C ($S.cm^2.mol^{-1}$) | Ionicity (%) |
|---|---|---|---|---|---|---|
| **Ionogel EMImTFSI** | 67.9 | 40.0 | / | 3.74 | 3.06 | 81.9 |
| **Ionogel EMImTFSI + 0.1M LiTFSI** | 67.1 | 39.3 | 30.6 | 3.65 | 3.15 | 86.3 |
| **Ionogel EMImTFSI + 0.5M LiTFSI** | 55.7 | 33.7 | 28.4 | 2.98 | 1.54 | 51.6 |
| **Ionogel EMImTFSI + 1M LiTFSI** | 45.1 | 28.9 | 27.7 | 2.42 | 1.63 | 67.5 |
| **Ionogel EMImTFSI + 0.1M $Mg(TFSI)_2$** | 61.3 | 38.7 | / | / | 2.50 | / |
| **Ionogel EMImTFSI + 0.5M $Mg(TFSI)_2$** | 40.4 | 34.8 | / | / | 1.99 | / |
| **Ionogel EMImTFSI + 1M $Mg(TFSI)_2$** | 29 | 31.8 | / | / | 1.83 | / |
| **Ionogel EMImTFSI + 0.1M $Zn(TFSI)_2$** | 62.0 | 39.6 | / | / | 3.22 | / |
| **Ionogel EMImTFSI + 0.5M $Zn(TFSI)_2$** | 43.3 | 36.2 | / | / | 1.91 | / |
| **Ionogel EMImTFSI + 1M $Zn(TFSI)_2$** | 32.7 | 33.2 | / | / | 1.96 | / |

# 5.5 Ionic coordination

Herein, the coordination sphere of the $Li^+$, $Mg^{2+}$ and $Zn^{2+}$ cations at the solid/liquid interface in ionogels arestudied. Raman spectrum for the ionogels series are shown in Figure 5.14.

First, there is a drastic decrease of the second population of TFSI coordinated with alkali/alkali earth cations in the ionogel. For all the studied concentrations, the shoulder which is specific to the ternary ILs (Chapter 4, Fig. 4.9 and 4.18) disappears with confinement (see black arrows on Figure 5.14). That means that the coordination number of metal cations in the confined ternary IL decreases. There are less TFSI in the close environment of $Li^+$, $Mg^{2+}$or $Zn^{2+}$. The main hypothesis is to attribute the decrease in coordination number to the migration of metal cations to the surface of the polymer, which is rich in fluorine non-binding doublets.

A second clue is the appearance of a new vibration band around 868 $cm^{-1}$ that does not exist in the ternary IL neither in the pure salt and PVDF Raman spectrum. This new band could be attributed to the C-F bonds vibration mode of the PVDF in presence of lithium, magnesium or zinc. The slight difference in energy shows that the interaction strength between monovalent and bivalent cations and the host matrix depends on the cation (867.3 $cm^{-1}$ for Li; 868.2 $cm^{-1}$ for Mg and Zn). This is another clue about the direct interaction between the metal cations and the polymer surface.

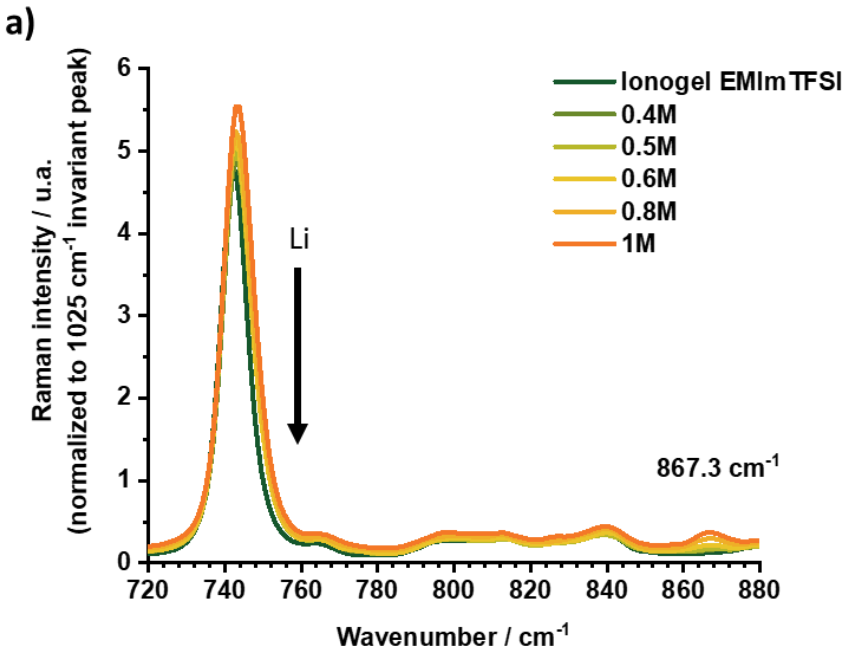

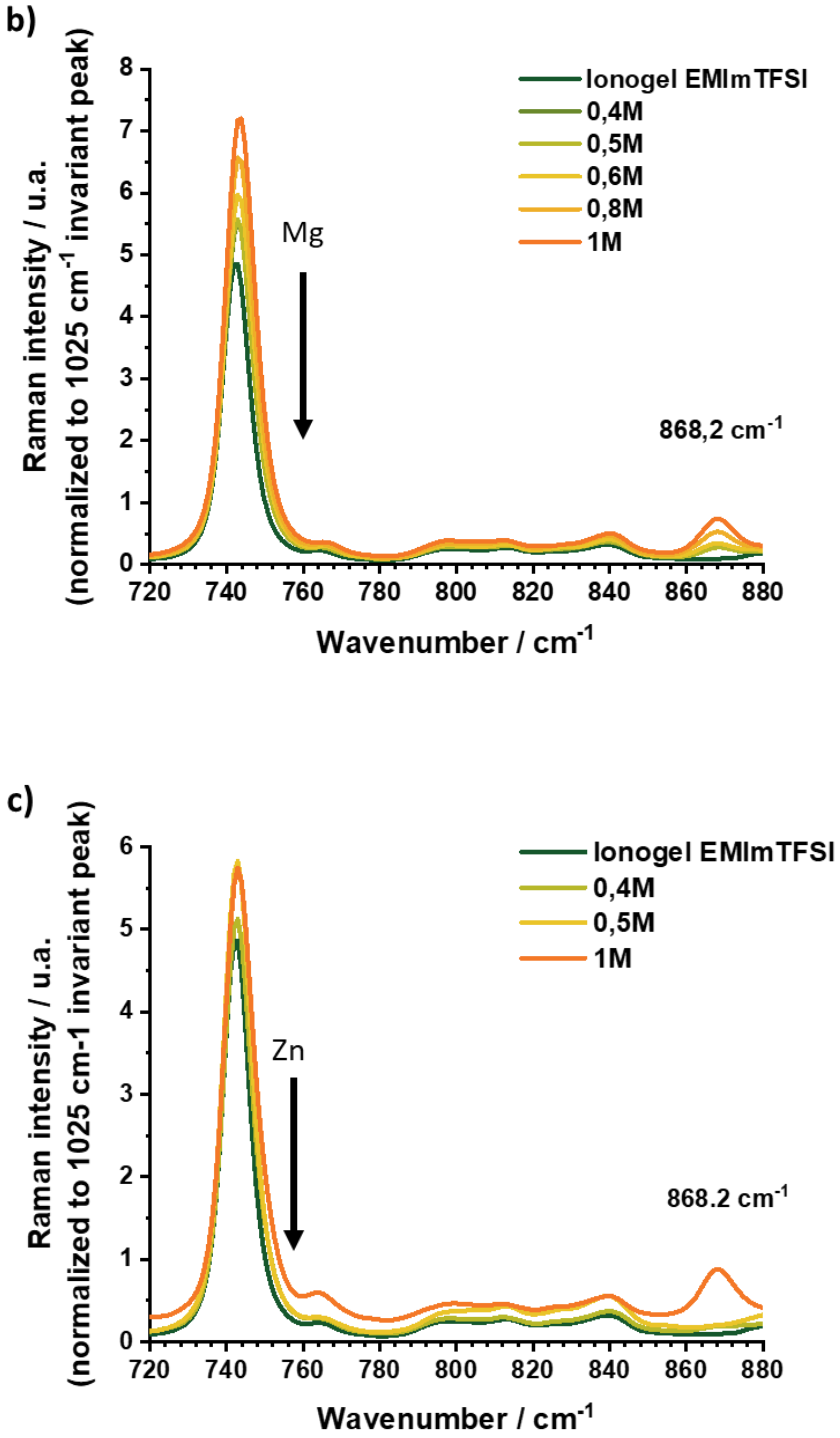


**Figure 5.14: Raman spectrum of a) ionogels with [EMImTFSI + LiTFSI] b) ionogels with [EMImTFSI + $Mg(TFSI)_2$] and c) ionogels with [EMImTFSI + $Zn(TFSI)_2$] at RT in the 720 to 880 $cm^{-1}$ region**

Finally, the coordination number around $Li^+$, $Mg^{2+}$ and $Zn^{2+}$ in ionogels drastically decrease compared to the coordination sphere of metal cations in ternary ILs (Figure 5.15). $TFSI^-$ molecules are not coordinating the metal cations in the same way in the confined ILs than in the non-confined ILs. There could be two main explanations for this result: either the internal pressure exerted on the IL by the polymer chains does not allow the formation of aggregates, or the fluorine non-binding electronic doublets on the polymer chain attract the metal cation. The correct explanation is probably a combination, an average, of both.

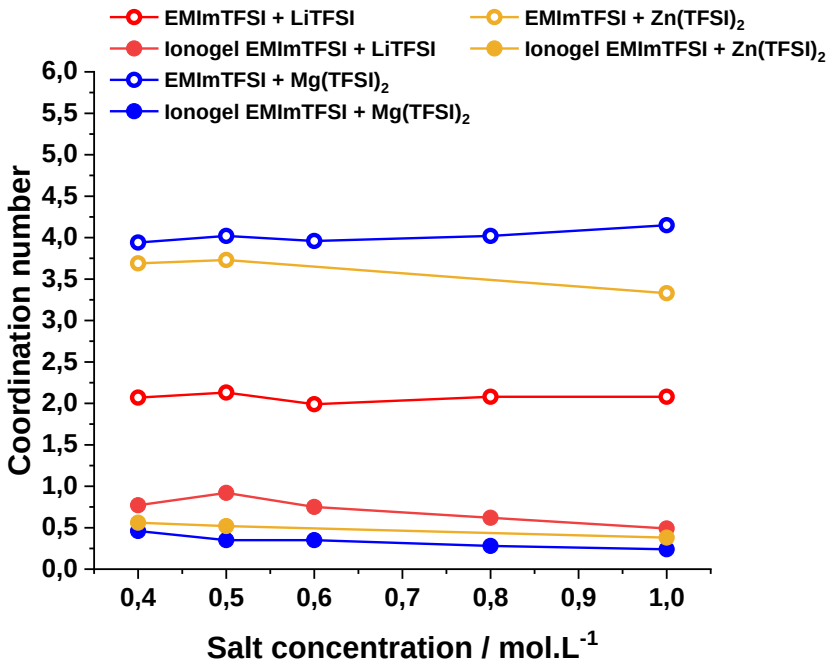


**Figure 5.15: Coordination number around $Li^+$, $Mg^{2+}$ and $Zn^{2+}$ cations in ternary ILs vs. ionogels**

# Conclusion

In summary, biphasic solid-liquid electrolytes have been obtained and characterized in the perspective of transport properties. The comparison between liquid (non confined ILs) and solid (ionogels) samples shows that there is a major difference in the ionic conductivity dependency on salt concentration for non-confined ionic liquids compared to confined ionic liquids. The drops of diffusion and ionic conductivity brought by the salt addition are more important in non confined ILs than in ionogels. Inevitably, the transport properties become better in the confined IL than in the non-confined one above a given concentration, which depends on the metal cation.

PVDF- based ionogels with a [0.83:0.17] composition shows very good ionic conductivities confirmed by the high diffusion of all ions of the electrolyte. Indeed, self-diffusion coefficients measurements reveal that confinement facilitates the diffusion in terms of diffusion action energies.

Many clues about the migration of $Li^+$, $Mg^{2+}$ and $Zn^{2+}$ to the solid liquid interface and the direct interaction between this metal cation and the polymer chains are established. Especially, the increase of the crystallized PVDF melting temperatures with the salt concentration, but also the drastic drop of the metal cations coordination number in ionogels observed thank to Raman spectra.

The free doublet electrons rich PVDF-matrix could lower the expected aggregation phenomenon that occurs in ILs-based electrolytes. Therefore, the confinement is a strategy to tackle the viscosity increase in highly concentrated electrolytes.

$Li^+$ diffusion is better in highly concentrated ionogel than in highly concentrated ionic liquids. This is an essential result because this is the evidence that the metal cation is mobile at the solid-to-liquid interface and is not immobilized by strong interactions with the host network. Moreover, thanks to the coupled EIS and PFG NMR and the activations energies decrease for $EMIm^+$ and $TFSI^-$ in ionogels, the enhanced diffusion of $Mg^{2+}$ and $Zn^{2+}$ in confined ILs is a reasonable assumption.

Finally, due to the abrupt decrease of $Li^+$ diffusion activation energy in ionogels (20 $kJ.mol^{-1}$) compared to the non-confined ternary ILs (45 $kJ.mol^{-1}$), a hypothesis on the diffusion mechanism could be proposed. $Li^+$ diffuses in the thin layer of less viscous layer at the solid-liquid interface with a facilitated 2D translational displacement along with a possible Grotthus mechanism on the fluorine free doublets of the PVDF.

# References


(1) Zhang, S.; Zhang, J.; Zhang, Y.; Deng, Y. Nanoconfined Ionic Liquids. *Chem. Rev.* **2017**, *117* (10), 6755–6833. https://doi.org/10.1021/acs.chemrev.6b00509.

(2) Wang, Y.-L.; Li, B.; Sarman, S.; Mocci, F.; Lu, Z.-Y.; Yuan, J.; Laaksonen, A.; Fayer, M. D. Microstructural and Dynamical Heterogeneities in Ionic Liquids. *Chem. Rev.* **2020**, *120* (13), 5798–5877. https://doi.org/10.1021/acs.chemrev.9b00693.

(3) Guyomard-Lack, A.; Delannoy, P.-E.; Dupré, N.; Cerclier, C. V.; Humbert, B.; Le Bideau, J. Destructuring Ionic Liquids in Ionogels: Enhanced Fragility for Solid Devices. *Phys. Chem. Chem. Phys.* **2014**, *16* (43), 23639–23645. https://doi.org/10.1039/C4CP03187C.

(4) Costa, C. M.; Cardoso, V. F.; Martins, P.; Correia, D. M.; Gonçalves, R.; Costa, P.; Correia, V.; Ribeiro, C.; Fernandes, M. M.; Martins, P. M.; Lanceros-Méndez, S. Smart and Multifunctional Materials Based on Electroactive Poly(Vinylidene Fluoride): Recent Advances and Opportunities in Sensors, Actuators, Energy, Environmental, and Biomedical Applications. *Chem. Rev.* **2023**, *123* (19), 11392–11487. https://doi.org/10.1021/acs.chemrev.3c00196.

(5) Susan, Md. A. B. H.; Kaneko, T.; Noda, A.; Watanabe, M. Ion Gels Prepared by in Situ Radical Polymerization of Vinyl Monomers in an Ionic Liquid and Their Characterization as Polymer Electrolytes. *J. Am. Chem. Soc.* **2005**, *127* (13), 4976–4983. https://doi.org/10.1021/ja045155b.

(6) Zhou, H. Facilitated Phase Transformation of PVDF in Its Composite with an Ionic Liquid. **2021**.

(7) Marie, A.; Said, B.; Galarneau, A.; Stettner, T.; Balducci, A.; Bayle, M.; Humbert, B.; Le Bideau, J. Silica Based Ionogels: Interface Effects with Aprotic and Protic Ionic Liquids with Lithium. *Phys. Chem. Chem. Phys.* **2020**, *22* (41), 24051–24058. https://doi.org/10.1039/D0CP03599H.

(8) Guillemin, T.; Douard, C.; Robert, K.; Asbani, B.; Lethien, C.; Brousse, T.; Le Bideau, J. Solid-State 3D Micro-Supercapacitors Based on Ionogel Electrolyte: Influence of Adding Lithium and Sodium Salts to the Ionic Liquid. *Energy Storage Materials* **2022**, *50*, 606–617. https://doi.org/10.1016/j.ensm.2022.05.041.

(9) Arano, K.; Begic, S.; Chen, F.; Rakov, D.; Mazouzi, D.; Gautier, N.; Kerr, R.; Lestriez, B.; Le Bideau, J.; Howlett, P. C.; Guyomard, D.; Forsyth, M.; Dupre, N. Tuning the Formation and Structure of the Silicon Electrode/Ionic Liquid Electrolyte Interphase in Superconcentrated Ionic Liquids. *ACS Appl. Mater. Interfaces* **2021**, *13* (24), 28281–28294. https://doi.org/10.1021/acsami.1c06465.

# General conclusion

## Conclusions on the present work

A contribution in understanding the dynamics in ILs-based electrolytes and ionogels was offered in this thesis. The objective to propose a robust, systematic methodology for demonstrating the improved transport properties of ionogels compared with conventional metal cations doped-ionic liquids is met. The systems chosen to synthetize performant bivalent cations-conductive ionogels are ideal systems for this study. The two last results chapters (4 & 5) summarize the results obtained for several series of non-confined and confined ternary ionic liquids with lithium, magnesium and zinc salts. Assessing the effect of confinement on the dynamics, thermal and structural properties of such electrolytes enables to bring fundamental conclusions and insights on how to optimize the transport of monovalent and bivalent metal cations in electrochemical devices.

For the last decades, research groups tried to bring a clear definition of ionic liquids properties and behaviour as a function of temperature or salt dopant. The conclusion on studying ternary ILs is that this family of molten salt is promising for energy storage electrolytes applications. Herein, we propose an interesting approach to overcome the disadvantages of using viscous and liquid ILs by confining the ternary ILs, as well as providing the ability to shape theme easily.

Obtaining solid biphasic electrolytes is an easy task, especially physical gels made of PVDF polymer chains. Nevertheless, the study of the dynamics in these complex electrolytes and understanding the diffusion mechanism is not trivial and the conclusions of the present work will be given next. Moreover, versatility of polymer networks and ionic liquids combinations ensures a promising future for ionogels science.

As a reference, three series of ternary ILs ([EMImTFSI + LiTFSI], [EMImTFSI + Mg(TFSI)2] and [EMImTFSI + Zn(TFSI)2]) have been characterized in term of some thermodynamic point of view, transport properties and coordination sphere around the metal cation. Adding monovalent or bivalent metal cations salt in the neat IL definitely changes the structural and transport properties with concentration. The decrease in self-diffusion and thus in macroscopic ionic conductivity has been shown to be due to the increasing viscosity brought by the aggregates formation in these complex concentrated electrolytes. First, this aggregation phenomenon is directly related to the polarizing power of the metal cation and its interaction ability toward $TFSI^-$ compared to the EMIm-TFSI interaction. The structure and proportion of these aggregates in the liquid phase are also depending

on the nature of the cation and the salt concentration. In particular, the TFSI coordination number of around $Li^+$ is two, around $Mg^{2+}$ is four and around $Zn^{2+}$ is between three and four. This ordered classification $Li^+ < Zn^{2+} < Mg^{2+}$ is often found in the thesis, meaning that the electronic configuration of the metal cations is the very essence of the observed properties. Secondly, transport properties of the mixtures were assessed in a second time thanks to the coupled EIS and PFG NMR. Numerous experimental data were tabulated, they will be the starting point to assess the effect of the confinement, and hopefully a trustable reference for future theoretical calculations.

In comparison, biphasic solid-liquid electrolytes have been obtained and characterized in the perspective of transport properties. The comparison between liquid (non-confined ILs) and solid (ionogels) samples shows that there is a major difference in the ionic conductivity dependency on salt concentration for non-confined ionic liquids compared to confined ionic liquids. The drops of diffusion and ionic conductivity brought by the salt addition are more important in non-confined ILs than in ionogels. Inevitably, the transport properties become better in the confined IL than in the non-confined one, above a given concentration, which depends on the metal cation.

The study of thermal behaviour in ionogels is limited by the quenching of transitions phases that make the observations of phase transitions difficult. However, the glass transition temperature is essential in predicting the viscosity of the liquid phase at higher temperatures. DSC measurements helped to hypothesize that the confined IL does not behave similarly at the solid-liquid interface or in the bulk IL. There is a local thin layer of ionic liquid adsorbed at the polymer surface, which shows unique structural and dynamical properties and where less energy is needed to trigger ions mobility. Indeed, PVDF- based ionogels with a [0.83:0.17] [IL:PVDF]composition shows very good ionic conductivities confirmed by the high diffusion of all ions of the electrolyte. Self-diffusion coefficients measurements reveal that confinement facilitates the diffusion in terms of diffusion activation energies.

Many clues about the migration of $Li^+$, $Mg^{2+}$ and $Zn^{2+}$ to the solid liquid interface and the direct interaction between this metal cation and the polymer chains are established, especially based on the increase of the crystallized PVDF melting temperatures with the salt concentration, but also on the drastic drop of the metal cations coordination number (less than one $TFSI^-$ molecule on average) in ionogels observed thanks to Raman spectra. The free doublet electrons rich PVDF-matrix could lower the expected aggregation phenomenon that occurs in ILs-based electrolytes. Therefore, we brought the evidence that confinement is a performant strategy to tackle the viscosity increase in highly concentrated electrolytes. $Li^+$ diffusion is better in highly concentrated ionogel than in highly concentrated ionic liquids. This is an essential result because this is the evidence that the metal cation

is mobile at the solid-to-liquid interface and is not immobilized by strong interactions with the host network. Moreover, thanks to the coupled EIS and PFG NMR and the activations energies decrease for $EMIm^+$ and $TFSI^-$ in ionogels, the enhanced diffusion of $Mg^{2+}$ and $Zn^{2+}$ in confined ILs is a reasonable prediction.

The final fundamental result is the abrupt decrease of $Li^+$ diffusion activation energy in ionogels (20 $kJ.mol^{-1}$) compared to that of the non-confined ternary ILs (45 $kJ.mol^{-1}$): this lead to the hypothesis that $Li^+$ diffuses in the thin layer of less viscous layer at the solid-liquid interface with a facilitated 2D translational displacement, along with a possible Grotthuss mechanism on the fluorine free doublets of the PVDF. This phenomenon still need to be investigated for bivalent metal cations.

# Perspectives

## Electrochemical characterization of electrolytes

Studying the dynamics in electrolytes is not enough to integrate ionogels in electrochemical devices such as hybrid supercapacitors. Other electrochemical characterizations need to be performed in order to assess the behaviour of these solid electrolytes under voltage and at metal interfaces. Here, we propose a protocol to obtain information on the Electrochemical Stability Window (ESW), the transference number of the metal cation and the reversibility of redox reactions at the electrolyte-to-electrode interface.

### 1. Linear Sweep Voltammetry – Measure of the ESW

The setups used during the thesis to measure the electrochemical stability windows of non-confined and confined ionic liquids are presented Figure 1. The main motivation was to develop cells where liquid and solid samples could be characterized in the same conditions. In Figure 2 are shown the results for EMImTFSI and a PVDF- based ionogels with a [0.83:0.17] composition.

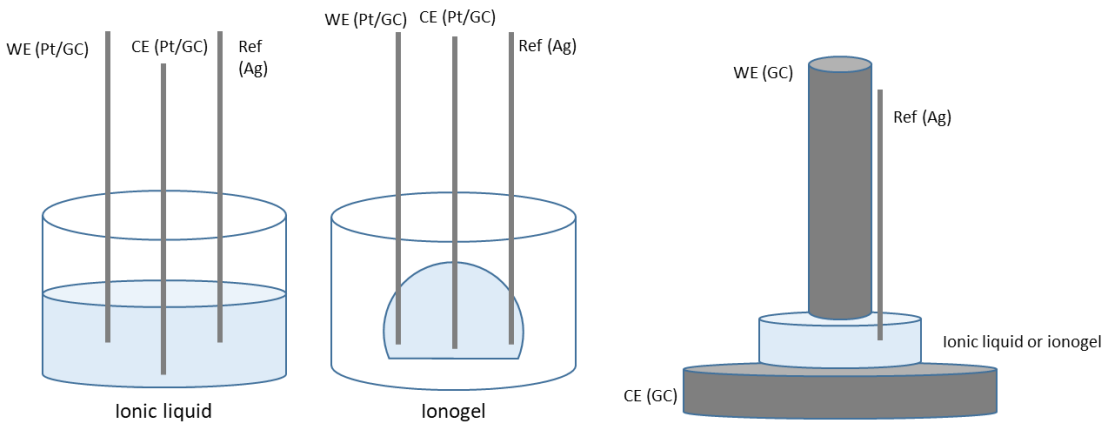


**Figure 1: LSV setups for ionic liquid and ionogels ESW measurement**

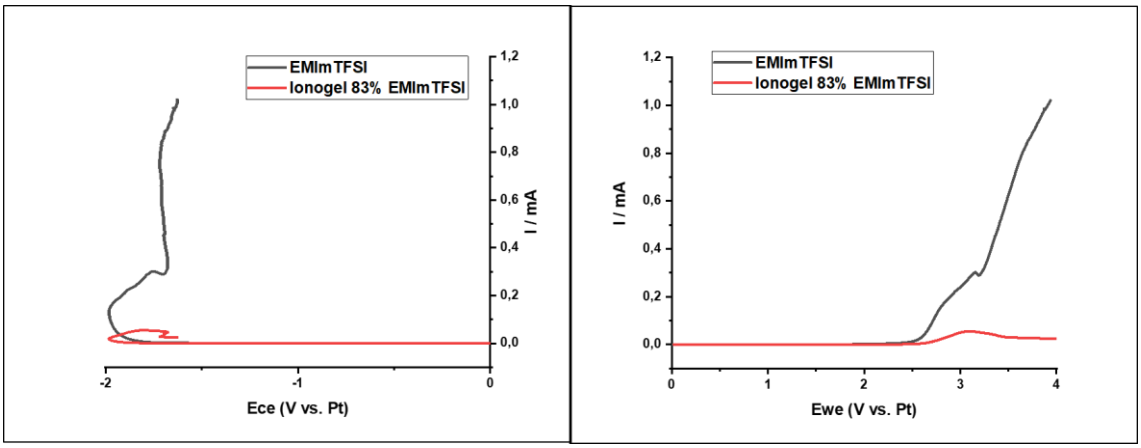


**Figure 2: Preliminary results on the stability window of EMImTFSI based IL and ionogel**

It is noteworthy that the reference used was a platinum wire and that the absolute potential is unknown, as a redox couple like $Fc/Fc^+$ is needed, and could be included in the ionogel synthesis. However, this measure enables to ensure that the entire stability window for EMImTFSI is around 4,5V between $TFSI^-$ oxidation at -2V and $EMIm^+$ reduction at +2,5V on the figure. Ohno et al. showed that the accurate potentials for the electrochemical decomposition of EMImTFSI are -2,5V for the oxidation of $TFSI^-$ and +2V for the reduction of $EMIm^+$ *vs* $Fc/Fc^+$. This method is still an interesting experiment to compare series of samples one to each other's.

## 2. Transference number measurement – Evans-Bruce-Vincent method

The transference number is a useful method to quantify the migration of a metal cation between two electrodes in a symmetric setup (Figure 3). In other words, this measurement assesses the electrolyte ability to transfer metal cation from one electrode to another after a DC polarization.

The transference number is a number comprised between 0 and 1, given by the Evans-Bruce-Vincent equation:

$$t^{+} = \frac{I_s(\Delta V - I_0 * R_0)}{I_0(\Delta V - I_s * R_s)}$$

Where $\boldsymbol{\Delta V}$ is a small dc applied to polarize the sample (between 20mV and 100 mV depending on the intensity of the current measured i.e. the quality of the electrolyte-electrode interface), $\boldsymbol{I_0}$ is an initial value of current upon polarization, $I_S$ is the steady-state current reached after the dc polarization, $\boldsymbol{R_0}$ and $\boldsymbol{R_s}$ are the resistance of the electrolyte before and after polarization, respectively.

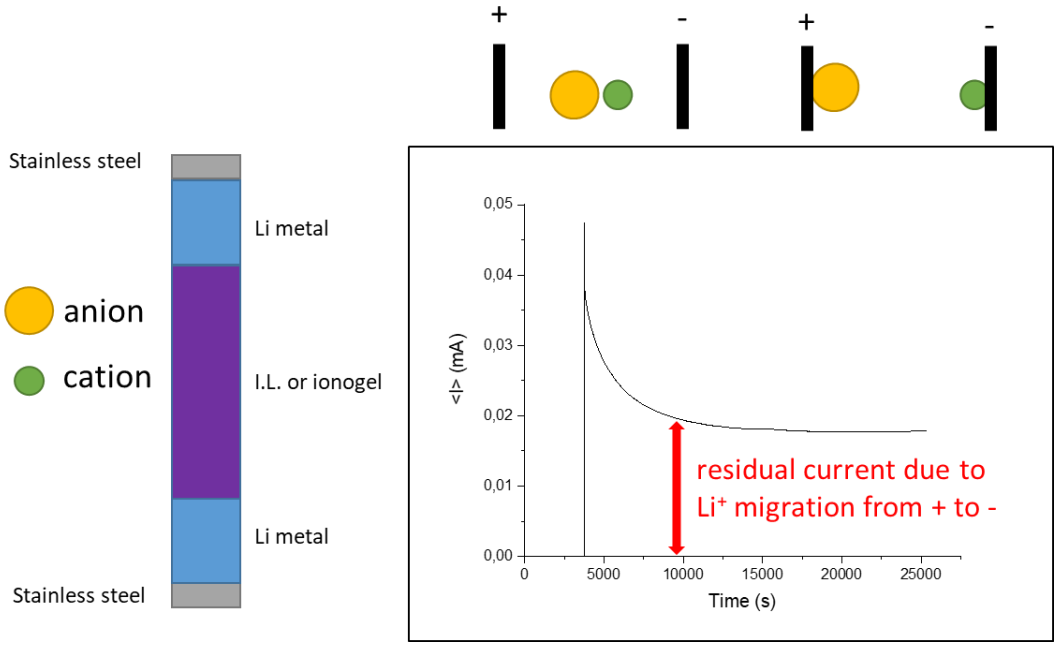


**Figure 3: Example of $Li^+$ transference number measurement in IL or ionogel electrolyte**

Some measurements has been performed but the accuracy of the calculations of transference numbers was not optimized and will need future developments. In particular, some issue with magnesium metal were encountered and studied. Artificial passivation layer at the surface of the metal was considered to prevent the formation of the ion-blocking resistive interface.

3. Stripping and plating – The reversibility of faradaic reactions

The last experiment that was considered and started during the PhD project is the reversible stripping and plating on metal electrodes in highly concentrated non-confined and confined ILs. Figure 4 shows the cyclic voltammetry at 0,1 $mV.s^{-1}$ and 5 $mV.s^{-1}$ of EMImTFSI + 1M LiTFSI between to lithium metal electrodes. Both oxidation and reduction of lithium are clearly visible in the ternary IL, showing that reversible redox reactions are possible at the electrolyte-electrode interface.

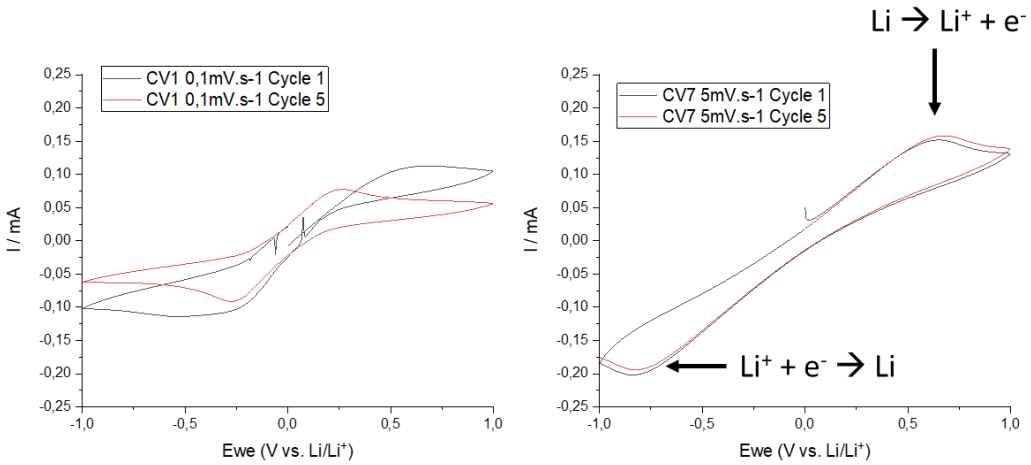


**Figure 4: Cyclic voltammetries for an ionic liquid sample containing 1M LiTFSI at different scan rates**

Overall, some studies on the electrochemical characterization on such electrolytes and their potential application on metal-ion device need to be developped and discussed, specifically for metal//ionogel//activated carbon systems and at which operating voltage.

## The chemistry of the host network

Some other polymer matrix were considered during the thesis in order to assess the impact of the surface chemistry of the confining matrix on the properties of the confined IL : these preliminary works deserve to be deepen in order to find the best synergetic effect between conined ternary IL and host network.

Among others, a new ionogel was synthetized succesfully with a co-polymer structure based on styrene and divinylbenzene backbone and poly(ethylene oxide) brushes. This ionogel is flexible and can host a relatively high amount of ionic liquid inside (Figure 4). The macroscopic ionic conductivities

of this Li and Mg-doped ionogel are very good regarding the liquid-to-solid ratio, which is slightly lower than in PVDF-based ionogels (Figure 5).

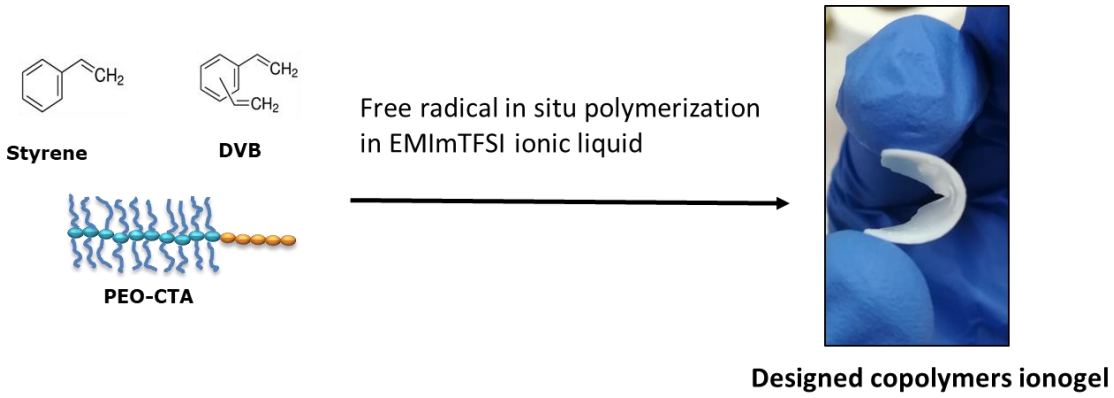


**Figure 5: Synthesis of a new co-polymer based ionogel with brush structure**

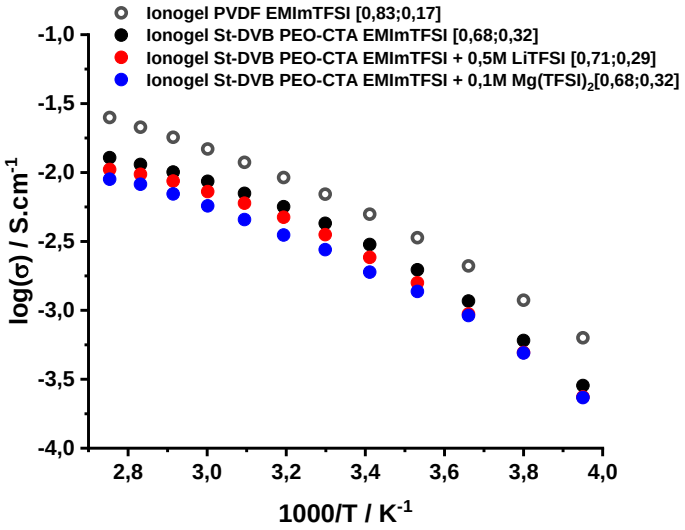


**Figure 5: Ionic conductivity performance of the new ionogel compared to PVDF based ionogel**

Some more work on complex polymer structures need to be done in order to correlate the topology and chemistry of the solid-to-liquid interface in ionogels with the observed enhanced transport properties of the electrolytes family.

# ANNEX 1: Standard deviation and uncertainties in EIS

$$\text{Ionic conductivity: } \sigma = \frac{e}{R.S}$$

Where $\sigma$ is the ionic conductivity in S.cm$^{-1}$; $e$ the thickness of the sample in cm; $S$ the surface area of the sample in contact with the stainless steel electrodes in cm$^2$ and $R$ the real part of the complex Impedance in Ω.

**Standard deviation**

Mean values of ionic conductivities are obtained with two measures on two identical samples. Standard deviation is given for these four values (Figure 1) and are calculated from the dispersion of the values measured. Error bars derived from statistics of the measurements are not shown in this manuscript.

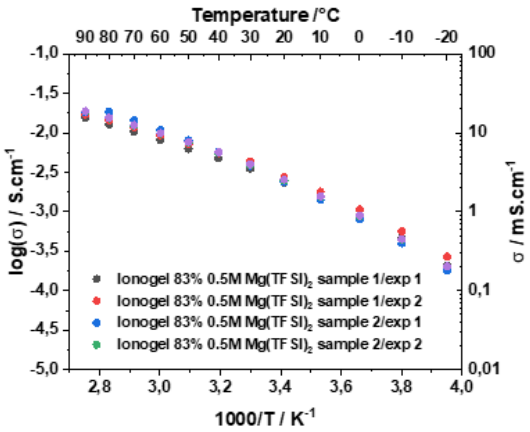


| | $\sigma_{50°C}$ *(mS.cm$^{-1}$)* |
|---|---|
| *EMIMTFSI* | 15.1 ±0.2 |
| *Ionogel 83% EMIMTFSI* | 11.8 ±0.2 |
| *EMIMTFSI +1M LiTFSI* | 7.3 ±0.2 |
| *Ionogel 83% EMIMTFSI +1M LiTFSI* | 6.6 ±0.4 |
| *EMIMTFSI + 1M Mg(TFSI)$_2$* | 2.5 ±0.6 |
| *Ionogel 83% EMIMTFSI +1M Mg(TFSI)$_2$* | 6.9 ±0.7 |

**Figure 1: Ionic conductivity measurements repeatability and standard deviations for few samples at 50°C**

**Uncertainties**

Uncertainties due to the shape factor of the sample are easy to calculate depending on the accuracy of the calliper tool used to obtain the dimension of the Teflon ring, in the case of liquid samples, or ionogels. This is important to mention that these uncertainties are always inferior to the standard deviation mentioned above and make the measurement of R the most significant factor in the determination of errors.

As it is very complicated to assess the uncertainty attributed to the measurement on the potentiostat itself, we propose here a method to obtain a confidence interval for each R measurements.

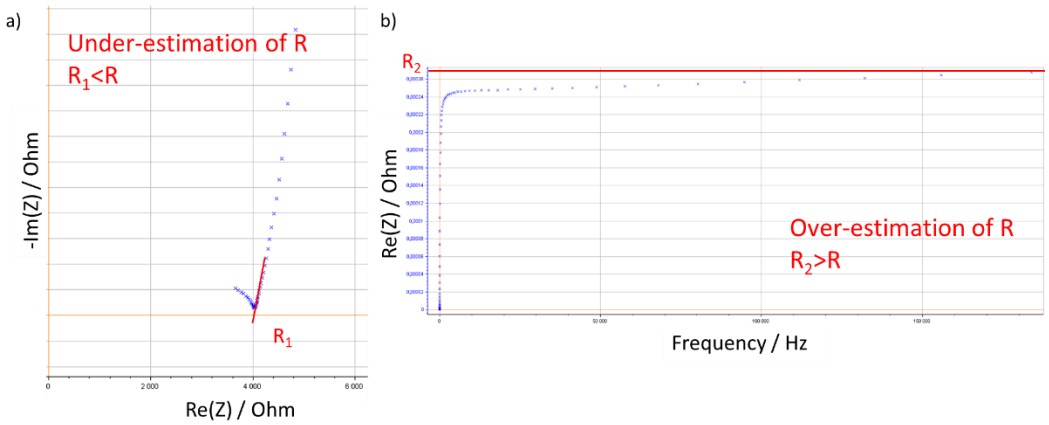


**Figure 2: (a) Nyquist plot and (b) resistance vs. frequency for one sample at a given temperature**

The data processing can involve two R-value determinations. The first one is via the Nyquist plot, the real part of impedance $R_1$ is underestimated by fitting the linear part at low frequencies where the value for Im(Z) is zero. The second method consists of plotting the tangent at infinite frequency on the Re(Z) vs. frequency plot. The $R_2$ value overestimates the resistance.

In the end, the measured value R is between $R_1$ and $R_2$. This information is an approximate uncertainty on the impedance measurement by EIS.

COLLEGE ED MATIERE,MOLECULES
DOCTORAL MATERIAUX ET
PAYS DE LA LOIRE GEOSCIENCES

Nantes Université

University of South Australia

**Titre :** Electrolytes ionogels solides conducteurs d'ions divalents pour applications métal-ion

**Mots clés :** Electrolyte, ionogel, tout-solide, métal-ion, magnésium, zinc

**Résumé :** Le développement de dispositifs de stockage d'énergie tout solide implique l'utilisation de nouveaux matériaux innovants incluant les électrolytes. Ils doivent être compétitifs vis-à-vis des électrolytes liquides commerciaux en termes de conductivité ionique et de stabilité électrochimique. Les liquides ioniques (LIs) sont déjà utilisés pour leurs propriétés intéressantes telles que leur pression de vapeur très faible, leur point de fusion bas, leur non flammabilité et leur large fenêtre électrochimique. Néanmoins, ils restent liquides et présentent des problèmes de fuite et donc de packaging. Le confinement de liquides ioniques dans le polymère polyfluorure de vinylidène (ionogels) permet de limiter les risques d'emballement thermique dans les dispositifs électrochimiques. Les ionogels sont des matériaux biphasiques à interface bicontinue entre un liquide ionique et la matrice solide qui le confine (silice ou polymères).

Les ionogels présentent une conductivité ionique très élevée. L'ajout de sels de Li, Mg ou Zn dans le LI permet d'adapter les ionogels à des applications spécifiques telles que les supercondensateurs et les batteries.

Le passage des cations monovalents aux cations divalents garantit une densité d'énergie théorique plus élevée dans le dispositif.

Ces travaux de recherche se concentrent sur les interactions et la mobilité des ions dans les ionogels. Nous étudions les interactions coulombiennes en compétition entre le cation d'intérêt ($Li^+/Mg^{2+}/Zn^{2+}$) et, soit avec l'anion de l'IL, soit avec la matrice solide de confinement. Ces études apportent des connaissances sur la surprenante diffusivité de ces cations dans les ionogels. Les propriétés chimiques et physiques du polymère jouent un rôle essentiel dans ces mécanismes de diffusion à l'interface solide-liquide. Le confinement permet de sélectionner une interaction privilégiée avec le réseau hôte pour les cations d'intérêt, avec une diffusion par sauts possible à l'interface continue. Enfin, les ionogels conçus pour les prototypes de supercondensateurs hybrides métal-ion pourront être étudiés dans des cellules symétriques afin de confirmer que les propriétés de transport sont meilleures dans les ionogels fortement concentrés que dans les liquides ioniques eux-mêmes.

**Title :** Bivalent cations conductive solid ionogel electrolytes for metal-ion applications

**Keywords :** Electrolyte, ionogel, all-solid state, metal-ion, magnesium, zinc

**Abstract:** The development of all-solid-state energy storage devices calls for the use of new, innovative materials including electrolytes. These must be competitive with commercial liquid electrolytes in terms of ionic conductivity and electrochemical stability. Ionics liquids (ILs) are already used for their interesting properties such as very low vapour pressure, low melting point, non-flammability, and wide electrochemical windows. Nevertheless, they remain liquid and present leakage and therefore packaging problems. The confinement of ionic liquids in polyvinylidene fluoride polymer (ionogels) limits the risk of thermal runaway in electrochemical devices. These are biphasic materials with continuous interfaces between an ionic liquid and the solid matrix (silica or polymer) that confines it.

Ionogels feature very high ionic conductivity. By adding Li, Mg or Zn salts to IL, ionogels can be tailored to specific applications such as supercapacitors and batteries.

The switch from monovalent to bivalent cations guarantees a higher theoretical energy density in the device.

The present work focuses on the interactions and mobility of ions in ionogels. We are studying the competitive coulombic interactions either between the cation of interest ($Li^+/Mg^{2+}/Zn^{2+}$) and the IL anion or with the confining solid matrix. These studies shed light on the surprising diffusivity of these cations in ionogels. The chemical and physical properties of the polymer play an essential role in these diffusion mechanisms at the solid-liquid interface. Confinement allows the cations of interest to select a preferred interaction with the host polymer, with a possible hopping diffusion mechanism at the continuous interface. Finally, ionogels designed for prototype metal-ion hybrid supercapacitors can be studied in symmetrical cells to confirm that transport properties are better in highly concentrated ionogels than in the ionic liquids themselves.